Characterisation of the sulphydryl oxidoreductase system of the mitochondrial intermembrane space

A thesis submitted to The University of Manchester for the degree of

Ph.D

In the Faculty of Life Sciences

2010

Swee Kim Ang

LIST OF CONTENTS

LIST OF FIGURES

LIST OF TABLES

ABSTRACT

In *Saccharomyces cerevisiae*, about 98% of all mitochondrial proteins are synthesised in the cytosol and are translocated into different mitochondrial subcompartments. The biogenesis of many cysteine-containing proteins in the mitochondrial intermembrane space (IMS) is driven by a sulphydryl oxidoreductase system known as the mitochondrial import and assembly (MIA) machinery that catalyses disulphide bond formation. The MIA machinery contains two essential components: the import receptor Mia40 and the FAD-dependent sulphydryl oxidase Erv1. Current model suggests that Erv1 oxidises Mia40, which in turn transfers a disulphide bond to substrate proteins. However, it was unclear how Erv1 oxidises Mia40. In this study, the roles of individual disulphide bonds of Erv1 and the mechanism of Mia40-Erv1 interaction were investigated. Erv1 contains three disulphide bonds arranged in two CXXC motifs (Cys30-Cys33 and Cys130-Cys133) and one $CX_{16}C$ motif (Cys159-Cys176). Three double cysteine mutants with each cysteine pair corresponding to individual disulphide bonds were generated. Systematic analyses using a wide range of *in vitro*, *in organello* and *in vivo* methods showed that both the CXXC disulphides are required for Erv1 enzymatic function, while the $CX_{16}C$ disulphide has a dual role in stabilising protein folding and mitochondrial import of Erv1. This study showed that Cys30-Cys33 functions as a shuttle disulphide that transfers electrons to the active-site disulphide Cys130-Cys133, and both intersubunit and intermolecular electron transfer can occur. The shuttle disulphide of Erv1 receives electrons from the CPC disulphide (Cys296-Cys298) of Mia40 through formation of a mixed disulphide intermediate. Characterisation of single cysteine mutant proteins of Mia40 and Erv1 suggested that Cys298 of Mia40 favours mixed disulphide bond formation with Cys30 of Erv1, although different mixed disulphides can be formed between all other cysteine combinations *in vitro*. GSH may play an isomerisation-like role in counteracting non-productive Mia40-Erv1 mixed disulphides. In addition, it was found that Erv1 has a strong affinity towards zinc binding, which inhibits its enzymatic function. The inhibitory effects of zinc can be counteracted in the presence of a chelating agent.

DECLARATION

No portion of the work referred to in the thesis has been submitted in support of an application for another degree or qualification of this or any other university or other institute of learning.

COPYRIGHT STATEMENT

i. The author of this thesis (including any appendices and/or schedules to this thesis) owns certain copyright or related rights in it (the "Copyright") and s/he has given The University of Manchester certain rights to use such Copyright, including for administrative purposes.

ii. Copies of this thesis, either in full or in extracts and whether in hard or electronic copy, may be made only in accordance with the Copyright, Designs and Patents Act 1988 (as amended) and regulations issued under it or, where appropriate, in accordance with licensing agreements which the University has from time to time. This page must form part of any such copies made.

iii. The ownership of certain Copyright, patents, designs, trade marks and other intellectual property (the "Intellectual Property") and any reproductions of copyright works in the thesis, for example graphs and tables ("Reproductions"), which may be described in this thesis, may not be owned by the author and may be owned by third parties. Such Intellectual Property and Reproductions cannot and must not be made available for use without the prior written permission of the owner(s) of the relevant Intellectual Property and/or Reproductions.

iv. Further information on the conditions under which disclosure, publication and commercialisation of this thesis, the Copyright and any Intellectual Property and/or Reproductions described in it may take place is available in the University IP Policy (see http://www.campus.manchester.ac.uk/medialibrary/policies/intellectual-property.pdf), in any relevant Thesis restriction declarations deposited in the University Library, The University Library's regulations (see http://www.manchester.ac.uk/library/aboutus/regulations) and in The University's policy on presentation of Theses.

ACKNOWLEDGEMENTS

I would like to thank all past and present members of the Lu, Bulleid, Grant and Swanton labs for their selfless help throughout the course of my study. Special thanks go to my supervisor Dr. Hui Lu, who gave me the opportunity to pursue this study and to develop my skills as a scientist. I have learnt a lot of valuable soft skills from her. I would like to thank my former boss Prof. Mary Jane Cardosa, for the excellent training when I was working as a research assistant in her super-advanced lab. The research skills I have learnt there have contributed significantly towards this study. I would like to thank Prof. Sim Soon Liang for being my referee when I was applying for financial support in pursuing this study. I would also like to thank all my family and friends. The greatest appreciation goes to my family especially my Mum, for all their support in everything over the years; the heartiest thanks go to my loving partner for the care and spiritual support, and the Kean family for the enjoyable Western culture experience. Lastly, I would like to thank the Faculty of Life Sciences for the Faculty Bursary that partially funded my study.

LIST OF ABBREVATIONS

AMS: 4-acetamido-4’-maleimidylstilbene-2,2’-disulphonic acid

ALR: Augmenter of liver regeneration

CCHL: Cytochrome c heme lyase

Ccp1: Cytochrome c peroxidase

Ccs1: Copper chaperone of Sod1

CD: Circular dichroism

Cyt c: Cytochrome c

DOX: Doxycycline

Dsb: Disulphide bond forming protein

DTT: Dithiothreitol

EDTA: Ethylenediaminetetraacetic acid

EGTA: Ethylene glycol-bis (β-aminoethylether) N,N,N’,N’-tetraacetic acid

ER: Endoplasmic reticulum

FAD: Flavin adenine dinucleotide

GSH: Reduced glutathione

GST: Glutathione-S-Transferase

HSP: Heat shock protein

IAM: Iodoacetamide

IM: Inner membrane

IMS: Intermembrane space

IPTG: Isopropyl-β-D-thiogalactopyranoside

ISC: Iron-sulphur cluster

LB: Luria broth

MALDI-Tof: Matrix assisted laser desorption ionisation time-of-flight

MIA: Mitochondrial import and assembly

MISS/ITS: Mitochondrial IMS sorting signals/ IMS-targeting signals

MPP: Mitochondrial processing peptidase

OD: Optical density

OM: Outer membrane

PAM: Presequence translocase-associated motor

PMSF: Phenyl methane sulphonyl fluoride

PDI: Protein disulfide isomerase

QSOX: Quiescin sulfhydryl oxidase

ROS: Reactive oxygen species

SAM: Sorting and assembly machinery

SDS-PAGE: Sodium dodecyl sulphate polyacrylamide gel electrophoresis

Sod1: Super oxide dimutase

TCEP: Tris- (2-carboxyethyl) phosphine membrane

TIM: Translocase complex of the inner membrane

TOM: Translocase complex of the outer membrane

WT: Wild type

PREFACE

Several results obtained from this study have been published (see appendix 2). The published materials were presented in this report with permission from the co-authors, together with other unpublished data.

1. INTRODUCTION

Mitochondrion is a discrete organelle housed in most eukaryotic cells. It contains double membranes, enabling the organelle to be divided into four distinct subcompartments (Figure 1.1, inset): the outer membrane (OM), the inner membrane (IM), the intermembrane space (IMS) and the matrix (Perkins and Frey, 2000, Frey and Mannella, 2000). The IM is highly folded and invaginated into the matrix, forming tubular structures called cristae. This feature further divides the IM into two different subdomains: the inner boundary membrane (IBM), which is closely opposed to the OM; and the cristae membrane, which reaches the matrix. The two IM subdomains therefore result in two IMS subdomains: the external IMS, which is separated by the OM and IBM; and the intracristal space, which is separated by cristae membranes opposite to each other.

The high compartmentalisation nature of mitochondrion enables the organelle to perform a wide range of metabolic functions. Fundamentally, mitochondrion supports aerobic metabolism and produces more than 90% of cellular energy (Chance et al., 1979) in the form of adenosine triphosphate (ATP) through two metabolic processes: the Kreb's cycle and the electron transport chain. Therefore, in metabolically active cells, such as cardiac muscle, liver and brain, mitochondria are found in a large number (Veltri et al., 1990). Throughout the ATP production process by oxidative phosphorylation that requires continuous flow of electrons, reactive oxygen species (ROS) are generated as by-products of the electron transport chain. Therefore, mitochondrion is a major source of ROS (Murphy, 2009) that play important signalling roles in a number of redox-dependent processes, including apoptosis (Jiang and Wang, 2004) and cell proliferation (Fruehauf and Meyskens, 2007). Furthermore, mitochondrion also plays important roles in cellular Ca^{2+} homeostasis (Graier et al., 2007) and Fe-S cluster biogenesis (Muhlenhoff and Lill, 2000).

Due to the significant roles of the mitochondrion in various cellular processes, mitochondrial dysfunction potentially causes a broad range of diseases in human, including diabetes, cardiovascular and neurological disorders (Schapira, 2006, Pieczenik and Neustadt, 2007). Since mitochondrial proteins are the key players of the essential intracellular metabolic pathways, studying the biogenesis and functions of mitochondrial proteins is fundamentally important to understand the associated diseases. In the following sections, the various mitochondrial protein import pathways into different subcompartments will be described,

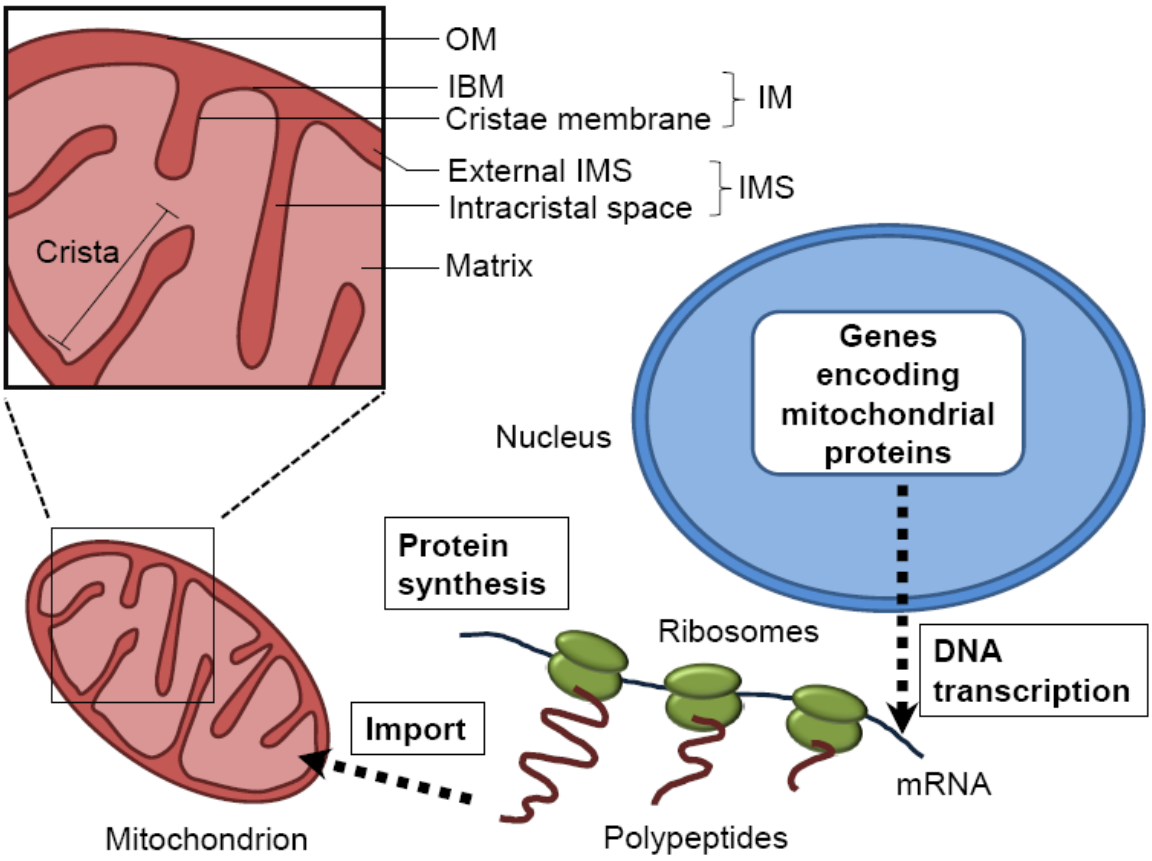

Figure 1.1 Biogenesis of mitochondrial proteins.

A majority of mitochondrial proteins are encoded by nuclear genes. They are synthesised on cytosolic ribosomes and subsequently translocated into the organelle. Inset: structural features of a mitochondrion. The outer membrane (OM) and inner membrane (IM) enclose a narrow space known as the intermembrane space (IMS). The IM encloses the matrix and is highly invaginated forming tubular structures known as cristae. These structures subdivide the IM into the inner boundary membrane (IBM) and the cristae membrane; and the IMS into the external IMS and the intracristal space.

with an emphasis on the redox-dependent MIA pathway in the IMS. The various aspects of disulphide bond formation pathways in the mitochondrial IMS will also be compared with those in endoplasmic reticulum and bacterial periplasm. Finally, current knowledge on the structural and functional properties of a key component of the MIA pathway, Erv1 which is the focus of this study will be reviewed in detail.

1.1 Biogenesis of mitochondrial proteins

Mitochondrion contains a distinct genome made of a single, circular DNA molecule which enables the organelle to self-replicate independently from the nuclear genome. This unique feature raised a general belief that the mitochondria are originated from bacteria captured by proto-eukaryotic cells which gradually evolved through endosymbiosis (Margulis, 1981). Throughout the evolution process, the bacteria lost their genes due to redundancy and transfer to the host cells; therefore resulting in much smaller mitochondrial genome size compared to the nuclear genome, and also gene distribution in between the two genomes (Gray et al., 1999, Margulis, 1981). In the last 10 years, the availability of complete genome sequence data of several mitochondrial, prokaryotic and nuclear genomes confirmed that the mitochondrial genome was descended from an α-proteobacterial ancestor (Gray et al., 2001).

The 86kb mitochondrial genome of yeast contains 46 genes coding for 19 polypeptides and 27 structural RNAs; whilst the 13kb mitochondrial genome of human contains 37 genes coding for 13 polypeptides and 24 structural RNAs (Foury et al., 1998, Anderson et al., 1981). The mitochondrial encoded proteins are mainly components of the respiratory complexes, comprising only about 1-2% of total estimated 800 (yeast) to 1300 (human) proteins in the mitochondria (Taylor et al., 2003, Sickmann et al., 2003). A vast majority of the remaining proteins are nuclear genome encoded and translated on the cytosolic ribosomes (Figure 1.1). Hence, there is a requirement for the synthesised proteins to be transported from the cytosol into the mitochondria. Mitochondrial proteins contain unique sorting signals that determine their translocation into specific subcompartments within the mitochondria using different pathways (Figure 1.2) (Neupert and Herrmann, 2007, Chacinska et al., 2009). In the following sections, the four major protein import pathways in different mitochondrial subcompartments will be reviewed.

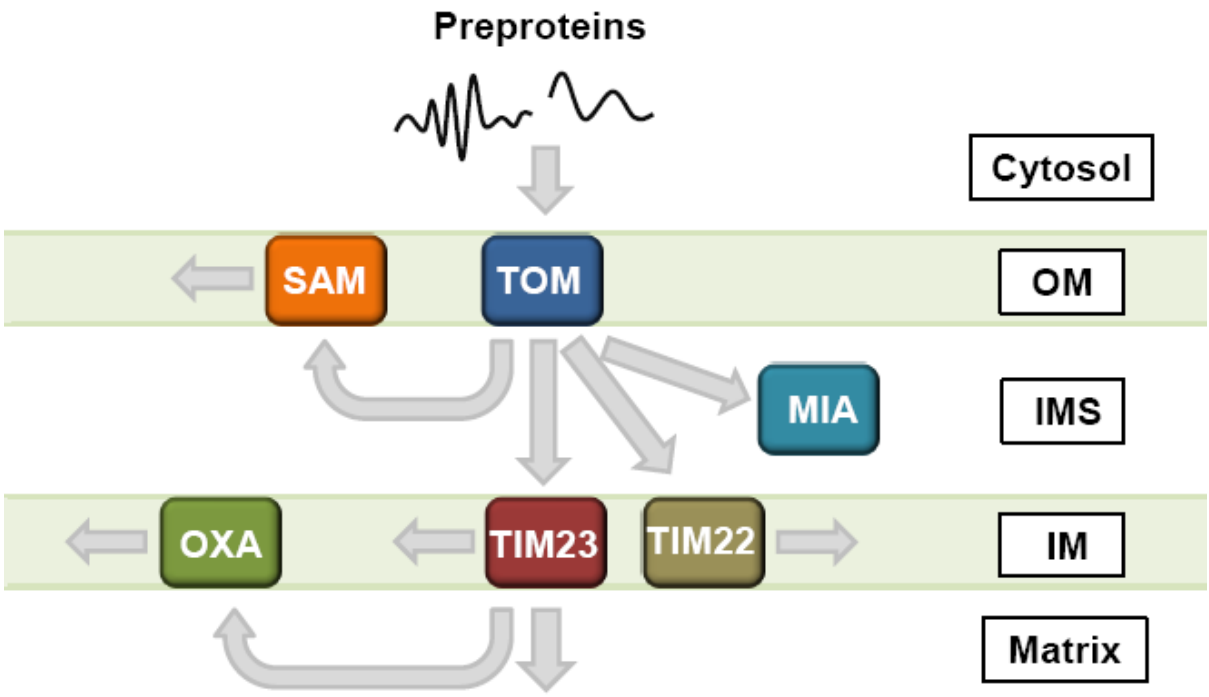

Figure 1.2 Import pathways of mitochondrial proteins.

Preproteins are translocated into the mitochondria through a general entrance known as the translocase of the outer membrane (TOM complex). Subsequently, the preproteins are sorted into different mitochondrial subcompartments using different pathways. SAM, sorting and assembly machinery for β-barrel OM proteins; MIA, mitochondrial import and assembly machinery for cysteine-rich IMS proteins; TIM23 complex, translocase of the inner membrane for presequence-containing IM and matrix proteins; TIM22 complex, translocase of the inner membrane for multiple-transmembrane IM proteins; OXA complex, cytochrome oxidase activity insertase for IM proteins that are initially translocated into the matrix. Figure adapted from Chacinska et al. (2009).

1.1.1 Matrix proteins

A vast majority of mitochondrial proteins are harboured in the matrix. Typically, matrix proteins contain cleavable N-terminal presequences with varying length from 10 to 80 amino acids (von Heijne, 1986). These presequences are mitochondrial targeting signals in the form of amphipathic α-helices containing a hydrophobic and a positively charged site. Biogenesis of matrix proteins, which is known as the presequence pathway can be distinguished into five steps (Figure 1.3) as follow:

Step 1: Binding and channelling across Tom40. The matrix preproteins are translocated in the form of loosely folded linear polypeptide chains led by the N-terminal presequences. The hydrophobic site on the presequence is initially recognised by the hydrophobic groove in the TOM complex receptor Tom20 (Saitoh et al., 2007). The preproteins are subsequently transferred to the central receptor Tom22 by binding to the positively charged site on the presequence, and then to Tom40 channel with the help of Tom5 (Yamano et al., 2008, Moberg et al., 2004, Esaki et al., 2004).

Step 2: Serial binding to IMS binding sites. Following channelling across the OM, the preproteins interact with a series of IMS binding sites of the TOM complex: Tom7 and the IMS domains of Tom22 and Tom40 (Esaki et al., 2003, Bolliger et al., 1995). This serial chain of presequence binding sites with increasing binding affinity, which pull the preproteins across the OM, continues with the components of the translocase of the inner membrane (TIM23 complex), therefore forming the basis of the binding chain hypothesis (Kanamori et al., 1999, Komiya et al., 1998).

Step 3: Transfer to Tim23 channel. The TIM23 complex together with the associated PAM complex in the matrix, are responsible for driving the import of the preproteins across the inner membrane into the matrix. As the preproteins emerge from the TOM complex, Tim50 of the TIM23 complex is the first receptor that interacts directly with the preproteins (Mokranjac et al., 2009, Tamura et al., 2009). This Tim50-preprotein interaction is required to stabilise binding of preproteins to the IMS domain of Tom22. The preproteins are released from Tom22 by a transient Tim21-Tom22 interaction, and subsequently transferred to the Tim23 channel with the help of Tim50 (Geissler et al., 2002, Mokranjac et al., 2003, Yamamoto et al., 2002).

Step 4: Chanelling across Tim23 and binding to PAM complex. The insertion of preproteins into the Tim23 channel requires membrane potential ($\Delta\Psi$) that activates the Tim23 and generates an electrophoretic force on the presequence (van der Laan et al., 2007, Krayl et al., 2007, Shariff et al., 2004). The $\Delta\Psi$-dependent insertion of preproteins is also facilitated by the close association of Tim21 with complexes of the electron transport chain (van der Laan et al., 2006, Wiedemann et al., 2007). However, further import that pulls the preproteins across the Tim23 channel into the matrix requires ATP, and the process is mediated by the presequence translocase-associated motor (PAM) complex. The central subunit of the PAM complex, the molecular chaperone heat shock protein 70 (mtHsp70) associated to Tim44 binds to the preproteins.

Step 5: Translocation into the matrix. The preproteins bound to mtHsp70 are driven into the matrix in a reaction cycle that requires ATP hydrolysis (Ungermann et al., 1996, Ungermann et al., 1994). The activity of mtHsp70 is regulated by the membrane-bound cochaperones Pam16, Pam17 and Pam18 (Kozany et al., 2004, Li et al., 2004, Mokranjac et al., 2006, Hutu et al., 2008). Following ATP hydrolysis, the nucleotide cofactor, Mge1 promotes the release of ADP from mtHSP70, allowing a new cycle of ATP binding and protein translocation (Miao et al., 1997). In the matrix, the presequences are proteolytically cleaved off by the mitochondrial processing peptidase (MPP), and the matrix proteins mature into their active forms (Gakh et al., 2002).

There are two competing models of protein translocation mechanism driven by mtHsp70 (Neupert and Brunner, 2002): 1) the trapping model, where the precursor proteins are trapped in the matrix by binding to mtHsp70, and the inward-directed movement of the preproteins is promoted by additional binding to mtHsp70; and 2) the pulling model, where the partially folded preproteins are stretched by binding to several mtHsp70 molecules, therefore promoting the active pulling into the matrix. However, a number of recent findings that revealed the high complexity of the import motor and the nature of the preprotein folding state during import suggested a combination of both mechanisms (Krayl et al., 2007, Wilcox et al., 2005).

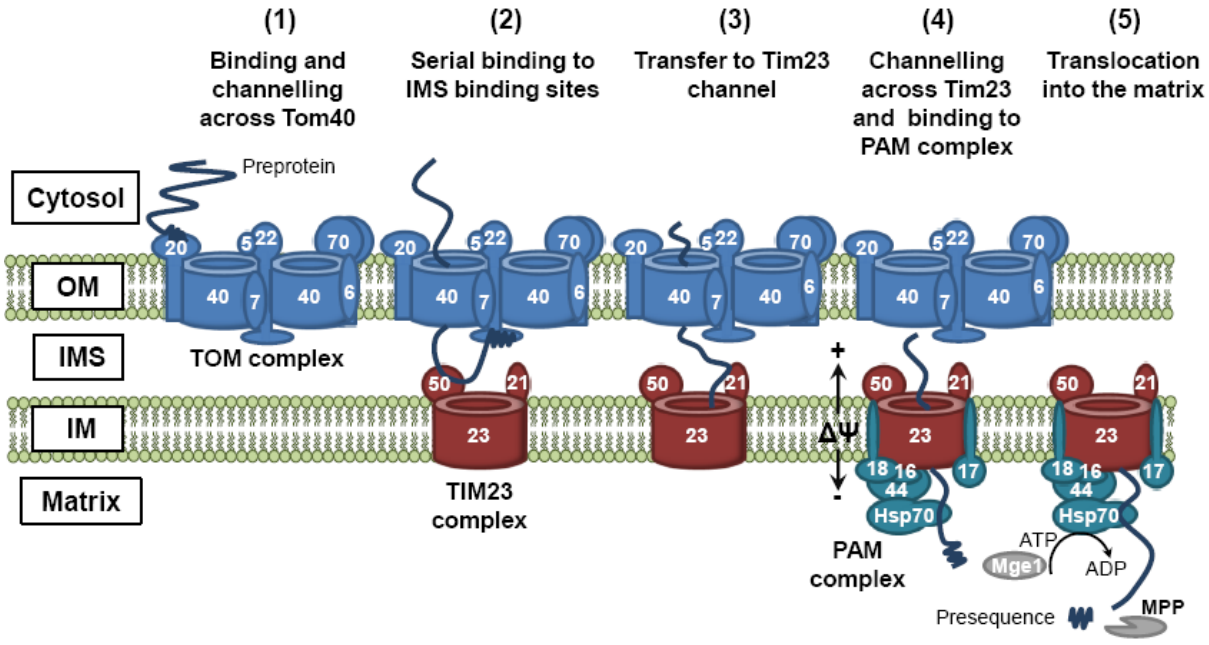

Figure 1.3 Presequence pathway of the matrix proteins.

The matrix preprotein is recognised by receptors Tom20 and Tom22 of the TOM complex and subsequently transferred to the channel-forming Tom40 (step 1). As the preprotein emerges from the TOM complex, it is serially bound to IMS domains of Tom7, Tom22, Tom40 and Tim50 (step 2). The preprotein is released from Tom22 and transferred to Tim23 channel (step 3). In a membrane potential-dependent ($\Delta\Psi$) manner, the preprotein is translocated across Tim23 and subsequently bound to the PAM complex (step 4). The preprotein is translocated into the matrix in a reaction cycle that requires ATP hydrolysis driven by the central unit of the PAM complex, heat shock protein 70 (Hsp70), and followed by proteolytic cleavage of the presequence by mitochondrial processing peptidase (MPP) (step 5).

1.1.2 Inner membrane proteins

Members of the carrier protein family and some membrane anchored subunits of the TIM complexes follow a major pathway that depends on the TIM22 complex for biogenesis. Preproteins of the TIM22-dependent pathway (Figure 1.4) contain non-cleavable multiple transmembrane domains, forming even-numbered modules that contain targeting information (Endres et al., 1999, Wiedemann et al., 2001, Pebay-Peyroula et al., 2003). Among these proteins, the ADP/ATP carrier protein (AAC) is the most widely studied substrate of the TIM22 complex. Biogenesis of AAC can be distinguished into five steps as follow (Pfanner and Neupert, 1987):

Step 1: Transportation by cytosolic targeting factors. Preproteins synthesised in the cytosol are bound by cytosolic chaperones Hsp70 and Hsp90 (Young et al., 2003). This chaperone binding is crucial to prevent aggregation of hydrophobic proteins in the aqueous cytosolic environment.

Step 2: Signal recognition and delivery to TOM complex. At the surface of mitochondria, the preprotein-chaperone complexes are recognised by the receptor Tom70, which contains binding sites for both the chaperones and the preproteins (Wiedemann et al., 2001, Young et al., 2003, Wu and Sha, 2006, Zara et al., 2009). For each precursor binding, as many as three Tom70 receptors are required, probably to prevent protein aggregation (Wiedemann et al., 2001). In an ATP-dependent manner, the preproteins are realeased from Tom70 molecules and the chaperones, into the TOM channel in a hairpin-like conformation such that the internal part of the preproteins move in first, leaving both termini are at the cytosolic surface (Wiedemann et al., 2001).

Step 3: Transportation across the IMS. The hydrophobic transmembrane domains of the preproteins are recognised and bound to the Tim9-Tim10 hexameric complex in the IMS (Vasiljev et al., 2004, Curran et al., 2002), which facilitates the release of the entire preproteins from the TOM channel (Truscott et al., 2002). The N-terminal domains of both Tim9 and Tim10 monomeric subunits in the Tim9-Tim10 complex provide substrate binding sites for the incoming preproteins (Vergnolle et al., 2005, Vergnolle et al., 2007, Baker et al., 2009). It appears that all the three transmembrane modules of AAC contain targeting signals that are important for translocation into the IMS (Endres et al., 1999, Brandner et al., 2005). The Tim9-Tim10 complex chaperones the preprotein across the IMS to the TIM22 complex,

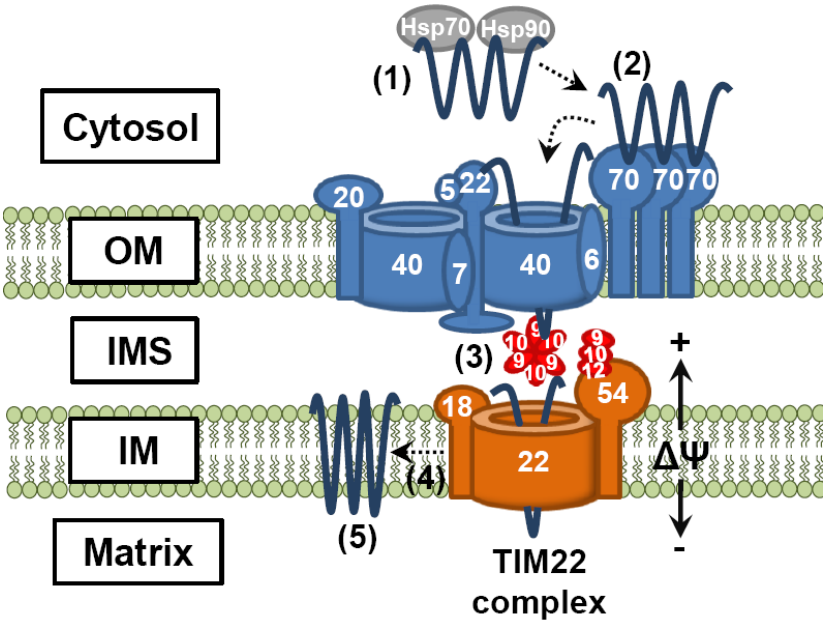

Figure 1.4 TIM22-dependent pathway of inner membrane carrier proteins.

Preproteins of TIM22-dependent pathway contain non-cleavable multiple transmembrane domains that form even-numbered modules. They are transported by cytosolic chaperones Hsp70 and Hsp90 (step 1) to the receptor Tom70 that delivers the preproteins into the TOM channel in a hairpin-like structure (step 2). The preproteins are chaperoned by Tim9-Tim10 complex across the IMS to the TIM22 complex (step 3), and subsequently inserted into the IM in a ΔΨ-dependent manner (step 4), before final assembly into their matured forms (step 5).

where the associated Tim9-Tim10-Tim12 plays a receptor role (Sirrenberg et al., 1998). Release of preprotein from the Tim9-Tim10 complex is probably mediated by Hot13 that reduces the small Tims subunits (Curran et al., 2004). Following release, the transmembrane domains of preproteins bind directly to the N-terminal domain of Tim12 that serves as a substrate sensor (Lionaki et al., 2008).

Step 4: Insertion into the IM. The precursor proteins associated to TIM22 complex are subsequently inserted into the IM in a ΔΨ-dependent manner by an unknown mechanism. Integration into the IM only requires the most C-terminal module (Brandner et al., 2005, Endres et al., 1999). It appears that Tim22 that forms the essential core of the TIM22 complex is important to drive insertion of AAC into the IM, in the absence of the other complex subunits Tim54 and Tim18 (Kovermann et al., 2002). The exact functions of Tim54 and Tim18 are still unclear. It was proposed that the Tim54 that exposes a large domain to the IMS may contribute tethering site for Tim9-Tim10-Tim12 (Wagner et al., 2008, Kerscher et al., 1997), while Tim18 may play a role in the assembly of the TIM22 complex (Wagner et al., 2008).

Step 5: Protein maturation. The preproteins are released from TIM22 complex as monomers (Dyall et al., 2003). Subsequent assembly occurs through dimerisation of incoming monomers with monomeric endogenous AAC (Rehling et al., 2003, Dyall et al., 2003). The conserved cysteine residues of AAC are required for dimerisation process to mature into its native form (Dyall et al., 2003).

In addition to TIM22 pathway, some IM proteins that carry matrix targeting presequences and/or hydrophobic transmembrane segments are imported using different import pathways. This class of IM proteins have a very similar import mechanism to the presequence-containing matrix proteins, which depends on TIM23 complex for biogenesis (Figure 1.5). There are two TIM23-dependent import pathways identified for IM proteins: 1) Conservative sorting pathway and 2) Stop-transfer pathway.

Preproteins of the conservative sorting pathway (Figure 1.5A) carry a matrix targeting presequence followed by multiple transmembrane domains (Hartl et al., 1987, Hartl et al., 1986). Like the matrix proteins, the presequences confer their translocation into the matrix through TIM23 complex in a ΔΨ and ATP-dependent manner. In the matrix, after presequence MPP-cleavage, the preproteins are integrated into the IM in an export-like

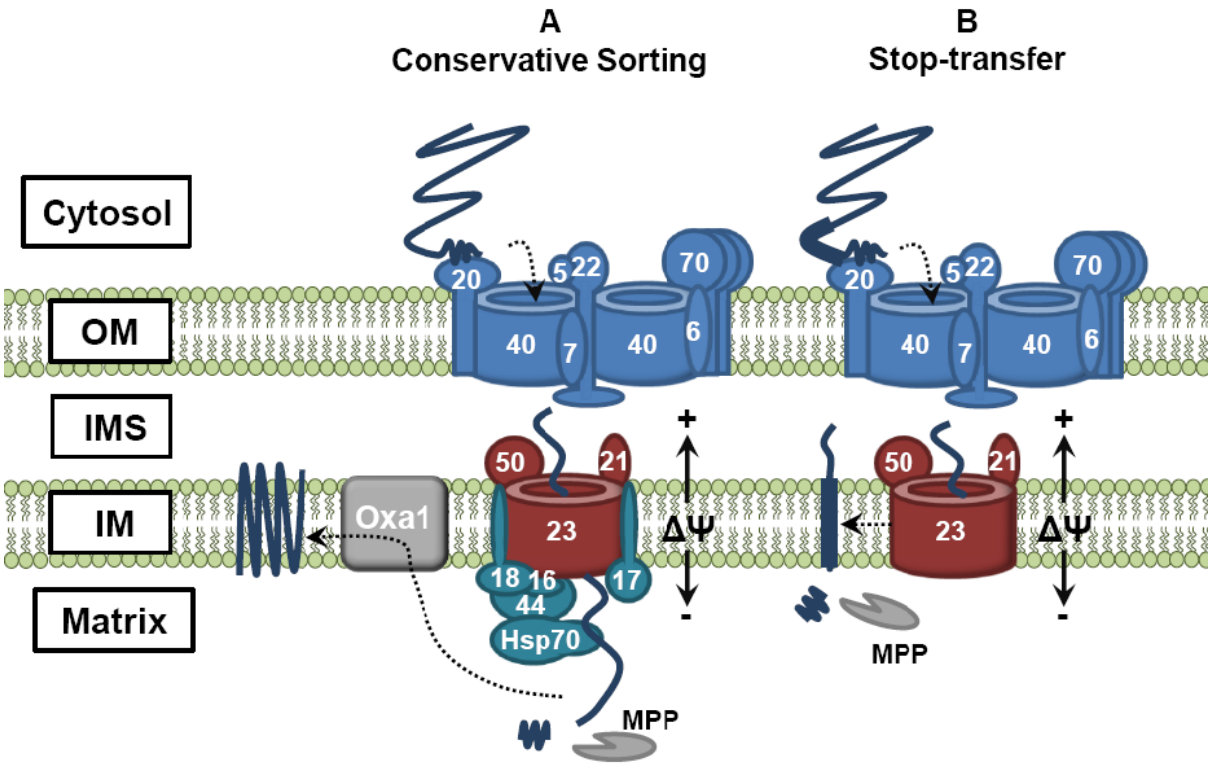

Figure 1.5 TIM23-dependent pathways of inner membrane proteins.

A. Conservative sorting pathway. Preproteins that follow this pathway contain a matrix-targeting presequence followed by multiple transmembrane domains. They are initially translocated into the matrix using the import pathway of matrix proteins (Figure 1.3), followed by insertion into the IM through the Oxa1 complex in an export-like manner.

B. Stop-transfer pathway. Preproteins of this pathway contain a matrix-targeting presequence followed by a hydrophobic domain. They are translocated into the TIM23 complex in the same manner like matrix-targeting proteins, but further translocation into the matrix is stopped by the hydrophobic domain. The presequence is cleaved by MPP in the matrix, and the preproteins are subsequently inserted laterally into the IM.

manner mediated by the Oxa1 complex of the IM, in a process that is driven by ΔΨ (Rojo et al., 1995, Herrmann et al., 1997, Hell et al., 1998). Examples of protein that follow this pathway are Mrs2 and Yta10 (Baumann et al., 2002).

Preproteins that follow the stop-transfer pathway (Figure 1.5B) have a presequence, which targets the preproteins into the mitochondria using the general import pathway of matrix proteins (Glaser et al., 1990, van Loon et al., 1986). The presequence is followed by a hydrophobic transmembrane domain, which is recognised by the TIM23 complex. This signal recognition arrests the preproteins at the TIM23 complex from being further imported into the matrix, hence facilitating their lateral insertion into the IM in a ΔΨ-dependent manner, without requiring the import motor of the PAM complex. The presence of the hydrophobic transmembrane domain itself is not sufficient for translocation arrest which also requires additional clusters of charged amino acid residues at their C-termini (Rojo et al., 1998). The TIM23 complex interacts with these charges to slow down the import process, allowing the transmembrane domain to be inserted laterally into the IM (Meier et al., 2005). In addition, the translocation arrest is also contributed to by the amino acid composition of the transmembrane domain. For arrested preproteins, their transmembrane domain is enriched with tyrosine and phenylalanine residues, and therefore is more hydrophobic than those of conservative sorted proteins (Meier et al., 2005). Proline residues are found to be absent in arrested transmembrane, but are typically present in transferred domain of conservative sorted proteins (Meier et al., 2005). A majority of stop-transferred proteins are inserted into the IM with the N-terminus facing into the matrix and the C-terminus facing the IMS (N_{in}-C_{out} topology) (Jensen and Dunn, 2002). Examples of proteins that follow this import pathway include yeast Mia40 (Naoé et al., 2004), lactate dehydrogenase (Rojo et al., 1998) and Cox5a (Glaser et al., 1990).

1.1.3 Outer membrane proteins

The β-barrel proteins of the OM, such as porin and Tom40 utilise the sorting and assembly (SAM) machinery for biogenesis (Figure 1.6). The precursors of β-barrel proteins contain internal targeting signals that target them to the TOM complex through receptor binding to Tom20 and Tom22, which facilitate their translocation across the Tom40 channel into the IMS (Kutik et al., 2008). In the aqueous IMS, the precursors are chaperoned by the Tim9-

Tim10 and Tim8-Tim13 complexes to the SAM complex, which then mediated their insertion and assembly into the OM (Hoppins and Nargang, 2004, Wiedemann et al., 2003, Wiedemann et al., 2004). The SAM core complex consists of three subunits: 1) Sam50, that forms the channel of the complex (Kozjak et al., 2003, Paschen et al., 2003, Gentle et al., 2004); 2) Sam35, that resides in between Sam50 molecules and serves as a direct receptor for incoming β-barrel preproteins (Kutik et al., 2008); and 3) Sam37, that facilitates the release of preproteins from the SAM complex (Chan and Lithgow, 2008). For β-barrel assembly into the OM, additional factors, such as Mdm10 that forms complexes with several other membrane proteins are required. Mdm10, that was originally proposed to maintain mitochondrial morphology, associates with another two membrane proteins, Mdm12 and Mmm1 (Boldogh et al., 2003). This complex mediates OM assembly of all known β-barrel proteins (Meisinger et al., 2007). For assembly of mature TOM complex however, after Tom40 insertion, sequential assembly of other receptor subunits requires Mdm10 that is in association with SAM complex (Meisinger et al., 2004), together with an additional protein factor Mim1 (Waizenegger et al., 2005). Mim1 is important for later stages of TOM complex assembly (Ishikawa et al., 2004, Waizenegger et al., 2005), and may regulate SAM function by a transient association with SAM complex (Becker et al., 2008). It is clear that the import and assembly of TOM complex involve several highly regulated protein complexes, but the exact biogenesis pathway is still unknown.

In addition to β-barrel proteins, the OM contains α-helical proteins, which are anchored to the OM by hydrophobic α-helical transmembrane domains. The translocation pathway of α-helical proteins varies, depending on the targeting signals and the orientation of protein insertion into the OM. Unlike β-barrel proteins, there is no requirement for α-helical proteins to be imported into the IMS before insertion into the OM. Some α-helical proteins depend on the components of TOM complex, such as Tom20, Tom22 and Tom70 for substrate recognition (Otera et al., 2007, Stojanovski et al., 2007). The factors that facilitate insertion of many α-helical proteins are largely unknown, although some of them seem depend on SAM complex (Stojanovski et al., 2007) and Mim1 (Popov-Celeketić et al., 2008, Becker et al., 2008). The mechanism of α-helical protein biogenesis in general is still poorly understood. Components of the import machineries that direct their integration into the OM are still yet to be identified.

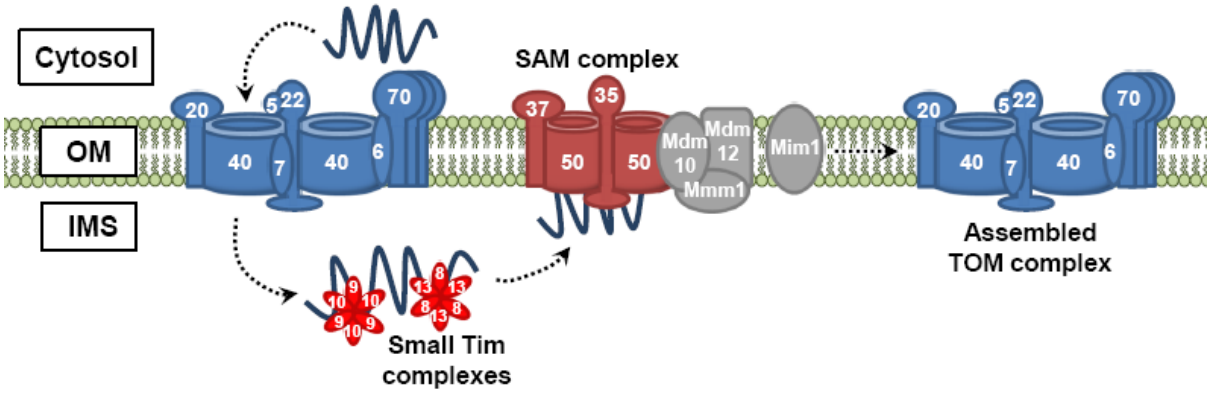

Figure 1.6 SAM-dependent pathway of outer membrane β-barrel proteins.

Preproteins of β-barrels are translocated into the IMS via the TOM complex. They are chaperoned in the IMS by Tim9-Tim10 and Tim8-Tim13 complexes to the SAM complex. The essential subunits of the SAM complex, Sam50 and Sam35 cooperate with the associated Mdm12 and Mmm1 in insertion of preproteins into the OM. Additional factors, Mdm10 and Mim1 are required for assembly of the oligomeric TOM complex.

1.1.4 Intermembrane space proteins

The IMS proteins are among the major components that play essential roles in mitochondrial function and biogenesis. These include electron transport chain components, metabolic enzymes, and transporters of polypeptides, redox equivalents and metal ions. All the IMS proteins are synthesised in the cytosol. Although the functions of many IMS proteins have been studied extensively, relatively little is known about their mitochondrial import mechanisms. The IMS protein import mechanisms can be divided into three categories (Herrmann and Hell, 2005, Neupert and Herrmann, 2007): 1) Bipartite-signal sorting, 2) Affinity binding, and 3) Folding trap.

A group of IMS proteins are characterised by containing a bipartite sorting signal: a typical N-terminal matrix-targeting presequence followed by a hydrophobic sorting sequence. Amongst the most extensively studied proteins that fall within this category are cytochrome b_2 (Glick et al., 1992), Mgm1 (Herlan et al., 2003, Sesaki et al., 2003) and cytochrome c peroxidise (Ccp1) (Esser et al., 2002). An extended list with details of bipartite-signal structures is covered elsewhere (Herrmann and Hell, 2005). The translocation pathway for this group of proteins is very similar to that of stop-transfer pathway used by many IM proteins, in such a way that the preproteins are translocated into the mitochondria in a matrix protein-like manner directed by the presequence, followed by halting at TIM23 channel and lateral insertion of the hydrophobic sorting sequence into the IM lipid bilayer in an N_{in}-C_{out} topology. The matured proteins are subsequently released into the IMS by peptidase cleavage. Typically, the N-terminal presequence exposed to the matrix is removed by MPP, followed by a second cleavage of bipartite sequence at the IM-IMS interface by inner membrane peptidase (Imp1) to release the C-terminal matured protein into the IMS (Gakh et al., 2002, Schneider et al., 1991).

Some IMS proteins are imported by associating to binding sites at the surface of OM or IM. To date, heme lyases are the best studied members within this group (Steiner et al., 1995, Diekert et al., 1999). They do not have presequences and their import is independent of ATP, $\Delta\Psi$ and any of the TIM complexes. Protein folding that is achieved after channelling through the TOM complex does not seem to provide the driving force for protein import (Steiner et al., 1995). It was proposed that a complex pattern of hydrophilic residues in heme lyases might serve as targeting signals recognised by binding sites on the IM (Diekert et al., 1999).

Therefore, it appears that the affinity to binding factors provides the driving force for import reactions across the OM. Some other members, like the creatine kinase have affinity binding sites, both on the OM and IM for protein biogenesis (Adams et al., 1989).

Preproteins that utilise a folding trap mechanism for biogenesis in the IMS are typically small in size (7-22kDa), lack N-terminal presequences and contain conserved patterns of cysteine or histidine residues that enable disulphide bond formation or cofactor binding (Herrmann and Hell, 2005, Herrmann and Kohl, 2007). They are translocated through the TOM complex into the IMS, where they interact with substrate specific factors which function as either receptors that bind transiently to imported preproteins, and/or as folding catalysts that stimulate stable protein folding via cofactor-binding and/or disulfide bond formation. The folded conformation therefore irreversibly traps the protein in the IMS. Instead of having just one general receptor, there are three substrate-specific import factors identified in the IMS so far. The first classical example of a receptor is the IM bound cytochrome c heme lyase (CCHL) which is responsible for biogenesis of cytochrome c (Cyt c) (Diekert et al., 2001, Dumont et al., 1988, Nargang et al., 1988). CCHL binds transiently to the newly imported apo-Cyt c and catalyses the covalent attachment of heme cofactor to the protein, which then matures into its folded, soluble holoform in the IMS. Another example of receptor is the copper chaperone of Sod1 (Ccs1), which is responsible for biogenesis of copper-zinc superoxide dismutase (Cu,Zn-Sod1) (Field et al., 2003, Furukawa et al., 2004). Ccs1 binds to newly imported Sod1 through a transient mixed disulphide bond. Following copper uptake, Sod1 is then released from Ccs1 through formation of an intermolecular disulphide bonded dimer, which retains the protein in the IMS. The mechanism of zinc incorporation into Sod1 is still unclear. The last but most widely used IMS protein import factors are the most recently identified Mia40 (mitochondrial import and assembly) (Naoé et al., 2004) and Erv1 (essential for respiration and vegetative growth) (Lee et al., 2000), which are responsible for biogenesis of many cysteine-containing IMS proteins in a redox-sensitive manner. Mia40 and Erv1 catalyse disulphide bond formation of substrate proteins in the IMS. A detailed mechanism of disulphide formation pathway in the mitochondrial IMS will be reviewed in Section 1.3.

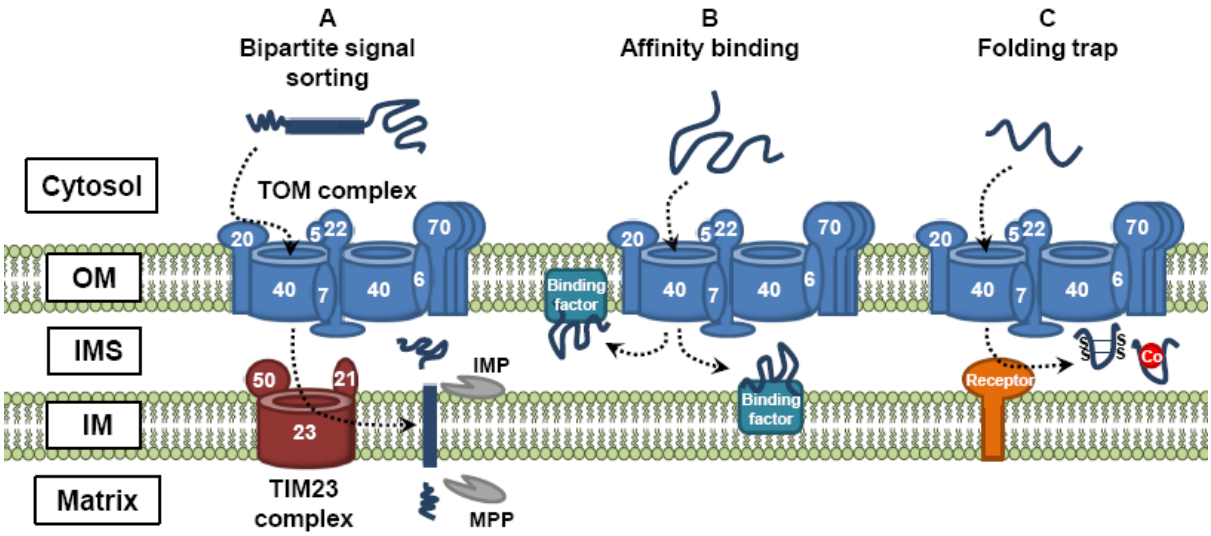

Figure 1.7 Biogenesis of intermembrane space proteins.

A. Bipartite signal sorting mechanism. Preproteins that follow this import mechanism contain a bipartite-sorting signal: a matrix-targeting presequence followed by a transmembrane domain. They are translocated across the TOM channel into the TIM23 complex using the import pathway of matrix proteins. Further translocation into the matrix is stopped by the transmembrane domain, which is then inserted laterally into the IM in a similar manner like the stop-transfer pathway of IM proteins (Figure 1.5B). The matured proteins are subsequently released into the IMS by inner-membrane peptidase (IMP).

B. Affinity binding mechanism. Precursors of some IMS proteins are translocated across the TOM complex into the compartment by permanently associating to binding factors on the OM or IM. The targeting signals for this class of IMS proteins are still poorly understood.

C. Folding trap mechanism. Preproteins that follow this import mechanism are usually small in size and contain conserved patterns of cysteines or histidines. They are translocated across the TOM complex into the IMS by binding to substrate specific receptors. The receptor promotes folding of substrate proteins by disulphide bond formation or cofactor binding, which permanently traps the proteins in the compartment.

1.2 Cellular disulphide bond formation pathways

Proteins achieve their correctly folded structures through a range of chemical interactions, such as van der waals forces, ionic bonds, hydrogen bonds and hydrophobic interactions between their amino acid side chains. An additional covalent interaction in between cysteine residues, known as a disulphide bond is crucial to maintain the three-dimensional structure of proteins. Many proteins of the secretory pathway contain disulphide bonds, which play important roles in a wide array of biological processes, such as in enzyme catalysis (Cappel and Gilbert, 1988), stabilisation of protein folding (Creighton, 1986) and regulation of biological activity (Abate et al., 1990, Staal et al., 1990). The formation of disulphide bonds is a versatile oxidation process. It generates two protons and two electrons (Gilbert, 1995), as shown the following equation:

$$2R\text{-}SH \leftrightarrow R\text{-}S\text{-}S\text{-}R + 2H^{+} + 2\bar{e}$$

In this reaction, the presence of an oxidant is required to accept the electrons produced. To form protein disulphide bonds *in vitro*, dissolved molecular oxygen can act as the oxidant or final electron acceptor, as demonstrated in a classical protein folding experiment using ribonuclease A (Anfinsen, 1973). The kinetics of oxygen association with protein thiols is slow, but it can be accelerated by redox intermediates like flavin or transition metals (Sevier and Kaiser, 2002). The formation of disulphide bonds *in vivo* is enzymatically catalysed by a variety of oxidoreductases, through a series of thiol-disulphide exchange reactions. To initiate a thiol-disulphide exchange reaction (Figure 1.8), a thiolate anion (S^{-}), generated by deprotonation of a free thiol group (SH), nucleophilically attacks the disulphide bond of another molecule. This causes displacement of a sulphur atom in the disulphide bond to form a short-lived mixed disulphide bond, which is then resolved by a second nucleophilic attack by the thiolate anion derived from the remaining thiol group. This results in reduction of the originally oxidised molecule, whist leaving the initially reduced molecule in oxidised form.

In the cell, disulphide bonds are preferably formed in oxidative environments. Therefore, disulphide bond containing proteins are predominately found in extra-cytoplasmic cellular compartments, such as in the perisplasmic space of gram-negative bacteria (Kadokura et al., 2004) and in the endoplasmic reticulum (ER) of eukaryotic cells (Sevier et al., 2007). In addition, the eukaryotic mitochondrial IMS, which was regarded as a continuous

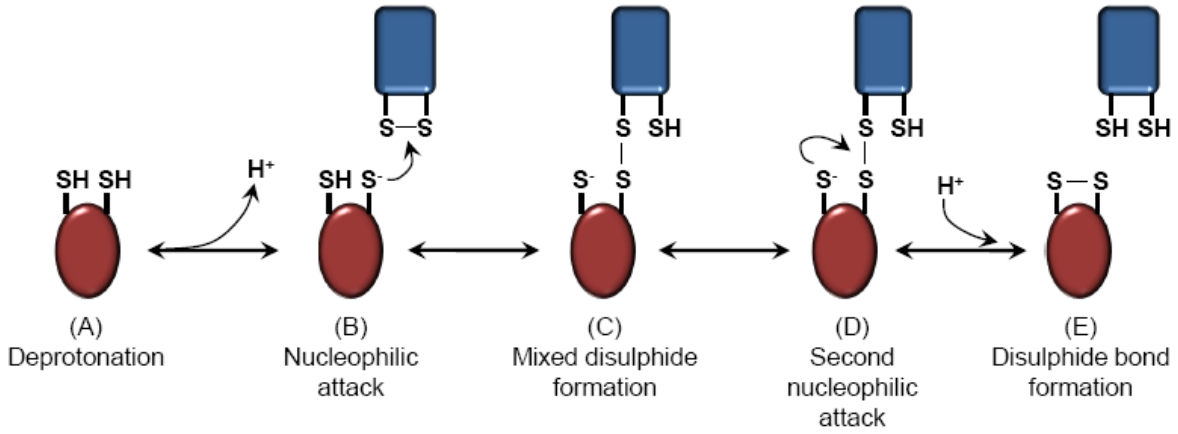

Figure 1.8 Thiol-disulphide exchange reaction.

The first step of a thiol-disulphide exchange reaction involves deprotonation of a thiol group (SH) to generate a thiolate anion (S^-) group. This group nucleophilically attacks disulphide bond of another molecule, leading to the formation of a mixed disulphide intermediate. The production of a second S^- group resolves the mixed disulphide bond by a second nucleophilic attack. As a result, a disulphide bond is formed in the initially reduced molecule. Meanwhile, the initially oxidised molecule becomes reduced.

compartment with a reducing cytosolic environment through the OM porins (Herrmann and Kohl, 2007, Koehler et al., 2006), has also been identified for accommodating protein thiol-disulphide exchange reactions (Mesecke et al., 2005). In agreement with this, a recent study showed that the redox environment in the mitochondrial IMS is actually more oxidising than the cytosol, and is maintained independently (Hu et al., 2008). However, the likelihood of disulphide bond formation is not solely determined by the redox environment, as thiol-disulphide exchange events have been shown to occur in the reducing cytosolic environment (Senkevich et al., 2002).

Although the disulphide bond formation pathways in each cellular compartment are catalysed by different oxidoreductase systems respectively, some parallels can be drawn from each system (Figure 1.9). The acquisition of disulphide bonds within substrate proteins in each compartment is mediated by a chain reaction catalysed by dedicated oxidoreductase systems that drive the transfer of oxidising equivalents. Each system contains a disulphide carrier which directly oxidises the substrate protein. The disulphide carriers are kept in an oxidised state by disulphide generating enzymes, which acquire the ultimate oxidising power from molecular oxygen or components of the respiratory chain as electron acceptors. In the following sections, the principles of thiol-disulphide exchange systems established in the bacterial periplasm, ER and cytosol will be described, as a basis to discuss the mitochondrial IMS oxidoreductase machinery.

1.2.1 Bacterial periplasm

The periplasm of gram-negative bacteria contains a group of oxidoreductases that are important to catalyse disulphide bond formation in proteins secreted into the compartment. These enzymes are known as the Dsb (disulphide bond) proteins. In *Escherichia coli*, these proteins participate in two major pathways: 1) Oxidation pathway, that involves DsbA and DsbB; and 2) Isomerisation pathway, that involves DsbC, DsbD and DsbG.

In the oxidation pathway (Figure 1.10), DsbA functions as the primary donor of disulphide bonds, which directly oxidises newly translocated substrate proteins (Bardwell et al., 1991, Kamitani et al., 1992). DsbA contains a thioredoxin domain, with an active-site disulphide

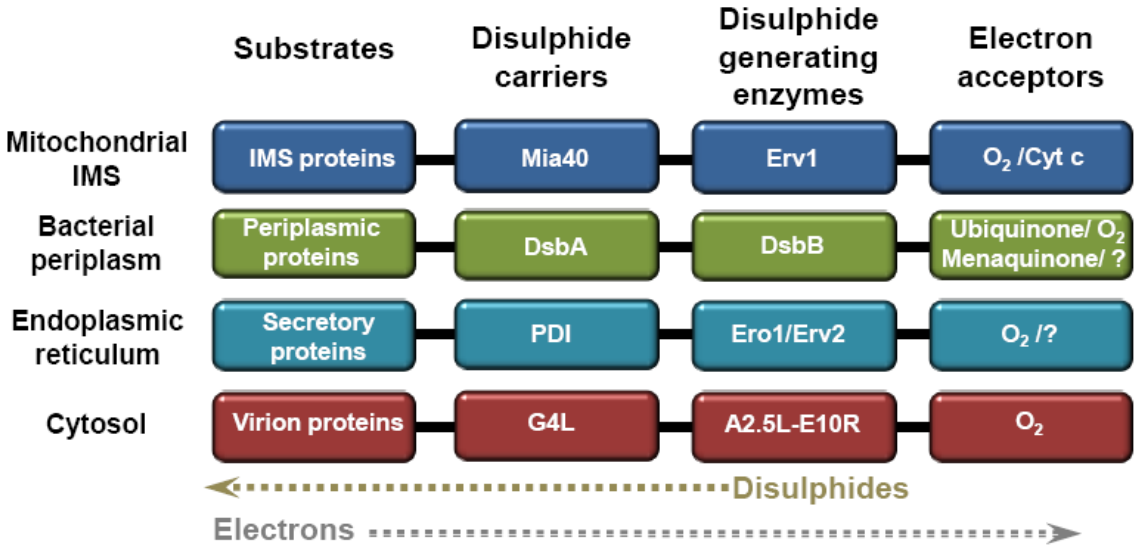

Figure 1.9 Comparison of the protein oxidative folding pathways in the mitochondrial IMS, bacterial periplasm, endoplasmic reticulum and cytosol.

In each system, disulphide bonds are transferred to substrate proteins directly through a disulphide carrier, which in turn is maintained in an oxidised state by a disulphide generating enzyme. The oxidising equivalent of disulphide generating enzymes in each system is derived from molecular oxygen, components of the respiratory chain or unknown factors as the final electron acceptors. The flows of disulphide bond and electron transfer are indicated. Figure adapted from Chacinska et al. (2009).

formed by the cysteine pair Cys30 and Cys33. The Cys30 has a very low pK_a value of 3.5, making it present almost entirely as a thiolate anion at physiological pH (Nelson and Creighton, 1994). Therefore, the active-site disulphide has a very high redox potential (E'_o) of -119mV (Zapun et al., 1993). DsbA has a high tendency to be reduced, due to its strong oxidising properties (Grauschopf et al., 1995). After transferring a disulphide bond to a folding substrate protein, the reduced DsbA is oxidised by the membrane embedded DsbB to allow for another cycle of incoming substrate protein oxidation (Bardwell et al., 1993, Bader et al., 1999). DsbB has four transmembrane helices and two periplasmic loops, each containing a disulphide bond, Cys41-Cys44 and Cys104-Cys130, respectively (Jander et al., 1994). The Cys41-Cys44 disulphide maintains the Cys104-Cys130 disulphide in an oxidised state, which interacts directly with DsbA (Kadokura and Beckwith, 2002, Kishigami and Ito, 1996, Kobayashi and Ito, 1999). It has been shown that DsbA and DsbB interact through formation of a mixed disulphide bond in between the Cys30 of DsbA and Cys104 of DsbB (Inaba et al., 2006, Malojcić et al., 2008). However, Cys104-Cys130 disulphide of DsbB has a much lower redox potential of -224mV (Inaba et al., 2005), which thermodynamically disfavours the electron flow from DsbA to DsbB. A recent work suggests that the uphill transfer of electrons in between the two enzymes is facilitated by conformational changes in DsbB upon DsbA binding, which might also play an important role to ensure unidirectional flow of electrons from DsbA to DsbB (Inaba et al., 2009). After oxidation of DsbA, reduced DsbB has to transfer the electrons from Cys44 to an acceptor for its reoxidation. Under aerobic conditions, reduced DsbB passes electrons to ubiquinone (Q) and then onto cytochrome oxidases *bd* and *bo*, which finally shuttles electrons to molecular oxygen (Bader et al., 1999). Under anaerobic conditions, menaquinone (MQ) receives electrons from DsbB before transferring them to fumarate reductase (Takahashi et al., 2004).

DsbA is not a specific oxidant because it has a broad range of substrates that contain at least two cysteines (Hiniker and Bardwell, 2004). Together with the fact that DsbA is a very powerful oxidant, there is a potential for non-native disulphide bonds to be introduced to newly translocated proteins. Therefore, there is an isomerisation requirement in the bacterial periplasm to prevent protein misfolding and aggregation (Figure 1.11). In *E. coli*, there are two protein disulphide isomerases identified, namely DsbC (Missiakas et al., 1994) and DsbG (Bessette et al., 1999). DsbC has very similar redox properties to those of DsbA, but it is kept in reduced form in the periplasm (Zapun et al., 1995), unlike DsbA that is found in an

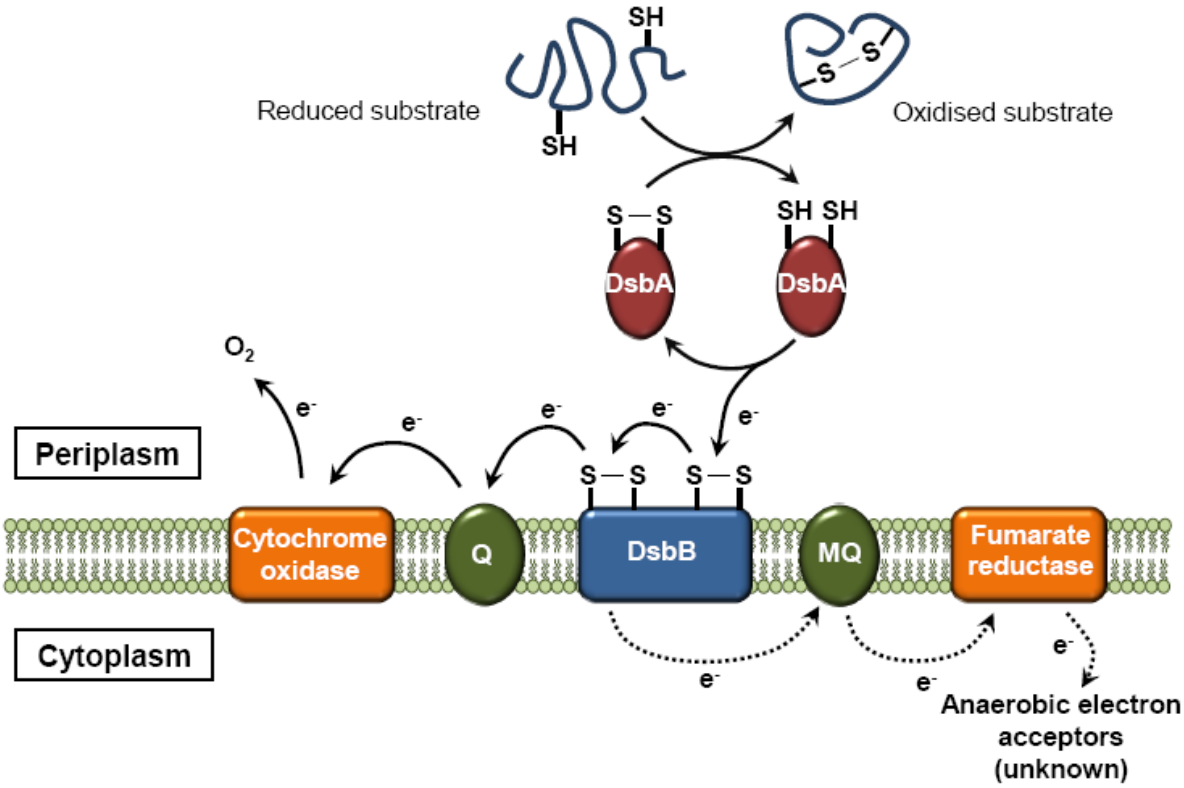

Figure 1.10 Oxidation pathway in the bacterial periplasm.

Reduced periplasm proteins are directly oxidised by DsbA. After transferring each disulphide bond to substrate protein, DsbA becomes reduced. The reduced DsbA is maintained in an oxidised form by the membrane-anchored DsbB. Under aerobic condition, after oxidation of DsbA, reduced DsbB is reoxidised by transferring electrons to ubiquinone (Q) and then onto cytochrome oxidases *bd* and *bo*, which finally transfer the electrons to molecular oxygen. Under anaerobic conditions, the electrons are transferred from reduced DsbB to menaquinone (MQ) and then onto fumarate reductase, which finally transfers the electrons to unknown alternative terminal electron acceptors.

oxidised form. The reduced DsbC functions as an isomerase by nucleophilically attacking and subsequently rearranging non-native disulphide bonds in substrate proteins. DsbC is also found in a dimeric form, which might be crucial for its isomerisation function (Sun and Wang, 2000). More importantly, the dimeric structure of DsbC also prevents oxidation of the protein by DsbB (Inaba et al., 2006, Bader et al., 2001). There is a large kinetic barrier to separate the oxidation pathway from the isomerisation pathway, enabling the organism to accommodate both pathways in the same compartment.

The second protein disulphide isomerase, DsbG is less abundant in the periplasm. The co-existence of two isomerases within the periplasm suggests that both isomerases might have different substrate specificity. DsbG contains negative charged surface that efficiently interact with folded proteins (Heras et al., 2004). Thus, DsbG may be better suited to reducing proteins containing single cysteine or odd-numbered cysteines (Depuydt et al., 2009). DsbC contains an inner surface with hydrophobic residues that may preferably interact with unfolded proteins containing non-native disulphides (Heras et al., 2004). In addition, the structural differences between DsbC and DsbG near the dimer interface may also indicate different functions of the two enzymes (Yeh et al., 2007). Both DsbC and DsbG are maintained in reduced form by the membrane embedded DsbD, which receives electrons from thioredoxin in the cytoplasm (Rietsch et al., 1997, Bessette et al., 1999). The reducing power of cytoplasmic thioredoxin is derived from thioredoxin reductase and reduced nicotiamide adenine dinucleotide phosphate (NADPH) (Rietsch et al., 1997).

1.2.2 Endoplasmic reticulum

The eukaryotic ER harbours a number of oxidoreductase to facilitate the oxidative folding and assembly of secretory proteins. Similar to those in the bacterial periplasm, these enzymes participate in two main pathways: 1) Oxidation pathway, that involves PDI (protein disulphide isomerase), Ero1 (ER oxidase 1) and Erv2 (essential for respiration and viability oxidase 2); and 2) Isomerisation/reduction pathway, that involves GSH (γ-L-glutamyl-L-cysteinyl-glycine) and/or PDI and Ero1.

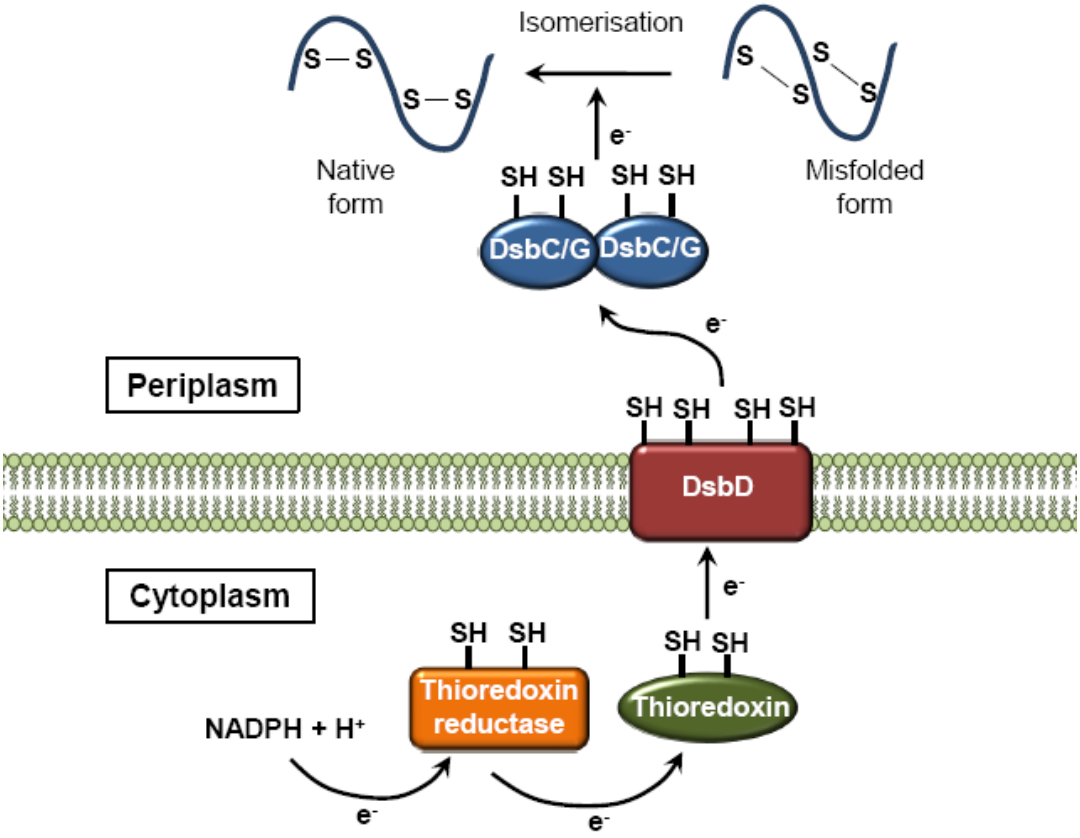

Figure 1.11 Isomerisation pathway in the bacterial periplasm.

The bacterial protein disulphide isomerases DsbC and DsbG in reduced states nucleophilically attack non-native disulphides in misfolded substrates to promote rearrangement of disulphide bonds into correctly folded proteins. Both DsbC and DsbG are maintained in reduced states by the membrane embedded DsbD, which receives electrons from thioredoxin in the cytoplasm. The reducing power of thioredoxin is derived from thioredoxin reductase, which is maintained in a reduced state by the reduced nicotiamide adenine dinucleotide phosphate (NADPH) in the cytoplasm.

PDI is a member of the thioredoxin superfamily that is characterised by the presence of one or more thioredoxin domains, a signal sequence and an ER retention signal (Appenzeller-Herzog and Ellgaard, 2008, Sevier and Kaiser, 2006a). The ER contains a large number of PDI homologues (19 in human and 5 in yeast) that might participate in specialised substrate folding pathways. PDI itself has two catalytic thioredoxin domains (a and a'), each containing an active CXXC motif; and two non-catalytic thioredoxin domains (b and b') lacking the active cysteines (Tian et al., 2006). It is an essential protein for cell viability in yeast (LaMantia et al., 1991) with versatile functions in catalysing protein disulphide bond formation, reduction and isomerisation, depending on the redox environment in the ER lumen and also the nature of substrate proteins (Wilkinson and Gilbert, 2004). The redox functions of the PDI are determined by the active CXXC motifs. Under steady-state conditions, PDI is found in a mixture of both oxidised and reduced forms *in vivo*, with about 70% of the oxidised form in yeast (Xiao et al., 2004). The oxidised PDI is important to catalyse protein disulphide bond formation, whilst reduced PDI is required for protein isomerisation/reduction (Laboissiere et al., 1995, Mezghrani et al., 2001).

Currently, two oxidation pathways of protein disulphide bond formation have been identified in the ER (Figure 1.12). The major pathway involves PDI and Ero1. PDI mediates the direct transfer of disulphide bonds from Ero1 to substrate protein through its peptide binding site at one of the thioredoxin domains, preferentially the a domain with an active-site CXXC disulphide (Mezghrani et al., 2001, Vitu et al., 2010). After transferring disulphide bonds to substrate proteins, the reduced PDI is reoxidised by Ero1 (Frand and Kaiser, 1999). Consistent with this, the Ero1 orthologues of yeast and human have been found forming mixed disulphide intermediates with PDI (Mezghrani et al., 2001, Benham et al., 2000, Tu et al., 2000, Frand and Kaiser, 1999). Therefore, PDI and Ero1 play equivalent roles as DsbA and DsbB of the bacterial periplasm respectively (Section 1.2.1). Ero1 interacts with reduced PDI through its CX_4C shuttle disulphide located in an unfolded polypeptide loop (Gross et al., 2004). After donating a disulphide bond to PDI, the reduced shuttle disulphide is reoxidised by transferring electrons to the active-site CXXC disulphide located adjacent to the isoalloxazine moiety of the flavin adenine dinucleotide (FAD) cofactor (Frand and Kaiser, 2000, Sevier and Kaiser, 2006b). The reduced active-site disulphide is maintained in an oxidised state by transferring the reducing equivalent via the bound FAD to molecular oxygen (Tu and Weissman, 2002). Under anaerobic condition, Ero1 can also be reoxidised by

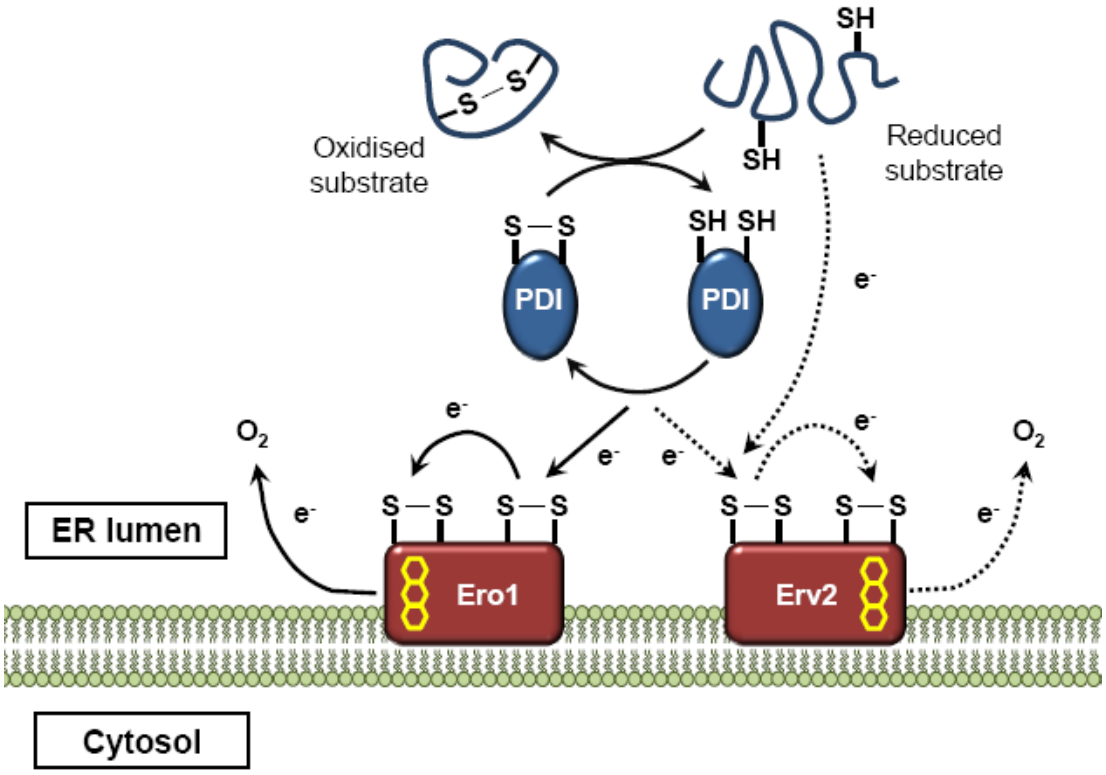

Figure 1.12 Oxidation pathway in the endoplasmic reticulum.

Reduced proteins in the endoplasmic reticulum (ER) are directly oxidised by PDI, which itself is maintained in an oxidised state by two parallel pathways. In the first pathway, after transferring each disulphide bond to substrate protein, reduced PDI is reoxidised by the membrane-anchored FAD-dependent oxidase Ero1. Alternatively, reduced PDI is reoxidised by a second membrane-anchored FAD-dependent oxidase Erv2. Reduced substrate proteins may directly be oxidised by Erv2. In both pathways, molecular oxygen is utilised as the final source of oxidising equivalents.

transferring electrons to unidentified electron acceptors (Sevier et al., 2001).

Besides Ero1, there is another membrane-associated, FAD-dependent oxidase Erv2 (Gross et al., 2002, Sevier et al., 2001, Gerber et al., 2001, Stein and Lisowsky, 1998) that forms the second disulphide bond formation pathway in the ER. Erv2 has been shown to directly catalyse the oxidation of substrate protein *in vitro* (Gerber et al., 2001, Sevier et al., 2001). Hence, it is suggested that Erv2 may possibly oxidise substrates *in vivo* directly, or via the PDI. Unlike Ero1, the Erv2 is not essential for cell viability, but *ERV2* deletion has a moderate effect on protein oxidation in the ER (Sevier et al., 2001). Therefore, Erv2 is possibly a minor disulphide bond formation pathway in the ER compared to Ero1, or is substrate-specific towards a group of unidentified, non-essential proteins.

Protein oxidative folding is sensitive to the redox environment in the ER lumen. Whilst an overly reducing condition in the ER disfavours protein disulphide bond formation (Braakman et al., 1992), a too oxidising condition leads to protein misfolding by formation of non-native disulphide bonds (Marquardt et al., 1993). Therefore, there is a requirement for isomerisation/reduction reactions in the ER to catalyse the rearrangement of wrongly formed disulphide bonds. In the ER isomerisation/reduction pathway (Figure 1.13), GSH serves as a net reductant to counteract the oxidation pathway driven by Ero1 and PDI (Cuozzo and Kaiser, 1999, Molteni et al., 2004). Currently, it is still poorly understood how exactly GSH participates in the ER isomerisation/reduction pathway. A number of recent findings have proposed the roles of GSH participating in two possible mechanisms: 1) direct reduction of misfolded proteins; and 2) redox activity regulation of the ER oxidoreductase.

The cytosol is the source of GSH that is required to modulate the ER protein folding during redox stress (Jessop and Bulleid, 2004, Molteni et al., 2004). To maintain the reducing power required for protein reduction, a continuous flux of GSH from the cytosol into the ER might be necessary, since a pathway to generate GSH in the ER is still unidentified. Consistent with this, a selective transport of GSH over oxidised glutathione (GSSG) has been observed in the ER membrane (Bánhegyi et al., 1999). A higher ratio of GSSG:GSH in the ER compared to the cytosol might also be an indication that GSH is being used for protein reduction, generating a pool of GSSG that is trapped in the ER (Hwang et al., 1992). A direct role of GSH in protein reduction/isomerisation pathway is further confirmed by the finding that a

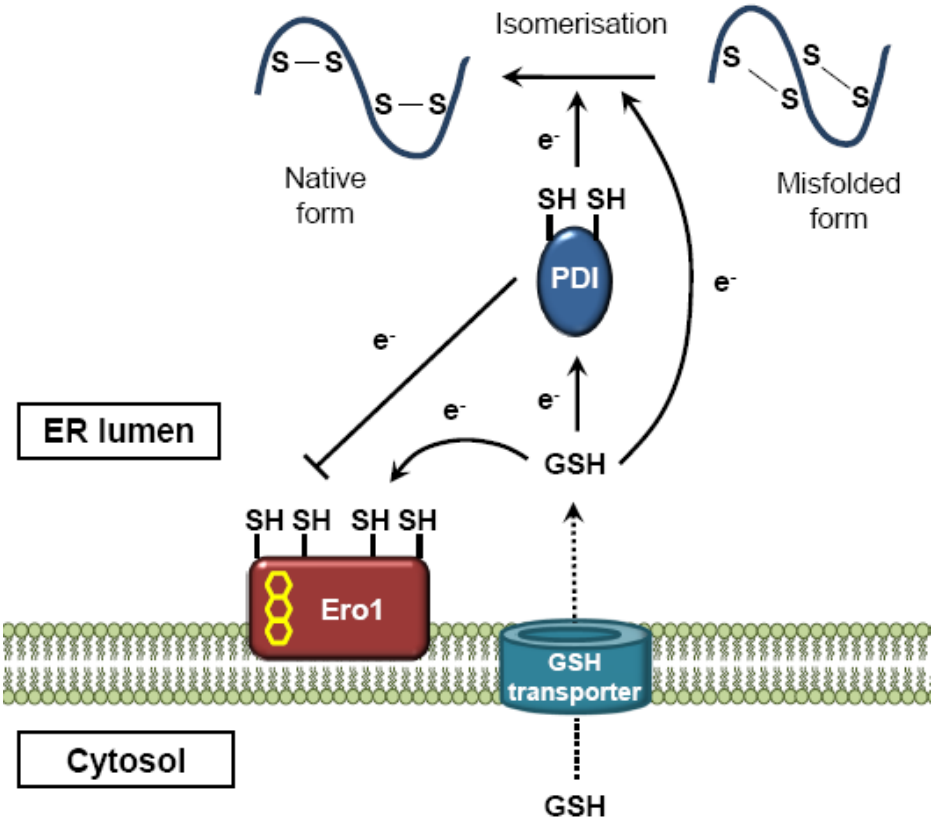

Figure 1.13 Isomerisation pathway in the endoplasmic reticulum.

The net reducing power of the isomerisation pathway in the endoplasmic reticulum (ER) is derived from GSH. The GSH is transported from the cytosol into the ER lumen by an unknown GSH transporter. GSH functions in ER protein isomerisation both directly and indirectly. GSH can directly reduce non-native disulphide bonds in misfolded proteins to allow for rearrangement of disulphide bonds into correctly folded proteins. Alternatively, GSH may regulate the redox states of oxidoreductases in the ER. PDI is kept in a reduced form by GSH to serve as an isomerase. To maintain PDI in reduced form to enable the enzyme to continuously function as an isomerase, regulatory disulphide of Ero1 is reduced by GSH to inactivate the enzyme from oxidising PDI.

large proportion of the GSH in the ER is associated with proteins in mixed-disulphide intermediates (Bass et al., 2004).

The redox reaction (oxidation, reduction or isomerisation) catalysed by an oxidoreductase is governed by the redox state of their redox-active disulphides. Therefore, maintaining the oxidoreductases in reduced form is required to enable their function in the ER isomerisation/reduction pathway. This can be achieved by using the reducing power of GSH. In agreement with this, the human PDI family member, ERp57 that is important in quality control of newly synthesised glycoprotein is unable to resume to its reduced state after oxidative stress in GSH-depleted cells, suggesting a role for GSH in direct reduction of ERp57 (Jessop and Bulleid, 2004). Therefore, a difference between the eukaryotic and the prokaryotic isomerisation/reduction pathway is the use of small molecule GSH in the eukaryotic system, rather than oxidoreductases in the prokaryotic system (Section 1.2.1) as the carrier of reducing equivalents.

In addition, GSH has also been proposed for having an indirect role in regulating the PDI redox activity by feedback regulation of Ero1 (Molteni et al., 2004, Gross et al., 2004). The yeast Ero1 contains two regulatory disulphides, Cys90-Cys349 and Cys150-Cys295 that control Ero1 activity by limiting the motion of its flexible loop containing the shuttle disulphide (Sevier et al., 2007, Appenzeller-Herzog et al., 2008, Baker et al., 2008, Inaba et al., 2010). The oxidase function of Ero1 is activated by a sequential reduction of Cys150-Cys295 by an unknown GSH-independent factor, followed by reduction of Cys90-Cys349 by GSH or a GSH-dependent redox-active enzyme (Sevier et al., 2007, Appenzeller-Herzog et al., 2008). This multiple-factor-dependent regulation of Ero1 activity is important to ensure that Ero1 is only activated under defined ER redox conditions, therefore avoiding undesirable oxidation of reductases or isomerases in the ER, which are required to be in reduced form to calalyse reduction/isomerisation of misfolded proteins. When Ero1 is inactivated, more reduced PDI is available as a reductase or isomerase to catalyse the reshuffling of non-native disulphide bonds of misfolded proteins (Mezghrani et al., 2001); and also the unfolding, dislocation and degradation of irreparably misfolded proteins during oxidative stress (Tsai et al., 2001, Fagioli et al., 2001). Therefore, by regulation of Ero1 to control the PDI activity, only a single oxidoreductase is required in both oxidation and reduction/isomerisation pathways in the eukaryotic ER, as opposed to the distinct oxidation (DsbA-DsbB) and

reduction (DsbC/G-DsbD) pathways in the prokaryotic periplasm that are separated by kinetic barriers (Section 1.2.1).

1.2.3 Cytosol

It is generally assumed that the reducing environment in the cytosol disfavours disulphide bond formation. However, discoveries of some intracellular mature vaccinia virion components containing stable disulphide bonds (Locker and Griffiths, 1999) prove that protein oxidative folding can also occur in the cytosol. Vaccinia virus contains three oxidoreductases, known as G4L, E10R, and A2.5L that participate in disulphide bond formation of virion membrane proteins (Figure 1.14) (Senkevich et al., 2000, Senkevich et al., 2002, White et al., 2002). G4L is a vaccinia virus thioredoxin homolog that has thiol transferase activity (Gvakharia et al., 1996) required for formation of disulphide bonds in two virion membrane proteins, L1R and F9L, and the subsequent assembly of vaccinia virions (White et al., 2000, White et al., 2002). E10R belongs to the eukaryotic ERV/ALR protein family, which contains a conserved CXXC motif and a FAD-binding domain (Senkevich et al., 2000). Therefore, it is likely that E10R utilises molecular oxygen as a final electron acceptor, like the other member of the protein family Erv2 (Gross et al., 2002, Sevier et al., 2001). G4L and E10R interact through a small α-helical protein containing a CXXXC motif, called A2.5L which forms a stable disulphide-linked heterodimer with E10R and a transient mixed disulphide intermediate with G4L (Senkevich et al., 2002). Therefore, E10R and A2.5L can be regarded as a unit that is functionally homologous to the prokaryotic DsbB and the eukaryotic Ero1/Erv2, whilst G4L fulfils a similar role to the prokaryotic DsbA and the eukaryotic PDI.

1.3 Disulphide bond formation pathway of the mitochondrial intermembrane space

The mitochondrial IMS was normally regarded as a compartment with similar redox properties to that of the cytosol because they are connected by porins in the OM that allow free passage of small molecules. Before the discovery that the mitochondrial IMS is more oxidising than the cytosol (Hu et al., 2008), it was a surprise when the IMS was found harbouring cysteine-rich proteins that form disulphide bonds like those in the bacterial

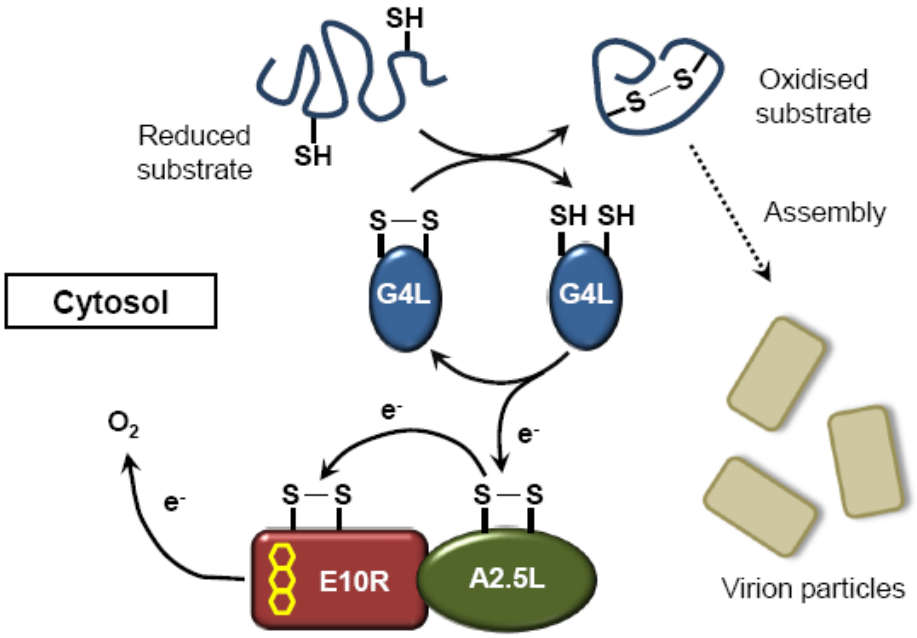

Figure 1.14 Oxidation pathway of vaccinia virion proteins in the cytosol.

The poxvirus membrane proteins L1R and F9L are directly oxidised by G4L. The reduced G4L, after catalysing each cycle of disulphide bond formation in substrate proteins, is kept in an oxidised state by the small α-helical protein A2.5L, which is covalently associated to the FAD-dependent oxidase E10R. The oxidising equivalent of A2.5L is ultimately derived from molecular oxygen through E10R

periplasm and the ER. The IMS protein disulphide bond formation pathway, which is also known as the MIA (mitochondrial import and assembly) pathway consists of two major components: the redox-sensitive import receptor Mia40 (Naoé et al., 2004) and the FAD-dependent sulphydryl oxidase Erv1 (Lee et al., 2000). These proteins constitute the MIA machinery that is essential for import and oxidative folding of cysteine-containing proteins in the mitochondrial IMS (Herrmann and Kohl, 2007, Stojanovski et al., 2007). In the following sections, an overview of the MIA pathway will be discussed, followed by a detailed review of components of the MIA pathway. In particular, the structural and functional properties of MIA substrates, Mia40 and Erv1 will be discussed as a basis to understand the mechanism of MIA pathway in further detail, including the downstream electron transfer pathways.

1.3.1 The MIA pathway: An overview

There are currently two competing models of disulphide bond formation pathway in the IMS. The first model suggests a disulphide relay system (Mesecke et al., 2005) that introduces disulphide bonds to substrate proteins through a serial thiol-disulphide exchange reactions between substrate protein, Mia40 and Erv1; while the second model suggests that the introduction of disulphide bonds in substrate proteins is mediated by multiple thiol-disulphide reactions through a ternary complex of substrate protein, Mia40 and Erv1 (Stojanovski et al., 2008a).

The disulphide relay system model consists of four steps (Figure 1.15):

Step 1: Import and substrate recognition by Mia40. Precursor proteins are imported in a reduced form into the IMS, where they directly interact with the oxidised Mia40 to form mixed disulphide bonds (Chacinska et al., 2004, Mesecke et al., 2005, Müller et al., 2008). It appears that only the oxidised form of Mia40 is able to form mixed disulphide intermediates, but not the reduced Mia40.

Step 2: Oxidation of substrate protein. The interaction of substrate protein with Mia40 leads to transfer of disulphide bonds from Mia40 to substrate proteins, which are subsequently released in oxidised forms in the IMS.

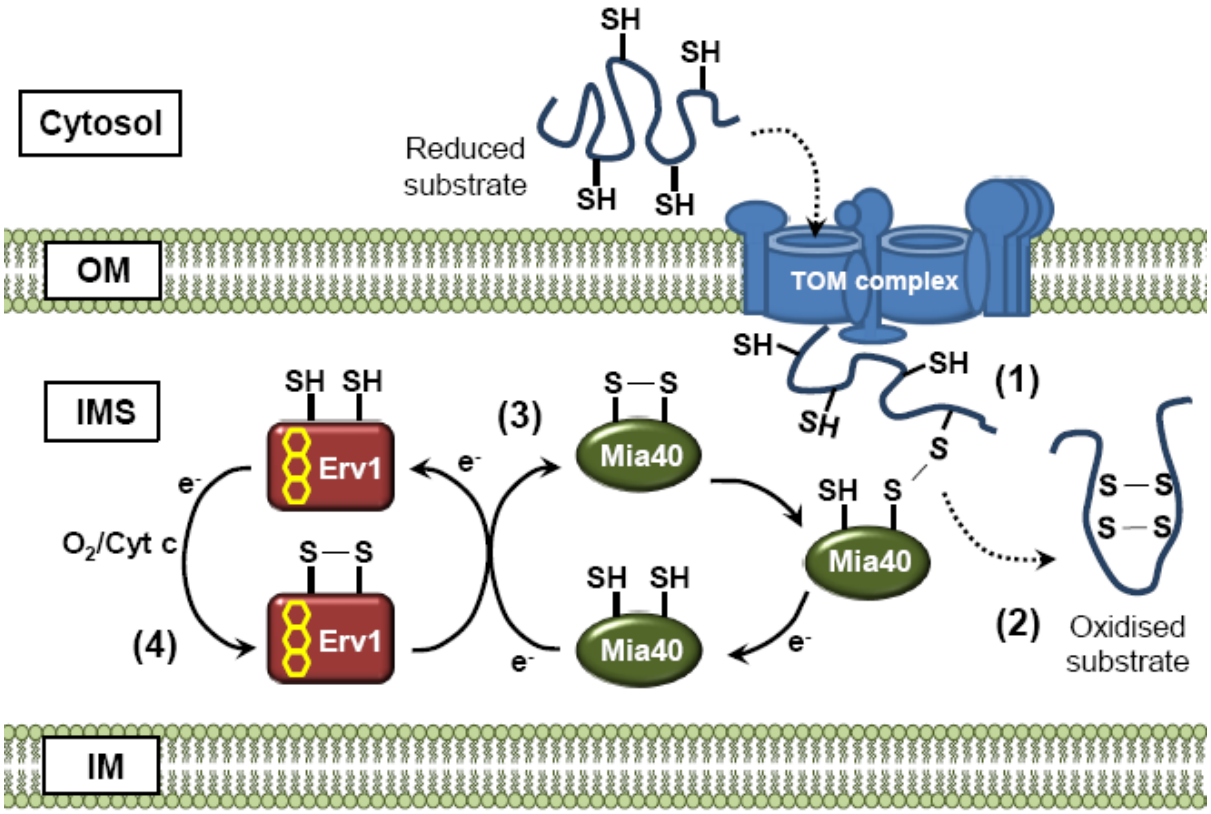

Figure 1.15 The first model of MIA pathway: A disulphide relay system.

Preproteins are translocated from the cytosol into the mitochondrial IMS in a reduced state. Upon channelling through the TOM complex, the reduced preproteins are recognised by Mia40 through formation of a mixed disulphide intermediate (step 1). Disulphide bond formation of substrate protein is catalysed by Mia40, which in turn becomes reduced after donating each disulphide bond (step 2). Reduced Mia40 is reoxidised by Erv1 to allow for another cycle of substrate oxidation (step 3). Erv1 is maintained in an oxidised state by molecular oxygen or cytochrome c (Cyt c), which are the ultimate source of oxidising equivalents (step 4).

Step 3: Reoxidation of Mia40. After donating disulphide bonds to substrate proteins, Mia40 becomes reduced, which is then reoxidised by Erv1 to allow Mia40 for another reaction cycle with newly imported substrate proteins. This is supported by the observations that in an *erv1* conditional mutant of yeast, Mia40 stays in reduced form (Mesecke et al., 2005, Rissler et al., 2005); and that Erv1 interacts with Mia40 via formation of mixed disulphide bonds (Grumbt et al., 2007, Tienson et al., 2009, Lionaki et al., 2010).

Step 4: Reoxidation of Erv1. After catalysing reoxidation of Mia40, Erv1 in turn becomes reduced. Erv1 is then reoxidised by molecular oxygen or Cyt c for another reaction cycle with reduced Mia40 (Daithankar et al., 2009, Tienson et al., 2009, Dabir et al., 2007, Bihlmaier et al., 2007).

Clearly, a series of independent thiol-disulphide exchange events in between the substrate protein, Mia40 and Erv1 are required to promote oxidative folding of substrate proteins. Presumably, the initial thiol-disulphide exchange step occurs in between one molecule of reduced substrate protein and one molecule of oxidised Mia40. In such case, Mia40 can only donate one disulphide bond from the redox-active CPC disulphide (Section 1.3.3) to substrate protein in a single thiol-disulphide exchange event. However, all the substrates of Mia40 studied so far contain at least two disulphide bonds (Section 1.3.2), therefore requiring further thiol-disulphide exchange steps for the same Mia40 molecule to be reoxidised by Erv1 before donating a second disulphide to the partially oxidised substrate protein. In fact, there are a number of observations that contradict with the model of disulphide relay system. Firstly, it is suggested that Erv1, instead of only keeping Mia40 in oxidised state, might be playing another role in the ultimate step of release, oxidative folding and assembly of substrate protein that is bound to Mia40. Rissler et al. (2005) demonstrated that in *erv1* mutant yeast strains, small IMS proteins remained associated with Mia40 and were not assembled into mature oligomeric complexes. This is in agreement with a recent *in organello* study showing that full oxidation of substrate protein requires functional Erv1, and substrate protein oxidation only happens after precursor interaction with Mia40, before final assembly into protein complexes (Müller et al., 2008). In addition, *in vitro* reconstitution assays using purified proteins found that oxidation of reduced substrate protein requires both Mia40 and Erv1, but not Mia40 alone (Grumbt et al., 2007, Tienson et al., 2009). The participation of Erv1 in IMS protein oxidative folding is further clarified by a recent striking finding that successfully trapped a ternary complex of Erv1, Mia40 and substrate protein during the early

stage of IMS protein import into mitochondria (Stojanovski et al., 2008a). This ternary complex might be required to facilitate the transfer of multiple disulphide bonds from Erv1 to substrate proteins containing more than one disulphide bond, through Mia40. Therefore, independent thiol-disulphide exchange events in between Mia40, Erv1 and substrate protein that require multiple collision steps in between molecules, as proposed in the model of disulphide relay system can be avoided. Based on the observation of the ternary complex, a second model of the disulphide bond formation pathway in the mitochondrial IMS is proposed (Figure 1.16).

Besides Mia40 and Erv1, a non-essential IMS protein, called Hot13 (helper of Tim13) has been proposed as the third component of the MIA machinery (Curran et al., 2004, Mesecke et al., 2008). Hot13 contains a highly conserved zinc-finger domain enriched with histidine and cysteine residues. In the absence of Hot13, the steady-state level of small Tim proteins (substrates of the MIA pathway, Section 1.3.2) in the mitochondria is significantly decreased (Curran et al., 2004). Although mitochondria lacking Hot13 are still competent for import of small Tim proteins at a slightly decreased level, the assembly of imported small Tims into complexes is impaired (Curran et al., 2004). These suggest that Hot13 might only be required after substrate binding to Mia40. Consistently, Hot13 has recently been found to play a second role as a zinc chelator in the mitochondrial IMS (Mesecke et al., 2008). Zinc can be bound to both Mia40 (Mesecke et al., 2008) and Erv1 (Morgan et al., 2009), and thus has an overall inhibitory effect to the MIA pathway. Hot13 may facilitate protein oxidative folding in the mitochondrial IMS by counteracting the inhibitory effects of zinc ions (Figure 1.17).

There are some unknown aspects in the MIA pathway. For instance, other possible alternative mechanisms by which Mia40 and Erv1 function. Mia40 has been found absent among members of the protozoan parasite family which contain substrates of the MIA pathway and an Erv1 orthologue, suggesting that the ancestral MIA pathway only requires Erv1 (Allen et al., 2008). Therefore, it is not clear that whether Erv1 can directly oxidise substrate proteins without Mia40 in yeast. There might be some other components required in the MIA machinery for protein oxidative folding. The detailed mechanism of Mia40-Erv1 interaction in biogenesis of cysteine rich IMS precursor proteins is still unclear. Hence, it is necessary to establish *in vitro* assays by using purified proteins to verify the detailed function of Erv1 and Mia40 in their interaction with precursor proteins.

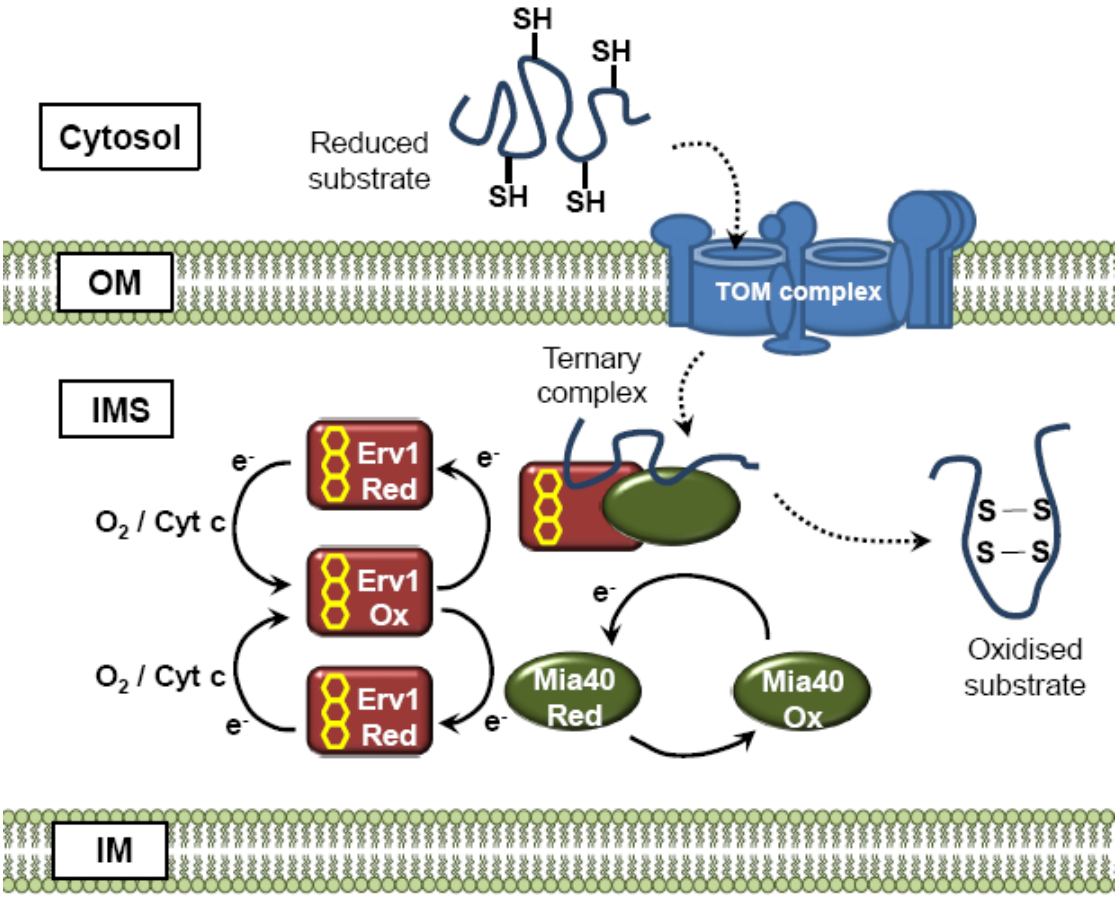

Figure 1.16 The second model of MIA pathway: A ternary complex formation.

The reduced substrate preprotein, following translocation across the TOM channel, forms a ternary complex with both Mia40 and Erv1 in the IMS. This complex formation is crucial to transfer more than one disulphide bond to substrate proteins to promote their full oxidation. Following substrate oxidation, both Mia40 and Erv1 are released in a reduced form. To allow for another cycle of substrate oxidation, the reduced Mia40 and Erv1 are subsequently reoxidised by oxidised Erv1 and oxygen/Cyt c, respectively.

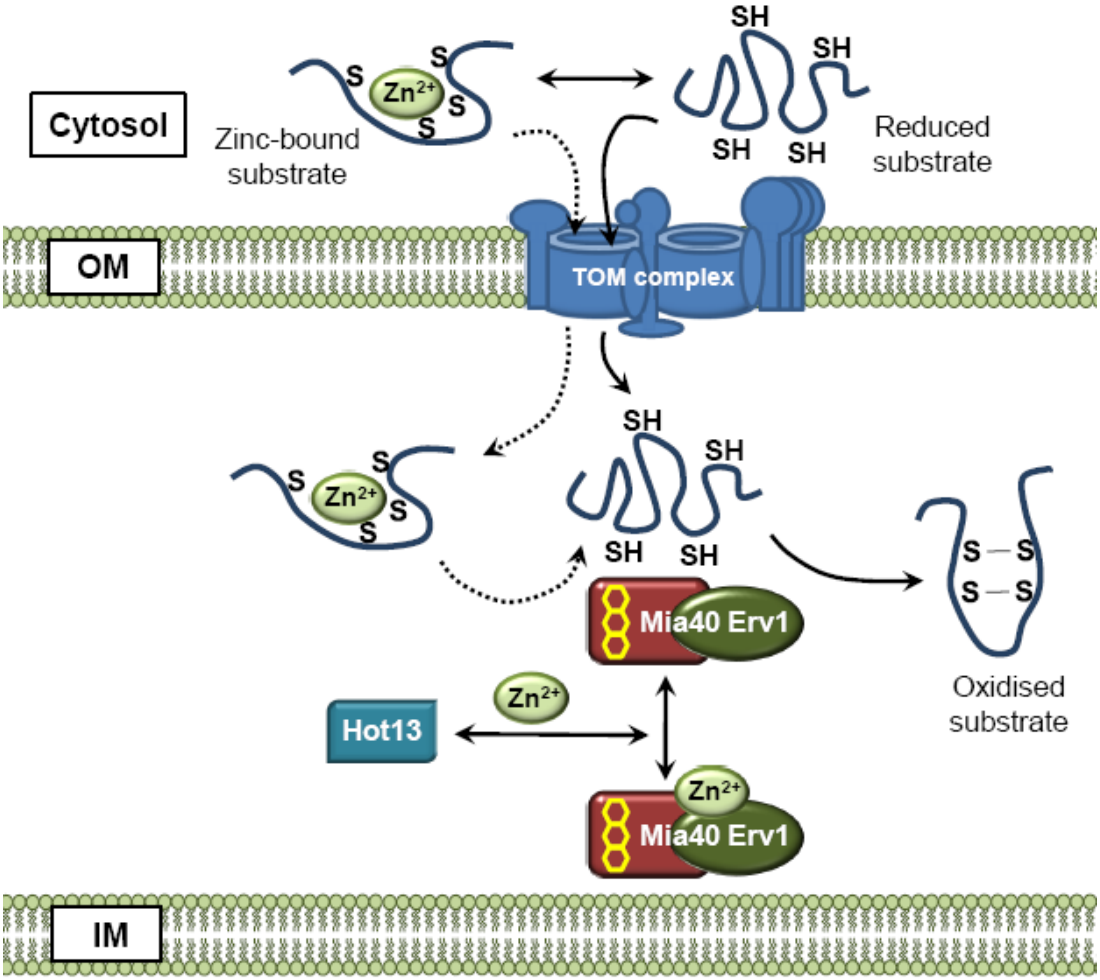

Figure 1.17 The role of Hot13 as a zinc chelator in the MIA pathway.

The zinc-finger small Tim proteins, substrates of the MIA pathway can be imported into the IMS in a fully reduced apo-form or a zinc-bound form. Most of the preproteins are imported into IMS in a fully reduced apo-form (solid arrow), which are subsequently oxidised by the Mia40/Erv1 system. A small fraction of the proteins may be imported into the IMS in a zinc-bound form (dashed arrow), which may inhibit the activity of the Mia40/Erv1 system. The inhibitory effect of zinc is counteracted by Hot13, which functions as a zinc chelator in the MIA pathway.

In contrast to the bacterial periplasm (Section 1.2.1) and eukaryotic ER (1.2.2), there are still no known reduction/isomerisation pathways in the mitochondrial IMS. There is a possibility that reduction/isomerisation pathways are not required in the mitochondrial IMS because most cysteine containing IMS proteins are small, with only one or two disulphide bonds. However, a very recent finding using *in vitro* reconstitution assays suggests that protein oxidative folding in the MIA pathway is also susceptible to form kinetically trapped mixed disulphide intermediates in between Mia40 and substrate proteins (Bien et al., 2010). These non-productive intermediates can be counteracted by physiological concentration of GSH to accelerate the oxidative folding of substrate proteins. Therefore, GSH in the mitochondrial IMS is playing a similar reduction/isomerisation role as in the ER. It is still not known whether GSH has any regulatory effects on the MIA machinery and whether any unidentified oxidoreductase exists in the mitochondrial IMS. To fully verify whether reduction/isomerisation pathways exist in the mitochondrial IMS, it remains to be elucidated whether protein misfolding could occur *in vivo* during protein oxidative folding. There are a few examples of protein reduction in the mitochondrial IMS, which might partly constitute the reduction pathway in the compartment. In the TIM22-dependent pathway of carrier proteins (Section 1.1.2), the translocation arrest of carrier proteins into the mitochondrial IM requires reduction and disassembly of small Tim complex, which might be catalysed by an unknown reductase (Curran et al., 2004). Another example is a flavoprotein known as Cyc2 which participates in the reduction pathway by maintaining the newly imported apo-Cyt c in reduced form to facilitate insertion of its heme cofactor (Bernard et al., 2005).

1.3.2 Substrates of the MIA pathway

Cysteine residues of the IMS proteins are highly conserved and are essential for functionality (Herrmann and Kohl, 2007). They often present as an invariant CXnC motif, where 'X' denotes any amino acids other than cysteine, and 'n' denotes the number of amino acids in between the two cysteines. These conserved cysteine motifs are important for translocation into the mitochondrial IMS following a disulphide bond formation route. The substrates of the MIA pathway are typically small in molecular weight. To date, there are mainly two different classes of identified substrates in the MIA pathway that differ in their characteristic cysteine signatures: the twin CX_3C motif and the twin CX_9C motif (Endo et al., 2010, Herrmann and Kohl, 2007).

1.3.2.1 Twin CX_3C motifs

The first group of MIA pathway substrates comprises members of the small Tim proteins (Tim8, Tim9, Tim10, Tim12 and Tim13) (Koehler, 2004). Small Tim proteins are about 10kDa in size, with a helix-loop-helix fold. Each helix contains a twin CX_3C motif, in which the two cysteines are separated by three amino acids. The helices are connected by two parallel disulphide bonds formed in between cysteines 1-4 and 2-3. Small Tim proteins assemble in 70kDa heterohexameric complexes of $[Tim9\text{-}Tim10]_3$ and $[Tim8\text{-}Tim13]_3$. Each complex has an α-propeller topology containing flexible helical tentacles that function to chaperone hydrophobic membrane proteins through the hydrophilic IMS (Webb et al., 2006, Baker et al., 2009). In addition, Tim9, Tim10 and Tim12 can form a hetero-oligomeric complex in a 3:2:1 ratio (Adam et al., 1999, Koehler et al., 1998). This complex is associated with the TIM22 complex and functions to mediate the insertion of substrate protein into IM.

There are two requirements for biogenesis of small Tim proteins in the mitochondrial IMS (Lu et al., 2004). Firstly, the proteins have to be in reduced forms in order to be competent for translocation into mitochondria. Secondly, formation of intramolecular disulphide bonds is required to retain the proteins in the IMS. The oxidised forms of small Tim protein monomers are required for subsequent complex formation (Lu et al., 2004). Therefore, the intramolecular interactions between the cysteine residues of small Tims are crucial in protein import, oxidative folding and complex formation. A mutation in the last cysteine in the human homologue of Tim8 causes neurodegenerative disorders in affected individuals due to the failure of Tim8-Tim13 complex formation (Hofmann et al., 2002, Roesch et al., 2002).

All the small Tim proteins contain a conserved twin CX_3C zinc-finger motif that coordinates one zinc ion (Sirrenberg et al., 1998). It has been shown that small Tim proteins can bind zinc ions at a molar ratio of 1:1 *in vitro* with their cysteine in reduced states (Lu et al., 2004, Ivanova et al., 2008). Small Tim proteins that are bound to zinc ions are incompetent for complex formation (Lu et al., 2004). Zinc ions might be playing a role in maintaining the small Tim proteins in a reduced state in order to be import-competent, since oxidative folding inhibits the import of these proteins (Lu and Woodburn, 2005, Morgan and Lu, 2008).

1.3.2.2 Twin CX_9C motifs

The second group of MIA pathway substrates is proteins with CX_9C motif, in which the two cysteines are separated by nine amino acids. The best characterised member in this group is the copper metallochaperone Cox17 that participates in the biogenesis of cytochrome c oxidase (COX) (Banci et al., 2008a, Horng et al., 2004). Cox17 transfers copper to COX through the proteins Cox11 and Sco1. Like the small Tim proteins, Cox17 also has a helix-loop-helix structure (Banci et al., 2008b). The helices are connected by two disulphide bonds formed by juxtaposed cysteines of the twin CX_9C motif, which play a structural role to maintain the protein conformation. Cox17 also contains another two cysteines at the N-terminus which are found in both oxidised and copper-bound states (Banci et al., 2008b). Therefore, it has been proposed that the transfer of copper by Cox17 is regulated by the redox states of this cysteine pair. Besides Cox17, there are several other IMS proteins containing twin CX_9C motif that are involved in COX biogenesis. Among them, only Cox19, Cmc1, Cmc2 and Cmc3 have been experimentally confirmed as substrates of the MIA pathway (Chacinska et al., 2004, Longen et al., 2009). In addition, many other proteins containing twin CX_9C motif with unknown functions have been revealed through bioinformatic searches (Longen et al., 2009). All of them are potential substrates of the MIA pathway, but only a few of them (Cmc4, Mic14 and Mic17) have been confirmed experimentally (Gabriel et al., 2007, Longen et al., 2009).

One of the key components of the MIA machinery, Mia40 also contains the signature twin CX_9C motif. It has been shown that partial mutation of this motif in its human homologue leads to a decreased level of import into the mitochondria, whereas complete mutation of all four cysteine residues in this motif inhibits Mia40 import (Hofmann et al., 2005). Therefore in higher eukaryotes, the twin CX_9C motif is specifically required for import and stability of Mia40 in mitochondria. Interestingly, the IM-anchoring yeast Mia40 has been shown to contain double mitochondrial sorting signals (Chacinska et al., 2008). The full-length yeast Mia40 utilises the N-terminus presequence and the IM-sorting transmembrane domain for translocation into IM through TIM23 complex using the stop-transfer pathway (Section 1.1.2). In the absence of IM-sorting signal, yeast Mia40 alternatively utilises the twin CX_9C motif that follows the MIA pathway for translocation into IMS.

1.3.2.3 Others

Apart from the above-mentioned two classes of proteins, there are some other IMS proteins without twin CX_3C or CX_9C that utilise MIA pathway for protein biogenesis import. Erv1 itself with two CXXC and a $CX_{16}C$ motifs has also been experimentally shown as a substrate of the MIA pathway (Gabriel et al., 2007, Terziyska et al., 2007). These studies have remarkably demonstrated that the MIA pathway has a broader spectrum to transport other cysteine containing proteins independently of the twin CX_3C or CX_9C motifs. However, it is not clear whether the twin CXXC motif of Erv1 is required for translocation into IMS. Terziyska et al. (2007) have demonstrated that the cysteine to serine Erv1 mutants in CXXC motif are able to be imported into mitochondria with unaffected efficiencies as compared to the wild type Erv1. If it is true that Erv1 does not require the CXXC motifs for import, Erv1 might be a MIA-dependent substrate that possibly utilises cysteines of the $CX_{16}C$ motif.

In addition, Ccs1, which was previously thought as the import receptor for Sod1 also depends on the MIA pathway for import into IMS (Reddehase et al., 2009). Ccs1 contains a CXXC and CXC motifs and is currently the largest substrate of the MIA pathway, with a size of 27kDa. This indicates that substrates of the MIA pathway are not only limited to low molecular weight proteins like the small Tims. Both Ccs1 and Sod1 are dually localised in both the cytosol and mitochondrial IMS. Their retention in the mitochondrial IMS significantly depends on the level of Mia40 and Erv1 (Mesecke et al., 2005, Khalimonchuk et al., 2008). Based on the observation that only Ccs1, but not Sod1 has been shown to directly interact with Mia40 by a mixed disulphide bond (Reddehase et al., 2009), together with the fact that Ccs1 is the folding factor for Sod1 (Furukawa et al., 2004), it has been suggested that the disulphide bond in Ccs1 is introduced by the MIA machinery, which is then transferred to newly imported Sod1.

There are some other IMS proteins with disulphide bonds that do not contain twin CX_3C or CX_9C motifs. Some of them contain cysteine residues with similar patterns, such as the CX_9C-$CX_{10}C$ in Cox12 (Arnesano et al., 2005, Tsukihara et al., 1995) that is likely functionally comparable to the twin CX_9C motif. It is still not known whether the disulphide bonds in these proteins are introduced by the MIA machinery, or other unidentified factors in the IMS.

1.3.3 Mia40: The import receptor

Mia40 is an essential protein in yeast (Naoé et al., 2004, Chacinska et al., 2004, Terziyska et al., 2005). It is found ubiquitously in the mitochondrial IMS of fungi and higher eukaryotes. It contains a highly conserved C-terminal domain with six cysteine residues arranged in a CPC and a twin CX_9C motif (Figure 1.18A) (Hofmann et al., 2005, Naoé et al., 2004). Mia40 homologues in fungi and higher eukaryotes are different in length. In fungi, in addition to the conserved C-terminus, Mia40 contains an N-terminal transmembrane domain that is tethered to the IM, with the soluble C-terminus facing the IMS (Naoé et al., 2004, Terziyska et al., 2005). In contrast, Mia40 in higher eukaryotes is shorter and exists as a soluble IMS protein without the N-terminal transmembrane segment (Hofmann et al., 2005). It has been shown that the yeast Mia40 can be functionally replaced by its human homologue (Chacinska et al., 2008), and only the highly conserved C-terminal IMS domain containing the cysteine residues is essential for function (Terziyska et al., 2009). Mia40 forms three disulphide bonds in its oxidised state: one disulphide in between the CPC cysteine pair, and two juxtapositional disulphides connecting the twin CX_9C cysteines in a hairpin structure (Grumbt et al., 2007). The CPC disulphide is redox sensitive, and can be selectively reduced from the two stable disulphides in the twin CX_9C motif; therefore suggesting a catalytic role for the CPC disulphide and a structural role for disulphides formed by the twin CX_9C motif (Grumbt et al., 2007, Terziyska et al., 2009).

Even though there are some similarities between the MIA pathway and those of the disulphide bond formation pathways in the bacterial periplasm (Section 1.2.1), eukaryotic ER (Section 1.2.2) and cytosol (Section 1.2.3), Mia40 shares no obvious homology to DsbA, PDI or G4L that function in a similar manner in the respective systems. The functional properties of Mia40 remained largely unknown until the NMR structure of human Mia40 (Banci et al., 2009) and the X-ray crystal structure of yeast Mia40 (Kawano et al., 2009) became available recently. The protein has a fruit dish-like structure that can be divided into two segments: 1) a lid segment containing the redox-active CPC disulphide and several hydrophobic residues that form a shallow hydrophobic cleft; and 2) a core segment containing two helices connected by two parallel disulphide bonds formed in between juxtaposed cysteines of the twin CX_9C motif (Figure 1.18B). The hydrophobic cleft is proposed as a substrate binding domain, as substitution of any hydrophobic residues with charged residues strongly interferes with substrate binding ability of Mia40 (Kawano et al., 2009). The second cysteine of the

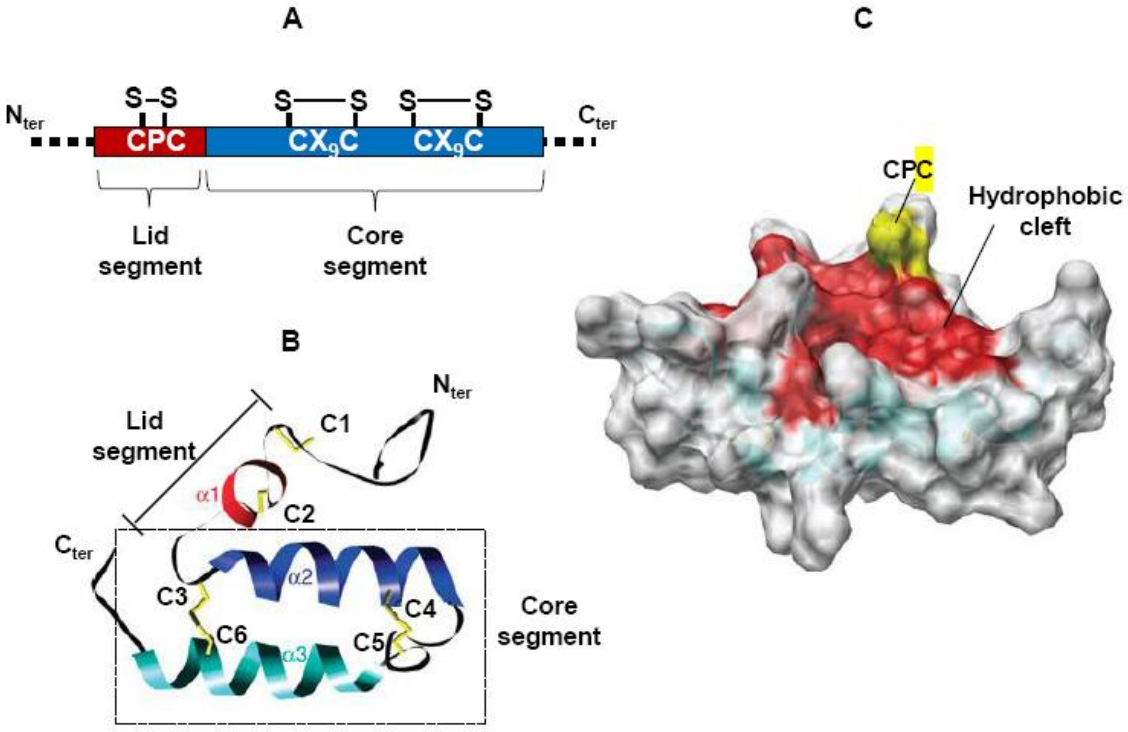

Figure 1.18 The structure of Mia40.

A. The primary structure of Mia40 functional domain. Mia40 contains six cysteine residues that constitute a CPC-CX_9C-CX_9C motif. The functional domain is divided into a lid segment containing the CPC redox-active disulphide, and a core segment containing the structural disulphides formed by the twin CX_9C motif.

B. The ribbon structure of human MIA40 with CPC disulphide in reduced form and both structural disulphides of twin CX_9C motif in oxidised form. Helix α1 of the lid segment is shown in red. Helices α2 and α3 of the core segment are shown in blue and cyan respectively. The cysteine residues are indicated in yellow.

C. Surface representation of MIA40 structure as in (B). The hydrophobic cleft on the surface of MIA40 is indicated in red. The structural core segment is indicated as a ribbon diagram in transparent cyan. The second cysteine of the CPC motif, which is located in close proximity to the hydrophobic cleft, is indicated in yellow. Figure adapted from Banci et al. (2009)

CPC motif is slightly exposed above the hydrophobic cleft (Figure 1.18C), hence further confirming its crucial role in substrate recognition by mixed disulphide formation demonstrated in previous biochemical studies (Terziyska et al., 2009, Tienson et al., 2009).

In addition, it was not clear whether Mia40 generally interacts with any cysteine-rich proteins or specifically recognises proteins translocated into the IMS. This question was clarified by two very recent studies that discovered targeting signals in substrate proteins that are specifically recognised by Mia40 (Milenkovic et al., 2009, Sideris et al., 2009). These signals are known as MISS (mitochondrial IMS sorting signals) or ITS (IMS-targeting signals). MISS/ITS is characterised by a consensus sequence of hydrophobic residues located at the $\pm 3^{rd}$, $\pm 4^{th}$ and $\pm 7^{th}$ positions from the docking cysteine with Mia40 (Figure 1.19). These hydrophobic residues are positioned upstream of the first cysteine in small Tims (Figure 1.19A), but downstream of the third cysteine in human Cox17 (Figure 1.19B). In yeast Cox17 in which the docking cysteine is the fourth one, the hydrophobic residues are positioned upstream of the fourth cysteine. MISS/ITS forms an amphipathic helix with the hydrophobic residues and the docking cysteine located on one side, and charged residues located on the opposite side. The hydrophobic residues are essential for binding to the hydrophobic cleft of Mia40, as substitution of any of them to charged residues inhibits the mixed disulphide bond formation between substrate and Mia40. The charged residues are not essential for binding to Mia40, but they play a cooperative role to maintain the overall conformation of the amphipathic helix. By compiling the structural data of Mia40 together with the discovery of MISS/ITS, a two-step sliding-docking model (Figure 1.20) of the interaction of substrate protein with Mia40 is proposed: 1) the substrate is guided by the MISS/ITS to slide into the hydrophobic cleft of Mia40 through weak non-covalent interactions; followed by 2) docking of the substrate cysteine to the second cysteine of Mia40 CPC to form a mixed disulphide intermediate (Sideris et al., 2009).

Clearly, the docking of substrate cysteine to Mia40 is facilitated by the MISS/ITS. This determines the specificity of substrate recognition by Mia40 and also the correct priming of cysteines in between substrate and Mia40 for covalent interaction. Therefore, the formation of unproductive disulphide bonds is less likely to occur in the mitochondrial IMS, compared to the bacterial periplasm and ER that require isomerisation/reduction pathway to unfold misoxidised proteins. In contrast, a recent study showed that unproductive mixed disulphide intermediates of Mia40 and substrate can be formed *in vitro* (Bien et al., 2010). Therefore, it

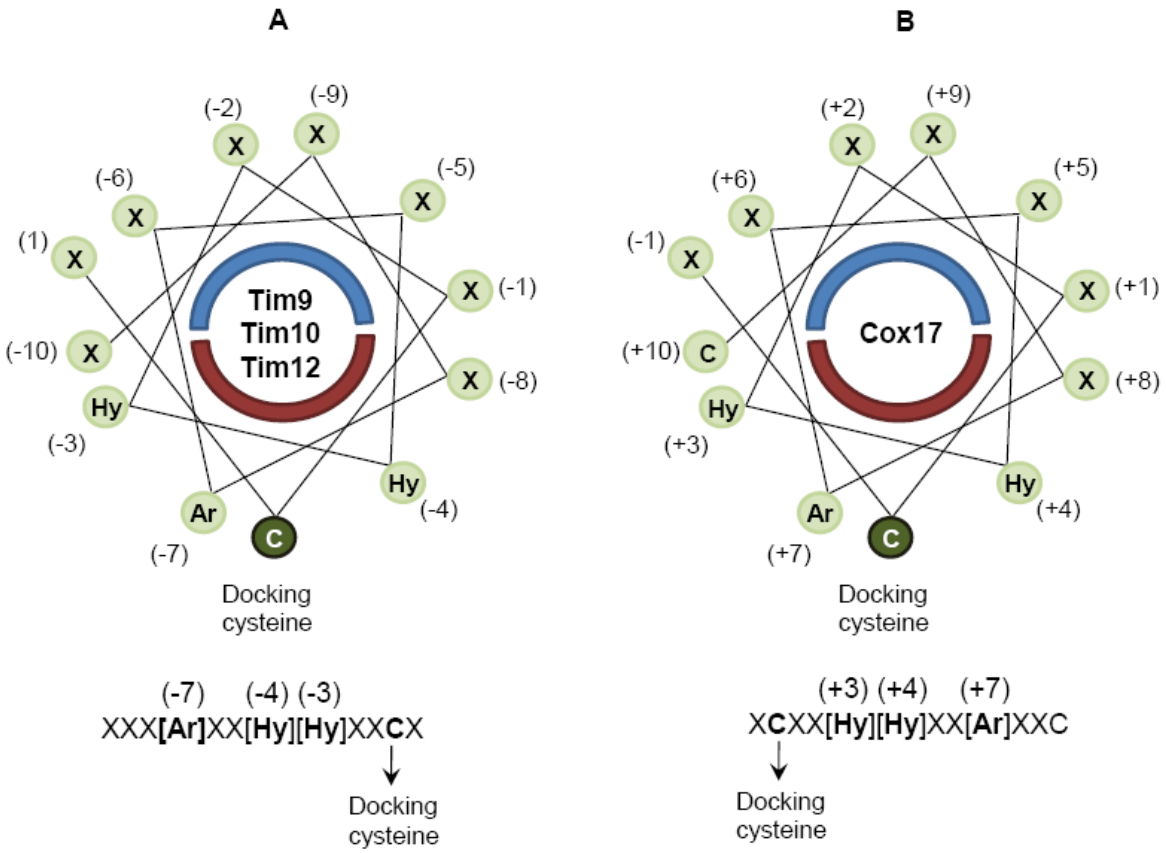

Figure 1.19 Helical wheel representation of MISS/ITS in substrates of the MIA pathway.

A. The MISS/ITS of the yeast Tim9, Tim10 and Tim12 forms an amphipathic α helix with the docking cysteine located next to the aromatic residue at position -7 and two other hydrophobic residues at positions -3 and -4 on the same hydrophobic face (red). The other amino acid residues are positioned at the opposite site as hydrophilic face (blue).

B. The MISS/ITS of human COX17 also forms an amphipathic α helix as in yeast small Tims (A), but the aromatic residue and two other hydrophobic residues are located at positions +7, +4 and +3 from the docking cysteine. Figure adapted from Sideris et al. (2009).

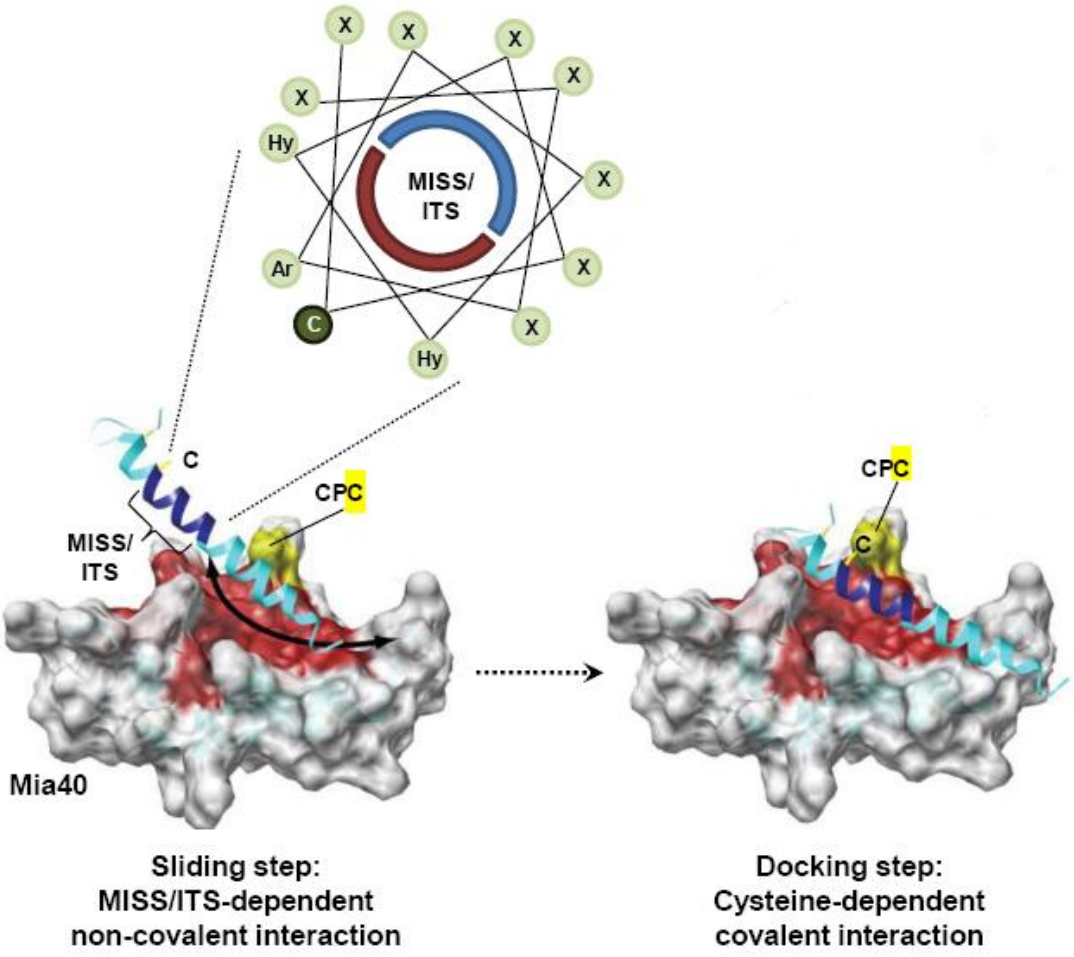

Figure 1.20 The sliding-docking model of substrate binding to Mia40.

The hydrophobic face of MISS/ITS in substrate protein (inset) is oriented to interact non-covalently with hydrophobic residues (red) on the binding cleft of Mia40 (sliding step). The docking cysteine of substrate protein is then primed to the second cysteine of the Mia40 CPC for covalent interaction (docking step). Figure adapted from Sideris et al. (2009).

remains to be investigated whether protein misfolding can occur *in vivo* in the mitochondrial IMS.

1.3.4 Erv1: The FAD-dependent sulphydryl oxidase

Erv1 is the only flavin-dependent sulphydryl oxidase found in the mitochondrial IMS of many eukaryotic cells (Fass, 2008). The enzyme is non-covalently bound to a flavin cofactor FAD which mediates the redox activity of the enzyme. Erv1 has a diverse range of functions in the cell, other than mediating the oxidative folding of IMS proteins in the MIA pathway. Classically, Erv1 has been shown to be essential for respiration and vegetative growth in yeast (Lisowsky, 1992). It can influence the biogenesis of mitochondria in different aspects, such as formation of criatae at the IM and maintenance of mitochondrial genome (Lisowsky, 1994, Lisowsky, 1996, Becher et al., 1999). Erv1 also plays an important role in maintaining the stability and normal morphology of mitochondria in the cell (Becher et al., 1999, Hofhaus et al., 1999). In addition, Erv1 has been identified as a novel factor that is required for cytosolic iron-sulfur (Fe/S) protein maturation, surprisingly not the mitochondrial Fe/S proteins (Lange et al., 2001). Mitochondria play an important role in the biogenesis of cellular Fe/S proteins localised in both the cytosol and in the mitochondria (Craig et al., 1999, Lill et al., 1999, Lill and Kispal, 2000). This organelle contains iron-sulfur cluster (ISC) assembly machinery that is essential for biogenesis of Fe/S proteins within the mitochondria, such as the subunits of complexes I, II and III of the respiratory chain. The ISC assembly machinery is also involved in the maturation of cytosolic Fe/S proteins like Leu1 and Rli1 (Kispal et al., 1999, Kaut et al., 2000, Lange et al., 2000, Li et al., 2001). The only previously identified mitochondrial component with specific function in Fe/S maturation is Atm1 of the IM, which has been proposed to export a component required for Fe/S protein assembly and maturation from the mitochondria (Bekri et al., 2000). Since Erv1 is localised in the IMS, it may operate downstream of Atm1 in the Fe/S protein maturation pathway (Lange et al., 2001). However, the mode of action for Erv1 in maturation of Fe/S proteins outside the mitochondria is still unknown. Clearly, Erv1 has a diverse range of effects in the cell. This has led to the suggestion that Erv1 either interacts with a number of different substrates, or with only one factor of general importance (Herrmann and Kohl, 2007). To date, the only

identified substrate of Erv1 is the Mia40, which can be regarded as a factor of general importance, as it serves as an import receptor for IMS proteins.

One common feature shared among FAD-dependent sulphydryl oxidases is that, the enzymes can catalyse the electron transfer from substrate molecules like protein thiols via the FAD cofactor to molecular oxygen or oxidised Cyt c (Thorpe and Coppock, 2007). Sulphydryl oxidases can be divided into three groups: 1) Ero1 enzymes, 2) quiescin sulphydryl oxidases (QSOX) and 3) ERV/ALR proteins.

The first sulphydryl oxidase, Ero1 is a large multi-helical membrane associated FAD-dependent enzyme found in the ER of yeast and higher eukaryotes. It contains at least five disulphide bonds, with only two of them conserved. The conserved cysteines, which are essential for the enzyme catalytic activity of Ero1, form the active site disulphide CXXC and shuttle disulphide CX_4C (Frand and Kaiser, 2000, Gross et al., 2004). The remaining non-conserved disulphide bonds have been demonstrated recently to play a regulatory role in both yeast and mammalian Ero1 (Sevier et al., 2007, Baker et al., 2008, Appenzeller-Herzog et al., 2008). The redox activity of Ero1 involving both redox active and regulatory disulphides in the ER disulphide bond formation pathway has been discussed earlier in Section 1.2.2.

The second group of sulphydryl oxidase, QSOX is found in diverse intracellular locations including the ER, Golgi apparatus, secretory granules (Tury et al., 2004) and the nuclear and plasma membranes (Wittke et al., 2003). In higher eukaryotes, QSOX is commonly found in secreted fluids, and therefore is proposed to play important physiological functions (Thorpe and Coppock, 2007, Coppock and Thorpe, 2006). Unlike Ero1, the multi-domain QSOX consists of one or more N-terminal thioredoxin-like domains containing a CXXC motif fused to an ERV/ALR module containing two CXXC motifs. The presence of thioredoxin-like domains in addition to the ERV/ALR domain has greatly enhanced enzymatic activities of QSOX to perform many important functions of disulphide bond formation in higher eukaryotes (Thorpe et al., 2002). It has been proposed that the CXXC in the thioredoxin domain initially interacts with substrate thiols before transferring electrons to the CXXC motifs and FAD in the ERV/ALR domain (Raje and Thorpe, 2003). However, the roles of these three CXXC motifs in the enzyme function of QSOX are still largely unknown.

Erv1 belongs to the single domain ERV/ALR protein family, which also includes the mammalian homologue of Erv1 known as augmenter of liver regeneration (ALR),

Arabidopsis thaliana Erv1 (AtErv1), and yeast Erv2 of the ER lumen. The ERV/ALR enzymes are characterised by a highly conserved central catalytic core of around 100 amino acids containing a CXXC motif (Cys130-Cys133 for Erv1), a $CX_{16}C$ motif (Cys159-Cys176 for Erv1) and residues required for FAD binding. Based on the partial crystal structure data of rat ALR (Wu et al., 2003), Erv2 (Gross et al., 2002) and AtErv1 (Vitu et al., 2006), the catalytic core of ERV/ALR protein contains a four-helix bundle forming the FAD-binding site with the active site CXXC motif located in close proximity to the isoalloxazine ring of FAD (Figure 1.21A). In addition, the $CX_{16}C$ motif forms a long range disulphide bond that brings the short fifth helix to the four-helix bundle in proximity to the adenine ring of FAD. Thus, the $CX_{16}C$ disulphide bond may play a structural role in stabilising the FAD binding and/or protein folding. However, there is still no direct experimental evidence to verify the roles of $CX_{16}C$ disulphide.

Other than the catalytic core, the other parts of the proteins are non-conserved and seem unstructured. All members of the ERV/ALR family have one additional disulphide bond located in the non-conserved N- or C-terminal region to the catalytic core (Figure 1.21B). This additional disulphide bond is hypothesised as a shuttle disulphide based on the partial crystal structure of Erv2 (Gross et al., 2002). The hypothesised shuttle disulphides of Erv2 CXC and AtErv1 CX_4C are located at the C terminus. On the other hand, Erv1 (Cys30-Cys33) and ALR have a CXXC shuttle disulphide located at the N-terminus to the catalytic core. Furthermore, the spacing and the identity of amino acid residues in between cysteines forming the shuttle disulphide is not conserved among members of the ERV/ALR proteins. In an *in vivo* study using Erv2 as a model (Vala et al., 2005), the enzyme function is unaffected with 1-4 spacing; but is inactive with 0 or 5 amino acids in between the shuttle cysteines. The identity of the amino acid in between the shuttle cysteines does not seem to be crucial for Erv2 function. In addition, the length of the flexible shuttle arm of Erv2 is found to be important for enzyme activity in substrate recognition.

An oxygen channel has been observed in some of the members of ERV/ALR proteins. The structures of Erv2 (Gross et al., 2002) and AtErv1(Vitu et al., 2006), poss a short hydrophobic channel on the protein surface leading to the N5 nitrogen of isoalloxazine ring. This channel is proposed to be the route for molecular oxygen to reach the FAD redox centre.

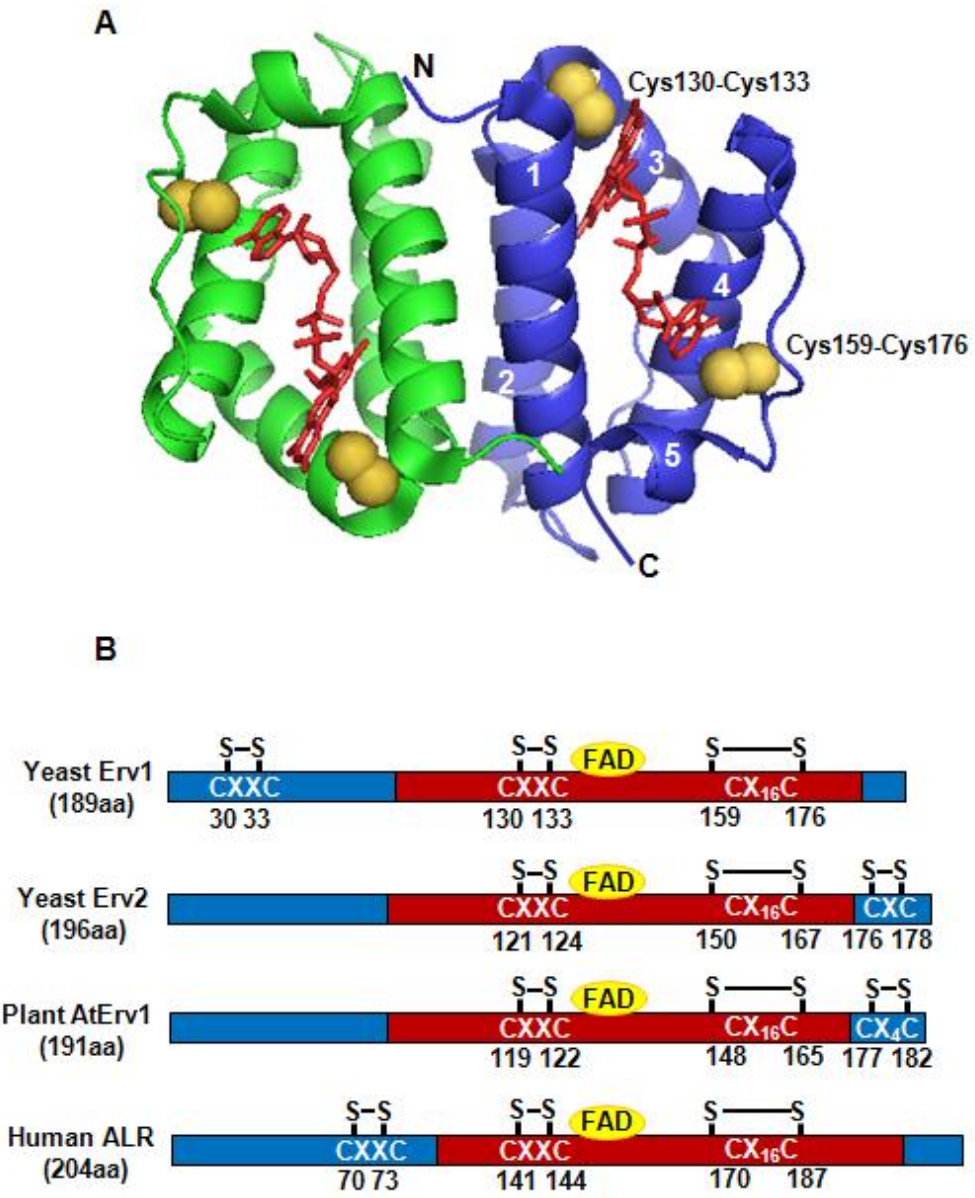

Figure 1.21 The structure and conserved cysteine motifs of ERV/ALR enzymes.

A. A modelled structure of the conserved catalytic core domain of the Erv1 dimer based on the crystal structure data of AtErv1 (Protein Data Bank accession number 2HJ3, residues 73–173, the helix 1 starts from residue 75) generated using Pymol program. The helices of the four-helix bundle and the short fifth helix are labelled from 1 to 5. The two disulphides and the cofactor FAD are shown as yellow spheres and red sticks, respectively.

B. The primary structure of yeast, plant, and human sulphydryl oxidase with the conserved cysteine motifs. The conserved catalytic core domains and the non-conserved domains are shown in red and blue, respectively. The cofactor FAD is located in close proximity to the CXXC disulphide of the catalytic core.

However, such oxygen channel is not observed in the structure of rat ALR, which possibly explains why oxygen is a poor electron acceptor for the enzyme (Wu et al., 2003). The unresolved Erv1 structure is predicted to have an oxygen channel, as it has been shown to utilise oxygen as electron acceptor (Dabir et al., 2007).

Erv1 contains 189 amino acids with a total of six cysteine residues forming three pairs of disulphide bonds (Cys30-Cys33, Cys130-Cys133 and Cys159-Cys176) as described above. It forms a homodimer of 44kDa based on non-reducing SDS-PAGE studies, suggesting that the monomer subunits are covalently linked, through intermolecular disulphide bonding (Lee et al., 2000, Hofhaus et al., 2003). However, structural and biochemical data have suggested that hydrophobic forces in between the two subunits are enough for the protein to dimerise (Bien et al., 2010, Vitu et al., 2006). A previous study (Hofhaus et al., 2003) using Erv1 single cysteine mutants demonstrated that all three disulphide bonds are essential for Erv1 function *in vivo*. However, only the Cys130-Cys133 disulphide is required for the oxidase activity of Erv1 *in vitro* by using an artificial substrate dithiothreitol (DTT) as electron donor. In addition, the proteins with Cys30 and Cys130 mutated had abnormal colour changes. These were probably caused by protein misfolding or formation of non-native disulphides due to the presence of an unpaired redox active cysteine. However, the protein with Cys159 mutated was colourless, indicating the absence of bound FAD. This was in agreement with previous structural data suggesting that the $CX_{16}C$ disulphide of ERV/ALR proteins has a stabilisation role for FAD binding (Gross et al., 2002). So far, it is clear that Cys130-Cys133 is the active site disulphide, but direct experimental evidence for the roles of Cys30-Cys33 and Cys159-Cys176 disulphides is still lacking.

1.3.5 Downstream electron transfer of the MIA pathway

In the MIA pathway, reduced Erv1 has to be reoxidised to allow for another cycle of substrate oxidation. There are three pathways in which reduced Erv1 can be reoxidised (Figure 1.22). Fundamentally, Erv1 is able to shuttle electrons directly to molecular oxygen (Figure 1.22, pathway 1) to produce hydrogen peroxide (H_2O_2), as shown in several *in vitro* studies (Daithankar et al., 2009, Tienson et al., 2009, Dabir et al., 2007, Bihlmaier et al., 2007). Alternatively, Cyt c can also serve as the oxidising agent for Erv1, suggesting that the

MIA pathway is linked to the respiratory chain (Figure 1.22, pathway 2 and 3) (Allen et al., 2005, Bihlmaier et al., 2007, Dabir et al., 2007, Bien et al., 2010).

Dabir et al. (2007) identified the role of cytochrome c peroxidase (Ccp1) as a potential candidate in electron shuttling from Erv1 (Figure 1.22, pathway 2). Two alternative mechanisms in which reduced Erv1 is reoxidised were proposed in this study. In the first mechanism, Cyt c serves directly as the electron acceptor of Erv1, and the reduced Cyt c can then be reoxidised using Ccp1 that subsequently reduces the accumulated H_2O_2. Alternatively, Erv1 uses oxygen as a direct electron acceptor and produces H_2O_2 that is efficiently reduced by Ccp1 to water. Oxidised Ccp1 is then reduced by Erv1-reduced Cyt c.

Interestingly, another study showed that the relative redox states of Mia40 in mitochondria actually depend on the activity of Cyt c and the respiratory chain complexes, i.e. cytochrome *c* reductase (complex III) and cytochrome *c* oxidase (complex IV) (Figure 1.22, pathway 3) (Bihlmaier et al., 2007). By using the mutants or inhibitors of the respiratory chain, reduced Cyt c and Mia40 accumulate upon inhibition of cytochrome c oxidase activity. On the other hand, the amount of oxidized Cyt c and Mia40 increases when cytochrome c reductase activity is blocked. These observations suggested that the respiratory chain is important for the activity of the MIA pathway in the IMS. Hence, a physical interaction between Erv1 and Cyt c is proposed to prevent the generation of H_2O_2 that is toxic to the cell. In agreement with this, *in vitro* experiments demonstrated that ALR, the human homologue of Erv1 is able to reduce oxidized Cyt c more efficiently, suggesting that Cyt c is a better electron acceptor than molecular oxygen (Farrell and Thorpe, 2005). However, under fermentative condition when the electron transport chain is not working, Cyt c could not serve as the electron acceptor of Erv1. Since the MIA pathway is still strictly essential under fermentative conditions, an alternative electron acceptor for Erv1 is still to be identified (Stojanovski et al., 2008b).

Therefore, it is likely that Erv1 is able to utilise diverse pathways for electron shuttling in the IMS, depending on the physiological condition of the cell. However, how Erv1 oxidation is regulated in the presence of numerous oxidising agents *in vivo*, is still a largely unknown question.

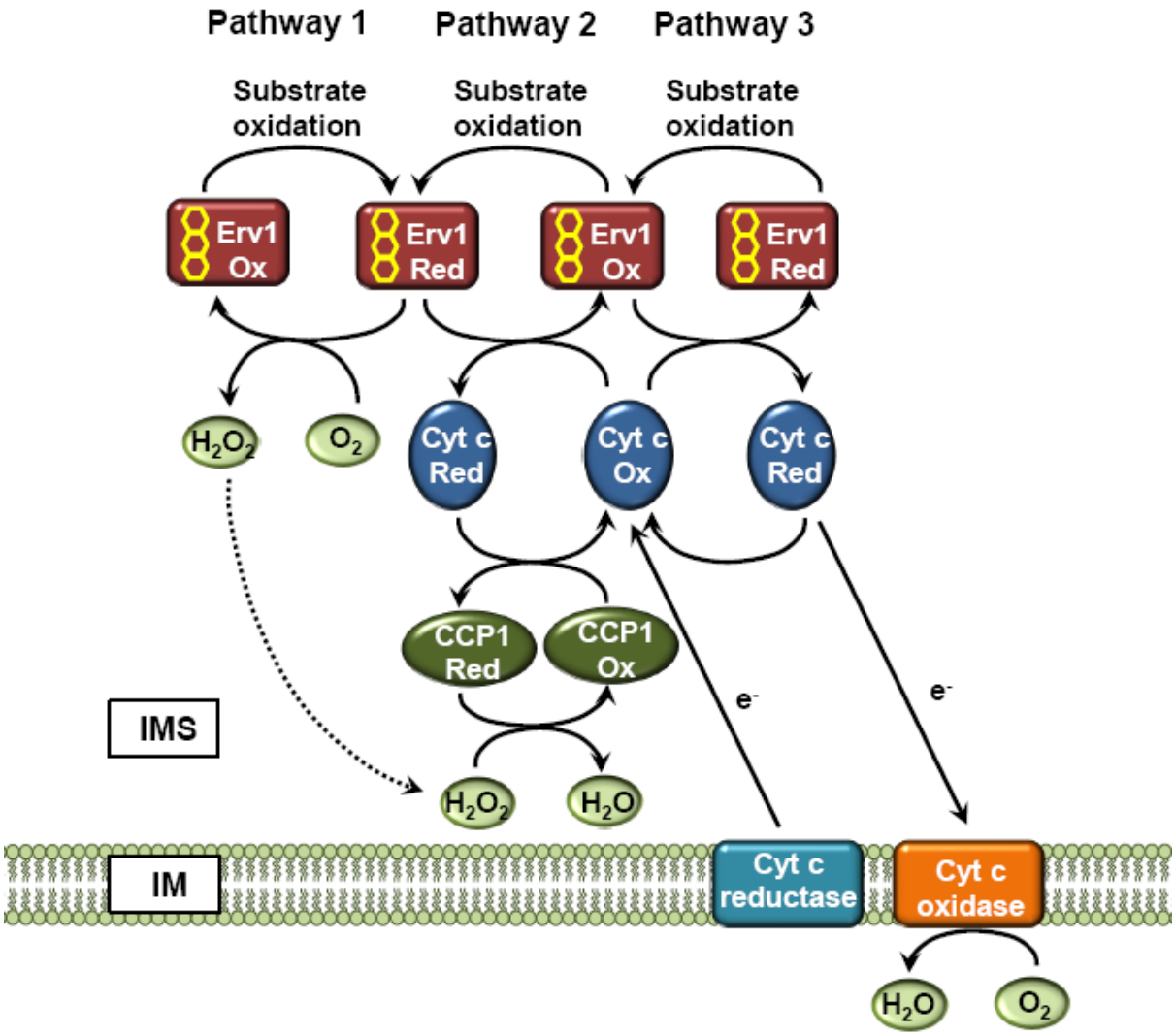

Figure 1.22 Alternative pathways of Erv1 oxidation.

After catalysing substrate oxidation, Erv1 is maintained in an oxidised state by three different pathways. Reduced Erv1 can either be directly oxidised by molecular oxygen (pathway 1) or cytochrome c (Cyt c, pathway 2 and 3). Hydrogen peroxide produced from pathway 1 maintains cytochrome c peroxidise (CCP1) in an oxidised state, which in turn provides oxidising equivalent to Erv1 through Cyt c (pathway 2). Alternatively, Erv1 is oxidised by connecting to components of the respiratory chain through Cyt c, which is kept in an oxidised state by cytochrome c oxidase that acquires the ultimate oxidising equivalent from molecular oxygen (pathway 3).

1.4 Aims and objectives

The MIA pathway of the mitochondrial IMS, which is the main focus of this study, is currently a very hot research topic. The protein characteristics and functional mechanism of Mia40 have extensively been studied recently. During the course of this project, the mechanism of Mia40-substrate interaction became well understood following the identification of targeting signals in substrate proteins and the availability of Mia40 structural data. Although several aspects of Erv1, the other key component of the MIA machinery have been studied, many questions still remain to be answered. The overall aim of this study was to understand the functional mechanism of Erv1 and its interaction with Mia40, as briefly outlined below:

A. Defining the structural roles of Erv1 disulphide bonds.

In this study, three disulphide bonds of Erv1 were mutated individually by replacing the corresponding cysteine pairs to serine residues. The purified wild-type and mutant proteins were characterised in terms of oligomerisation states, spectrometric properties and protein stability. In addition, the effects of zinc binding on the enzymatic activities of Erv1 were also to be studied.

B. Investigating the functional roles of Erv1 disulphide bonds.

The effects of individual disulphide bond mutation on Erv1 enzymatic function were studied by oxygen consumption assays. Artificial (DTT and TCEP) and native (partially reduced Mia40) substrates were used as electron donors in the assays. In addition, the roles of each disulphide bond in Erv1 protein biogenesis and cell viability in yeast were also being studied by using mitochondrial import and cell phenotype testing assays, respectively.

C. Understanding the interaction between Mia40 and Erv1, and the role of GSH in the interaction.

The individual cysteines of both Mia40 and Erv1 that can potentially be primed for mixed disulphide bond formation were characterised by using single cysteine to serine mutant proteins. The mutant proteins were used to study the covalent interaction between Mia40 and Erv1. In addition, the effects of GSH on Mia40-Erv1 interaction were also to be studied.

The results of this study have contributed to two publications, which together with other unpublished data, will be presented in this report in three result chapters (Chapters 3-5).

2. MATERIALS AND METHODS

All chemicals were provided by Sigma (St. Louis, USA), unless otherwise stated.

2.1 *In vitro* techniques

2.1.1 DNA cloning

All the oligonucleotides (Eurofins MWG Operon, Germany), DNA templates and cloning vectors used in this study are listed in Appendix 1. To generate inserts for DNA cloning, the target DNA fragments were amplified by polymerase chain reactions (PCR). Typically, each PCR reaction contained 0.3mM of deoxynucleoside triphosphate mix, 20pmol of each primer, 1.5mM of $MgCl_2$, and 2.5U of *Taq* DNA polymerase (Fermentas, Hanover, MD, USA) with 1 X working concentration of the reaction buffer system. The PCR was performed at 95^{o}C for 5 minutes followed by 35 cycles at 95^{o}C for 30 seconds, 55^{o}C for 15 seconds, and 72^{o}C for 30 seconds. The annealing temperature and extension time were adjusted accordingly, with different oligonucleotides used and expected length of PCR products. A final extension of 5 minutes at 72^{o}C completed the PCR.

The PCR products were examined by 1X Tris-Acetic Acid agarose gel electrophoresis and subsequently purified from agarose gels using QIAGEN Gel Extraction Kit (Qiagen) or GENECLEAN III kit (Bio101, Vista, CA, USA) according to the manufacturer's protocol with an additional drying step prior to elution. Purified PCR products were digested with 10 units of each of FastDigest® restriction enzymes (Fermentas, Hanover, MD, USA) at 37^{o}C for 4 hours or overnight and then purified from agarose gels before ligating into linearised vector DNA treated with the same restriction enzymes. The ligation reaction was carried out at 22^{o}C for 1 hour or 16^{o}C overnight using 2.5U of T4 DNA ligase (Fermentas, Hanover, MD, USA) in 1X concentration of the reaction buffer.

Transformation was achieved by incubating 5μl of the ligation mixture with 50μl of competent *Escherichia coli* TOP10 cells (Invitrogen Carlsbad, CA, USA) for 1 hour on ice followed by a heat-shock at 42^{o}C for 50 seconds. Cell growth was achieved by addition of 250μl of pre-warmed (37^{o}C) SOC medium followed by incubation at 37^{o}C with shaking at 220rpm for 1 hour. Approximately 50μl of the culture was plated on LB agar plates containing either 50 μg/ml of kanamycin or 100 μg/ml of ampicillin depending on the vector used, and incubated for 16-20 hours at 37^{o}C before colonies were screened by PCR. The PCR

products with the desired size were purified from agarose gels and sequenced using ABI prism Big Dye terminator kit (Applied Biosystems, Foster City, USA) to compare with the respective DNA sequences deposited in the public database GenBank at the NCBI web site (http://www.ncbi.nlm.nih.gov/BLAST/). Plasmid DNA with desired insert was extracted using QIAGEN Plasmid Miniprep kit (Qiagen) or MiniPrep Express Matrix (Bio101, Vista, CA, USA) according to manufacturer's guidelines before transforming into competent *E. coli* Rosetta-gami 2 cells (Novagen, San Diego, CA) or BL21 (DE3) cells (Stratagene, La Jolla, USA) for protein expression.

2.1.2 Site-directed mutagenesis

The Erv1 and Mia40 cysteine to serine mutants used in this study were created by PCR site-directed-mutagenesis. The oligonucleotides (listed in Table) were designed with a single base pair change in the codon for cysteine residues into serine residues. The PCR was performed using 10ng of wild-type construct as template DNA in a 20μl reaction containing 0.3mM of deoxynucleoside triphosphate mix, 12.5pmol of each primer set and 2.5U of Pfu DNA polymerase (Fermentas, Hanover, MD, USA) with 1 X working concentration of the reaction buffer system. The PCR was performed at 95^{o}C for 30 seconds followed by 18 cycles of 95^{o}C for 30 seconds, 55^{o}C for 1 minute and 68^{o}C for 13 minutes. The parental plasmid DNA was digested with 10U of Dpn1 (Stratagene, La Jolla, USA) at 37^{o}C for 1 hour before transforming into competent *E. coli* TOP10 cells (Invitrogen Carlsbad, CA, USA). Colonies were screened by DNA sequencing as described in Section 2.1.1. To generate double cysteine mutants, a single cysteine mutant construct was used as the template for mutagenesis reaction with the primers for the second cysteine mutation. The plasmid DNA containing desired mutation was transformed into competent *E. coli* Rosetta-gami 2 cells (Novagen, San Diego, CA) or BL21 (DE3) cells (Stratagene, La Jolla, USA) for protein expression.

2.1.3 Protein expression and purification from *Escherichia coli*

2.1.3.1 Solutions

Buffer A: 50mM Tris-(hydroxymethyl)aminomethane (Tris)-HCl pH 7.4, 150mM NaCl

Buffer AE: Buffer A + 1mM EDTA

Binding Buffer: Buffer A + 10mM Imidazole

Washing Buffer 1: Buffer A + 20mM Imidazole

Washing Buffer 2: Buffer A + 40mM Imidazole

Elution Buffer: Buffer A + 250mM Imidazole

2.1.3.2 Erv1 full-length and C-terminal domain

The wild-type (WT), cysteine-to-serine mutant and C-terminus Erv1 proteins were expressed as C-terminal 6-Histidine tagged recombinant proteins from Rosetta-gami 2 cells. Overnight culture grown in Luria Broth (LB) media at 37^{o}C with shaking at 220rpm was diluted 1:50 into fresh LB containing 50μg/ml of kanamycin. Cells were grown until the OD_{600} reaches 0.6-0.8. Protein expression was achieved by an overnight induction at 16^{o}C with 0.5mM isopropyl-β-D-thiogalactopyranoside (IPTG, Bioline, London, UK) and 10μM flavin adenine dinucleotide (FAD). The cell pellets from 1l culture were resuspended in 20ml of Buffer A containing 50μM FAD and one tablet of complete EDTA free protease inhibitor cocktail (Roche, Germany). Cell breakage was facilitated by 10 cycles of 9-second sonication with 1 minute intervals on ice, using a tapered tip at 35% amplitude. The soluble fraction containing the majority of the protein of interest was separated from the pellet by centrifugation at 20,000g for 15 minutes at 4^{o}C. Clarified sup fraction containing most of the protein of interest was 0.2μM filtered and applied onto a column with 2ml packed volume of Ni^{2+} charged His.Bind Resin (Novagen, Madison, WI, USA) equilibrated with 10mM imidazole in Buffer A at 4^{o}C. After a washing step with 10 volumes of Washing Buffer 1 and 10 volumes of Washing Buffer 2, the protein was eluted with 3 volumes of Elution Buffer. The imidazole was removed from the eluates by dialysis against 2-3 successive changes of 1l Buffer AE at

4°C. For maximal cofactor binding to Erv1, 100μM FAD was supplemented before storage at -80°C in 500μl aliquots.

2.1.3.3 Erv1 N-terminal domain

The N-terminus of Erv1 was expressed as C-terminal 6-Histidine tagged recombinant protein from BL21 (DE3) cells. All cell growth conditions, protein expression, cell breakage and protein purification procedures were the same as for the full-length and the C-terminus, except that no free FAD was supplemented throughout the process.

2.1.3.4 Mia40c

The wild-type and the cysteine-to-serine mutant Mia40c proteins were expressed as Glutathione-S-Transferase (GST) fusion proteins in *E. coli* BL21 (DE3) cells (Stratagene, La Jolla, USA). All cell growth conditions, protein expression and cell breakage procedures were performed as described in Section 2.1.3.2, unless otherwise stated. Protein expression was achieved by 0.5mM IPTG overnight induction at 16°C in LB media containing 100μg/ml ampicillin. For each litre of culture, cell pellets were resuspended in 20ml of Buffer AE containing one tablet of complete EDTA free protease inhibitor cocktail (Roche, Germany) before cell breakage. The soluble fraction containing the majority of the protein of interest was clarified by centrifugation and then 0.2μm filtered before being applied onto 4ml packed volume of Gluthathione Sepharose 4B beads (Amersham Pharmacia, Uppsala, Sweden) equilibrated with Buffer AE at 4°C for 1 hour. The beads were washed by 15 volumes of Buffer AE before resuspended in 6ml of Buffer AE containing 20U/ml of thrombin and subsequently incubated for 16-20 hours at 4°C to facilitate protein cleavage from the GST tag. The protein was eluted with 2 volumes of Buffer AE and kept at -80°C in 500μl aliquots for long term storage.

2.1.4 Gel filtration

Before any protein assay, the affinity purified proteins were further purified by size exclusion chromatography using a Superdex 75 10/30 column (Amersham Pharmacia, Uppsala, Sweden) connected to an AKTA Purifier FPLC system (Amersham Pharmacia, Uppsala, Sweden) operated by Unicorn software. Protein samples were centrifuged at maximum speed for 5 minutes in a bench-top centrifuge for removal of any protein precipitate before injection into the system. Buffer A was used as running buffer at a flow rate of 0.5ml/minute. The protein eluates were collected in 0.5ml fractions.

2.1.5 Multiangle laser light scattering

The affinity purified Erv1 and its mutants were sent to the Biomolecules Core Facility (Manchester, UK) for light scattering analyses. Protein samples were applied to a Superdex 200 gel filtration column (Amersham Pharmacia, Uppsala, Sweden) running with Buffer A. Protein eluted from the column passed through an in-line DAWN EOS laser photometer set at 682nm and an Optilab rEX refractor. To calculate the weight-averaged molecular mass, the light scattering intensity and eluant refractive index were analysed using ASTRA version 4.8 software. The light scattering analysis is courtesy of Marj Howard (Biomolecular Core Facility, Manchester, UK).

2.1.6 Determination of the extinction coefficients

UV-Vis absorption spectra of Erv1 and its mutants were measured using a Cary 300 spectrophotometer at 1nm intervals from 250 to 700nm. Quartz cells with path-length of 1cm were used for all measurements at room temperature (20^{o}C). All spectra were baseline corrected using the corresponding buffer. The extinction coefficients and the percentage of enzyme-bound FAD for the WT and mutant Erv1 were calculated based on a molar extinction coefficient of 11.3 $mM^{-1}\,cm^{-1}$ at 450 nm for free FAD and 72.68 $mM^{-1}\,cm^{-1}$ for Erv1 at 275 nm as reported previously (Dabir et al., 2007). FAD was released from the proteins by addition of 1% SDS.

2.1.7 Circular dichroism

Circular dichroism (CD) analysis was performed using a JASCO J810 spectropolarimeter with a 1mm path-length quartz cuvette. Far-UV CD spectra were measured at 25°C with 300µl of 10-15µM proteins. Each spectrum represents an average of four scans from 200-260 nm at 0.2 nm intervals with the spectra for buffer alone subtracted. CD spectra were normalised by protein molar concentration and number of residues. Thermal denaturation was measured at 222 nm, at 1ºC intervals over 5-90ºC with temperature increase at 1ºC/min. CD analysis of WT and cysteine-to-serine mutants of Erv1 is courtesy of Hui Lu (Manchester, UK).

2.1.8 Proteinase K digestion

In reaction volumes of 20µl, 5µM Erv1 and its mutants were incubated with 50µg/ml proteinase K at 25ºC for 30 minutes. Protease activity was inhibited by addition of 10mM PMSF for 10 minutes. Mock controls were treated in exactly the same manner.

2.1.9 Preparation of partially reduced Mia40c

The Mia40c was incubated with 0.5mM TCEP at room temperature for 10 minutes in reaction volumes of 500µl. Partially reduced Mia40 (Mia40c-pR) was buffer exchanged against 1ml of Buffer A using NAP5 columns (Amersham Pharmacia, Uppsala, Sweden). To avoid excessive loss of protein concentration and presence of reducing agent co-eluted with the protein, only the fraction from 200-750µl of the elution was collected for subsequent assays.

2.1.10 Ellmann's assays

In reaction volumes of 1ml, 50µl Mia40c-pR was incubated with 2mM Ellmann's reagent in 50mM Tris-HCl buffer, pH 7.5 and 0.1% SDS for 5 minutes at room temperature. The absorbance at 412nm corresponding to free thiols was measured using a Cary 300 spectrophotometer in quartz cells with path-length of 1cm. The concentration of Mia40c-pR

was calculated using a molar extinction coefficient of 13.6 mM^{-1} cm^{-1} after baseline correction using the same buffer.

2.1.11 Oxygen consumption assays

Erv1 oxidase activity was measured using a Clark-type oxygen electrode (Hansatech Instrument Ltd, England). The electrode was calibrated with a few grains of sodium dithionite to set the range of oxygen level measurement from 0 to 100%. All measurements were carried out in a 0.5ml reaction volume at 25^{o}C in Buffer AE, unless otherwise stated. For measurements with DTT, TCEP and GSH as substrates, Erv1 was pre-equilibrated at 25°C followed by addition of substrate to initiate the reaction. For measurements with Mia40c-pR as substrate, freshly prepared Mia40c-pR was pre-equilibrated at 25°C followed by addition of Erv1 to catalyze the reaction. Data analysis of the oxygen consumption profile and the calculation of reaction slope were performed using the Microcal™ Origin™ statistical software package.

2.1.12 AMS alkylation assays

Redox states of protein cysteines were examined by using the thiol alkylation agent 4-acetamido-4'-maleimidylstilbene-2,2'-disulphonic acid (AMS, Molecular Probes, Invitrogen) at an excess amount. AMS is covalently linked to any free thiol groups resulting in an increase of molecular weight by 0.5kDa per thiol. AMS was prepared in 2X non-reducing SDS-PAGE sample buffer and incubated with an equal volume of protein samples in dark for 15 minutes before resolving on 16% tricine SDS-PAGE gels (Section 2.1.14).

2.1.13 Mass spectrometry analysis

The WT Erv1 (5μM) was incubated with 0 or 50μM freshly prepared Mia40c-pR for about 10s, and then the reaction was stopped by addition of non-reducing SDS-PAGE sample buffer containing 4mM iodoacetamide (IAM). The proteins were separated by non-reducing SDS-PAGE. The bands corresponding to Erv1 were excised and digested with AspN.

Peptides were analysed by mass spectrometry on a Bruker MALDI-Tof using a positive reflection method. Mass spectrometry analysis is courtesy of Emma Keevill (Biomolecular Core Facility, Manchester, UK).

2.1.14 Tricine SDS-PAGE

All tricine SDS-PAGE (sodium dodecyl sulfate polyacrylamide gel electrophoresis) gels (Schagger and Von Jagow, 1987) were run using the Biorad mini-Protean III system. For non-reducing condition, samples were resuspended either in an equal volume of 2X SDS-PAGE (4% (w/v) SDS, 8% (v/v) glycerol, 0.02% (w/v) bromophenol blue, 80mM Tris-HCl, pH6.8) sample buffer. For reducing condition, samples were resuspended in sample buffer with DTT to give a final concentration of 0.1M. All the samples were heated at 95^{o}C for 5 minutes and spun for 10 minutes on a bench-top centrifuge at maximum speed before loading.

2.1.15 Gel transfer

Gels for western blot analysis were transferred onto nitrocellulose membranes using a Hoefer TE 22 mini tank transfer gel electrophoresis unit in chilled Towbin buffer (25mM Tris, 192mM glycine, 20% (v/v) methanol). Transfer was carried out for 1 hour at 0.3A.

2.1.16 Western blotting and antibodies

Generally, transferred membranes were blocked with 0.5% (w/v) skimmed milk in 1X phosphate buffer saline tween (PBST, 137mM NaCl, 2.7mM KCl, 10mM Na_2HPO_4, 2mM NaH_2PO_4, pH7.4, 0.1% Tween-20) for 1 hour at room temperature or overnight at 4^{o}C. For western blotting with anti-His antibody, 0.5% (w/v) bovine serum albumin (BSA) was used as blocking agent. Primary antibody diluted in PBST with 0.5% (w/v) blocking agent was added for 2 hours at room temperature or overnight at 4^{o}C. The membranes were washed with PBST for 10 minutes, up to 3 times before addition of secondary antibody diluted in PBST with 0.5% (w/v) blocking agent for 2 hours at room temperature. The membranes were

washed with PBST as described earlier before addition of enhanced chemiluminescence (ECL, GE Healthcare) substrate solution and exposure to Kodak Biomax MR film.

The primary antibody specific for Erv1 was produced in New Zealand White Rabbits and purified by Eurogentec. The antibody was raised against a peptide corresponding to the last 10 amino acid residues of the Erv1 C-terminal domain, and was used at 1/2500 dilution. The Goat anti-Rabbit IgG-HRP secondary antibody was purchased from Invitrogen, and was used at 1/5000 dilution. The HisDetector™ Nickel-HRP to detect His-tagged protein was purchased from KPL and was used at a dilution of 1/2500. The mouse anti-myc primary antibody (Invitrogen) and the Goat anti-Mouse IgG-HRP (Invitrogen), both used at 1/1000 dilution, were kindly given by Chris Grant (Manchester, UK).

2.2 *In organello* techniques

2.2.1 Solutions

Breaking Buffer: 0.6M Sorbitol, 20mM HEPES-KOH pH 7.4

2x Import Buffer: 1.2M Sorbitol, 100mM HEPES-KOH pH 7.4, 100mM KCl, 1.5mg/ml L-methionine, 2mg/ml fatty acid free BSA

Trypsin buffer: 0.6M Sorbitol, 20mM HEPES-KOH pH 7.4, 50μg/ml trypsin

2.2.2 Radiolabelled protein production

Radiolabelled Erv1 precursors were synthesised in TNT® T7 Coupled Reticulocyte Lysate System (Promega, Fitchburg, USA) according to the manufacturer's protocol using ^{35}S-methionine and the same plasmid constructs used for protein purifications as DNA template, at 30^{o}C for 90 minutes. The reaction was stopped following a centrifugation step at 55,000g, 4^{o}C for 15 minutes using a TLA.100 rotor in a Beckman Optima™ MAX ultracentrifuge to remove ribosomes preventing any further translation. The supernatant containing ^{35}S-Erv1 precursor was used for import assays.

2.2.3 Mitochondrial protein import assays

Mitochondria were isolated from the wild-type yeast D273-10B strain (MATα) by Bruce Morgan (Manchester, UK). Before import reactions, mitochondria thawed from -80^{o}C on ice were diluted tenfold in chilled Breaking Buffer and reisolated by centrifugation at 13,000g for 5 minutes at 4^{o}C. The mitochondria were washed once and resuspended to 10mg/ml in the same buffer until use. Import assays were carried out in 150µl reactions consisting 75µg mitochondria, 5% (v/v) ^{35}S-Erv1 and 2mM EDTA in 1x Import Buffer. Import reactions were performed at 30°C for 30 minutes and the unimported materials were digested by incubation with Trypsin Buffer at 4ºC for 20 min. The protease reaction was stopped by the addition of 1mg/ml soybean trypsin inhibitor at 4^{o}C for 10 min. Mitochondria were reisolated by centrifugation, before resuspended in gel sample buffer for Tris/Tricine SDS-PAGE analysis and visualisation by autoradiography. Import level was quantified by two-dimensional densitometry using an Aida image analyser (Version 4.00).

2.3 *In vivo* techniques

2.3.1 Construction of *ERV1* repressible *Saccharomyces cerevisiae* strain

The *ERV1* repressible yeast strain was constructed based on a method described by(Yen et al., 2003), as illustrated in Figure 2.1. Briefly, a PCR product encoding a KanMX4 cassette, the *tet*O_2 promoter and flanking regions that are homologous to 45bp of *ERV1* promoter 105bp upstream from ATG and the first 45bp of the gene was amplified from plasmid template pCM324. By using lithium-acetate method (Gietz et al., 1992), this PCR product was transformed into yeast strain CML476 to disrupt the endogenous *ERV1* promoter by homologous recombination. The transformants were initially screened by resistance to 400µg/ml G418 before phenotype testing by spotting on YPD media (1% bactoyeast extract, 2% bactopeptone, 2% glucose) containing 50µg/ml doxycycline to confirm repression of the *ERV1* gene. PCR was then used to further confirm that the KanMX4-*tet*O_2 cassette had been integrated into the correct location. The construction of *tet*0_2-regulated *ERV1* strain is courtesy of Nianshu Zhang (Cambridge, UK).

2.3.2 Complementation of the *tet*O_2 *ERV1* strain with plasmid encoded Erv1

The pRS414 vector encoding for the WT and mutant Erv1 with its promoter and terminator sequence were transformed individually into the *tet*0_2 *ERV1* strain and were selected using SD agar media (0.67% yeast nitrogen base, 2% glucose, 2% agar) supplemented with 0.1% (w/v) Trp Drop-out Synthetic Complete Amino Acid (Formedium, UK). Tryptophan was omitted from the media to allow for pRS414 vector selection. For co-expression of two different Erv1 mutants within the same cell, with one of them in pRS414, and the other in pRS416, SD-Trp-Ura was used as selection media. Transformed cells were liquid-cultured in respective selection media until stationary phase. For phenotype testing, the cells were diluted to OD_{600}= 1, and followed by 4 subsequent 1/7 serial dilutions using the same selection media on respective selection agar media supplemented with or without 50μg/ml doxycycline.

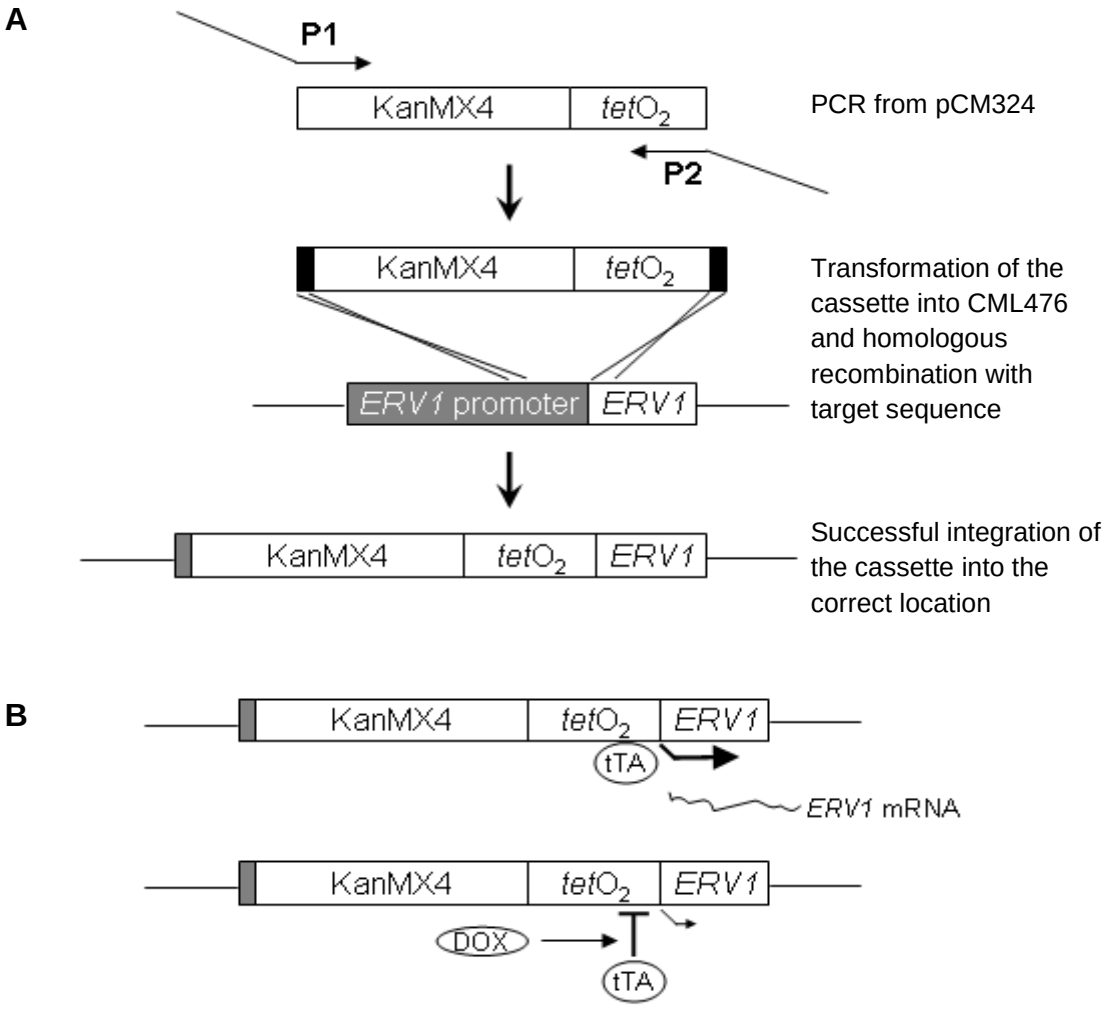

Figure 2.1 Schematic of the procedures for constructing *ERV1* repressible *S. cerevisiae* strain and doxycycline induced repression of the gene.

A. The KanMX4-*tet*O_2 cassette containing the *ERV1* gene flanking regions (black boxes) was synthesised by PCR. The bending parts of the arrows represent the 45bp regions of the primers (P1 and P2) homologous to the target sequences in the *ERV1* gene. The PCR product transformed into CML476 strain of *S. cerevisiae* was integrated upstream of the *ERV1* gene through homologous recombination, replacing the *ERV1* promotor.

B. The *tet*O_2 allows for *ERV1* expression as normal upon activation by tTA transactivator produced by the yeast genome, unless tTA binding is blocked by the presence of doxycycline (DOX).

3. RESULTS AND DISCUSSION I: PROTEIN PURIFICATION AND CHARACTERISATION

3.1 Introduction

Erv1 contains six cysteine residues arranged in a CXXC motif at the non-conserved N-domain, a CXXC and a $CX_{16}C$ motif at the conserved C-domain (Figure 3.1). Each pair of cysteine motifs forms a disulphide bond, which is individually named as Cys30-Cys33, Cys130-Cys133 and Cys159-Cys176, respectively. Based on the partial crystal structure data of other members of the ERV/ALR protein family (Gross et al., 2002, Wu et al., 2003, Vitu et al., 2006), the C-domain CXXC disulphide located in close proximity to the isoalloxazine ring of FAD has been suggested as the active-site disulphide. The long range $CX_{16}C$ disulphide that brings the short fifth helix to the four-helix bundle in proximity to the adenine ring of FAD is suggested to play a role in stabilisation of FAD binding and/or protein structural folding. Each member of the ERV/ALR protein family contains a disulphide located on the N- or C-terminal non-conserved flexible domain, which is suggested to act as a shuttle disulphide.

A previous study using single cysteine mutant proteins of Erv1 was only able to experimentally confirm the role of C-domain CXXC disulphide (Cys130-Cys133) as an active site disulphide by using DTT as an artificial substrate (Hofhaus et al., 2003). Whilst all the cysteine residues were demonstrated to play essential roles for cell viability in yeast, direct experimental evidence showing the exact functions of the N-domain CXXC disulphide (Cys30-Cys33) and the C-domain $CX_{16}C$ disulphide (Cys159-Cys176) is still lacking. Furthermore, the single cysteine mutant proteins of Erv1 showed different biophysical properties, some of which had non-specific protein aggregation possibly due to the unpaired cysteine, which caused difficulties in handling. In this study, to understand the roles of each disulphide bond of Erv1, both the cysteine residues corresponding to each of the three disulphides were mutated to serines (Figure 3.1). The mutant proteins were named as C30/C33S, C130/C133S and C159/C176S, respectively in the rest of the report.

In this chapter, the wild-type (WT) and the three individual disulphide mutant proteins of Erv1 were characterised. The oligomerisation states, spectrometric properties and thermal stability of the proteins were studied by using biophysical tools. In addition, the enzymatic function of the WT protein was tested by oxygen consumption assays under different buffer

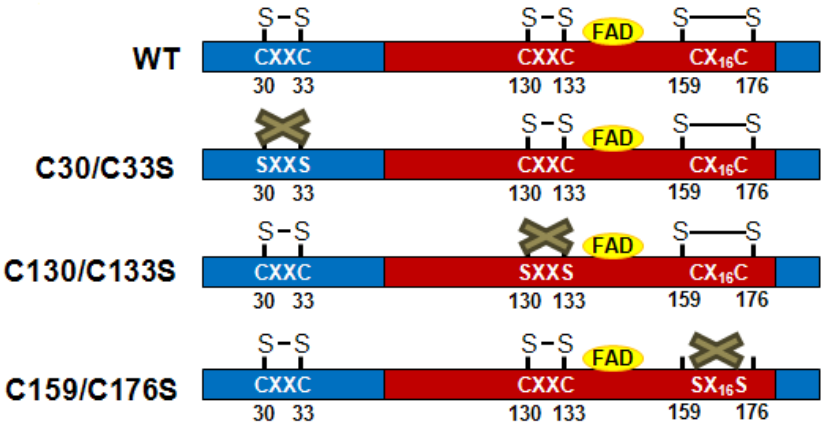

Figure 3.1 Primary structures of the WT and three double cysteine mutants of Erv1. Each disulphide bond of Erv1 was mutated by replacing the corresponding cysteine pair with serine residues. The conserved catalytic core domain and the non-conserved domain are shown in red and blue, respectively.

conditions. Finally, the effects of zinc on the oxidase activity of Erv1 were also studied. The findings from this chapter provided some basic information in optimising the conditions to study the functional properties of Erv1, which will be presented in the next chapter.

3.2 Purification and oligomerisation states of Erv1 proteins

The WT and the individual disulphide mutant proteins of Erv1 were successfully purified as C-terminally 6x His-tagged recombinant proteins from *E. coli* using the same procedure (see Materials and Methods, Section 2.1.3.2). All the three purified mutant proteins were yellowish in colour similar to the WT. SDS-PAGE analysis of affinity purification (Figure 3.2) showed that the WT and all three mutant proteins were soluble and found mainly in the supernatant after cell lysis (lane 4), and the purified proteins (lane 7) were found to be more than 90% pure. The WT and all three mutant proteins remained soluble throughout the purification process. Interestingly, the C130/133S formed white protein precipitates during dialysis when excess free FAD was removed, and re-supplementation of 100µM free FAD completely resolubilised the protein, suggesting that the Cys130-Cys133 disulphide may play a role in stabilising FAD binding that facilitates the overall protein structural folding.

To investigate the oligomerisation states of purified proteins, the WT and all 3 mutant proteins were analysed by gel filtration chromatography on Superdex 75 (Figure 3.3A). The WT was eluted in two peaks at 7.3ml (peak 1) and 8.2ml (peak 2) at about 1:2 ratio (black curve). Similarly, C30/C33S was also eluted in two peaks at the same fractions, but it was found to be more dominated by peak 2 with the ratio of peak 1 to peak 2 at about 1:8 (red curve). In contrast, C159/C176S showed about an equal ratio of peak 1 to peak 2, with a slightly shifted elution fraction for the second peak at about 8.3ml (green curve). For C130/C133S however, apart from the two peaks, a third main peak (peak 3) was eluted at about 9ml (blue curve). In comparison with the molecular weight markers, peak 1 likely contained aggregated or high oligomeric proteins, where as peak 2 may be a tetramer. All the proteins prepared from different batches of purification had consistent gel filtration profiles with the same peak ratios. The lowest peak fractions of the WT and mutant Erv1, which likely contained correctly folded proteins, were used for subsequent assays.

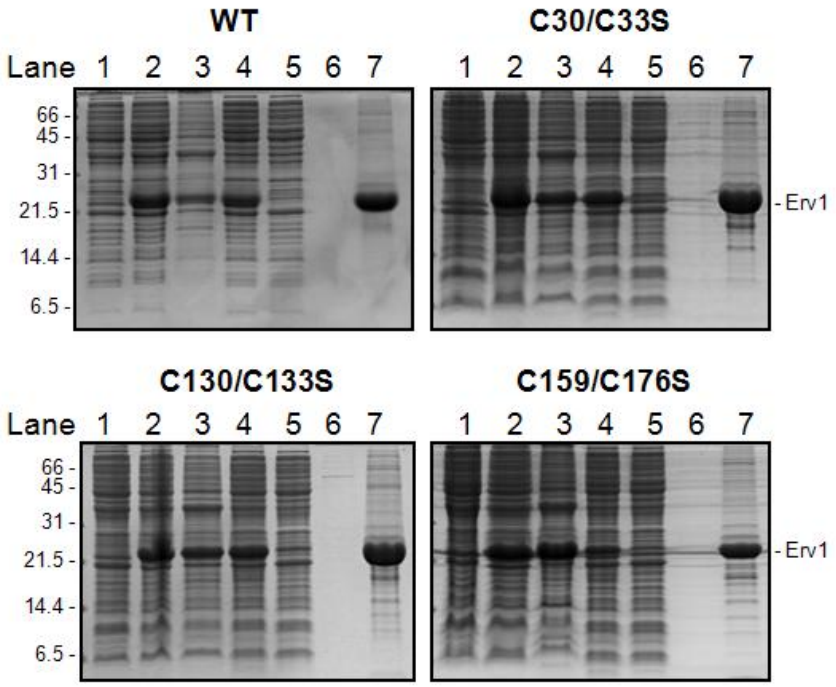

Figure 3.2 SDS-PAGE analysis of protein purification for 6x His-tagged WT and mutant proteins of Erv1.

The cells were grown to log phase (lane 1) before induction overnight at 16^{o}C (lane 2). Induced cells were broken by sonication and separated into pellet (lane 3) and sup fractions (lane 4). The proteins from sup fractions were applied to anti-His beads (lane 5). After a few washing steps (lane 6), the Erv1 were eluted (lane 7) from the column. The proteins were analysed under reducing condition and visualised by coomassie-blue staining.

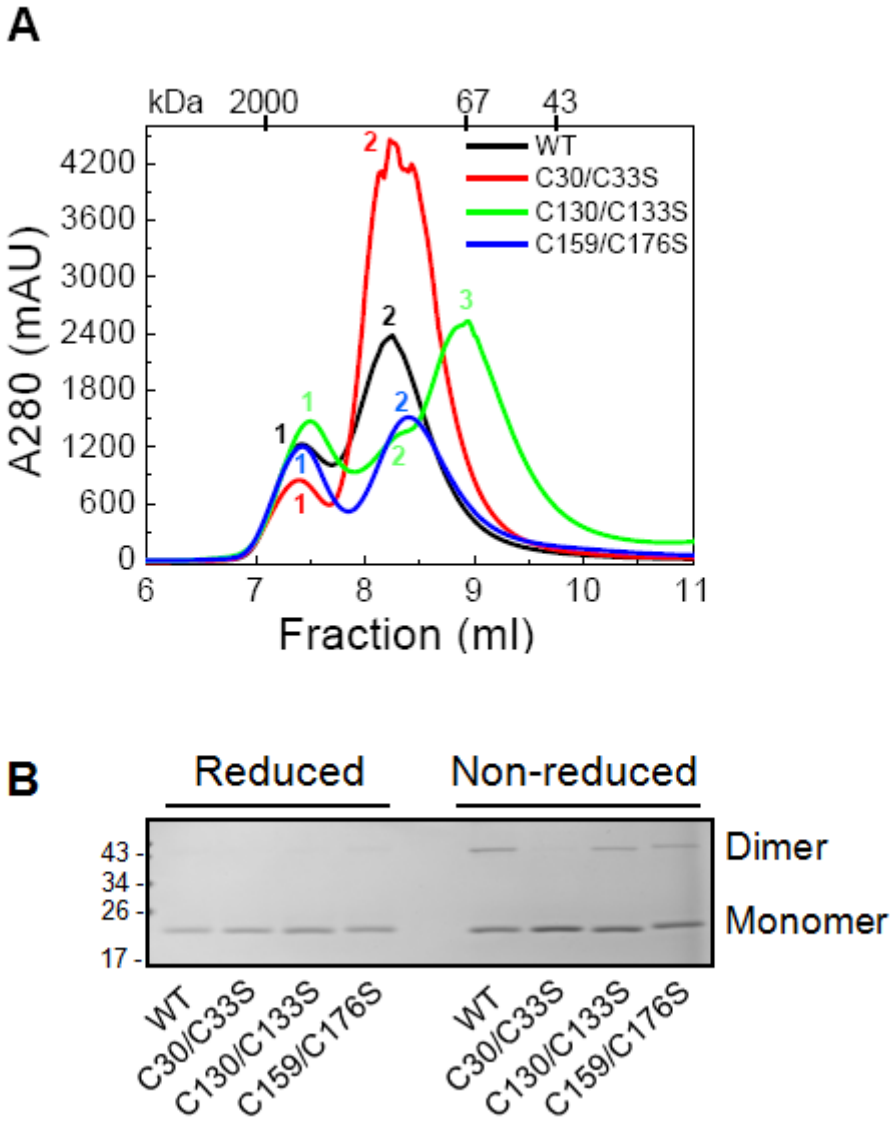

Figure 3.3 Oligomerisation states of the WT and double cysteine mutants of Erv1.

A. Gel filtration profiles of the WT and mutant proteins on Superdex 75 column. The molecular weight markers and the corresponding peak fractions were indicated. The lowest peaks containing the correctly folded proteins were used for subsequent downstream assays.

B. 16% Tricine SDS-PAGE of the WT and mutant proteins under reducing and non-reducing conditions. Samples were treated with (reducing) or without (non-reducing) 1mM TCEP for 5 minutes and resuspended in sample buffer containing 10mM IAM before loading. Proteins were visualised by coomassie-blue staining.

Next, to investigate whether the individual disulphide bond plays a role in Erv1 oligomerisation, the proteins were checked by reducing and nonreducing SDS-PAGE (Figure 3.3B). For all the proteins except C30S/C33S mutant, a fraction of ~20% proteins migrated slowly on the nonreducing gel with an apparent molecular weight corresponding to a dimer. This showed that Cys30-Cys33 disulphide is involved in formation of an intermolecular disulphide bonded dimer, which was in agreement with a previous study using the C-terminal domain of Erv1 (Lee et al., 2000).

In order to determine oligomeric states of the purified Erv1 proteins more accurately, light scattering coupled with gel filtration analysis on Superdex 200 was used. The peak 1 fractions of the WT and all mutant proteins were confirmed to be aggregates due to high molecular weights of >200kDa (results not shown). The peak 2 fractions of the WT, C30/C33S and C159/C176S were determined to have a molecular weight of about 80kDa, 88kDa and 81kDa respectively, showing that they are tetramers, where as for C130/C133S with molecular weight determined to be 70kDa was likely to be a trimer or mixture of dimer and tetramer (results not shown). These results were different from a recent report showing that the purified protein of WT Erv1 only formed dimer (~44kDa) under native conditions (Bien et al., 2009). It was revealed that the protein was purified without supplementing free FAD, which was different from the procedure used in this study (see Materials and Methods, Section 2.1.3.2). Consistently, earlier trials of Erv1 protein purification without FAD supplementation in this study also yielded Erv1 that formed dimer with only about 45% bound FAD and was less active (data not shown). It was later found out that Erv1 purified with FAD supplementation contain nearly 100% of proteins with bound FAD (Section 3.3). Since FAD binding is essential for enzymatic function of Erv1, the percentage of protein FAD binding was maximised by supplementing free FAD during the protein purification procedure. The lowest peak fractions of the WT and mutant proteins, which likely correspond to the correctly folded active forms, were used in the rest of this study.

3.3 Effects of individual disulphide mutation on the spectrometric properties of Erv1

The UV-visible spectrum of the WT Erv1 showed a characteristic bound FAD spectrum with a maximum absorbance at 460 nm and a shoulder peak at ~485 nm (Figure 3.4A). Upon addition of 1% SDS, the absorption maximum was ~10 nm blue-shifted to 450 nm, the same

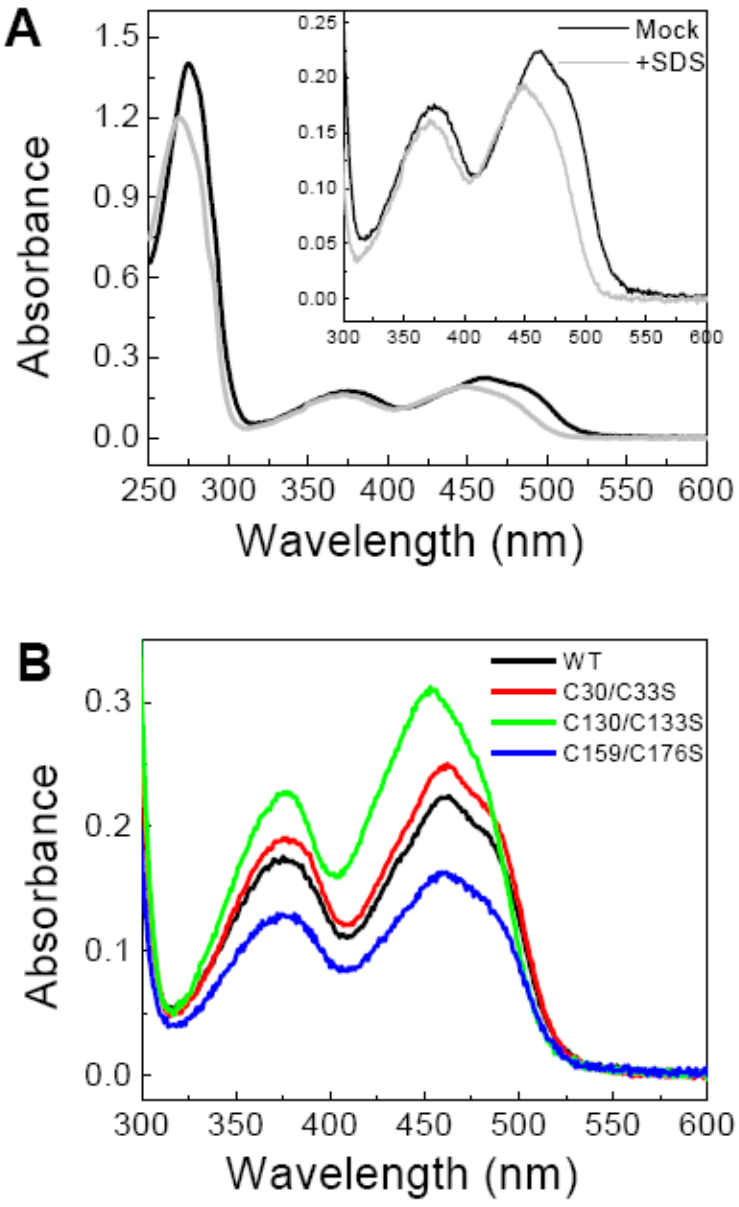

Figure 3.4 Spectroscopic measurements of the WT and double cysteine mutants of Erv1.

A. Absorption spectra of the WT protein in 150mM NaCl, 50mM Tris, pH7.4 in the absence (black) and presence of 1% SDS (light grey).

B. Absorption spectra of the WT and mutant proteins. The concentrations of FAD- bound for WT, C30/C33S, C130/C133S and C159/C176S were 18.9, 22.6, 25.8 and 13.7 µM, respectively.

wavelength as that of free FAD, confirming the release of cofactor FAD. The same FAD spectrum as that of the WT was observed for C30S/C33S and C159S/C176S, but a slightly blue-shifted spectrum with the maximum at 453nm was obtained for C130S/C133S (Figure 3.4B). It is consistent with the fact that the active site Cys130–Cys133 disulphide is located proximal to the isoalloxazine ring of FAD and the mutation changed bound-FAD absorption slightly. The molar extinction coefficients for the bound FAD in the WT and all three mutant proteins were determined (see Materials and Methods, Section 2.1.6) to be 11.9, 11.1, 12.1, and 11.9$mM^{-1}cm^{-1}$ at the corresponding wavelength of the absorption maximum (Table 3.1). These values are similar to each other and to that of other members of ERV/ALR family. The same FAD-binding yield of about 93% was obtained for the WT and all the mutants. Taken together, these results showed that all three Erv1 double cysteine mutant proteins can be purified as the WT with FAD bound at a molar ratio of 1:1. None of the three individual disulphide bonds of Erv1 is essential for FAD binding.

Table 3.1: Spectrometric properties of the WT and double cysteine mutants of Erv1.

Erv1	λ_{max} (nm)	Extinction coefficient ($mM^{-1}\,cm^{-1}$)	FAD-binding (%)
WT	460	11.9	93±2
C30/C33S	460	11.1	93±2
C130/C133S	453	12.1	93±2
C159/C176S	460	11.9	91±2

The extinction coefficients and the percentage of protein bound FAD were calculated based on 11.3 $mM^{-1}\,cm^{-1}$ at 450 nm for free FAD and 72.68 $mM^{-1}\,cm^{-1}$ at 275 nm for Erv1 protein. The error bars represent standard errors, n=3.

3.4 Effects of individual disulphide mutation on the folding and stability of Erv1

The effects of disulphide bond mutation on the overall conformation of Erv1 were investigated using far-UV CD spectra. The WT and all mutant proteins had a similar spectrum profile with a conformation dominated by α-helical structures as expected, based on the crystal structure data of the other ERV/ALR members (Gross et al., 2002, Wu et al., 2003, Vitu et al., 2006) (Figure 3.5A). However, an intensity decrease was observed for C30S/C33S.

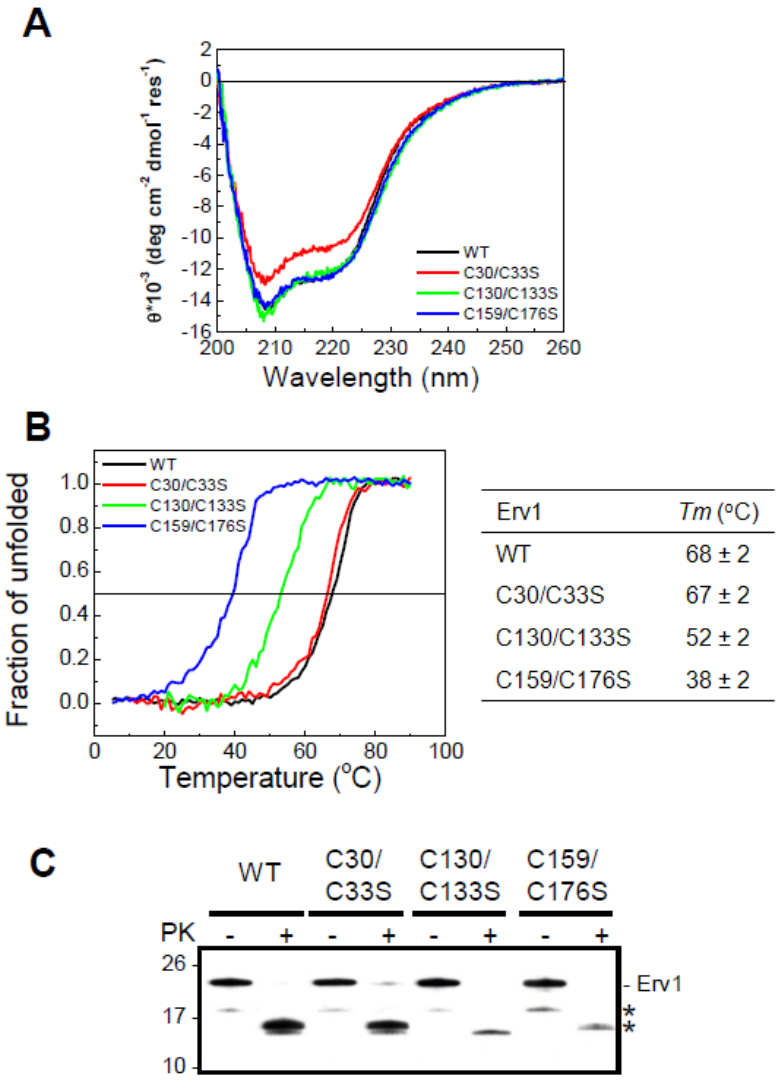

Figure 3.5 Folding and stability of WT and double cysteine mutants of Erv1.

A. Far UV CD spectra of the WT and double cysteine mutant proteins. For all measurements, proteins at a concentration of 10μM were used.

B. Thermal denaturation of the WT and double cysteine mutant proteins measured by CD intensity change at 222 nm. The T_m of the WT (black line), C30/C33S (red line), C130/C133S (green line) and C159/C176S (blue line) mutant were determined to be 68, 67, 52, and 38ºC, respectively.

C. Western blotting of the WT and double cysteine mutant proteins using an antibody against the C-terminus of Erv1. The proteins were untreated or treated by incubation with 0.05mg/ml proteinase K at 25ºC for 30 minutes, and followed by addition of 10mM PMSF before separation by SDS-PAGE. The full length Erv1 and the protease-resistant fragments (*) are indicated.

To understand the possible structural role played by each disulphide bond, thermal denaturation of the WT and mutant proteins was studied by following the intensity change of CD at 222 nm (Figure 3.5B). The WT was stable against heat denaturation with a melting temperature (*Tm*) of 68°C. Mutation of the N-terminal CXXC disulphide bond (Cys30-Cys33) had no apparent effect on the overall stability of the protein. In contrast, mutation of both the core domain disulphide bonds (Cys130-Cys133 and Cys159-Cys176) had a clear effect on the stability of the protein, with a *Tm* of 52°C for C130S/C133S and 38°C for C159S/C176S. Notably, mutation of the Cys159-Cys167 disulphide alone resulted in a decrease of 30°C in *T*m of the protein. A fraction of the C159S/C176S mutant was unfolded at the physiological temperature and as low as ~25°C. This result showed that the Cys159–Cys176 disulphide plays a key role in stabilising the overall folding of Erv1.

Next, the effects of the individual disulphide mutations on the stability of Erv1 were confirmed by proteinase K (PK) digestion, followed by Western blot analysis using an antibody against the C terminus of Erv1 (Figure 3.5C). In the presence of PK, the WT and all three mutant proteins were digested. Although a stable C-terminal fragment of ~15 kDa was clearly observed for the WT and C30S/C33S, the intensity of the same fragment was very weak for C130S/C133S and C159S/C176S, and no other bands were detectable. Thus, the results of PK digestion are consistent with those of the thermal denaturation study.

Both CD and PK digestion studies suggested that the C-terminal domain of Erv1 was folded and resistant to PK digestion but not the N-terminal domain. To confirm further, the N-terminal domain (Erv1N, amino acid 1-83) and C-terminal domain (Erv1C, amino acid 84-189) of Erv1 were purified and subjected to the same CD and PK analysis as for the WT and double cysteine mutant proteins. CD analysis (Figure 3.6A) revealed that the C-terminal domain is folded, with a spectrum profile of α-helical structures similar to that of full length proteins, whlist the N-terminal domain is unfolded. Consistently, the C-terminal domain was resistant to PK digestion, showing the same ~15kDa fragment, and the N-terminal domain was fully digested (Figure 3.6B).

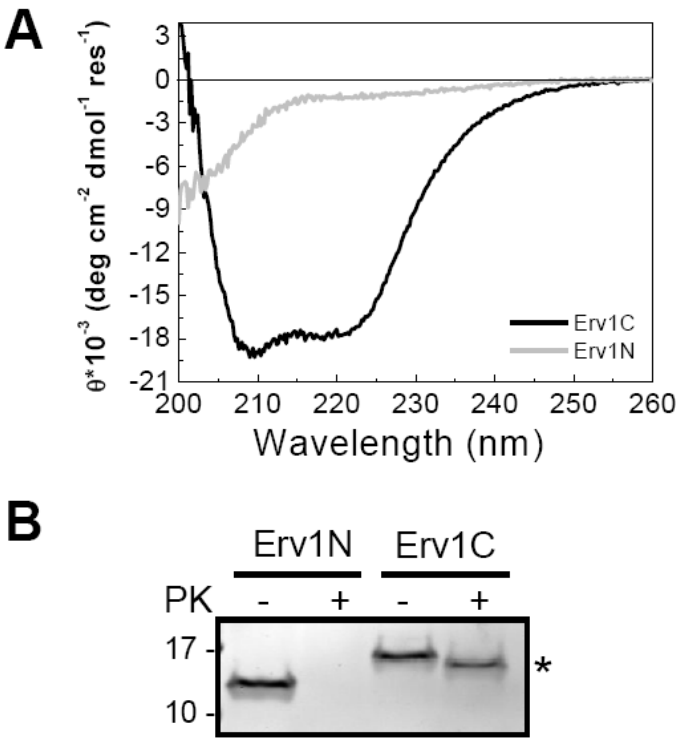

Figure 3.6 Folding and stability of N- and C-terminal domains of Erv1.

A. Far UV CD spectra analysis was the same as in Figure 3.5A, but using the N- and C-terminal domains of Erv1 at a concentration of 15μM.

B. Proteinase K digestion analysis same as in Figure 3.5C, but using the N- and C-terminal domains of Erv1. Proteins were visualised by coomassie-blue staining. The protease-resistant fragment (*) is indicated.

Taken together, the Cys30–Cys33 disulphide has no observable effect on the overall stability of Erv1, as the N-terminal domain is unfolded. Both the C-terminal disulphides play a role in stabilising the folding of the protein, especially the Cys159–Cys176 disulphide.

3.5 Effects of Zn^{2+} on the enzymatic function of Erv1

It was previously shown that Zn^{2+} has an inhibitory effect towards the oxidase activity of Erv2 (Wang et al., 2007). Therefore, it was hypothesised that Erv1 may have an affinity towards zinc. To address this, the Erv1 oxidase activity in various buffer conditions was used as a parameter to measure Zn^{2+} binding using oxygen electrode assays, with which molecular oxygen is utilised as final electron acceptor for Erv1. A commonly used reducing agent, TCEP was used as electron donor for Erv1. TCEP was used as of substrate to test the effect of zinc on Erv1 oxidase activity because it does not bind Zn^{2+}, unlike the thiol-containing DTT (Krezel et al., 2003).

Firstly, to test whether the purified Erv1 is functional, the oxidase activity of the WT protein was measured in mock buffer (Figure 3.7A, curve a). As soon as TCEP was added to initiate the reaction, oxygen was consumed immediately, showing that the purified Erv1 was active, with an initial rate of oxygen consumption determined to be 0.62μM/s. Interestingly, in the presence of EDTA, the Erv1 oxidase activity was increased by about 28% (Figure 3.7A, curve b). However, the Erv1 oxidase activity was strongly impaired by addition of 1μM Zn^{2+} (Figure 3.7A, curve c), which gave the molar ratio of Erv1 to zinc as 1:1. The Erv1 oxidase activity was completely inhibited in the presence of 10μM Zn^{2+} (Figure 3.7A, curve d), and the activity can be recovered by addition of EDTA (Figure 3.7A, curve e). These results showed that Erv1 has a high affinity towards zinc, which can inhibit its oxidase activity.

To measure the affinity of Erv1 towards zinc, a method based on Erv1 oxidase activity and the use of a metal chelator was used. In the presence of an excess amount of Zn^{2+}, the metal chelator functions in controlling the free Zn^{2+} concentration available in the buffer for Erv1 binding. Assuming that Zn^{2+} can bind to Erv1 at a molar ratio of 1:1, the dissociation constant (K_d) of zinc-binding of Erv1 is equivalent to the free Zn^{2+} concentration in the buffer when Erv1 has 50% of its oxidase activity, as such that 50% of Erv1 is in zinc-bound form (ZnErv1), and the other 50% is in zinc-free active form (apoErv1), based on Equation (1).

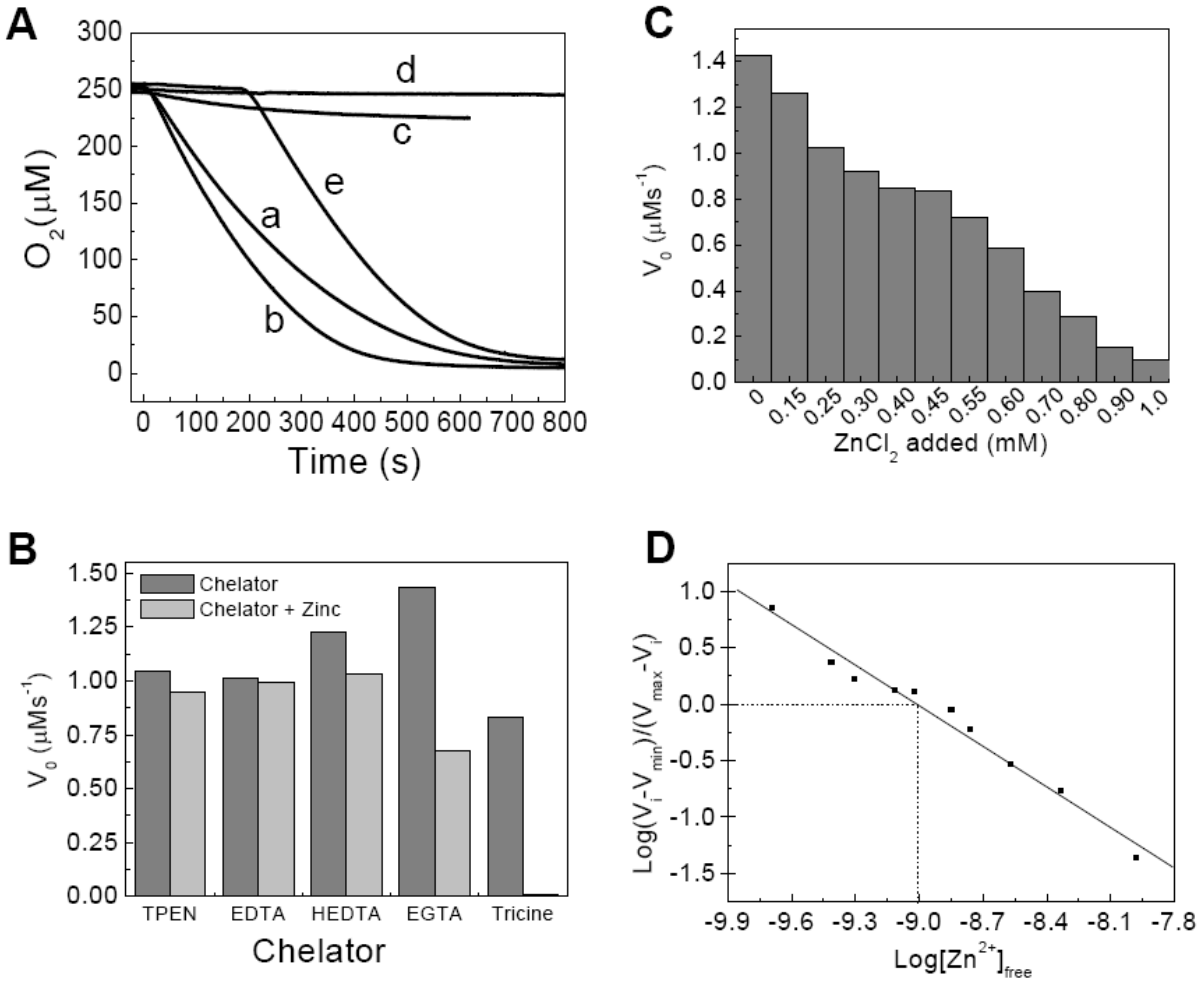

Figure 3.7 Zinc binding properties of Erv1.

A. Time courses of oxygen consumption with 2.5mM TCEP as electron donor in the presence of 1μM Erv1 WT at 25°C in all conditions: mock buffer (a), 1mM EDTA (b), 1μM (c) or 10μM $ZnCl_2$ (d,e). To chelate zinc ions, 1mM EDTA was added to at 180s (e).

B. Erv1 oxidase activities in the presence of 0.5mM $ZnCl_2$ and 1mM of different metal chelators.

C. Erv1 oxidase activities in the presence of 0-1mM of $ZnCl_2$ and 1mM of EGTA.

D. A double log Hill's plot showing the Erv1 response of free Zn^{2+} is linear with an x-intercept of -9.01 ± 0.50 at 25°C, which equals to the log of the apparent dissociation constant (log K_d = -9.01 ± 0.50, or $K_d = 9.74 \times 10^{-10}$). The free Zn^{2+} concentration in each buffer was calculated using WEBMAXC STANDARD program (http://maxchelator.stanford.edu).

$$K_d = [\text{apoErv1}] \times [Zn^{2+}]_{free} / [\text{ZnErv1}] \quad (1)$$

Firstly, a suitable chelating agent that provides a more quantitative determination of Erv1 zinc-binding affinity was selected. To screen for a wider range of Zn^{2+} concentrations, a number of metal chelators with different zinc-binding affinities (Dawson et al., 1986) were used to control the concentration of free Zn^{2+}. Erv1 oxidase activity was measured in different buffers containing 1mM of each chelating agent in the presence or absence of 0.5mM of Zn^{2+} (Figure 3.7B). Among the chelating agents tested, EGTA appeared to be the best candidate, as the Erv1 oxidase activity in the presence of Zn^{2+} was significantly different to that with the absence of Zn^{2+}. This showed that EGTA could provide a good Zn^{2+} buffer for a more accurate measurement, in comparison to the stronger Zn^{2+} chelating EDTA, HEDTA and TPEN, and the weaker tricine.

Next, to determine the apparent dissociation constant K_d of ZnErv1, the Erv1 oxidase activity was measured in the presence of various free Zn^{2+} concentrations, which were achieved by using 1mM EGTA with 0-1mM free Zn^{2+} added (Figure 3.7C). The free Zn^{2+} concentration in each buffer was calculated using WEBMAXC STANDARD program and the data were analysed based on the double log Hill's equation (Equation 2) to calculate the K_d of ZnErv1 (Figure 3.7D).

$$\text{Log}\{(V_i - V_{min})/(V_{max} - V_i)\} = \log[Zn^{2+}]_{free} - \log K_d \quad (2)$$

V_i is the observed initial rate of Erv1 oxygen consumption at different concentrations of free Zn^{2+}. V_{min} and V_{max} are the controls representing the respective initial oxygen consumption rate of ZnErv1 and apoErv1, which were measured in the buffer containing 1mM EGTA with 1 or 0 mM of Zn^{2+}. The K_d value of ZnErv1 was determined to be 9.74×10^{-10} ($\log K_d = -9.01$), which was comparable to the calculated K_d values of other strong Zn^{2+} chelators, such as EGTA (1.19×10^{-9}), HEDTA (1.27×10^{-12}) and EDTA (3.50×10^{-14}) under the same condition using WEBMAXC STANDARD program.

Taken together, these results showed that the purified Erv1 was active, with a strong zinc binding affinity, which inhibits its oxidase activity. However, how Zn^{2+} binds to Erv1 is still unknown. Importantly, based on the results, to maintain Erv1 oxidase activity, a chelating agent such as EDTA was used in the subsequent functional characterisation assays of this study.

3.6 Discussion

3.6.1 Protein folding and oligomerisation states of Erv1

All the three double cysteine mutant proteins of Erv1 can bind FAD at a molar ratio of 1:1 as that of the WT, indicating that none of the three conserved disulphides is essential for FAD-binding to Erv1. The mutant proteins revealed the same spectra profile as the WT protein with FAD absorbance maximum at 460nm, except for C130/C133S with slightly shifted absorbance at 453nm (Figure 3.3B). There was also no massive protein aggregation observed for the purified mutant proteins, except for C130/C133S upon removal of excess free FAD. The protein precipitates of C130/C133S were white, indicating the absence of FAD. It was likely that mutation of both Cys130 and Cys133 of the redox centre affects the stability of FAD binding. Nevertheless, these results overall showed that it is advantageous to use double cysteine mutants for studying the roles of each disulphide bond in Erv1, compared to with single cysteine mutant proteins in a previous study (Hofhaus et al., 2003).

It was previously shown that N-terminal deletion of Erv1 abolished protein dimerisation through disulphide bonding, and that the WT protein expressed in yeast cells formed dimers under non-reducing SDS-PAGE (Lee et al., 2000). Consistently, the same result was observed with C30/C33S mutant in this study. Therefore, the N-terminal cysteines are essential for disulphide linked dimer formation. However, light scattering data revealed that the WT Erv1 forms tetramers under native condition, indicating that there are non-covalent interactions in between protein subunits. Surprisingly, C30/C33S also formed tetramers even in the absence of disulphide linked dimer. These data suggested that in Erv1, four protein molecules maybe interacted non-covalently with or without co-existence of disulphide bond within a pair of protein subunit in the tetramer. A very recent study showed that Erv1 can only form dimer through non-covalent interactions (Bien et al., 2010). The formation of dimer, instead of tetramer was possibly due to no free FAD supplementation during the process of protein purification. It seems likely that FAD binding affected the Erv1 oligomerisation states, but how exactly excess FAD promoted tetramer formation is unknown. While it could not be excluded that tetramer formation was only observed *in vitro*, the physiological native oligomerisation state of Erv1 is yet to be investigated.

As shown by CD spectra, mutation of individual disulphides had no obvious effects on Erv1 secondary structure, except for C30/C33S mutant with a slight decreased intensity. It may be

due to the absence of intermolecular disulphide bonded dimer, or the Cys30–Cys33 disulphide may be important for the overall folding of the non-FAD-binding N-terminal domain. However, both the thermal denaturation and limited protease digestion studies showed that both disulphides (Cys130-Cys133 and Cys159-Cys176) of the C-terminus contributed to the overall stability of the protein. While C130/C133S had a decreased T_m of 53°C, C159/C176S had an even lower T_m of 38°C. A fraction of C159/C176S mutant was unfolded at a temperature as low as 25°C. Thus, this result provided a good explanation for single mutation of C159S that resulted in a temperature sensitive phenotype in yeast that could grow at 24°C, but not at 37°C (Hofhaus et al., 2003).

3.6.2 The inhibitory effects of Zn^{2+} on the MIA pathway

Oxygen consumption of Erv1 in the presence or absence of Zn^{2+} and/or EDTA showed that Zn^{2+} is a strong inhibitor of the oxidase activity of Erv1. Consistently, Zn^{2+} also had a similar inhibition effect on the yeast sulphydryl oxidase Erv2 (Wang et al., 2007), suggesting that Zn^{2+} might have a general inhibitory effect on the activity of sulphydryl oxidases. An increase of Erv1 oxidase activity by ~28% in the presence of metal chelator, compared to that in the mock buffer that contained trace amount of Zn^{2+} suggested that Erv1 had a very high affinity towards zinc binding. Assuming that Zn^{2+} can bind to Erv1 at 1:1 ratio, the K_d of ZnErv1 was measured to be 9.74×10^{-10}, which was very close to the K_d of ZnTim10 (8.00×10^{-10}) in a previous study (Ivanova et al., 2008). The similar affinity of Erv1 and small Tim proteins towards zinc supported the hypothesis that small Tim proteins are imported into the mitochondrial IMS in an apo form, rather than Zn^{2+}-bound form (Morgan et al., 2009). Otherwise, Zn^{2+} can impair the Erv1 activity and the entire MIA pathway. Consistently, a recent study suggested that Hot13 in the IMS may promote Mia40 oxidation by Zn^{2+} removal (Mesecke et al., 2008). Therefore, it was likely that Zn^{2+} may bind to the reduced cysteines of Mia40. Likewise, Zn^{2+} may inhibit reduced Erv1 from being regenerated/reoxidised by binding to the reduced cysteines of Erv1, probably Cys30-Cys33 on the N-terminal domain that may function as a shuttle disulphide. Since the availability of free zinc in the mitochondria is present at nanomolar to picomolar scale (Peck Jr and Ray Jr, 1971, Atar et al., 1995, Simons, 1991), how Zn^{2+} is regulated under different physiological conditions that interferes with Erv1 activity and the overall MIA pathway *in vivo* are still unknown.

Nevertheless, to optimise the oxidase activity of Erv1, removal of Zn^{2+} is required, thus 1mM EDTA was used in all the assays for studying Erv1 oxidase function.

3.7 Conclusions

The WT and the three individual disulphide bond mutant proteins of Erv1 purified in this study were correctly folded, as judged by FAD binding, CD and absorbance spectroscopy. The disulphide bonds at the C-terminal domain played a structural role that contributed to the overall protein stability, especially the long range disulphide Cys159-Cys176. The WT was also shown to be enzymatically active, and its oxidase activity can be strongly inhibited by Zn^{2+}-binding. An optimal oxidase activity can be obtained in the presence of a chelating agent, such as EDTA. Overall, the studies of this chapter provided good quality starting materials and essential information for subsequent *in vitro* assays to study the functional roles of each disulphide bond, as described in the next chapter.

4. RESULTS AND DISCUSSION II: FUNCTIONAL ROLES OF DISULPHIDE BONDS OF ERV1

4.1 Introduction

From the results obtained from the last chapter, it is now clear about the roles of each disulphide bond in Erv1 that contributes to the spectrometric properties, oligomerisation states and folding of the protein. In this chapter, the functional roles played by the individual disulphide bonds will be addressed. A wide range of approaches involving *in vitro*, *in vivo* and *in organello* techniques were used to understand this issue comprehensively.

The effects of individual disulphide mutation on Erv1 enzymatic function were studied using the oxygen consumption assays. Both small molecules (DTT and TCEP) and native protein substrate (Mia40) were used as electron donors for Erv1 to systematically dissect the functional roles of each disulphide bond, as opposed to previous studies (Lee et al., 2000, Hofhaus et al., 2003) that only used non-native substrates (DTT and reduced lysozyme).

In addition to enzymatic function, the roles of individual disulphides in the biogenesis of Erv1 were investigated. Erv1 has been shown to use the MIA pathway for protein biogenesis, and its import into the mitochondrial IMS is redox-regulated (Gabriel et al., 2007, Terziyska et al., 2007). It has been claimed that cysteines in both the CXXC motifs are essential for Erv1 mitochondrial import, even though the import level of Erv1 with mutations in the CXXC motif was not significantly different to that of the WT protein (Terziyska et al., 2007). To address this question, roles of individual cysteine motifs in Erv1 protein biogenesis were studied by comparing the mitochondrial import levels of the WT to the double cysteine mutant proteins.

Finally, the effects of individual disulphide bond mutation in Erv1 on yeast cell viability were studied to verify the roles of individual disulphides in enzymatic function and protein biogenesis of Erv1 obtained based on *in vitro* and *in organello* assays.

4.2 Effects of individual disulphide mutation on Erv1 oxidase activity using DTT as substrate

The roles of individual disulphide bonds in the oxidase function of Erv1 were studied using oxygen consumption assays. First, the commonly used reducing agent DTT was employed as the electron donor for the WT and double cysteine mutant proteins. The WT Erv1 started to consume oxygen immediately when DTT was added (Figure 4.1A, black curve). The k_{cat} was determined to be 1.3 ± 0.1 s^{-1}, which was ~50% higher than those reported previously (Hofhaus et al., 2003, Dabir et al., 2007). The K_m for molecular oxygen was determined to be 57μM (Figure 4.1B and Table 4.1). Different effects on the oxidase activity were observed with the three double cysteine mutants. As expected, the active site C130S/C133S mutant showed no or very little activity (Figure 4.1A, green curve), similar to that of a previous study using single cysteine mutants (Hofhaus et al., 2003). Interestingly, the N-terminal disulphide mutant C30S/C33S (Figure 4.1A, red curve) showed ~15% higher oxidase activity (k_{cat}= 1.5 ± 0.1 s^{-1}) than that of the WT enzyme. This was in contrast with a previous study using the corresponding single cysteine mutants showing only ~30–50% activity of the WT enzyme (Hofhaus et al., 2003). For the C159S/C176S mutant, a decreased activity was observed (Figure 4.1A, blue curve), and the k_{cat} and K_m values were determined to be 0.8 s^{-1} and 87μM, respectively (Table 4.1). The enzyme specificity, ratio of k_{cat}/K_m for the WT and C30S/C33S was the same ($2.3 \times 10^4\ M^{-1}\ s^{-1}$), which was similar to those of Ero1 proteins ($4–8 \times 10^4\ M^{-1}\ s^{-1}$) (Gross et al., 2006, Wang et al., 2009). Taken together, these results showed that by using DTT as substrate, only Cys130–Cys133 disulphide is required for the oxidase activity of Erv1, confirming that it is the active site disulphide.

4.3 Both Cys30-Cys33 and Cys130-Cys133 disulphides are required for Erv1 oxidase activity towards its physiological substrate

Since DTT is a strong reductant, and an artificial electron donor for Erv1, it might not reduce Erv1 disulphides in a physiological relevant manner. Therefore, it is important to know whether all three disulphides are essential for the oxidase activity towards Erv1's native substrate protein Mia40. Thus, the partially reduced Mia40c (Mia40c-pR), with the cysteines of CPC in the reduced form and CX_9C motifs in the oxidised form, was prepared and used as an electron donor for Erv1. Oxygen consumption of 50μM Mia40c-pR in the presence of

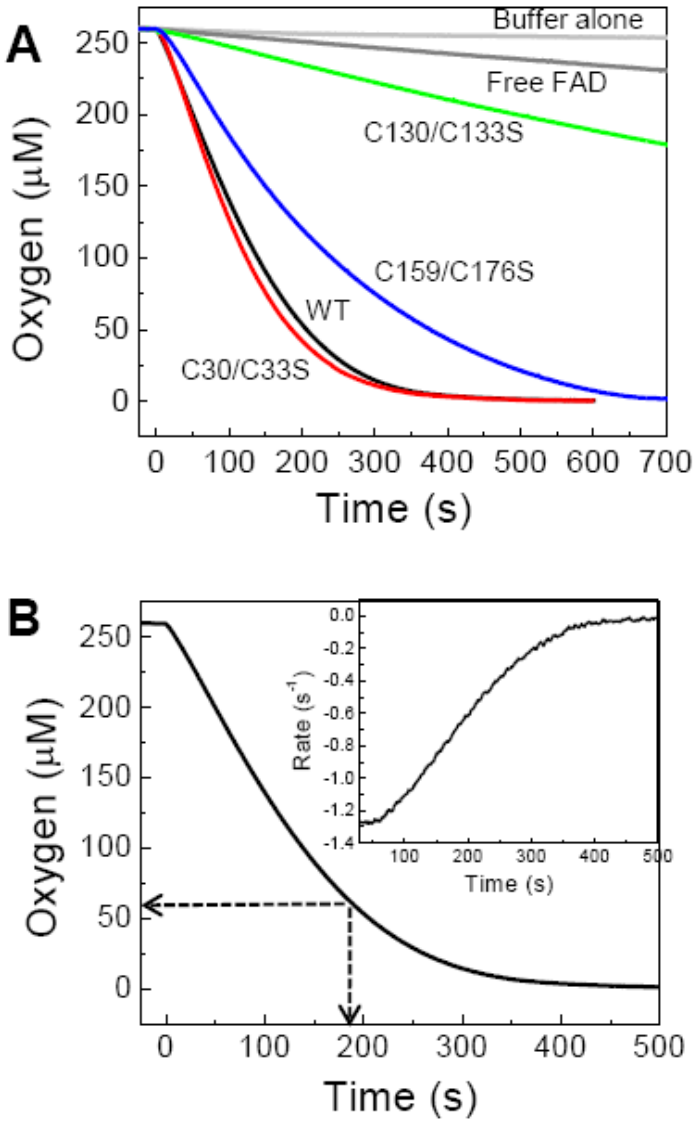

Figure 4.1 Oxygen consumption of DTT catalysed by the WT and double cysteine mutants of Erv1.

A. Oxygen consumption profiles of 10mM DTT in the presence of 1μM of the WT (black), C30/C33S (red), C130/C133S (green), and C159/C176S (blue), respectively, and two controls of 10mM DTT in the buffer (50mM Tris, pH7.4 150mM NaCl, 1mM EDTA) alone (light grey) or plus 1μM free FAD (dark grey). For all measurements, DTT was injected to pre-equilibrated samples at 25°C at the time zero.

B. Oxygen consumption of 10mM DTT catalysed by the WT Erv1 and the time course of the rate change (inset) to show how k_{cat} and K_m were determined.

Table 4.1: Oxygen consumption kinetic parameters for the WT and double cysteine mutants of Erv1 using 10mM DTT as substrate.

Erv1	k_{cat} (s^{-1})	K_m (μM)	k_{cat}/Km (M^{-1} s^{-1})
WT	1.3±0.1	57±4	$2.3±0.2×10^4$
C30/C33S	1.5±0.1	62±5	$2.4±0.2×10^4$
C130/C133S	<0.1	-	-
C159/C176S	0.8±0.1	87±8	$9.2±0.2x10^3$

All experiments were carried out with 1μM Erv1 proteins in 50mM Tris buffer pH 7.4, 150 mM NaCl, 1mM EDTA, at 25°C. The error bars represent standard errors, n=3.

1μM WT or mutant Erv1 was measured. As shown in Figure 4.2A, whilst both the WT (black curve) and C159S/C176S (blue curve) Erv1 could catalyse the electron transfer from Mia40 to molecular oxygen, both C30S/C33S (red curve) and C130S/C133S (green curve) mutants were inactive. The initial rates for WT and C159S/C176S were ~0.6 ± 0.1 and 0.5 ± 0.1 s^{-1}, respectively. Thus, for Mia40 oxidation, although C159S/C176S mutant had no significant affected oxidase activity, both Cys30–Cys33 and Cys130–Cys133 disulphides were required.

Furthermore, changes in the redox state of Erv1 and Mia40c were analysed in parallel using a SDS-PAGE based AMS thiol-modification assay (see Materials and Methods, Section 2.1.12). As shown in Figure 4.2B, a fraction of oxidised Mi40c (O) was observed after addition of the WT or C159S/C176S Erv1 for 0.5 min, and all of the proteins were oxidised in 5 min (Figure 4.2B, lanes 3–5 and 12–14). When C30S/C33S or C130S/C133S mutant was used, Mia40c remained in the reduced form (R), even after 20 min (Figure 4.2B, lanes 6–11). Meanwhile, the redox state changes of Erv1 were revealed by Western blotting (Figure 4.2C). Again, the same pattern of redox state changes was observed for the Erv1 and C159S/C176S Erv1 (Figure 4.2C, lanes 1–4 and 13–16), which was in agreement with the time courses of Mia40c-pR oxidation (Figure 4.2A, black and blue curves). A fraction of reduced Erv1 was detected at 0.5 min, which was reoxidised/regenerated in 5 min when all of the Mia40c-pR was oxidised. Interestingly, a species with ~37kDa corresponding to Erv1-Mia40c adduct was observed immediately as soon as Mia40c-pR was added at 0.5 min, and stayed consistently throughout the same time course (Figure 4.2C, lanes 1–4 and 13–16). For

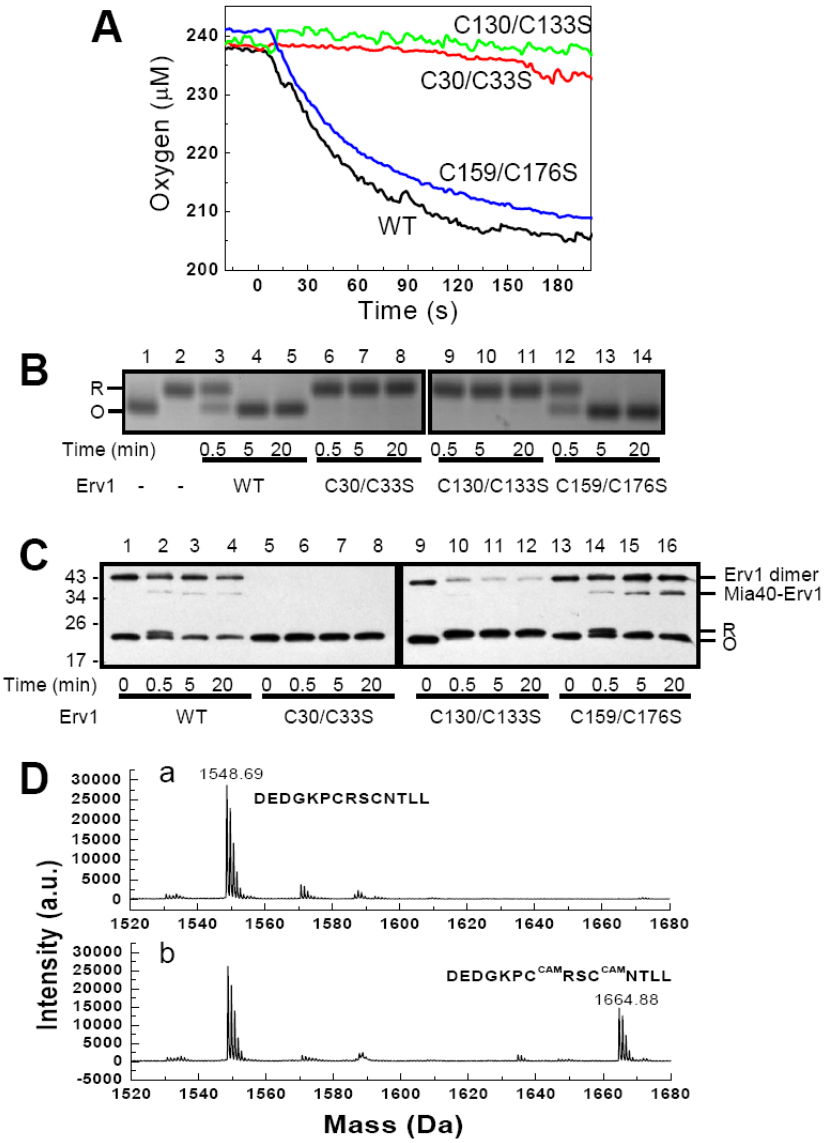

Figure 4.2 Oxygen consumption and redox state analyses of Mia40c-pR oxidation catalysed by the WT and double cysteine mutants of Erv1.

A. Oxygen consumption profiles of 50μM Mia40c-pR in the presence of 1μM the WT Erv1 (black), C30/C33S (red), C130/C133S (green), and C159/C176S (blue), respectively.

B. AMS assays of the redox state change analysis of Mia40c-pR. Mia40c was detected by coomassie-blue staining.

C. AMS assays of the redox state change analysis of the WT and mutants of Erv1. The proteins were detected by western blotting with antibody against Erv1.

D. Mass spectrometry analysis of WT Erv1 before (a) and after (b) incubation with Mia40c-pR for about 10s. The peptides containing Cys30 and Cys33 in the oxidised (1548.69 Da) or reduced and alkylated (1664.88) forms were shown.

C30S/C33S mutant, no redox state change was observed (Figure 4.2C, lanes 5-8), consistent with the observation that this mutant was inactive in oxygen consumption (Figure 4.2A, red curve). There was no Erv1-Mia40c adduct observed for this mutant (Figure 4.2C, lanes 5-8), suggesting that Cys30-Cys33 disulphide is required for interaction with Mia40. For C130S/C133S mutant, all the protein was reduced after 0.5 min and remained in the reduced form throughout the same time course (Figure 4.2C, lanes 9–12), although the mutant was enzymatically inactive (Figure 4.2A, green curve). Similar to the WT and C159/C176 mutant, the Erv1-Mia40c adduct was formed immediately with C130/C133 mutant after addition of Mia40c-pR at 0.5 min, but remained undetectable for the rest of the time course (Figure 4.2C, lanes 9–12). The instability of Erv1-Mia40c adduct in C130/C133 mutant, which could be due to a role played by the Cys130-Cys133 disulphide to stabilise the adduct, was consistent with the observation of a very recent study using *in organello* assays (Lionaki et al., 2010). Nevertheless, these results overall were consistent with the conclusion that Cys30–Cys33 acts as a shuttle disulphide, which was reduced by Mia40c-pR, and these two cysteine residues (Cys30 and Cys33) were modified by AMS. This conclusion was confirmed by proteinase digestion coupled with mass spectrometry analysis of Erv1 (Figure 4.2D) before (panel a) and after (panel b) brief incubation with Mia40c-pR. Although a peptide of 1548.69Da corresponding to 24–37 residues of Erv1 with Cys30–Cys33 disulphide bonded was identified in both samples, the same peptide with both Cys30 and Cys33 modified by iodoacetamide (1664.88 Da) was observed only in the sample mixed with Mia40c-pR.

In summary, oxygen consumption and AMS assays showed that both CXXC disulphides (Cys30–Cys33 and Cys130–Cys133) are essential for Erv1 oxidase activity towards the physiological substrate Mia40c. The $CX_{16}C$ disulphide had no obvious effect on Erv1 activity and thus was not required for Erv1 oxidase function. In addition, Cys30-Cys33 disulphide is required for interaction with Mia40 to form the Erv1-Mia40c adduct, which will be investigated further in the next chapter.

4.4 The active site disulphide Cys130-Cys133 is well protected and can be activated by Cys30-Cys33 through intermolecular electron transfer

To understand why Cys30–Cys33 is required to act as a shuttle disulphide for electron transfer from Mia40 to the redox active disulphide Cys130-Cys133 of Erv1, the oxygen

consumption experiments were repeated using TCEP as an electron donor. TCEP is a stronger reducing agent and has a slightly larger size (250Da) than DTT (154Da). In comparison with DTT, TCEP showed the same results for the two mutants: inactive C130S/C133S and decreased activity C159S/C176S mutants, respectively (compare Figures 4.1A and 4.3A). However, an opposite result was observed for the C30S/C33S mutant. While a slightly increased activity was observed with DTT (Figure 4.1A, red curve), little oxygen consumption was detected using TCEP as an electron donor (Figure 4.3A, red curve). In the absence of Cys30–Cys33 disulphide, TCEP is not a substrate for Erv1. Thus, these results showed that even TCEP could not access and reduce the active site disulphide of Erv1 directly, suggesting the active site disulphide (Cys130–Cys133) is buried and well protected. The oxygen consumption curves of TCEP oxidation were further analysed, and the k_{cat} values were determined to be 1.1 and 0.7 s^{-1} for the WT and C159S/C176S, respectively. The K_m values for oxygen were 27μM for the WT and 18μM for C159S/C176S (Table 4.2). A similar substrate specificity of 4×10^4 M^{-1} s^{-1} was obtained, which was ~2–4 times higher than that determined by using DTT (Table 4.2). Thus, TCEP is a better electron donor than DTT in terms of activation specificity. This was consistent with the finding that DTT not only can reduce Cys30–Cys33, but also Cys130–Cys133 and maybe even Cys159–Cys176; thus some enzyme activity may be lost during the assays using DTT.

Table 4.2: Oxygen consumption kinetic parameters for the WT and double cysteine mutants of Erv1 using 3.5mM TCEP as substrate.

Erv1	k_{cat} (s^{-1})	K_m (μM)	k_{cat}/Km (M^{-1} s^{-1})
WT	1.1±0.1	27±3	$4.1\pm0.3\times10^4$
C30/C33S	<0.1	-	-
C130/C133S	<0.05	-	-
C159/C176S	0.7±0.1	18±2	$3.9\pm0.3\times10^4$

All experiments were carried out with 1μM Erv1 proteins in 50mM Tris buffer pH 7.4, 150 mM NaCl, 1mM EDTA, at 25°C. The error bars represent standard errors, n=3.

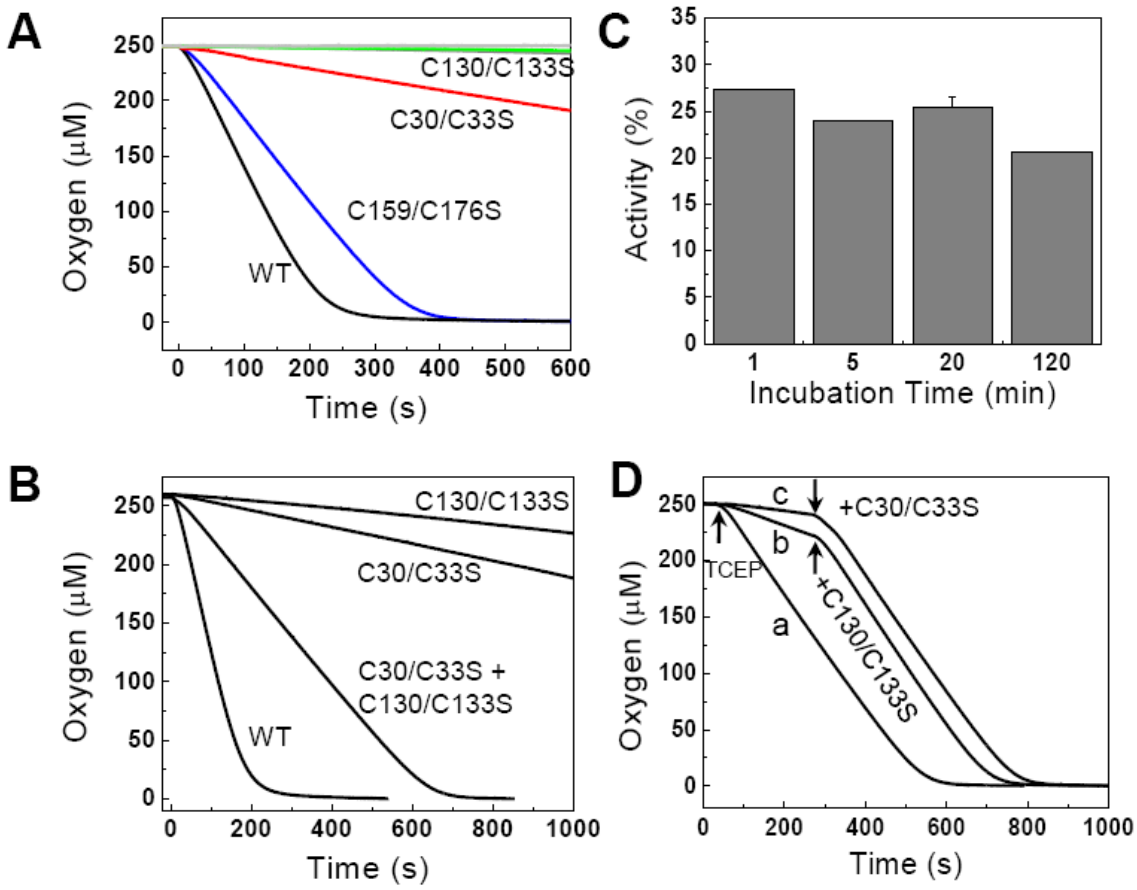

Figure 4.3 Oxygen consumption of TCEP catalysed by the WT and double cysteine mutants of Erv1.

A. Oxygen consumption profiles of 3.5mM TCEP in the presence of 1μM WT Erv1 (black), C30/C33S (red), C130/C133S (green), and C159/C176S (blue), respectively, and two controls of 3.5 mM TCEP in the buffer alone (light grey) or in the presence of 1μM free FAD (dark grey), as described for DTT in Figure 4.1.

B. Oxygen consumption of 3.5mM TCEP in the presence of a mixture of 1μM C30/C33S plus 1μM C130/C133S, or 2μM of the WT, C30/C33S, or C130/C133S, respectively.

C. The relative activity of C30/C33S plus C130/C133S plotted against the incubation time. Activity of the WT Erv1 was set as 100%.

D. Oxygen consumption of 3.5mM TCEP catalysed by 1μM C30/C33S plus 1μM C130/C133S. In curve (a), the two mutants were preincubated for 5 min before TCEP was injected. In curve (b), TCEP was injected to C30/C33S at 30s followed by addition of C130/C133S at 300s. In curve (c), TCEP was injected to C130/C133S at 30s followed by addition of C30/C33S at 300s.

Next, to confirm that Cys30–Cys33 acts as a shuttle disulphide, the activity assay was performed using TCEP as an electron donor in the presence of a total of 2μM enzyme(s): WT, C30S/C33S, or C130S/C133S alone, or a mixture of the two mutants (1μM each), respectively. As shown in Figure 4.3B, although both mutants alone were inactive, the mixture of these two mutants (preincubated for ~5 min) showed a clear oxidase activity. The rate of oxygen consumption was 0.33 ± 0.03 s^{-1}, which was ~24% of the WT enzyme (1.40 ± 0.10 s^{-1}) at the same condition (Figure 4.3B and Table 4.3). The result confirmed that Cys30–Cys33 disulphide of the C130S/C133S mutant could activate Cys130-Cys133 disulphide of the C30S/C33S mutant via intersubunit or intermolecular electron transfer. If the formation of a heteromeric species between the two mutant proteins is necessary for the activity, the activity will increase with the incubation time, which allows for scrambling of the two mutant proteins.

Interestingly, no obvious difference in the levels of activity was observed between 1, 5, and 20 min of incubation, but a slightly decreased activity was obtained when the proteins were preincubated for 2 h (Figure 4.3C). Thus, these results suggested that heteromeric formation is not required for the observed oxidase activity. To verify this, TCEP was first incubated with one of the mutants and followed by addition of the second mutant (Figure 4.3D, curves b and c). The same rate of oxygen consumption as that of preincubated proteins (curve a) was obtained as soon as the second mutant was added in both cases, indicating that intermolecular electron shuttling from Cys30-Cys33 to Cys130-Cys133 could occur without formation of a heteromeric species in between the two individually inactive mutant proteins.

Since only about a quarter (~24%) of the oxidase activity was recovered by mixing the two individually inactive mutant proteins, the hypothesis of intermolecular electron transfer mechanism in Erv1 would be further confirmed if a heteromeric form of the two mutants could recover more than 24% of the oxidase activity. As illustrated in Figure 4.4, the heteromeric mutant protein was generated by coexpression of these two mutant proteins encoded by different plasmids in *E. coli*. Both mutant proteins were individually tagged. The heteromeric mutant proteins containing both tags were purified in two steps, one after another using two different affinity beads against the individual tag. To verify whether the purified proteins were the heteromeric forms of the two mutants, the proteins were analysed by spectra measurements and Western blotting. The proteins showed a UV-visible spectroscopic profile with a maximum absorbance of bound FAD at 457nm, which was about in between

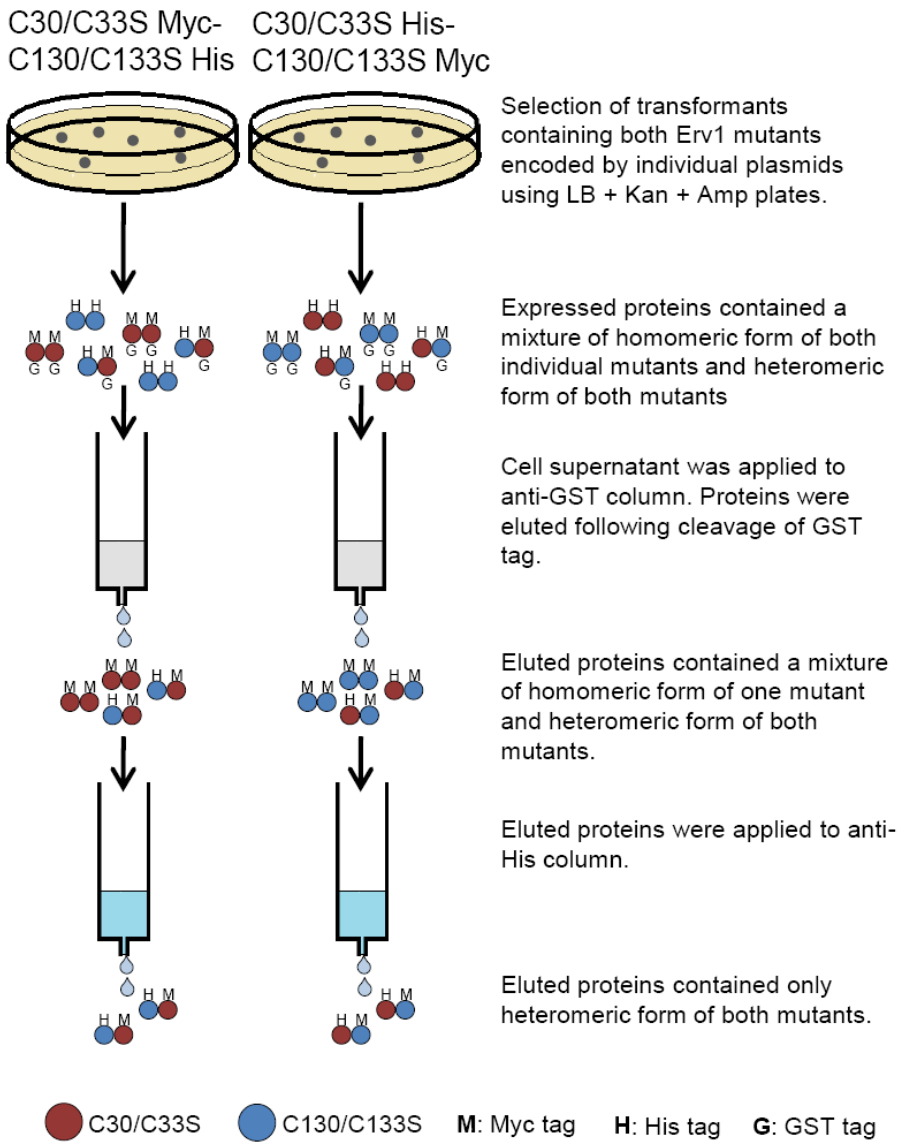

Figure 4.4 A schematic illustration of protein purification procedures of C30/C33S-C130/C133S heteromeric mutant proteins.

Individual DNA constructs coding for C30/C33 or C130/C130 mutant Erv1 were co-transformed into *E. coli* Rosetta-gami 2 cells. One of the mutant proteins contains an N-terminal GST tag and a C-terminal Myc tag, and the other contains a C-terminal 6x-His tag (see Appendix 1 for details of DNA constructs). The transformants containing both constructs were selected and used for co-expression of both mutant proteins, producing a mixture of homomeric mutant proteins (C30/C33S-C30/C33S and C130/C133S-C130/C133S) and heteromeric mutant proteins (C30/C33S-C130/C133S). The heteromeric mutant proteins, which contain both GST and His tags, were purified with anti-GST and anti-His affinity beads in two successive steps one after another.

both individual mutants (Figure 4.5A). Western blotting against the individual tags confirmed the existence of both mutants in the protein complex (Figure 4.5B). As expected, the heteromeric mutant proteins showed an increased oxidase activity of 0.54 ± 0.04 s^{-1}, which was ~39% of the WT enzyme under the same condition (Figure 4.5C, Table 4.3).

To further confirm the intermolecular interaction in between the Cys30-Cys33 and Cys130-Cys133 disulphides, Erv1N Erv1C were used. In this case, both Cys30-Cys33 and Cys130-Cys133 disulphides were located in individual molecules of N- and C- termini respectively. Firstly, oxygen consumption assays were performed using TCEP as an electron donor in the presence of WT, Erv1N alone, Erv1C alone or a mixture of Erv1N and Erv1C at equimolar concentrations (Figure 4.6A and Table 4.3). While Erv1N alone showed no oxidase activity as expected, Erv1C alone showed ~19% of oxidase activity relative to the WT enzyme. The partial activity recovery of Erv1C against TCEP indicated that in the absence of the N-terminal shuttle domain, the catalytic core of Erv1 is partially accessible to TCEP. In the presence of both N- and C-terminal domains, a higher relative oxidase activity of ~29% to the WT was recovered under the same condition, suggesting an intermolecular electron transfer from reduced Erv1N to Erv1C, although some of the oxidase activity was contributed from partial accessibility of Erv1C to TCEP. Nevertheless, to demonstrate the intermolecular electron transfer from Cys30-Cys33 disulphide to Cys130-Cys133 disulphide more directly, Erv1N with its Cys30-Cys33 disulphide reduced was used as a substrate for Erv1C and analysed by AMS assays (Figure 4.6B). About 50% of Erv1N was oxidised (O) after incubation with Erv1C for 0.5 min, and was then fully oxidised in 5 min. In the absence of Erv1C, all the Erv1N stayed in the reduced form throughout the time course. Therefore, electrons could be transferred from Cys30-Cys33 of one molecule to Cys130-Cys133 of another molecule.

Taken together, the results of this study demonstrated experimentally for the first time that Cys30–Cys33 functionally acts as a shuttle disulphide, passing electrons to the active site Cys130–Cys133 disulphide. Furthermore, electron transfer can occur between two different molecules via intermolecular interactions.

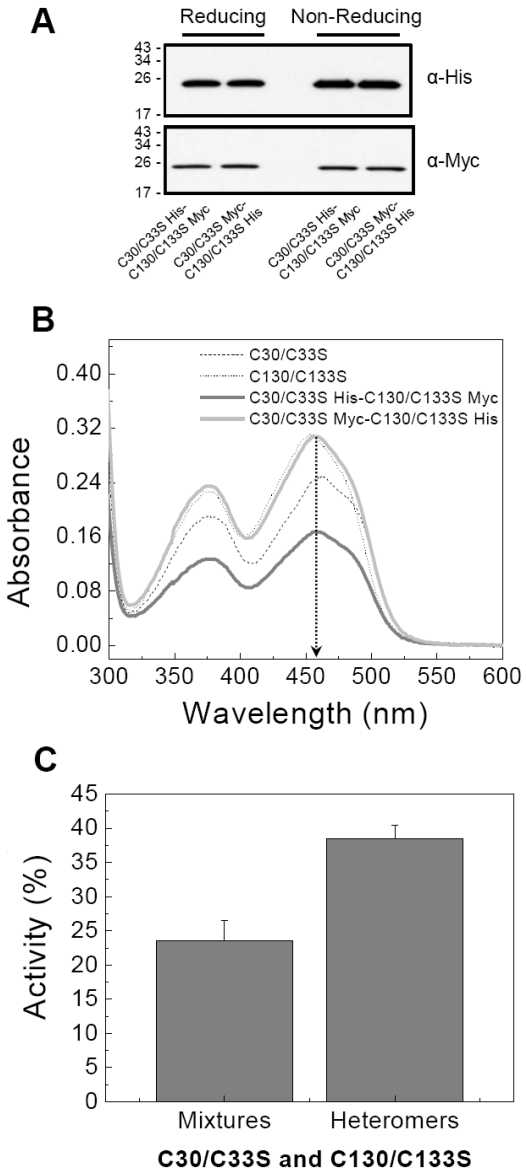

Figure 4.5 Confirmation of intermolecular interaction in between Cys30-Cys33 disulphide and Cys130-Cys133 disulphide by using C30/C33S-C130/C133S heteromeric mutant proteins.

A. Western blotting of purified heteromeric mutant proteins against the individual tags. The proteins were further purified by gel filtration on Superdex 75 column before analysis by SDS-PAGE under both reducing and non-reducing conditions.

B. Absorption spectra of heteromeric mutant proteins in 150mM NaCl, 50mM Tris, pH7.4, compared to the spectra profiles of the individual mutant proteins. The absorption maxima for protein-bound FAD of the heteromeric mutant proteins were determined to be 457nm, as indicated.

C. The relative activity of C30/C33S and C130/C133S mutant proteins in the form of mixtures (1µM each) and heteromers (2µM) normalised to that of the WT (2µM) as 100%. The oxidase activity was measured by oxygen consumption assays using 3.5mM TCEP as substrate. Error bars represent standard error, n=3.

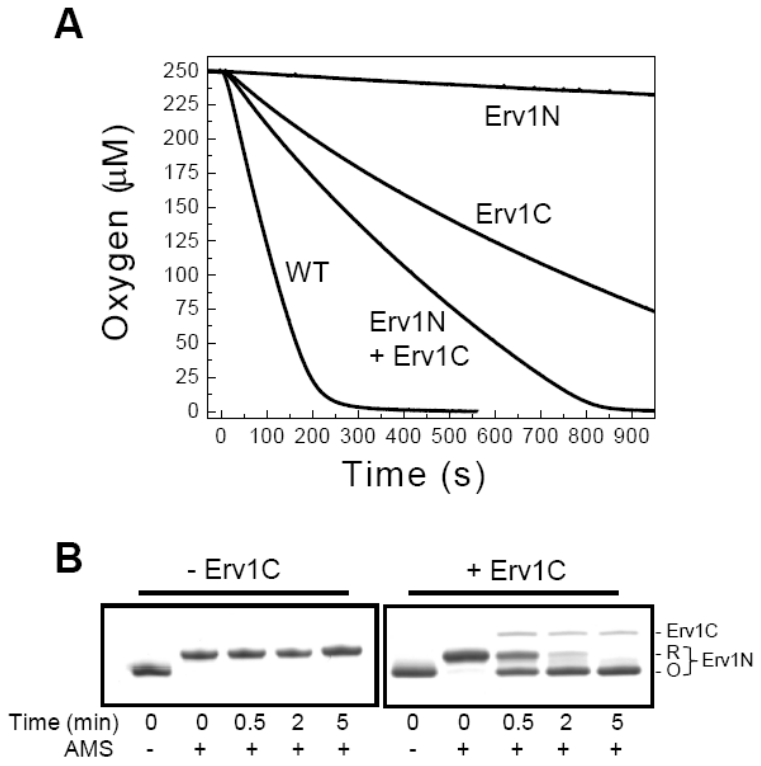

Figure 4.6 Further confirmation of intermolecular interaction in between Cys30-Cys33 disulphide and Cys130-Cys133 disulphide by using N- and C-terminal domains of Erv1.

A. Oxygen consumption of 3.5mM TCEP in the presence of 2μM of Erv1N alone, Erv1C alone or a mixture of 2μM each of Erv1N and Erv1C, compared to the oxygen consumption profile of 2μM WT Erv1 under the same condition.

B. AMS assay of the redox state change of 50μM Erv1N in the absence or presence of 5μM Erv1C. The proteins were detected by by coomassie-blue staining. The oxidised (O) and reduced (R) forms of Erv1N were indicated.

Table 4.3: Oxidase activities of the WT and mutants of Erv1 at a total concentration of 2μM using 3.5mM TCEP as substrate.

Erv1	k_{cat} (s^{-1})	Relative activity (%)
WT	1.40 ± 0.10	100
Mixtures of C30/C33S and C130/C133S	0.33 ± 0.03	24 ± 2
Heteromers of C30/C33S and C130/C133S	0.54 ± 0.04	39 ± 3
Erv1N	<0.05	-
Erv1C	0.26 ± 0.03	19 ± 2
Mixtures of Erv1N and Erv1C	0.41 ± 0.01	29 ± 1

All experiments were carried out in 50mM Tris buffer pH 7.4, 150 mM NaCl, 1mM EDTA, at 25°C. The error bars represent standard errors, n=3.

4.5 The $CX_{16}C$ cysteines are required for biogenesis of Erv1 in mitochondria

It was shown that biogenesis of Erv1 uses the redox sensitive MIA import pathway (Gabriel et al., 2007, Terziyska et al., 2007). While previous studies showed that individual mutation of Cys30, Cys33, Cys130 and Cys133 had no obvious effect on Erv1 import (Terziyska et al., 2007), the cysteine residue that is directly involved in the import of this protein has not been shown. Therefore, effects of the double cysteine mutants on the mitochondrial import of Erv1 were investigated. The ^{35}S-labelled precursor proteins of WT and mutant Erv1 were incubated with WT mitochondria at 30°C followed by trypsin treatment at indicated time points to quench the import reactions by digesting the unimported materials. The import level of the proteins was analysed by SDS-PAGE and autoradiography (Figure 4.7A and B). A 10% standard of individual precursor protein was used to calculate the import level of the corresponding protein, which was then normalised to that of the WT Erv1 set as 100%. The relative import level was about 57% for C30/C33S, 159% for C130/C133S, and 25% for C159/C176S (Figure 4.7C). These indicated that, while mutation of Cys30-Cys33 and Cys159-Cys176 disulphides had inhibitory effects on the import, mutation of Cys130-Cys133 disulphide resulted in an enhanced level of mitochondrial import. A significant decrease in the import level was observed for C159/C176S, suggesting the important roles of cysteines in $CX_{16}C$ motif for Erv1 biogenesis. This was further confirmed by the results of the

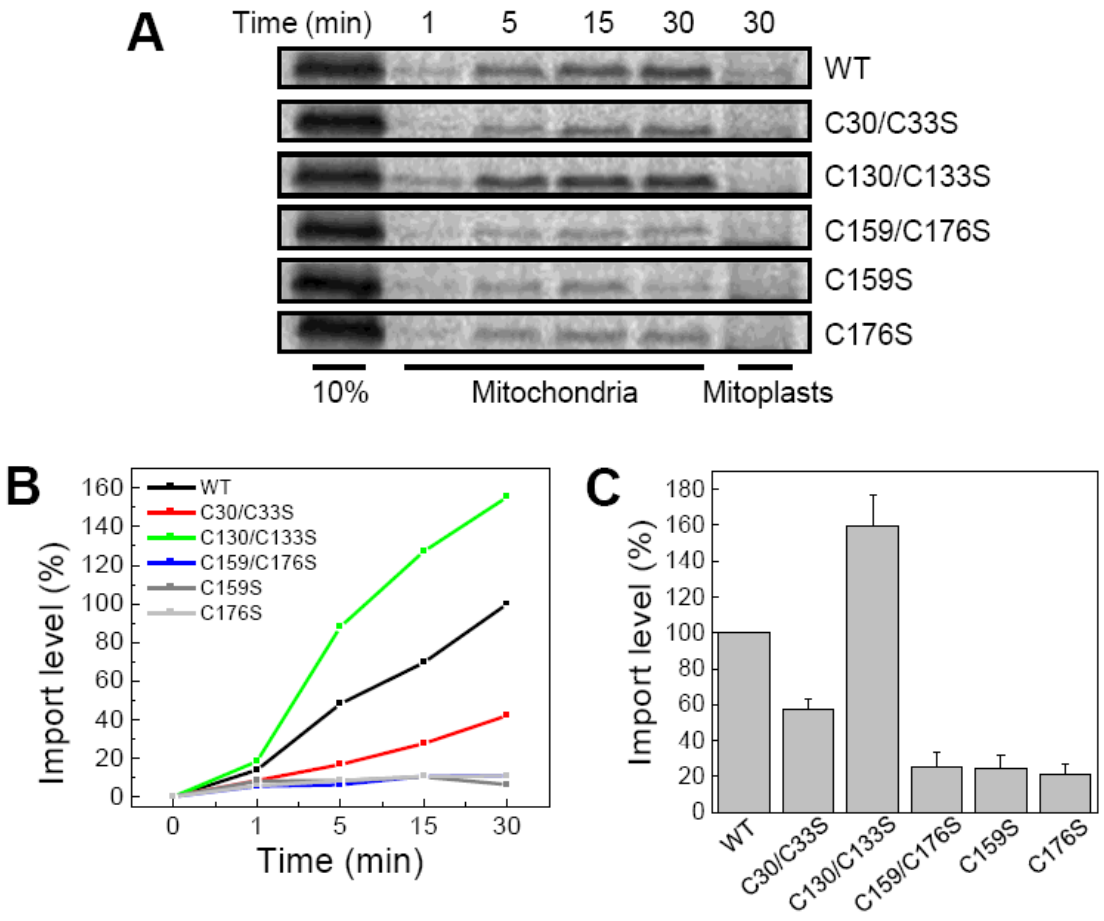

Figure 4.7 Mitochondrial import of ^{35}S-labelled WT and mutant Erv1.

A. SDS-PAGE analysis of 10% of the precursors (10%) and the mitochondrial imported proteins by time course from 1 minute to 30 minutes. Mitoplasts were re-isolated by 0.1% digitonin treatment on ice for 3 minutes before trypsin treatment.

B. Quantification of imported Erv1 as in A.

C. Relative import levels of the mutants normalised to that of the WT Erv1 as 100%. Error bars represent standard error, n=5

corresponding single cysteine mutants C159S and C176S showing similar import levels to that of the double cysteine mutant (Figure 4.7A-C).

4.6 All three disulphide bonds of Erv1 are essential for cell viability in yeast

To check the physiological relevance of the results obtained by *in vitro* and *in organello* approaches, the roles of each disulphide bond in Erv1 were tested genetically in yeast by using a *tet*O promoter regulated *ERV1* strain. An advantage of using *tet*-regulatable promoter system is that, the target gene expression is tightly regulated by doxycycline which does not alter growth medium composition as in the *GAL* system. Therefore, the overall cell metabolism remains unaffected and the transcriptional regulation is only specific to the genes being studied (Wishart et al., 2005).

To demonstrate that the *ERV1* gene expression is regulatable in the *tet*O promoter regulated *ERV1* strain, the phenotype of the constructed strain was spot-tested on YPD media in the presence or absence of doxycycline at 30^{o}C (Figure 4.8A). In the absence of doxycycline, the *tet*O promoter regulated *ERV1* strain was as viable as the wild type strain (Figure 4.8A, left panel). However, it became less viable when doxycycline was added (Figure 4.8A, right panel). Despite the fact that *ERV1* is an essential gene for cell viability (Lisowsky, 1992), the cell could still survive to a certain extend. It was possibly due to the residual Erv1 expressed from the stock culture in the absence of doxycycline, and/or incomplete *ERV1* gene suppression by doxycycline. The presence of a minute quantity of Erv1 enzyme, which is not required in a large quantity to maintain the cellular function as for other essential proteins like Mia40, would therefore result in a certain extend of cell viability.

Next, to test the effect of individual disulphide bond mutation of Erv1 on cell viability, the *tet*O promoter regulated *ERV1* strain carrying plasmid coding for the WT and the corresponding double cysteine mutants were spot-tested on SD media at 25^{o}C and 37^{o}C (Figure 4.8B). The cell viability of the strain itself without any plasmid copy of *ERV1* in the absence of doxycycline was used as a background (negative control). At 25^{o}C (left panel), the background strain had a very similar growth and was viable, both in the presence or absence of doxycycline. As a result, the effect of individual disulphide mutation on cell viability was undetectable at 25^{o}C. Therefore, the experiment was repeated at an elevated

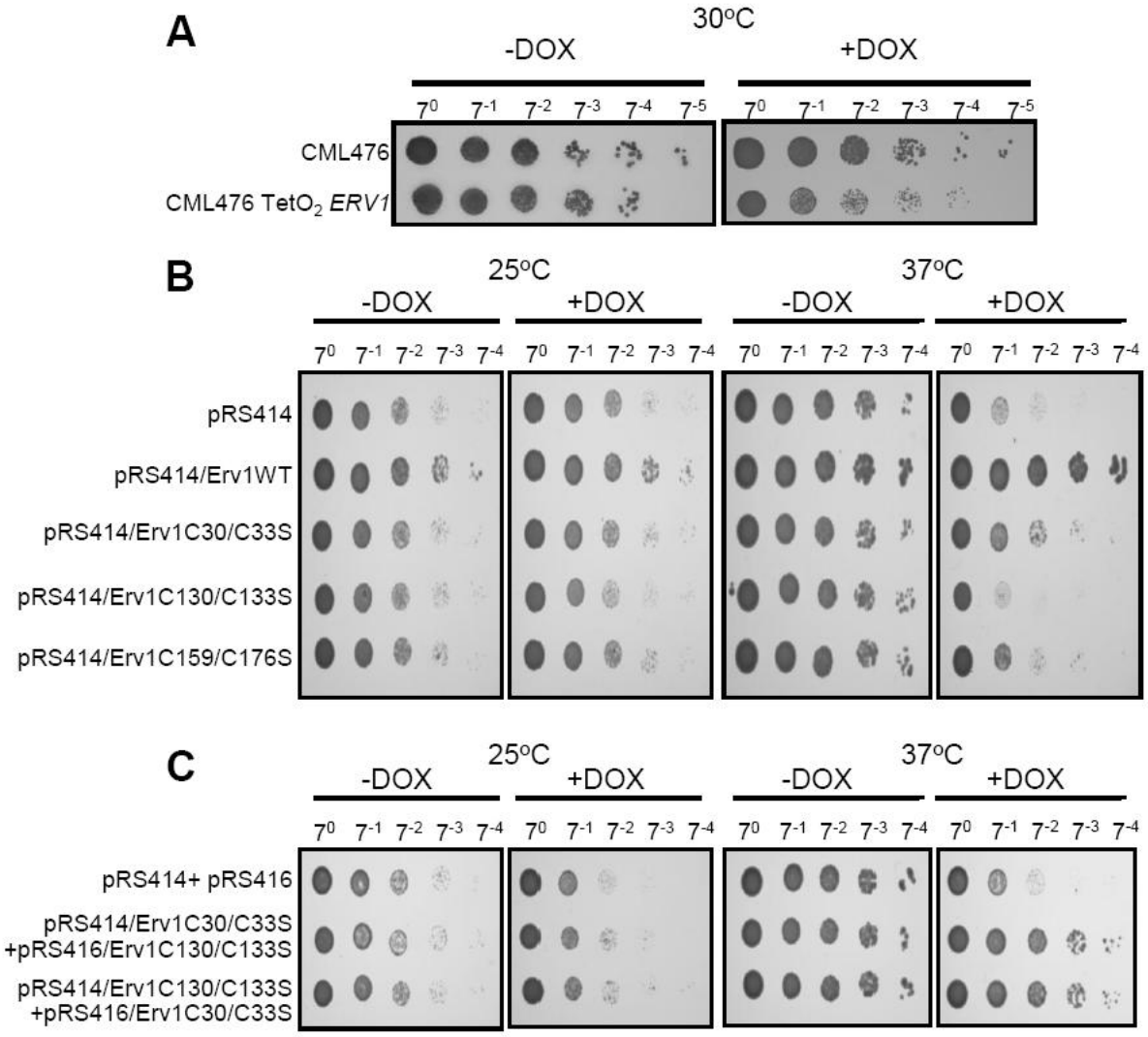

Figure 4.8 Cell viability tests of *tet*O_2 promoter regulatable *ERV1* yeast strains.

A. Phenotype testing of the constructed *tet*O_2 *ERV1* strain. Cells were grown at 30°C in YPD media until stationary phase before dilution to OD_{600}= 1, and followed by 1/7 serial dilutions using fresh YPD media. Diluted cells were spotted onto YPD plates with or without 50µg/ml of doxycycline (DOX) and incubated at 30°C for 48 hours. The original strain CML476 treated in the same manner was used as control.

B. The effects of Erv1 individual disulphide mutation on cell viability. The constructed *tet*O_2 *ERV1* strain individually transformed with pRS414 plasmids encoding for the WT or individual disulphide mutant gene of *ERV1* were grown at 30°C in SD –Trp media until stationary phase. Cells were diluted as in A using fresh SD –Trp media and spotted onto the same media with or without 50µg/ml of DOX. Cells were incubated at 25°C or 37°C for 48 hours. The *tet*O_2 *ERV1* strain carrying pRS414 plasmid alone was used as control.

C. The effects of C30/C33S and C130/C133S mutant co-expression on cell viability. The strains carrying both C30/C33S and C130/C133S mutant alternately encoded by pRS414 or pRS416 plasmids were treated in the same manner as in B, but using SD –Trp –Ura media to maintain both plasmids.

temperature of 37^{o}C (right panel). The cell was not viable in the presence of doxycycline at higher temperature, suggesting that this strain was temperature-sensitive. While the plasmid coding for WT *ERV1* rescued the cell viability, all the mutants failed. This was consistent with the *in vitro* and *in organello* results that all the three disulphide bonds of Erv1 play important roles in enzymatic function (Cys30-Cys33 and Cys130-Cys133), protein stability (Cys159-Cys176) or mitochondrial import (Cys159-Cys176).

Finally, to demonstrate an interaction between the Cys30-Cys33 disulphide and the Cys130-Cys133 disulphide in the cell, the phenotype of the strain carrying both C30/C33 and C130/C133 mutants encoded by different plasmids were tested (Figure 4.8C). At 37^{o}C, co-expression of both mutants rescued cell viability to a significant level (right panel), which was in agreement with *in vitro* results that mixing/scrambling of both mutants could resume Erv1 oxidase activity.

4.7 Discussion

4.7.1 The functional mechanism of Erv1

Studies of this chapter provided direct experimental evidence to show that the N-terminal Cys30-Cys33 disulphide is required to shuttle electrons from the physiological substrate Mia40 to the active site Cys130-Cys133 disulphide. Most previous *in vitro* studies on the function of FAD-dependent sulphydryl oxidases used model substrates (e.g. DTT, reduced lysozyme or *E coli* thioredoxin). In this study, both artificial substrates (DTT, TCEP) and the physiological substrate, partially reduced Mia40, were used to address the functional mechanism of Erv1. The results showed that the active-site disulphide of the WT Erv1 is accessible to DTT but not to TCEP and Mia40. Thus, in terms of biological relevance, TCEP is a better small molecule than DTT as substrate for Erv1. The C30/C33S mutant was more active than the WT towards DTT oxidation but was enzymatically inactive towards Mia40c and TCEP oxidation. Together with the fact that TCEP is a stronger reductant and larger (250 Da) than DTT (154 Da), the results suggested that the active-site disulphide is highly protected. It is not accessible to both Mia40 and TCEP in full-length proteins. The standard redox potential for Erv1 active site disulphide (Cys130-Cys133) has been determined to be of -150 mV (Dabir et al., 2007). The redox potentials for the mitochondrial IMS, GSH, and DTT

were determined to be of -255, -240 and -330 mV, respectively (Hu et al., 2008, Rothwarf and Scheraga, 1992), and an even lower value for TCEP was predicted (Krezel et al., 2003). Accordingly, the active site disulphide of Erv1 would be thermodynamically unstable in the IMS or against any of above thiol reducing reagents if it was not well protected. The inaccessible nature of the active site disulphide can also explain why DTT is a poor substrate for all members of ERV/ALR and Ero1 families in general. The conclusion was also in agreement with the finding that GSH was not a good substrate for Erv1 (results not shown) and other ERV enzymes, because GSH is not only a weaker reductant, but also a larger molecule (307Da) than TCEP. Thus, Cys30-Cys33 disulphide is required to serve as a shuttle disulphide to transfer electrons from substrate to the active-site Cys130-Cys133 disulphide.

4.7.2 Intermolecular electron transfer mechanism of Erv1

It was shown in this study that the Erv1 oxidase activity was partially recovered after mixing of the two individually inactive mutants, C30/C33S and C130/C133S (Figure 4.3B). The immediate recovery of only about 24% to that of the WT Erv1 enzyme activity suggested that the electron transfer from the shuttle Cys30-Cys33 disulphide to the active site Cys130-Cys133 disulphide had occurred via intermolecular rather than intersubunit reaction. This was confirmed by an increased activity recovery of ~39% for the C30/C33S-C130/C133S heteromeric mutant, and also the *in trans* oxidation of reduced Erv1N by Erv1C demonstrated in this study. Consistently, two recent studies also showed the intermolecular interaction in between the shuttle and active site disulphides of Erv1 using *in vivo* (Bien et al., 2010) and *in organello* (Lionaki et al., 2010) approaches. These results suggested that in the cell, Cys30-Cys33 disulphide can shuttle electrons to Cys130-Cys133 disulphide through both intersubunit and intermolecular reactions as illustrated in Figure 4.9. Similarly, for Ero1 a mechanism of both intra and intermolecular electron transfer has been suggested (Sevier and Kaiser, 2006b). Unlike Ero1, all known ERV/ALR enzymes form stable dimer or oligomers (Gross et al., 2002, Wu et al., 2003, Vitu et al., 2006). From the current understanding, the electron transfer mechanism in ERV/ALR enzymes only occurs through intersubunit interaction. The intermolecular electron transfer mechanism of Erv1 demonstrated in this study raised an interesting question about the physiological relevance for the oligomerisation

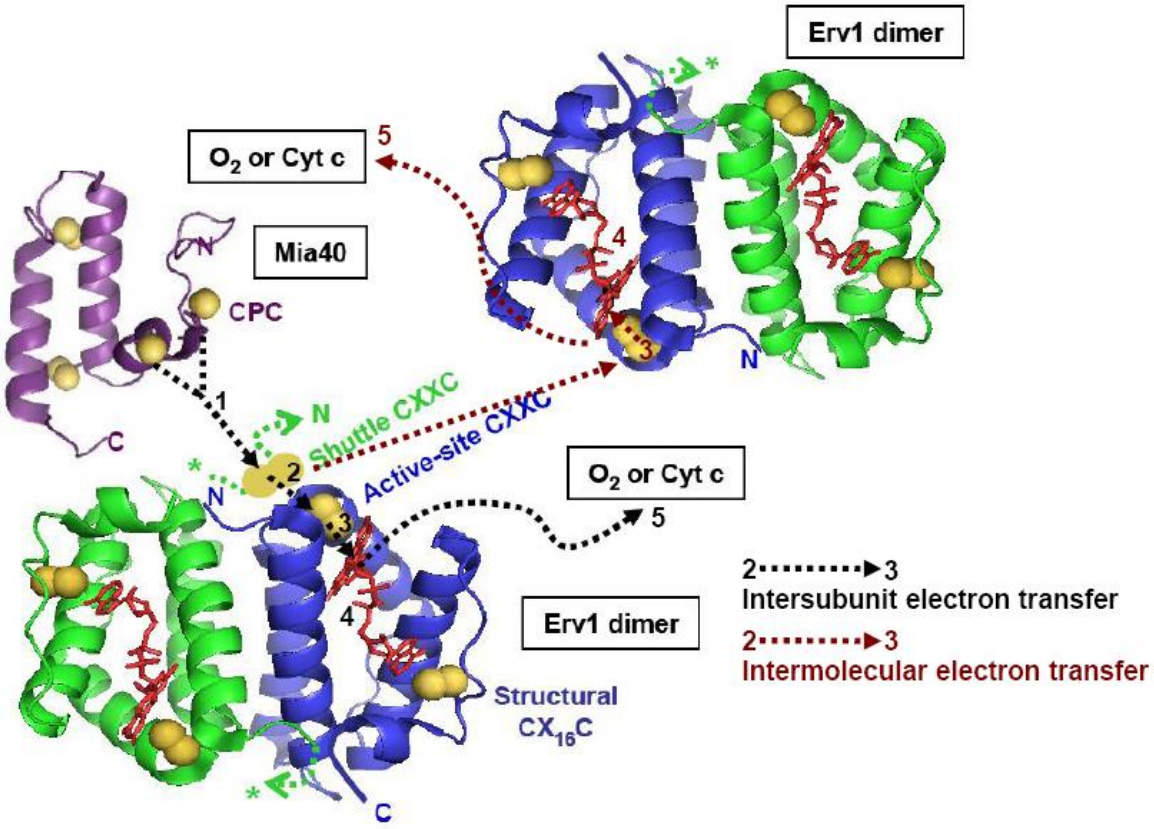

Figure 4.9 The electron transfer mechanisms of the MIA pathway.

Electrons are transferred from the reduced CPC cysteines of Mia40 to the N-terminal shuttle CXXC (Cys30-Cys33) disulphide of Erv1 (1→2). The reduced shuttle disulphide, after receiving electrons from Mia40, can alternatively transfer electrons to the active-site CXXC (Cys130-Cys133) disulphide of the other Erv1 subunit (2→3, black arrow) or other Erv1 molecule (2→3, red arrow). Subsequently, electrons are transferred from the reduced active-site disulphide to FAD (3→4), which then shuttles electrons to molecular oxygen or cytochrome c (Cyt c) (4→5).

requirement for Erv1. Therefore, the relationship between the native oligomerisation state and functional mechanism of Erv1 in the cell is still to be discovered.

4.7.3 A possible regulatory role of the N-terminal Cys30-Cys33 disulphide

The data from this study also suggested that Cys30-Cys33 disulphide and/or the flexible N-terminal region may play a role in regulating the accessibility of the active site disulphide through a conformation change induced by interacting with Mia40 and thiol/disulphide exchange. Based on the CD measurements, a clear conformation change was observed for the N-terminal C30/C33S mutant (Figure 3.4A), suggesting that a conformation change may occur in the flexible N-terminal region upon reduction of Cys30-Cys33 disulphide. Consistently, the important role of the flexible N-terminal region in regulating the accessibility of active site disulphide in the catalytic core is supported by the observation that TCEP is partially accessible to the active site disulphide of Erv1C (Figure 4.6A), but not to that of the full-length C30/C33S (Figure 4.3A). Thus, the Erv1 N-terminal region may play a protection role in mediating the accessibility of the active site disulphide. In this way, the oxidase activity of Erv1 can be regulated effectively and specifically, whilst circumventing or limiting non-specific and harmful oxidation of protein thiols. Recently, a similar regulatory role played by a disulphide was demonstrated for both yeast Ero1p and human Ero1α (Sevier et al., 2007, Baker et al., 2008, Appenzeller-Herzog et al., 2008). These regulatory disulphide bonds are among the non-conserved disulphides of Ero1 proteins. Whilst Erv1 has only three conserved disulphides, the location and the spacing between the two cysteine residues of the only shuttle disulphides (CX_nC, n=1, 2, or 4) are not strictly conserved among the ERV/ALR enzymes (Figure 1.21B). Accordingly, this disulphide may act as a regulative disulphide with substrate specificity.

4.7.4 The targeting signal for protein import and biogenesis of Erv1

The data from mitochondrial import studies suggested that cysteine residues of the $CX_{16}C$ play an important role during the mitochondrial import of Erv1, and both cysteine residues seem required (Figure 4.7). Interestingly, the $CX_{16}C$ motif is unique and only conserved among ERV/ALR enzymes, not the structure and functionally related Ero1 and QSOX

proteins. Consistently, except for Erv2, ERV/ALR enzymes are mainly located in the mitochondrial intermembrane space. Therefore, in addition to CX_3C and CX_9C motifs, proteins with $CX_{16}C$ motif may represent a new category of MIA substrates. Substrate recognition by Mia40 may occur in different orientations, depending on the substrate category. For small Tim proteins with CX_3C motifs, substrate binding to Mia40 strictly depends on the most N-terminal cysteine (Milenkovic et al., 2007, Sideris and Tokatlidis, 2007); whereas for Cox17 protein families with CX_9C motifs, C-terminal cysteines are important for recognition by Mia40 (Sideris et al., 2009). Therefore, Erv1 may be recognised by Mia40 in a very similar mechanism to those of Cox17 proteins, since the $CX_{16}C$ motif of Erv1 is located at the C-terminus of the protein and Cys176 is only 13 amino acids away from the end of the polypeptide chain. Apart from cysteines of $CX_{16}C$ motif, the N-terminal cysteines may play a role during import of Erv1 as well, as a decreased level of import (57%) was observed for C30/C33S mutant. Interestingly, the active site disulphide mutant C130/C133S showed a significant increase in the level of mitochondrial import compared with the WT Erv1. Since oxidative folding can compete with mitochondrial import of the IMS small Tim proteins (Morgan and Lu, 2008), the more effective import of C130/C133S mutant suggested that the precursor maybe unfolded or more resistant to oxidative folding than the WT Erv1 under the experimental conditions. Overall, while mutation of individual disulphide bond affects Erv1 mitochondrial import differently, the mechanism of how exactly Erv1 is imported into the mitochondria is still unclear. It seems that the two cysteines of the $CX_{16}C$ motif are required for import, but it still cannot be excluded from the possibility that the imported mutant proteins are unstable (see Results and Discussion, Section 3.4) and subsequently susceptible to degradation in the mitochondria. The mitochondrial targeting signals (MISS/ITS) that confer substrate recognition by Mia40 have recently been discovered in small Tims and Cox17 (Milenkovic et al., 2009, Sideris et al., 2009). The docking cysteine and MISS/ITS in Erv1 are still yet to be recognised.

4.8 Conclusions

In summary, by using *in vitro* assays coupled with *in organello* and *in vivo* approaches, it was demonstrated that all three pairs of disulphide bonds of Erv1 play essential but different roles in the function and biogenesis of the protein. While the N-terminal CXXC motif (Cys30-

Cys33) acts as shuttle disulphide and regulation of the accessibility of the active site disulphide (Cys130-Cys133), the C-terminal $CX_{16}C$ motif plays important roles in both protein folding and mitochondrial import of Erv1. The well protected active site disulphide (Cys130-Cys133) requires the shuttle disulphide (Cys30-Cys33) to transfer electrons from substrate, and both intersubunit and intermolecular transfer can occur.

5. RESULTS AND DISCUSSION III: INTERACTION BETWEEN ERV1 AND MIA40, AND THE ROLE OF GSH IN THE INTERACTION

5.1 Introduction

Mia40 is the native substrate of Erv1. However, little was known about how Erv1 interacts with Mia40 at the beginning of this project. *In vitro* studies in the last chapter demonstrated that the shuttle disulphide (Cys30-Cys33) of Erv1 interacts directly with the CPC cysteines of Mia40 (see Results and Discussion, Section 4.3), which was supported by two very recent studies using *in vivo* and *in organello* approaches (Bien et al., 2010, Lionaki et al., 2010). Erv1 and Mia40 interact to form a Mia40-Erv1 intermediate, which was observed to be persistent and unresolved in the *in vitro* assays of Mia40c-pR oxidation by Erv1 (Figure 4.2C). This observation led to the hypothesis that the Mia40-Erv1 intermediate could be a non-productive species caused by formation of non-native disulphides. Thus, there could be a requirement for isomerisation/reduction pathway in the mitochondrial IMS to mediate the reshuffling of misformed disulphides, as those identified in the bacterial periplasm and ER (see Introduction, Section 1.6.1 and 1.6.2). In the mitochondrial IMS, an oxidoreductase that plays an isomerisation role like DsbC/DsbG in the bacterial periplasm or PDI in the ER has not been identified. Therefore, reduced glutathione (GSH) has been proposed to fulfil an isomerisation role in the mitochondrial IMS (Bien et al., 2010).

To address this hypothesis, which was the main focus of this chapter, the Mia40-Erv1 interaction was studied using purified proteins. First, the interaction between Erv1 and Mia40 was tested on the WT proteins to verify that the Mia40-Erv1 intermediate was due to mixed disulphide bond formation. Next, to understand how the Mia40-Erv1 mixed disulphide intermediate was formed, single cysteine mutant proteins of Erv1 shuttle disulphide and Mia40 CPC disulphide were purified and characterised. The mutant proteins were used to understand how Mia40-Erv1 mixed disulphides are formed between cysteines of Mia40 and Erv1. Finally, to verify whether GSH plays an isomerisation role in Mia40-Erv1 interaction, the effects of GSH on the formation and dissociation of different Mia40-Erv1 intermediates were investigated.

5.2 Formation of mixed disulphide intermediate between Mia40 and Erv1

To study the interaction of Mia40 with Erv1, a time course of protein oxidation of Mia40c-pR catalysed by WT Erv1 was investigated. At indicated time points, the reactions were quenched by an excess amount of iodoacetamide (IAM) to alkylate any free thiols. The formation of Mia40-Erv1 intermediate was analysed by Western blotting against Erv1 (Figure 5.1). An adduct of ~37kDa was formed as soon as Erv1 was added to Mia40c-pR at 0.5min (lane 2), which persisted in an increasing amount (lane 2-5) throughout the time course. The adduct was disassociated under reducing condition, confirming that it was a mixed disulphide of Mia40-Erv1 (lane 6). To further understand how Mia40 and Erv1 interact to form a mixed disulphide intermediate, single cysteine mutants of Mia40 CPC and Erv1 shuttle disulphide were generated and used in this study, as described in the following sections.

5.3 Characterisation of single cysteine mutants of Erv1 shuttle disulphide

To understand how the Mia40-Erv1 mixed disulphide is formed, single cysteine mutants of the Erv1 shuttle disulphide (Cys30-Cys33) were generated and characterised. Both single cysteine mutant proteins were purified using the same method as for the WT protein. They were named Erv1^{C30S} and Erv1^{C33S} throughout the rest of the report (Figure 5.2A).

As previously reported (Hofhaus et al., 2003), the affinity purified Erv1^{C33S} was yellowish as for the WT protein, and Erv1^{C30S} was black. Protein misfolding and aggregation might have occurred to the single cysteine mutant(s), due to the fact that when a single cysteine of a disulphide bond is mutated, the remaining free cysteine may still be reactive. An abnormal colour observed for one of the single cysteine mutants, but not for the corresponding double cysteine mutant (see Results and Discussion, Section 3.2) was an indication of protein misfolding. Therefore, the oligomerisation states of both single cysteine mutant proteins were analysed.

Gel filtration chromatography profiles (Figure 5.2B) showed that the Erv1^{C30S} (dark grey curve) was eluted in 3 peaks at void (peak 1), 8.5ml (peak 2) and 9.75ml (peak 3) at a ratio of about 2:3:5. However for Erv1^{C33S} (light grey curve), two peaks were observed, with about 50% of the protein eluting as aggregates at void (peak 1) and the rest at 8.0ml (peak 2).

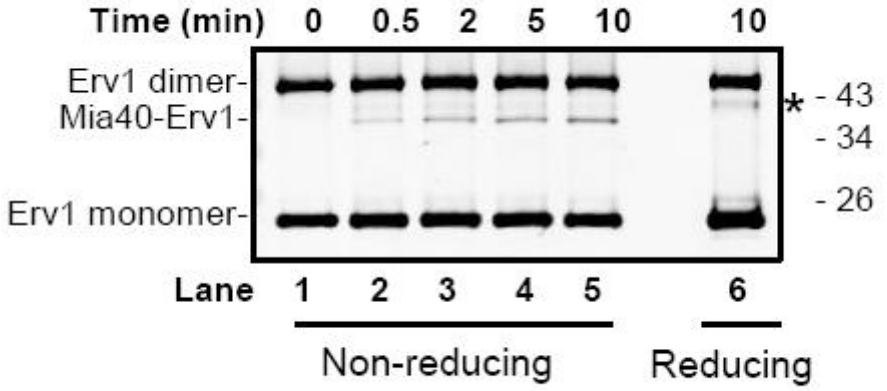

Figure 5.1 Formation of Mia40-Erv1 mixed disulphide during oxidation of Mia40c-pR by WT Erv1.

Time course of 50µM Mia40c-pR oxidation by 5µM WT Erv1 at room temperature (lane 2-5). The reactions were stopped by addition of sample buffer containing 20mM iodoacetamide (IAM). As control, the reaction at the end of the time course was analysed using sample buffer containing DTT (lane 6). The proteins were detected by western blotting with antibody against Erv1. An unknown protein species was indicated (*).

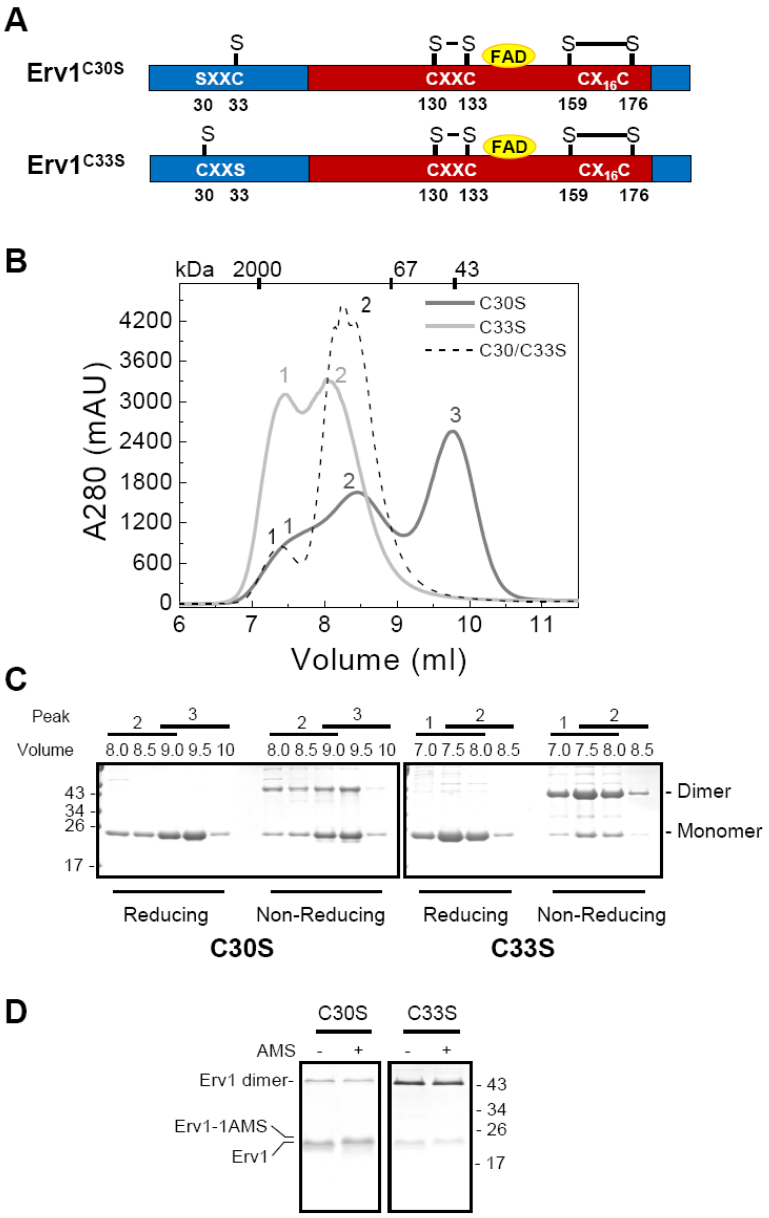

Figure 5.2 Oligomerisation states of the purified Erv1^{C30S} and Erv1^{C33S} mutant proteins.

A. Primary structures of Erv1^{C30S} and Erv1^{C33S} mutant proteins.

B. Gel filtration profiles of Erv1^{C30S} and Erv1^{C33S} compared to that of the corresponding double cysteine mutant C30/C33S on Superdex 75 column. The molecular weight markers and the corresponding peak fractions were indicated. The lowest peaks of the respective mutant protein were used for subsequent downstream assays.

C. 16% Tricine SDS-PAGE of Erv1^{C30S} and Erv1^{C33S} mutant proteins peak fractions in B under reducing and non-reducing conditions.

D. AMS alkylation of the free cysteine in Erv1^{C30S} and Erv1^{C33S} mutant proteins. Samples were treated with or without AMS in sample buffer before analysis by 16% Tricine SDS-PAGE.

In contrast, the double cysteine mutant (C30/C33S; dotted curve) was eluted with a vast majority of the protein at peak 2. These indicated that the protein aggregates in $Erv1^{C33S}$ were mostly due to the activity of Cys30 that may form non-native, intermolecular disulphide bonds with each other. Further analysis by reducing/non-reducing SDS-PAGE of the corresponding peak fractions confirmed that both $Erv1^{C30S}$ and $Erv1^{C33S}$ contained a significant amount of intermolecular disulphide bonded dimer (Figure 5.2C), as opposed to the C30/C33S double cysteine mutant which formed only monomer (see Results and Discussion, Section 3.2). In terms of monomer to dimer ratio, $Erv1^{C30S}$ formed mainly monomers with some dimers, in contrast to $Erv1^{C33S}$ which formed mainly dimers. To investigate the oligomerisation states under native condition, light scattering coupled with gel filtration chromatography revealed that the $Erv1^{C30S}$ peak 3 was a dimer (49kDa), whereas the $Erv1^{C33S}$ peak 2 was a pentamer (105kDa) (results not shown). The lowest peak fractions of each mutant protein were further analysed in subsequent assays.

To check whether the remaining cysteine of the mutated disulphide bond is free, the mutant proteins were analysed by AMS alkylation assays (Figure 5.2D). The monomers of the mutant proteins were slightly shifted to a higher molecular weight in the presence of AMS, which likely correspond to single cysteine modification, compared to those without AMS, thus confirming the availability of the remaining cysteine. For the dimers, no shift was observed. This indicated that the dimers were formed by intermolecular disulphide bonding between the remaining cysteine in the mutant proteins.

Since the two single cysteine mutant proteins have different colours, they were further analysed by spectroscopy (Figure 5.3). While $Erv1^{C33S}$ (light grey curve) showed the same spectra profile as the WT, with a bound FAD peak at around 460nm, $Erv1^{C30S}$ (dark grey curve) revealed a broadened peak at ~447nm and an additional absorbance at ~580nm. Addition of 1% SDS shifted the absorbance to 450nm, showing that FAD was bound to both mutant proteins. There was no electron paramagnetic resonance (EPR) signal detected for $Erv1^{C30S}$, thus the presence of a peak at ~580nm could be due to a charge-transfer complex formed between a persulphide anion and the FAD.

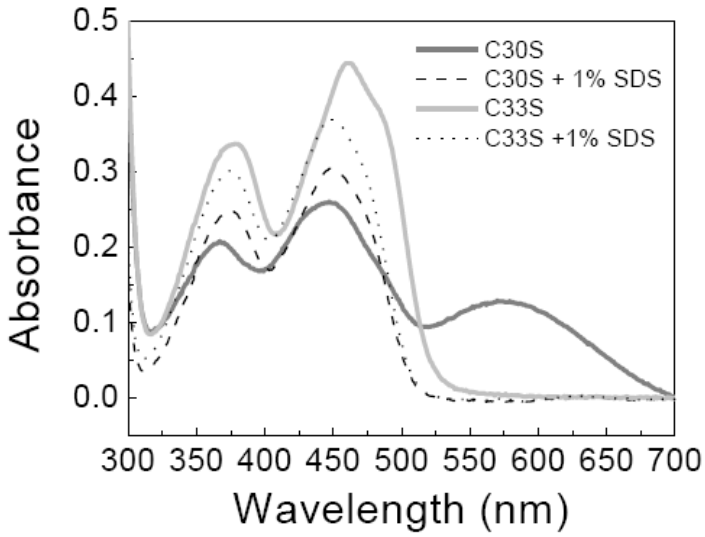

Figure 5.3 Effects of individual mutation of Cys30 and Cys33 on the FAD binding of Erv1.

Absorption spectra of the Erv1^{C30S} and Erv1^{C33S} mutant proteins in Buffer A in the absence and presence of 1% SDS.

Next, the oxidase activity of Erv1^{C30S} and Erv1^{C33S} were analysed using oxygen consumption assays (Figure 5.4 and Table 5.1). With DTT as substrate (Figure 5.4A), the normal coloured Erv1^{C33S} showed a slightly increased activity than the WT, with a k_{cat} value of 1.6 ± 0.1 s^{-1} which was very similar to that observed with the double cysteine mutant C30/C33S, while the black coloured Erv1^{C30S} had a decreased activity with a k_{cat} value of 0.3 ± 0.1 s^{-1} (Table 5.1). When TCEP was used as substrate (Figure 5.4B), the normal coloured Erv1^{C33S} also showed a very similar oxidase activity as the double cysteine mutant C30/C33S, but the black coloured Erv1^{C30S} mutants was completely inactive (Table 5.1).

Taken together, these results suggested that the first cysteine (Cys30) is more reactive than the second cysteine (Cys33) for intermolecular disulphide bond formation and/or causing protein aggregation. Mutation of Cys30 affected the spectrometric properties and enzymatic function of Erv1 against DTT, but not mutation of Cys33, although both mutant proteins were purified with bound FAD.

Table 5.1: Oxygen consumption kinetic parameters of Erv1^{C30S} and Erv1^{C33S} mutant proteins compared to those of the double cysteine mutant protein C30/C33S.

Electron donor	Erv1	k_{cat} (s^{-1})	K_m (μM)	k_{cat}/K_m (M^{-1} s^{-1})
10mM DTT	C30S	0.3±0.1	-	-
	C33S	1.6±0.1	59±5	$2.7±0.2×10^4$
	C30/C33S	1.5±0.1	62±5	$2.4±0.2×10^4$
3.5mM TCEP	C30S	<0.05	-	-
	C33S	<0.1	-	-
	C30/C33S	<0.1	-	-

All experiments were carried out with 1μM Erv1 proteins in 50mM Tris buffer pH 7.4, 150 mM NaCl, 1mM EDTA, at 25°C. The error bars represent standard errors, n=3.

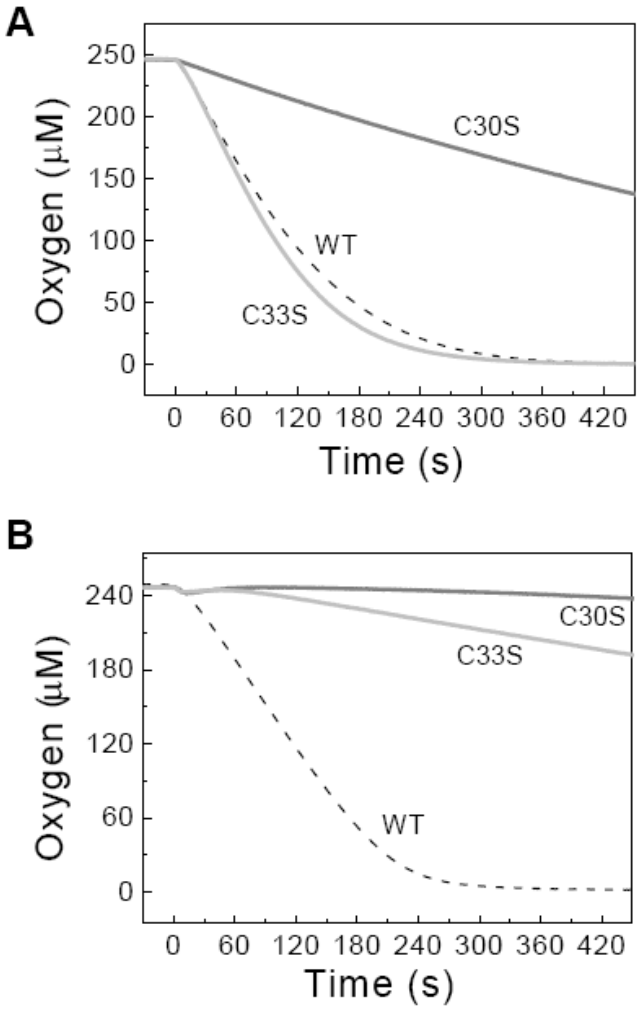

Figure 5.4 Effects of individual mutation of Cys30 and Cys33 on the enzymatic function of Erv1.

A. Oxygen consumption profiles of 10mM DTT in the presence of 1μM $Erv1^{C30S}$ or $Erv1^{C33S}$ mutant proteins. As control, the WT protein was used under the same condition. For all measurements, DTT was injected to pre-equilibrated samples at 25°C at the time zero.

B. Oxygen consumption profiles of 3.5mM TCEP in the presence of 1μM $Erv1^{C30S}$ or $Erv1^{C33S}$ mutant proteins compared to that of the WT protein under the same condition as in A.

5.4 Characterisation of single cysteine mutants of Mia40 CPC disulphide

Two single cysteine mutants of Mia40 CPC disulphide were generated and purified using the same method as for WT Mia40c. They were named Mia40c^{C296S} and Mia40c^{C298S} in the rest of the report (Figure 5.5A). Likewise, the oligomerisation states of the purified mutant proteins were analysed by gel filtration chromatography (Figure 5.5B). Mia40c^{C296S} was eluted in 3 peaks at 8ml (peak 1), 8.75ml (peak 2) and 10.25ml (peak 3) at about the same ratio (dark grey curve), which was very similar to that of the WT Mia40c (dotted curve). However, for Mia40c^{C298S}, two main peaks were observed, with about 10% of the protein was eluted at 8.75ml (peak 1), and the rest was eluted at 10.25ml (peak 2) (light grey curve). The high oligomers (peak 1 and peak 2) in Mia40c^{C296S} and WT Mia40c may be due to the activity of Cys298 that caused non-native intermolecular disulphide bonds between Mia40c. Consistently, reducing/non-reducing SDS-PAGE showed that the corresponding peak fractions of Mia40c^{C296S} mutant protein was dominated by high oligomers and dimers, as opposed to a mixture of dimers and monomers in the Mia40c^{C298S} mutant protein (Figure 5.5C). These suggested that the Cys298 of the Mia40 may be more susceptible for covalent intermolecular interaction compared to Cys296. The lowest peak fractions of each mutant protein were further analysed in subsequent assays.

Next, to verify whether the dimers in Mia40c^{C296S} and Mia40c^{C298S} were due to intermolecular disulphide bonding between the remaining cysteine in each mutant, the proteins were reduced by DTT followed by AMS alkylation analysis (Figure 5.5D). The mutant proteins were slightly shifted to a higher molecular weight in the presence of AMS, compared to those without AMS, suggesting single cysteine modification by AMS and the availability of the remaining cysteine.

In overall, these results suggested that in Mia40, the second cysteine (Cys298) is more reactive than the first cysteine (Cys296) for intermolecular disulphide bond formation and/or causing protein aggregation.

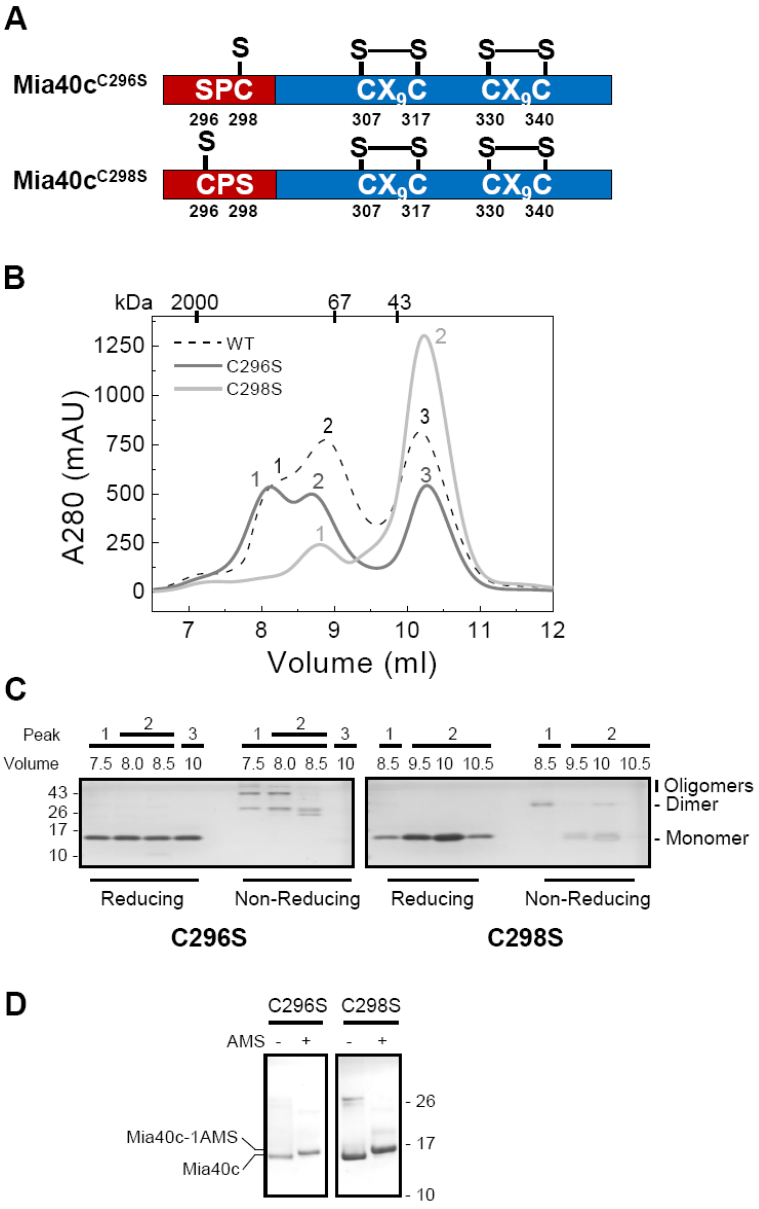

Figure 5.5 Oligomerisation states of the purified Mia40c^{C296S} and Mia40c^{C298S} mutant proteins.

A. Primary structures of Mia40c^{C296S} and Mia40c^{C298S} mutant proteins.

B. Gel filtration profiles of Mia40c^{C296S} and Mia40c^{C298S} compared to that of the WT Mia40c analysed under the same condition as in Figure 5.2B. The lowest peaks of the respective mutant protein were used for subsequent downstream assays.

C. 16% Tricine SDS-PAGE of Mia40c^{C296S} and Mia40c^{C298S} mutant proteins peak fractions in B under reducing and non-reducing conditions.

D. AMS alkylation of the free cysteine in Mia40c^{C296S} and Mia40c^{C298S} mutant proteins. The proteins were treated with 5mM DTT and buffer exchanged against Buffer A using NAP5 columns before AMS treatment and analysis by 16% Tricine SDS-PAGE.

5.5 Effects of single cysteine mutation on Mia40-Erv1 mixed disulphide formation

To investigate how Mia40-Erv1 mixed disulphides are formed between cysteines of Mia40 and Erv1, the single cysteine mutant proteins of Erv1 and Mia40c were incubated for 20 minutes in all four possible combinations. As shown in Figure 5.6, similar to that of the WT proteins, an adduct of ~37kDa was observed in all four cases (lane 3-4, 9-10). This adduct was dissociated under reducing condition (lane 5-6, 11-12), therefore confirming an intermolecular disulphide formation between the mutant proteins of Mia40 and Erv1. Since the highest amount of the adduct was detected in between Mia40c^{C296S} and Erv1^{C33S} (lane 9), it was likely that the mixed disulphide formed between the second cysteine of Mia40 (Cys298) and the first cysteine of Erv1 (Cys30) is most favourable and may be the native intermediate.

5.6 Effects of GSH on the Mia40-Erv1 intermediates

To understand whether GSH plays a reduction/isomerisation-like role in Mia40-Erv1 interaction, the effects of GSH on the mixed disulphides of Mia40 and Erv1 were investigated. Firstly, time courses of Mia40-Erv1 mixed disulphide formation between different mutant proteins were carried out for 10 minutes (Figure 5.7, left panel). As expected, Mia40c^{C296S}-Erv1^{C33S} showed the highest rate of mixed disulphide formation (Figure 5.7C, lane 1-5). Notably, the amount of Erv1^{C33S} dimer decreased at the same time as the Mia40-Erv1 intermediate increased, suggesting the reshuffling of disulphide bond from Erv1 dimer to Mia40-Erv1 intermediate. This was not observed for other mutant protein combinations that formed mixed disulphides, but at lower rates (Figure 5.7A, B and D, lane 1-5). Next, the effects of GSH on the dissociation of the mixed disulphides were studied (Figure 5.7, right panel). To this end, following the time courses of mixed disulphide formation, 10mM GSH was added to chase for 30 minutes (Figure 5.7 right panel). In the presence of GSH, whilst the mixed disulphide intermediates of Mia40c^{C298S} with Erv1^{C30S} and Erv1^{C33S} were dissociated immediately within 0.5min (Figure 5.7B and D, lane 7), a majority of the mixed disulphide intermediates of Mia40c^{C296S} with Erv1^{C30S} and Erv1^{C33S} were still detectable after 30 minutes (lane 11).

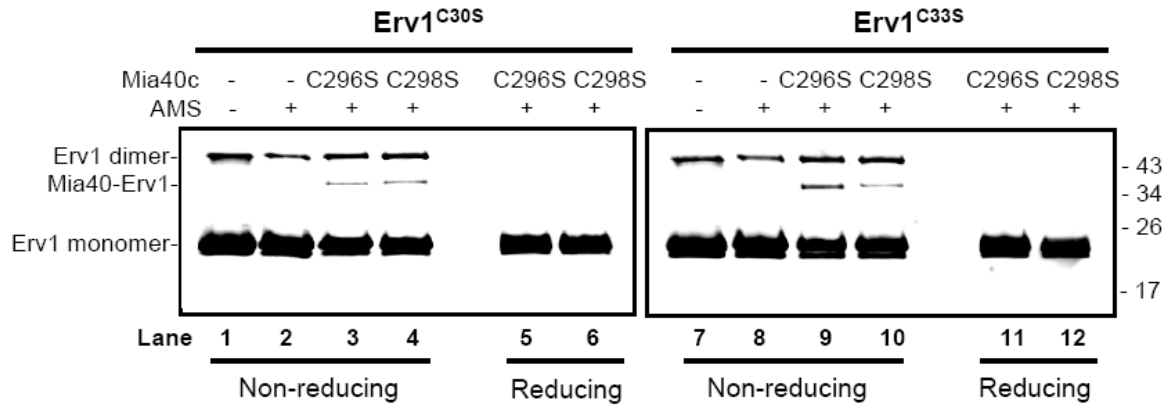

Figure 5.6 Mixed disulphide bond formation between different single cysteine mutants of Mia40c and Erv1.

The proteins were treated with 5mM DTT and buffer exchanged as in Figure 5.5D before incubation at equimolar concentrations for 20 minutes at room temperature. The reactions were stopped by addition of sample buffer with or without 1mM DTT for 5 minutes before alkylation by 2.5mM AMS. The proteins were detected by western blotting with antibody against Erv1.

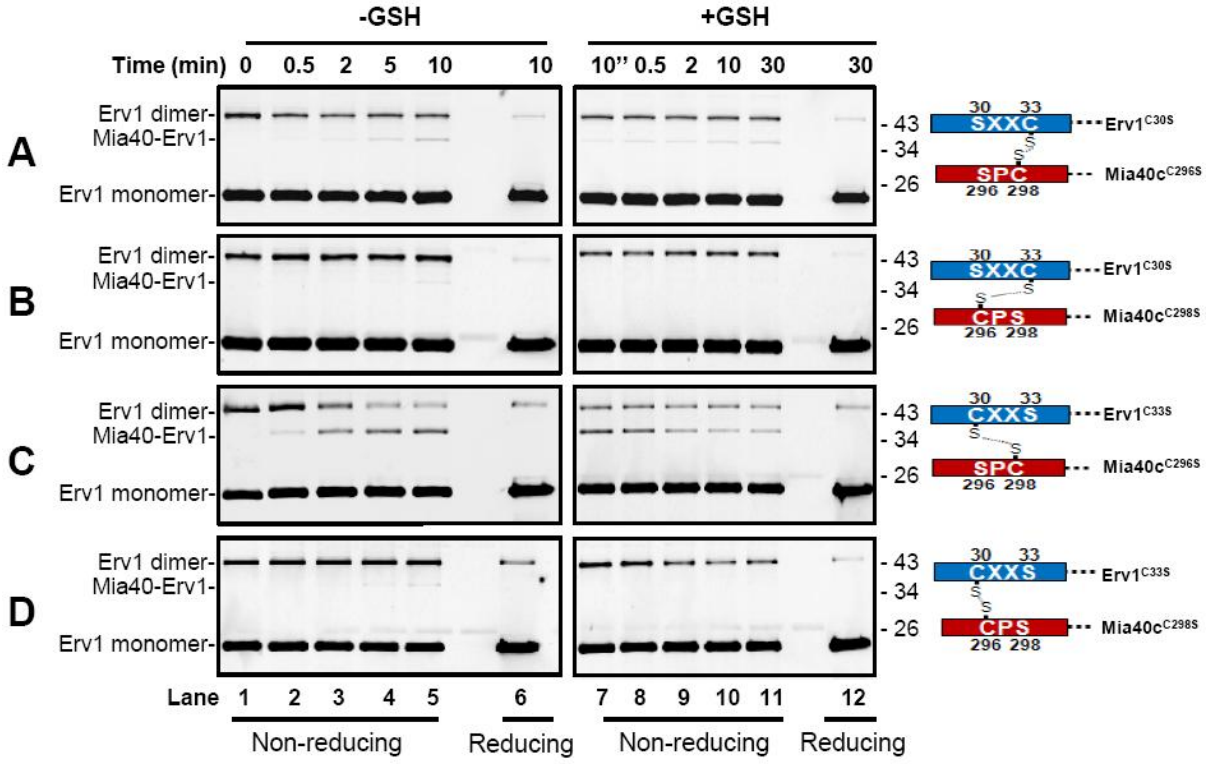

Figure 5.7 Effects of GSH on the mixed disulphide intermediates formed between different single cysteine mutant proteins of Mia40 and Erv1.

Time courses of mixed disulphide formation between single cysteine mutants of Mia40c and Erv1 in the absence of GSH (left panel), followed by chase assays after addition of 10mM GSH (right panel). The proteins were pre-treated with 5mM DTT and buffer exchanged against Buffer A using NAP5 columns before incubation at room temperature. The molar ratio concentration of Mia40 to Erv1 used was 10:1 (50µM Mia40, 5µM Erv1). The reactions were stopped by addition of sample buffer containing 20mM IAM. As control, the reactions after each time course were analysed under reducing condition by resuspending the reaction mixtures in sample buffer containing DTT. The proteins were detected by western blotting with antibody against Erv1. A: $Erv1^{C30S}$-$Mia40^{C296S}$, B: $Erv1^{C30S}$-$Mia40^{C298S}$, C: $Erv1^{C33S}$-$Mia40^{C296S}$, D: $Erv1^{C33S}$-$Mia40^{C298S}$.

Taken together, it was likely that GSH had different effects on Mia40-Erv1 disulphides formed between different cysteines. While mixed disulphides of Mia40/Cys296-Erv1/Cys30 and Mia40/Cys296-Erv1/Cys33 were less stable and could easily be dissociated by GSH, mixed disulphides of Mia40/Cys298-Erv1/Cys30 and Mia40/Cys298-Erv1/Cys33 were resistant to GSH.

5.7 Discussion

5.7.1 A possible role of Erv1 Cys30 in intermolecular interaction

By studying the functional properties of individual cysteine mutants of the Erv1 shuttle disulphide, results of this Chapter provided evidence of the electron transfer mechanism in between cysteines within Erv1. Firstly, it was found that the first cysteine (Cys30) of Erv1 was more reactive than the second cysteine (Cys33), based on the observation that Erv1 formed mainly high oligomers when Cys33 was mutated (leaving Cys30 free), while Cys30 mutation rendered Erv1 to form mainly low oligomers. Therefore, it was likely that Cys30 is the cysteine that first receives the reducing equivalent from its interacting molecules. Secondly, the results also suggested that the Cys33 transfers electrons to the redox centre by interacting with Cys130. This was supported by the observation that mutation of Cys30, but not Cys33, changed the colour and FAD spectrum of Erv1. Possibly, when Cys30 was mutated, the Cys33 could form a trapped disulphide bond with Cys130, leaving the Cys133 free to form a charge-transfer complex with FAD. Furthermore, the oxidase activity of $Erv1^{C30S}$ mutant was impaired, while the $Erv1^{C33S}$ mutant showed very similar oxidase activities to those of the double cysteine mutant C30/C33S against both DTT and TCEP. The observation that $Erv1^{C30S}$ mutant was inactive indicated that the trapped Cys33-Cys130 disulphide bond was probably buried, with little or no accessibility, or resistant to DTT. Lastly, the results also suggested that the FAD receives electrons from Cys133 before transferring to molecular oxygen, which was supported by the fact that Cys133 is located in close proximity to FAD (Gross et al., 2002, Wu et al., 2003, Vitu et al., 2006). Likewise, Cys130 mutation of the redox active disulphide caused a colour change (orange) in the mutant protein, but not Cys133 mutation (result not shown; Hofhaus et al., 2003). Similar to that observed with $Erv1^{C30S}$ mutant, this could also be logically explained by the charge-transfer in between Cys133 and the FAD. Taken together, a mechanism of electron transfer

between cysteines of Erv1 was proposed: Cys30 → Cys33 → Cys130 → Cys133 → FAD. In this way, Cys30 may be the first cysteine that receives the reducing equivalent from Mia40.

5.7.2 The mechanism of Mia40-Erv1 interaction

The shuttle disulphide of Erv1 on the flexible N-terminal domain is essential for interaction with the CPC disulphide of Mia40 (Bien et al., 2010, Lionaki et al., 2010). The preliminary data from this Chapter indicated that Mia40 and Erv1 possibly interact through the formation of a mixed disulphide bond between the second cysteine of Mia40 (Cys298) and the first cysteine of Erv1 (Cys30), based on the following observations in terms of Mia40: (1) the Mia40 Cys298 is more reactive than Cys296, as higher oligomers were formed in the presence of Cys298, even in the WT protein; (2) Mia40 Cys298 is more exposed than Cys296, which is slightly buried on the hydrophobic cleft, and therefore more reactive for interaction with other molecules (Banci et al., 2009, Kawano et al., 2009); (3) the mixed disulphide between Cys298 of Mia40 and Cys30 of Erv1 was formed more rapidly and abundantly compared to other cysteine combinations. Although Mia40-Erv1 mixed disulphides could be formed between the other cysteine combinations, they may be the off-pathway intermediates, due to their slow formation. Furthermore, in the presence of GSH, the intermediates formed between Cys296 of Mia40 and both cysteines of the Erv1 shuttle disulphide were easily counteracted. This was in agreement with a latest finding that suggested an isomerisation-like role of GSH in the mitochondrial IMS that reshuffles the disulphides of non-productive intermediates of Cox19-Mia40 to accelerate the oxidative folding of Cox19 (Bien et al., 2010). Interestingly, the intermediates formed between Cys298 of Mia40 and both cysteines of the Erv1 shuttle disulphide were very stable against GSH. The ability of Mia40 Cys298 to form stable intermediates with both cysteines of Erv1 shuttle disulphide was probably facilitated by the exposed Cys298 on hydrophobic binding cleft of Mia40 (Banci et al., 2009, Kawano et al., 2009), and the flexible nature of the Erv1 N-terminal arm. Although the results suggested that Cys298 of Mia40 favours the intermediate formation with Cys30 of Erv1, its interaction with Cys33 of Erv1 could also possibly co-exist in the cell.

5.8 Conclusions

Overall, whilst no clear conclusion can be drawn from the preliminary results obtained so far, the interesting observation about the different effects of GSH on Mia40-Erv1 mixed disulphides have provided a new basis to study the mechanism of the MIA pathway in further detail.

6. OVERALL CONCLUSIONS

The overall aim of this study was to understand the oxidoreductase system in the mitochondrial IMS, which mainly focused on Erv1 characterisation and Mia40-Erv1 interaction. In particular, the roles of individual disulphide bonds of Erv1, the effects of Zn^{2+} on the Erv1 activity, and the mechanism of Mia40-Erv1 interaction were investigated using *in vitro* purified proteins coupled with *in organello* and *in vivo* studies.

The first part of the study focused on general characterisation of Erv1 and the effects of Zn^{2+} on the oxidase activity of Erv1 using purified proteins. The effects of individual disulphide bond mutation on Erv1 oligomerisation states, spectrometric properties and stability were studied using the WT and double cysteine mutant proteins. In terms of protein oligomerisation, the results indicated that the purified WT Erv1 formed a tetramer under native conditions; and individual disulphide mutation had no obvious effect on tetramer formation except for the C130/C133S mutant that formed a smaller size. The UV/Vis spectra absorbance results showed that none of the three disulphides of Erv1 were essential for FAD-binding, as >90% of the purified WT and mutant proteins were bound to FAD. Thermal denaturation studies coupled with protease digestion analysis indicated that both the disulphides at the conserved catalytic core are important in maintaining the stability of the protein, especially the long range disulphide Cys159-Cys176. In addition, Zn^{2+} has a strong inhibitory effect on the enzymatic function of Erv1. The presence of a strong Zn^{2+} chelator such as EDTA is required to maintain the oxidase function of Erv1 *in vitro*.

The second part of the study focused on the functional roles of individual disulphide bonds of Erv1 in enzymatic function and protein biogenesis. The roles of individual disulphides in Erv1 enzymatic function were studied using DTT, TCEP and Mia40c-pR as electron donors. The results showed that both the CXXC disulphides, Cys30-Cys33 and Cys130-Cys133 are essential for Erv1 oxidase function. Cys30-Cys33 disulphide functions as a shuttle disulphide and may play a regulatory role to mediate the transfer of reducing equivalents to the well-protected redox centre of Erv1. Cys130-Cys133 disulphide is well-protected against large reducing molecules, such as TCEP and Mia40c-pR, and functions as a redox-active disulphide that receives electrons from the shuttle disulphide Cys30-Cys33. Both intersubunit and intermolecular electron transfer could occur, as the oxidase activity of the individually inactive mutant proteins lacking either the shuttle disulphide or redox-active disulphide was

partially recovered by mixing/scrambling the two mutant proteins together. Furthermore, mitochondrial import studies showed that Cys159-Cys176 disulphide may be crucial for biogenesis of Erv1, and both Cys159 and Cys176 seem required. Finally, yeast genetic studies showed that all three disulphide bonds of Erv1 are essential for cell viability. Co-expression of mutant Erv1 lacking the shuttle disulphide or redox-active disulphide rescued cell viability. Therefore, the *in vivo* studies confirmed the findings from *in vitro* data that both Cys30-Cys33 and Cys130-Cys133 are important for enzymatic function of Erv1.

The third part of the study focused on the formation of the intermolecular disulphide intermediate of Mia40 with Erv1. Although characterisation of single cysteine mutant proteins of Mia40 Cys296-Cys298 and Erv1 Cys30-Cys33 suggested that Cys298 of Mia40 favours mixed disulphide bond formation with Cys30 of Erv1, the Mia40-Erv1 mixed disulphides can be formed in all possible cysteine combinations *in vitro*. The Mia40-Erv1 mixed disulphides formed between Cys296 of Mia40 with both Cys30 and Cys33 of Erv1 are unstable and can easily be dissociated by GSH at physiological concentration, which was consistent with the hypothesis that GSH may play an isomerisation-like role in the mitochondrial IMS. In contrast, the intermediates formed between Cys298 of Mia40 with both Cys30 and Cys33 of Erv1 are GSH-resistant. The studies about how Mia40 and Erv1 interact and the role of GSH in Mia40-Erv1 interaction are still preliminary. While no clear conclusion can be drawn so far, this study provided essential materials and preliminary data for future studies.

7. QUESTIONS ARISING AND FUTURE DIRECTIONS

The findings from this study raised several interesting questions, which include:

(i) Why is there an oligomerisation requirement for Erv1, since the reducing equivalents can be transferred between Erv1 molecules?

All known ERV/ALR enzymes form stable dimers or oligomers (Gross et al., 2002, Wu et al., 2003, Vitu et al., 2006). Based on non-reducing SDS-PAGE studies, the monomer subunits of Erv1 are held together through disulphide bonding, which are contributed by the N-terminal Cys30-Cys33 disulphide (Lee et al., 2000, Hofhaus et al., 2003). Without the N-domain, Erv1 can also dimerise through hydrophobic interactions contributed by 6 amino acid residues at the C-domain between monomer subunits (Bien et al., 2010, Vitu et al., 2006). In this study, the purified protein of full-length WT Erv1 and C30/C33S mutant forms tetramer, where as the C-domain forms dimer under native condition (results not shown). This suggested that in the N-domain may contribute to Erv1 oligomerisation through non-covalent interactions. Therefore, in the WT Erv1, the four protein subunits are possibly held together through non-covalent interactions contributed by both N- and C-domain, with co-existence of covalent interaction within a pair of protein subunit contributed by Cys30-Cys33 disulphide. In contrast, the WT Erv1 purified in a very recent study only formed dimer (Bien et al., 2010). Early trials of Erv1 purification without excess FAD supplementation in this study also yielded dimers that had ~50% FAD binding (results not shown). Since the proteins used in this study were purified with excess FAD supplementation and had more than 90% FAD binding, it is likely that the oligomerisation states of Erv1 are caused by protein to FAD binding ratio. Although excess FAD supplementation during protein purification in this study may have promoted tetramer formation *in vitro*, whether the dimeric or tetrameric form resemble the native physiological oligomerisation state of Erv1 *in vivo* is still unknown. Based on the crystal structure data of the other ERV/ALR enzymes, the mechanism of electron transfer occurs between protein subunits, which may explain the oligomerisation requirement of this protein family. In this study however, it was demonstrated that other than intersubunit electron transfer mechanism, electrons can also be transferred between different dimers/oligomers of Erv1. Similarly, such intermolecular electron transfer mechanism has also been shown in Ero1, which only forms monomer (Sevier and Kaiser, 2006b). Since intermolecular electron transfer can occur in Erv1, the requirement of Erv1 to oligomerise in

a physiologically relevant manner is still to be discovered. To provide a better understanding of the correlation between oligomerisation requirement and functional mechanism of Erv1, the *in vivo* oligomerisation state of Erv1 needs to be investigated.

(ii) What is the correlation of the MIA pathway to metal ions homeostasis in the mitochondria?

In this study, an increase of Erv1 oxidase activity by ~28% in the presence of metal chelator, compared to that without metal chelator was observed. Although the affinity of Erv1 towards zinc was investigated, traces amount of other metal ions present in the buffer may also have effects on Erv1 oxidase activity. Correspondingly, Mia40, the physiological substrate of Erv1, has a strong affinity towards iron (Daithankar et al., 2009) and copper (Terziyska et al., 2004), other than zinc (Terziyaka et al., 2004, Mesecke et al., 2008). Together with the fact that substrates of the MIA pathway like the small Tims and Cox17 have affinity towards to zinc (Sirrenberg et al., 1998, Lu et al., 2004, Ivanova et al., 2008) and copper (Banci et al., 2008b, Beers et al., 1997, Heaton et al., 2001) respectively, the entire MIA pathway may have a strong correlation to the metal ion homeostasis in the mitochondria. Erv1 has previously been proposed as a component that participates in delivery of iron-sulphur (Fe/S) cluster to the cytosol for Fe/S protein maturation (Lange et al., 2001). However, Erv1 and its human homologue ALR have no direct association with Fe/S cluster (Lange et al., 2001, Daithankar et al., 2009). The strong ability of Mia40 to bind iron suggested that Mia40 may participate in Fe/S delivery, which may have been indirectly enabled by Erv1 (Daithankar et al., 2009). In addition, Mia40 may participate in copper delivery indirectly as well. Mia40 oxidises Cox17 that is translocated into mitochondrial IMS to its structured functional form, which can bind one copper for delivery into Cyt c oxidase through Sco1 (Banci et al., 2008b). This suggests that both Mia40 and Erv1 participate in metal iron homeostasis of mitochondria directly or indirectly. Other than zinc, iron and copper are required as cofactors for maturation of metalloenzymes. Calcium is another ion that may potentially be correlated to the MIA pathway, since mitochondria function in sequestration of calcium ions (Graier et al., 2007). To date, Erv1 is the only sulphydryl oxidase identified in the mitochondria. There may be other substrates of Erv1, other than Mia40 that participate in a wide range of

metabolic functions, including metal ion homeostasis. Therefore, other native substrates of Erv1 in the mitochondrial IMS are still yet to be identified.

(iii) How does Erv1 get imported into the mitochondrial IMS?

The data from mitochondrial import studies showed that mutation of individual disulphides had different effects on import of Erv1 into the mitochondrial IMS. Although the results suggested that cysteine residues of the $CX_{16}C$ motif are crucial for Erv1 biogenesis, the mixed disulphide intermediate formed between Erv1 precursor and Mia40 during Erv1 import has not been identified under the tested condition (results not shown). There are a number of factors that may contribute to the observed import defect of Erv1 with cysteines of $CX_{16}C$ mutated. Firstly, the mutant protein may be unstable and susceptible to degradation after import into the mitochondria. In addition, there is also a possibility that the mutant protein is more sensitive to oxidative folding that inhibits Erv1 import into the mitochondria in the presence of reticulocyte lysate, which contains a large number of redox active factors. These factors include thioredoxin, glutaredoxin, peroxiredoxins and glutathione peroxidases that may catalyse oxidative folding of Erv1 before mitochondrial import. However, the redox state changes of unimported Erv1 were unable to be detected due to poor image resolution (results not shown). The overall import level of WT Erv1 was much lower (only 3-5%) compared to those of small Tims (10-20%) under the same condition. Therefore, the import condition of Erv1 still needs to be optimised in the presence of reducing agent and/or denaturant in order to investigate whether oxidative folding of Erv1 affects mitochondrial import of Erv1. Due to the above-mentioned limitations of mitochondrial import assays, the roles of cysteines for Erv1 biogenesis can alternatively be investigated by yeast genetic approaches using the *tet*O promoter regulatable *ERV1* strains generated in this study. By down regulating the endogenous Erv1, the steady state level of plasmid encoded Erv1 tagged with 6xHis in the mitochondria of respective yeast strains may provide some information about role of cysteine motif that drives the mitochondrial import of Erv1.

(iv) Does disulphide reduction/isomerisation pathway exist in the mitochondrial IMS?

The crystal structures of Mia40 and identification of MISS/ITS signals in substrates of the MIA pathway suggested that hydrophobic interactions facilitate correct priming of cysteines for mixed disulphide formation between substrate protein and Mia40. This minimises non-native disulphide formation which may lead to protein misfolding in the mitochondrial IMS. Therefore, a disulphide reduction/isomerisation pathway may not be needed in the mitochondrial IMS unlike those in the ER and bacterial periplasm. However, Mia40-Cox19 mixed disulphide has been observed *in vitro* during oxidation of Cox19 by Mia40, and such an intermediate can be dissociated by GSH at physiological concentration, suggesting that GSH may play an isomerisation-like role in the IMS (Bien et al., 2010). In this study, it was demonstrated that Mia40-Erv1 mixed disulphides can be formed in all possible cysteine combinations *in vitro*. However, GSH only had the same effect as that observed for Mia40-Cox19 towards some of the Mia40-Erv1 mixed disulphides. The observed GSH-resistant Mia40-Erv1 mixed disulphides may be the intermediates required for full oxidation of MIA substrates by formation of a ternary complex between substrate Mia40 and Erv1. Together with the fact that all MIA substrates contain two to three disulphide bonds, such a complex formation that requires multiple thiol-disulphide exchange reactions may cause a possibility of non-native disulphide formation that lead to protein misfolding. Under oxidative stress, elevated levels of reactive oxygen species produced in the mitochondria may potentially lead to non-native disulphide formation and protein misfolding in the IMS. Other than GSH, there may be oxidoreductases in the mitochondrial IMS that play a similar role like the DsbC/G in the bacterial periplasm, since mitochondria are believed to be descended from the α-proteobacterial ancestor. Therefore, it would be interesting to investigate whether the cytoplasmic Trx1/2/Trr1 and Grx1/2/Glr1 systems or even the mitochondrial matrix Trx3/Trr2, Grx2/5Glr1 systems play an important reduction/isomerisation role in the mitochondrial IMS.

8. REFERENCES

ABATE, C., PATEL, L., RAUSCHER, F. J. & CURRAN, T. (1990) Redox regulation of fos and jun DNA-binding activity *in vitro*. *Science,* 249**,** 1157-1161.

ADAM, A., ENDRES, M., SIRRENBERG, C., LOTTSPEICH, F., NEUPERT, W. & BRUNNER, M. (1999) Tim9, a new component of the TIM22.54 translocase in mitochondria. *Embo J* 18**,** 313-319.

ADAMS, V., BOSCH, W., SCHLEGEL, J., WALLIMANN, T. & BRDICZKA, D. (1989) Further characterization of contact sites from mitochondria of different tissues: topology of peripheral kinases. *Biochim Biophys Acta,* 981**,** 213-225.

ALLEN, J. W. A., FERGUSON, S. J. & GINGER, M. L. (2008) Distinctive biochemistry in the trypanosome mitochondrial intermembrane space suggests a model for stepwise evolution of the MIA pathway for import of cysteine-rich proteins. *FEBS Lett,* 582**,** 2817-2825.

ALLEN, S., BALABANIDOU, V., SIDERIS, D. P., LISOWSKY, T. & TOKATLIDIS, K. (2005) Erv1 mediates the Mia40-dependent protein import pathway and provides a functional link to the respiratory chain by shuttling electrons to cytochrome c. *J Mol Biol,* 353**,** 937-944.

ANDERSON, S., BANKIER, A. T., BARRELL, B. G., DE BRUIJN, M. H., COULSON, A. R., DROUIN, J., EPERON, I. C., NIERLICH, D. P., ROE, B. A. & SANGER, F. (1981) Sequence and organisation of the human mitochondrial genome. *Nature,* 290**,** 457-465.

ANFINSEN, C. B. (1973) Principles that govern the folding of protein chains. *Science,* 181**,** 223-230.

APPENZELLER-HERZOG, C. & ELLGAARD, L. (2008) The human PDI family: versatility packed into a single fold. *Biochim Biophys Acta,* 1783**,** 535-548.

APPENZELLER-HERZOG, C., RIEMER, J., CHRISTENSEN, B., SORENSEN, E. S. & ELLGAARD, L. (2008) A novel disulphide switch mechanism in Ero1alpha balances ER oxidation in human cells. *Embo J,* 27**,** 2977-2987.

ARNESANO, F., BALATRI, E., BANCI, L., BERTINI, I. & WINGE, D. R. (2005) Folding studies of Cox17 reveal an important interplay of cysteine oxidation and copper binding. *Structure,* 13**,** 713-722.

ATAR, D., BACKX, P. H., APPEL, M. M., WEI DONG, G. & MARBAN, E. (1995) Excitation-transcription coupling mediated by zinc influx through voltage- dependent calcium channels. *J Biol Chem,* 270**,** 2473-2477.

BADER, M., MUSE, W., BALLOU, D. P., GASSNER, C. & BARDWELL, J. C. A. (1999) Oxidative protein folding is driven by the electron transport system. *Cell,* 98**,** 217-227.

BADER, M. W., HINIKER, A., REGEIMBAL, J., GOLDSTONE, D., HAEBEL, P. W., RIEMER, J., METCALF, P. & BARDWELL, J. C. (2001) Turning a disulfide isomerase into an oxidase: DsbC mutants that imitate DsbA. *Embo J,* 20**,** 1555-1562.

BAKER, K. M., CHAKRAVARTHI, S., LANGTON, K. P., SHEPPARD, A. M., LU, H. & BULLEID, N. J. (2008) Low reduction potential of Ero1alpha regulatory disulphides ensures tight control of substrate oxidation. *Embo J,* 27**,** 2988-2997.

BAKER, M. J., WEBB, C. T., STROUD, D. A., PALMER, C. S., FRAZIER, A. E., GUIARD, B., CHACINSKA, A., GULBIS, J. M. & RYAN, M. T. (2009) Structural and functional requirements for activity of the Tim9-Tim10 complex in mitochondrial protein import. *Mol Biol Cell,* 20**,** 769-779.

BANCI, L., BERTINI, I., CEFARO, C., CIOFI-BAFFONI, S., GALLO, A., MARTINELLI, M., SIDERIS, D. P., KATRAKILI, N. & TOKATLIDIS, K. (2009) MIA40 is an oxidoreductase that catalyzes oxidative protein folding in mitochondria. *Nat Struct Mol Biol,* 16**,** 198-206.

BANCI, L., BERTINI, I., CIOFI-BAFFONI, S., HADJILOI, T., MARTINELLI, M. & PALUMAA, P. (2008a) Mitochondrial copper(I) transfer from Cox17 to Sco1 is coupled to electron transfer. *Proc Natl Acad Sci USA,* 105**,** 6803-6808.

BANCI, L., BERTINI, I., CIOFI-BAFFONI, S., JANICKA, A., MARTINELLI, M., KOZLOWSKI, H. & PALUMAA, P. (2008b) A structural-dynamical characterization of human Cox17. *J Biol Chem,* 283**,** 7912-7920.

BÁNHEGYI, G., LUSINI, L., PUSKÁS, F., ROSSI, R., FULCERI, R., BRAUN, L., MILE, V., DI SIMPLICIO, P., MANDL, J. & BENEDETTI, A. (1999) Preferential transport of glutathione versus glutathione disulfide in rat liver microsomal vesicles. *J Biol Chem,* 274**,** 12213-12216.

BARDWELL, J. C., LEE, J. O., JANDER, G., MARTIN, N., BELIN, D. & BECKWITH, J. (1993) A pathway for disulfide bond formation *in vivo*. *Proc Natl Acad Sci USA,* 90**,** 1038-1042.

BARDWELL, J. C. A., MCGOVERN, K. & BECKWITH, J. (1991) Identification of a protein required for disulfide bond formation in vivo. *Cell,* 67**,** 581-589.

BASS, R., RUDDOCK, L. W., KLAPPA, P. & FREEDMAN, R. B. (2004) A major fraction of endoplasmic reticulum-located glutathione is present as mixed disulfides with protein. *J Biol Chem,* 279**,** 5257-5262.

BAUMANN, F., NEUPERT, W. & HERRMANN, J. (2002) Insertion of bitopic membrane proteins into the inner membrane of mitochondria involves an export step from the matrix. *J Biol Chem,* 277**,** 21405-21413.

BECHER, D., KRICKE, J., STEIN, G. & LISOWSKY, T. (1999) A mutant for the yeast scERV1 gene displays a new defect in mitochondrial morphology and distribution. *Yeast,* 15**,** 1171-1181.

BECKER, T., PFANNSCHMIDT, S., GUIARD, B., STOJANOVSKI, D., MILENKOVIC, D., KUTIK, S., PFANNER, N., MEISINGER, C. & WIEDEMANN, N. (2008) Biogenesis of the mitochondrial TOM complex: Mim1 promotes insertion and assembly of signal-anchored receptors. *J Biol Chem,* 283**,** 120-127.

BEERS, J., GLERUM, D. M. & TZAGOLOFF, A. (1997) Purification, characterization, and localization of yeast Cox17p, a mitochondrial copper shuttle. *J Biol Chem,* 272**,** 33191-33196.

BEKRI, S., KISPAL, G., LANGE, H., FITZSIMONS, E., TOLME, J., LILL, R. & BISHOP, D. F. (2000) Human ABC7 transporter: Gene structure and mutation causing X-linked sideroblastic anemia with ataxia with disruption of cytosolic iron-sulfur protein maturation. *Blood,* 96**,** 3256-3264.

BENHAM, A. M., CABIBBO, A., FASSIO, A., BULLEID, N., SITIA, R. & BRAAKMAN, I. (2000) The CXXCXXC motif determines the folding, structure and stability of human Ero1-Lα. *Embo J,* 19**,** 4493-4502.

BERNARD, D. G., QUEVILLON-CHERUEL, S., MERCHANT, S., GUIARD, B. & HAMEL, P. P. (2005) Cyc2p, a membrane-bound flavoprotein involved in the maturation of mitochondrial c-type cytochromes. *J Biol Chem,* 280**,** 39852-39859.

BESSETTE, P. H., COTTO, J. J., GILBERT, H. F. & GEORGIOU, G. (1999) *In vivo* and *in vitro* function of the *Escherichia coli* periplasmic cysteine oxidoreductase DsbG. *J Biol Chem,* 274**,** 7784-7792.

BIEN, M., LONGEN, S., WAGENER, N., CHWALLA, I., HERRMANN, J. & RIEMER, J. (2010) Mitochondrial disulfide bond formation is driven by intersubunit electron transfer in Erv1 and proofread by glutathione. *Mol Cell,* 37**,** 516-528.

BIHLMAIER, K., MESECKE, N., TERZIYSKA, N., BIEN, M., HELL, K. & HERRMANN, J. M. (2007) The disulfide relay system of mitochondria is connected to the respiratory chain. *J Cell Biol,* 179**,** 389-395.

BOLDOGH, I. R., NOWAKOWSKI, D. W., YANG, H. C., CHUNG, H., KARMON, S., ROYES, P. & PON, L. A. (2003) A Protein Complex Containing Mdm10p, Mdm12p, and Mmm1p Links Mitochondrial Membranes and DNA to the Cytoskeleton-based Segregation Machinery. *Mol Biol Cell,* 14**,** 4618-4627.

BOLLIGER, L., JUNNE, T., SCHATZ, G. & LITHGOW, T. (1995) Acidic receptor domains of both sides of the outer membrane mediate translocation of precursor proteins into yeast mitochondria. *Embo J,* 14**,** 6318-6326.

BRAAKMAN, I., HELENIUS, J. & HELENIUS, A. (1992) Manipulating disulfide bond formation and protein folding in the endoplasmic reticulum. *Embo J,* 11**,** 1717–1722.

BRANDNER, K., REHLING, P. & TRUSCOTT, K. N. (2005) The carboxyl-terminal third of the dicarboxylate carrier is crucial for productive association with the inner membrane twin-pore translocase. *J Biol Chem,* 280**,** 6215-6221.

CAPPEL, R. E. & GILBERT, H. F. (1988) Thiol/disulfide exchange between 3-hydroxy-3-methylglutaryl-CoA reductase and glutathione. A thermodynamically facile dithiol oxidation. *J Biol Chem,* 263**,** 12204-12212.

CHACINSKA, A., GUIARD, B., MULLER, J. M., SCHULZEÂ€“SPECKING, A., GABRIEL, K., KUTIK, S. & PFANNER, N. (2008) Mitochondrial biogenesis, switching the sorting pathway of the intermembrane space receptor Mia40. *J Biol Chem,* 283**,** 29723-29729.

CHACINSKA, A., KOEHLER, C. M., MILENKOVIC, D., LITHGOW, T. & PFANNER, N. (2009) Importing mitochondrial proteins: Machineries and mechanisms. *Cell,* 138**,** 628-644.

CHACINSKA, A., PFANNSCHMIDT, S., WIEDEMANN, N., KOZJAK, V., SANJUAN SZKLARZ, L. K., SCHULZE-SPECKING, A., TRUSCOTT, K. N., GUIARD, B., MEISINGER, C. & PFANNER, N. (2004) Essential role of Mia40 in import and assembly of mitochondrial intermembrane space proteins. *Embo J,* 23**,** 3735-3746.

CHAN, N. C. & LITHGOW, T. (2008) The peripheral membrane subunits of the SAM complex function codependently in mitochondrial outer membrane biogenesis. *Mol Biol Cell,* 19**,** 126-136.

CHANCE, B., SIES, H. & BOVERIS, A. (1979) Hydroperoxide metabolism in mammalian organs. *Phys Rev,* 59**,** 527-605.

COPPOCK, D. L. & THORPE, C. (2006) Multidomain flavin-dependent sulfhydryl oxidases. *Antioxid Redox Signal,* 8**,** 300-311.

CRAIG, E. A., VOISINE, C. & SCHILKE, B. (1999) Mitochondrial iron metabolism in the yeast *Saccharomyces cerevisiae*. *Biol Chem,* 380**,** 1167-1173.

CREIGHTON, T. E. (1986) Disulfide bonds as probes of protein folding pathways. *Methods Enzymol,* 131**,** 83-106.

CUOZZO, J. W. & KAISER, C. A. (1999) Competition between glutathione and protein thiols for disulphide-bond formation. *Nat Cell Biol,* 1**,** 130-135.

CURRAN, S. P., LEUENBERGER, D., LEVERICH, E. P., HWANG, D. K., BEVERLY, K. N. & KOEHLER, C. M. (2004) The role of Hot13p and redox chemistry in the mitochondrial TIM22 import pathway. *J Biol Chem,* 279**,** 43744-43751.

CURRAN, S. P., LEUENBERGER, D., OPPLIGER, W. & KOEHLER, C. M. (2002) The Tim9p-Tim10p complex binds to the transmembrane domains of the ADP/ATP carrier. *Embo J,* 21**,** 942-953.

DABIR, D. V., LEVERICH, E. P., KIM, S. K., TSAI, F. D., HIRASAWA, M., KNAFF, D. B. & KOEHLER, C. M. (2007) A role for cytochrome c and cytochrome c peroxidase in electron shuttling from Erv1. *Embo J,* 26**,** 4801-4811.

DAITHANKAR, V. N., FARRELL, S. R. & THORPE, C. (2009) Augmenter of liver regeneration: Substrate specificity of a flavin-dependent oxidoreductase from the mitochondrial intermembrane space. *Biochemistry,* 48**,** 4828-4837.

DAWSON, R. M. C., ELLIOTT, D. C., ELLIOTT, W. H. & JONES, K. M. (1986) Data for biochemical research. Oxford: Clarendon Press.

DEPUYDT, M., LEONARD, S. E., VERTOMMEN, D., DENONCIN, K., MORSOMME, P., WAHNI, K., MESSENS, J., CARROLL, K. S. & COLLET, J. F. (2009) A periplasmic reducing system protects single cysteine residues from oxidation. *Science,* 326**,** 1109-1111.

DIEKERT, K., DE KROON, A. I., AHTING, U., NIGGEMEYER, B., NEUPERT, W., DE KRUIJFF, B. & LILL, R. (2001) Apocytochrome c requires the TOM complex for translocation across the mitochondrial outer membrane. *Embo J,* 20**,** 5626-35.

DIEKERT, K., KISPAL, G., GUIARD, B. & LILL, R. (1999) An internal targeting signal directing proteins into the mitochondrial intermembrane space. *Proc Natl Acad Sci USA,* 96**,** 11752-11757.

DUMONT, M. E., ERNST, J. F. & SHERMAN, F. (1988) Coupling of heme attachment to import of cytochrome c into yeast mitochondria. Studies with heme lyase-deficient mitochondria and altered apocytochromes c. *J Biol Chem,* 263**,** 15928-15937.

DYALL, S. D., AGIUS, S. C., DE MARCOS LOUSA, C., TREZEGUET, V. & TOKATLIDIS, K. (2003) The dynamic dimerization of the yeast ADP/ATP carrier in the inner mitochondrial membrane is affected by conserved cysteine residues. *J Biol Chem,* 278**,** 26757-26764.

ENDO, T., YAMANO, K. & KAWANO, S. (2010) Structural basis for the disulfide relay system in the mitochondrial intermembrane space. *Antioxid Redox Signal*.

ENDRES, M., NEUPERT, W. & BRUNNER, M. (1999) Transport of the ADP/ATP carrier of mitochondria from the TOM complex to the TIM22.54 complex. *Embo J,* 18**,** 3214-3221.

ESAKI, M., KANAMORI, T., NISHIKAWA, S. I., SHIN, I., SCHULTZ, P. G. & ENDO, T. (2003) Tom40 protein import channel binds to non-native proteins and prevents their aggregation. *Nat Struct Biol,* 10**,** 988-994.

ESAKI, M., SHIMIZU, H., ONO, T., YAMAMOTO, H., KANAMORI, T., NISHIKAWA, S. I. & ENDO, T. (2004) Mitochondrial protein import. Requirement of presequence elements and TOM components for precursor binding to the TOM complex. *J Biol Chem,* 279**,** 45701-45707.

ESSER, K., TURSUN, B., INGENHOVEN, M., MICHAELIS, G. & PRATJE, E. (2002) A novel two-step mechanism for removal of a mitochondrial signal sequence involves the mAAA complex and the putative rhomboid protease Pcp1. *J Mol Biol,* 323**,** 835-843.

FAGIOLI, C., MEZGHRANI, A. & SITIA, R. (2001) Reduction of interchain disulfide bonds precedes the dislocation of Ig-mu chains from the endoplasmic reticulum to the cytosol for proteasomal degradation. *J Biol Chem,* 276**,** 40962-40967.

FARRELL, S. R. & THORPE, C. (2005) Augmenter of liver regeneration: A flavin-dependent sulfhydryl oxidase with cytochrome c reductase activity. *Biochemistry,* 44**,** 1532-1541.

FASS, D. (2008) The Erv family of sulfhydryl oxidases. *Biochim Biophys Acta,* 1783**,** 557-566.

FIELD, L. S., FURUKAWA, Y., O'HALLORAN, T. V. & CULOTTA, V. C. (2003) Factors controlling the uptake of yeast copper/zinc superoxide dismutase into mitochondria. *J Biol Chem,* 278**,** 28052-28059.

FOURY, F., ROGANTI, T., LECRENIER, N. & PURNELLE, B. (1998) The complete sequence of the mitochondrial genome of *Saccharomyces cerevisiae*. *FEBS Lett,* 440**,** 325-331.

FRAND, A. R. & KAISER, C. A. (1999) Ero1p oxidizes protein disulfide isomerase in a pathway for disulfide bond formation in the endoplasmic reticulum. *Mol Cell,* 4**,** 469-477.

FRAND, A. R. & KAISER, C. A. (2000) Two pairs of conserved cysteines are required for the oxidative activity of Ero1p in protein disulfide bond formation in the endoplasmic reticulum. *Mol Biol Cell,* 11**,** 2833-2843.

FREY, T. G. & MANNELLA, C. A. (2000) The internal structure of mitochondria. *Trends Biochem Sci,* 25**,** 319-324.

FRUEHAUF, J. P. & MEYSKENS, F. L. J. (2007) Reactive oxygen species: A breath of life or death? *Clin Cancer Res,* 13**,** 789–794.

FURUKAWA, Y., TORRES, A. S. & O'HALLORAN, T. V. (2004) Oxygen-induced maturation of SOD1: A key role for disulfide formation by the copper chaperone CCS. *Embo J,* 23**,** 2872-2881.

GABRIEL, K., MILENKOVIC, D., CHACINSKA, A., MULLER, J., GUIARD, B., PFANNER, N. & MEISINGER, C. (2007) Novel mitochondrial intermembrane space proteins as substrates of the MIA import pathway. *J Mol Biol,* 365**,** 612-620.

GAKH, O., CAVADINI, P. & ISAYA, G. (2002) Mitochondrial processing peptidases. *Biochim Biophys Acta,* 1592**,** 63-77.

GEISSLER, A., CHACINSKA, A., TRUSCOTT, K. N., WIEDEMANN, N., BRANDNER, K., SICKMANN, A., MEYER, H. E., MEISINGER, C., PFANNER, N. & REHLING, P. (2002) The mitochondrial presequence translocase: An essential role of Tim50 in directing preproteins to the import channel. *Cell,* 111**,** 507-518.

GENTLE, I., GABRIEL, K., BEECH, P., WALLER, R. & LITHGOW, T. (2004) The Omp85 family of proteins is essential for outer membrane biogenesis in mitochondria and bacteria. *J Cell Biol,* 164**,** 19-24.

GERBER, J., MUHLENHOFF, U., HOFHAUS, G., LILL, R. & LISOWSKY, T. (2001) Yeast ERV2p is the first microsomal FAD-linked sulfhydryl oxidase of the Erv1p/Alrp protein family. *J Biol Chem,* 276**,** 23486.

GIETZ, D., ST JEAN, A., WOODS, R. A. & SCHIESTL, R. H. (1992) Improved method for high efficiency transformation of intact yeast cells. *Nucleic Acids Res,* 20**,** 1425.

GILBERT, H. F. (1995) Thiol/disulfide exchange equilibria and disulfide bond stability. *Methods Enzymol,* 251**,** 8-28.

GLASER, S. M., MILLER, B. R. & CUMSKY, M. G. (1990) Removal of a hydrophobic domain within the mature portion of a mitochondrial inner membrane protein causes its mislocalization to the matrix. *Mol Cell Biol,* 10**,** 1873-1881.

GLICK, B. S., BRANDT, A., CUNNINGHAM, K., MULLER, S., HALLBERG, R. L. & SCHATZ, G. (1992) Cytochromes c1 and b2 are sorted to the intermembrane space of yeast mitochondria by a stop-transfer mechanism. *Cell,* 69**,** 809-822.

GRAIER, W., FRIEDEN, M. & MALLI, R. (2007) Mitochondria and Ca^{2+} signaling: Old guests, new functions. *Pflügers Archiv Eur J Physiol,* 455**,** 375–396.

GRAUSCHOPF, U., WINTHER, J. R., KORBER, P., ZANDER, T., DALLINGER, P. & BARDWELL, J. C. (1995) Why is DsbA such an oxidizing disulfide catalyst? *Cell,* 83**,** 947-955.

GRAY, M., BURGER, G. & LANG, B. F. (2001) The origin and early evolution of mitochondria. *Genome Biol,* 2**,** 1018.1 - 1018.5.

GRAY, M. W., BURGER, G. & LANG, B. F. (1999) Mitochondrial evolution. *Science,* 283**,** 1476-1481.

GROSS, E., KASTNER, D. B., KAISER, C. A. & FASS, D. (2004) Structure of Ero1p, source of disulfide bonds for oxidative protein folding in the cell. *Cell,* 117**,** 601-610.

GROSS, E., SEVIER, C. S., HELDMAN, N., VITU, E., BENTZUR, M., KAISER, C. A., THORPE, C. & FASS, D. (2006) Generating disulfides enzymatically: reaction products and electron acceptors of the endoplasmic reticulum thiol oxidase Ero1p. *Proc Natl Acad Sci USA,* 103**,** 299-304.

GROSS, E., SEVIER, C. S., VALA, A., KAISER, C. A. & FASS, D. (2002) A new FAD-binding fold and intersubunit disulfide shuttle in the thiol oxidase Erv2p. *Nat Struct Biol,* 9**,** 61-67.

GRUMBT, B., STROOBANT, V., TERZIYSKA, N., ISRAEL, L. & HELL, K. (2007) Functional characterization of Mia40p, the central component of the disulfide relay system of the mitochondrial intermembrane space. *J Biol Chem,* 282**,** 37461-37470.

GVAKHARIA, B. O., KOONIN, E. K. & MATHEWS, C. K. (1996) Vaccinia virus G4L gene encodes a second glutaredoxin. *Virology,* 226**,** 408-411.

HARTL, F. U., PFANNER, N. & NEUPERT, W. (1987) Translocation intermediates on the import pathway of proteins into mitochondria. *Biochem Soc Trans,* 15**,** 95-97.

HARTL, F. U., SCHMIDT, B., WACHTER, E., WEISS, H. & NEUPERT, W. (1986) Transport into mitochondria and intramitochondrial sorting of the Fe/S protein of ubiquinol-cytochrome c reductase. *Cell,* 47**,** 939-951.

HEATON, D. N., GEORGE, G. N., GARRISON, G. & WINGE, D. R. (2001) The mitochondrial copper metallochaperone Cox17 exists as an oligomeric, polycopper complex. *Biochemistry,* 40**,** 743-751.

HELL, K., HERRMANN, J. M., PRATJE, E., NEUPERT, W. & STUART, R. A. (1998) Oxa1p, an essential component of the N-tail protein export machinery in mitochondria. *Proc Natl Acad Sci USA,* 95**,** 2250-2255.

HERAS, B., EDELING, M. A., SCHIRRA, H. J., RAINA, S. & MARTIN, J. L. (2004) Crystal structures of the DsbG disulfide isomerase reveal an unstable disulfide. *Proc Natl Acad Sci USA,* 101**,** 8876–8881.

HERLAN, M., VOGEL, F., BORNHÖVD, C., NEUPERT, W. & REICHELT, S. (2003) Processing of Mgm1 by the rhomboid-type protease Pcp1 is required for maintenance of mitochondrial morphology and of mitochondrial DNA. *J Biol Chem,* 278**,** 27781-27788.

HERRMANN, J. & HELL, K. (2005) Chopped, trapped or tacked - Protein translocation into the IMS of mitochondria. *Trends Biochem Sci,* 30**,** 205-211.

HERRMANN, J. & KOHL, R. (2007) Catch me if you can! Oxidative protein trapping in the intermembrane space of mitochondria. *J Cell Biol,* 176**,** 559-563.

HERRMANN, J., NEUPERT, W. & STUART, R. A. (1997) Insertion into the mitochondrial inner membrane of a polytopic protein, the nuclear-encoded Oxa1p. *Embo J* 16**,** 2217-2226.

HINIKER, A. & BARDWELL, J. (2004) *In vivo* substrate specificity of periplasmic disulfide oxidoreductases. *J Biol Chem,* 279**,** 12967-12973.

HOFHAUS, G., LEE, J. E., TEWS, I., ROSENBERG, B. & LISOWSKY, T. (2003) The N-terminal cysteine pair of yeast sulfhydryl oxidase Erv1p is essential for in vivo activity and interacts with the primary redox centre. *Eur J Biochem,* 270**,** 1528-1535.

HOFHAUS, G., STEIN, G., POLIMENO, L., FRANCAVILLA, A. & LISOWSKY, T. (1999) Highly divergent amino termini of the homologous human ALR and yeast scERV1 gene products define species specific differences in cellular localization. *Eur J Cell Biol,* 78**,** 349-356.

HOFMANN, S., ROTHBAUER, U., MUHLENBEIN, N., BAIKER, K., HELL, K. & BAUER, M. F. (2005) Functional and mutational characterization of human MIA40 acting during import into the mitochondrial intermembrane space. *J Mol Biol,* 353**,** 517-528.

HOFMANN, S., ROTHBAUER, U., MUHLENBEIN, N., NEUPERT, W., GERBITZ, K. D., BRUNNER, M. & BAUER, M. F. (2002) The C66W mutation in the deafness dystonia peptide 1 (DDP1) affects the formation of functional DDP1.TIM13 complexes in the mitochondrial intermembrane space. *J Biol Chem,* 277**,** 23287-23293.

HOPPINS, S. C. & NARGANG, F. E. (2004) The Tim8-Tim13 Complex of Neurospora crassa Functions in the Assembly of Proteins into Both Mitochondrial Membranes. *J Biol Chem,* 279**,** 12396-12405.

HORNG, Y. C., COBINE, P. A., MAXFIELD, A. B., CARR, H. S. & WINGE, D. R. (2004) Specific copper transfer from the Cox17 metallochaperone to both Sco1 and Cox11 in the assembly of yeast cytochrome C oxidase. *J Biol Chem,* 279**,** 35334-35340.

HU, J., DONG, L. & OUTTEN, C. E. (2008) The redox environment in the mitochondrial intermembrane space is maintained separately from the cytosol and matrix. *J Biol Chem,* 283**,** 29126-29134.

HUTU, D. P., GUIARD, B., CHACINSKA, A., BECKER, D., PFANNER, N., REHLING, P. & VAN DER LAAN, M. (2008) Mitochondrial protein import motor: Differential role of Tim44 in the recruitment of Pam17 and J-complex to the presequence translocase. *Mol Biol Cell,* 19**,** 2642-2649.

HWANG, C., SINSKEY, A. J. & LODISH, H. F. (1992) Oxidized redox state of glutathione in the endoplasmic reticulum. *Science,* 257**,** 1496-1502.

INABA, K., MASUI, S., IIDA, H., VAVASSORI, S., SITIA, R. & SUZUKI, M. (2010) Crystal structures of human Ero1α reveal the mechanisms of regulated and targeted oxidation of PDI. *Embo J,* 29**,** 3330-3343.

INABA, K., MURAKAMI, S., NAKAGAWA, A., IIDA, H., KINJO, M., ITO, K. & SUZUKI, M. (2009) Dynamic nature of disulphide bond formation catalysts revealed by crystal structures of DsbB. *Embo J,* 28**,** 779-791.

INABA, K., MURAKAMI, S., SUZUKI, M., NAKAGAWA, A., YAMASHITA, E., OKADA, K. & ITO, K. (2006) Crystal structure of the DsbB-DsbA complex reveals a mechanism of disulfide bond generation. *Cell,* 127**,** 789-801.

INABA, K., TAKAHASHI, Y. H. & ITO, K. (2005) Reactivities of quinone-free DsbB from *Escherichia coli*. *J Biol Chem,* 280**,** 33035-33044.

ISHIKAWA, D., YAMAMOTO, H., TAMURA, Y., MORITOH, K. & ENDO, T. (2004) Two novel proteins in the mitochondrial outer membrane mediate β-barrel protein assembly. *J Cell Biol,* 166**,** 621-627.

IVANOVA, E., BALL, M. & LU, H. (2008) Zinc binding of Tim10: evidence for existence of an unstructured binding intermediate for a zinc finger protein. *Proteins,* 71**,** 467-475.

JANDER, G., MARTIN, N. L. & BECKWITH, J. (1994) Two cysteines in each periplasmic domain of the membrane protein DsbB are required for its function in protein disulfide bond formation. *Embo J* 13**,** 5121-5127.

JENSEN, R. E. & DUNN, C. D. (2002) Protein import into and across the mitochondrial inner membrane: role of the TIM23 and TIM22 translocons. *Biochim Biophys Acta,* 1592**,** 25-34.

JESSOP, C. E. & BULLEID, N. (2004) Glutathione directly reduces an oxidoreductase in the endoplasmic reticulum of mammalian cells. *J Biol Chem,* 279**,** 55341-55347.

JIANG, X. & WANG, X. (2004) Cytochrome C-mediated apoptosis. *Annu Rev Biochem,* 73**,** 87-106.

KADOKURA, H. & BECKWITH, J. (2002) Four cysteines of the membrane protein DsbB act in concert to oxidize its substrate DsbA. *Embo J,* 21**,** 2354–2363.

KADOKURA, H., TIAN, H., ZANDER, T., BARDWELL, J. C. A. & BECKWITH, J. (2004) Snapshots of DsbA in action: detection of proteins in the process of oxidative folding. *Science,* 303**,** 534-537.

KAMITANI, S., AKIYAMA, Y. & ITO, K. (1992) Identification and characterization of an Escherichia coli gene required for the formation of correctly folded alkaline phosphatase, a periplasmic enzyme. *Embo J,* 11**,** 57-62.

KANAMORI, T., NISHIKAWA, S. I., NAKAI, M., SHIN, I., SCHULTZ, P. G. & ENDO, T. (1999) Uncoupling of transfer of the presequence and unfolding of the mature domain in precursor translocation across the mitochondrial outer membrane. *Proc Natl Acad Sci USA,* 96**,** 3634-3639.

KAUT, A., LANGE, H., DIEKERT, K., KISPAL, G. & LILL, R. (2000) Isa1p is a component of the mitochondrial machinery for maturation of cellular iron-sulfur proteins and requires conserved cysteine residues for function. *J Biol Chem,* 275**,** 15955-15961.

KAWANO, S., YAMANO, K., NAOE, M., MOMOSE, T., TERAO, K., NISHIKAWA, S., WATANABE, N. & ENDO, T. (2009) Structural basis of yeast Tim40/Mia40 as an oxidative translocator in the mitochondrial intermembrane space. *Proc Natl Acad Sci USA,* 106**,** 14403-14407.

KERSCHER, O., HOLDER, J., SRINIVASAN, M., LEUNG, R. S. & JENSEN, R. E. (1997) The Tim54p-Tim22p complex mediates insertion of proteins into the mitochondrial inner membrane. *J Cell Biol,* 139**,** 1663-1675.

KHALIMONCHUK, O., RIGBY, K., BESTWICK, M., PIERREL, F., COBINE, P. A. & WINGE, D. R. (2008) Pet191 is a cytochrome c oxidase assembly factor in *Saccharomyces cerevisiae*. *Eukaryot Cell,* 7**,** 1427-1431.

KISHIGAMI, S. & ITO, K. (1996) Roles of cysteine residues of DsbB in its activity to reoxidize DsbA, the protein disulphide bond catalyst of *Escherichia coli*. *Genes Cells,* 1**,** 201–208.

KISPAL, G., CSERE, P., PROHL, C. & LILL, R. (1999) The mitochondrial proteins Atm1p and Nfs1p are essential for biogenesis of cytosolic Fe/S proteins. *Embo J,* 18**,** 3981-3989.

KOBAYASHI, T. & ITO, K. (1999) Respiratory chain strongly oxidizes the CXXC motif of DsbB in the *Escherichia coli* disulfide bond formation pathway. *Embo J,* 18**,** 1192–1198.

KOEHLER, C. M. (2004) The small Tim proteins and the twin CX_3C motif. *Trends Biochem Sci,* 29**,** 1-4.

KOEHLER, C. M., BEVERLY, K. N. & LEVERICH, E. P. (2006) Redox pathways of the mitochondrion. *Antioxid Redox Signal,* 8**,** 813-822.

KOEHLER, C. M., MERCHANT, S., OPPLIGER, W., SCHMID, K., JAROSCH, E., DOLFINI, L., JUNNE, T., SCHATZ, G. & TOKATLIDIS, K. (1998) Tim9p, an essential partner subunit of Tim10p for the import of mitochondrial carrier proteins. *Embo J,* 17**,** 6477-6486.

KOMIYA, T., ROSPERT, S., KOEHLER, C., LOOSER, R., SCHATZ, G. & MIHARA, K. (1998) Interaction of mitochondrial targeting signals with acidic receptor domains along the protein import pathway: Evidence for the 'acid chain' hypothesis. *Embo J,* 17**,** 3886-3898.

KOVERMANN, P., TRUSCOTT, K. N., GUIARD, B., REHLING, P., SEPURI, N. B., MULLER, H., JENSEN, R. E., WAGNER, R. & PFANNER, N. (2002) Tim22, the essential core of the mitochondrial protein insertion complex, forms a voltage-activated and signal-gated channel. *Mol Cell,* 9**,** 363-373.

KOZANY, C., MOKRANJAC, D., SICHTING, M., NEUPERT, W. & HELL, K. (2004) The J domain-related cochaperone Tim16 is a constituent of the mitochondrial TIM23 preprotein translocase. *Nat Struct Mol Biol,* 11**,** 234-241.

KOZJAK, V., WIEDEMANN, N., MILENKOVIC, D., LOHAUS, C., MEYER, H. E., GUIARD, B., MEISINGER, C. & PFANNER, N. (2003) An essential role of Sam50 in the protein sorting and assembly machinery of the mitochondrial outer membrane. *J Biol Chem,* 278**,** 48520-48523.

KRAYL, M., LIM, J. H., MARTIN, F., GUIARD, B. & VOOS, W. (2007) A cooperative action of the ATP-dependent import motor complex and the inner membrane potential drives mitochondrial preprotein import. *Mol Cell Biol,* 27**,** 411-425.

KREZEL, A., LATAJKA, R., BUJACZ, G. D. & BAL, W. (2003) Coordination properties of tris(2-carboxyethyl)phosphine, a newly introduced thiol reductant, and its oxide. *Inorg Chem,* 42**,** 1994-2003.

KREZEL , A., LATAJKA, R., BUJACZ, G. D. & BAL, W. (2003) Coordination properties of tris(2-carboxyethyl)phosphine, a newly introduced thiol reductant, and its oxide. *Inorg Chem,* 42**,** 1994-2003.

KUTIK, S., STOJANOVSKI, D., BECKER, L., BECKER, T., MEINECKE, M., KRUGER, V., PRINZ, C., MEISINGER, C., GUIARD, B., WAGNER, R., PFANNER, N. &

WIEDEMANN, N. (2008) Dissecting membrane insertion of mitochondrial β-barrel proteins. *Cell,* 132**,** 1011-1024.

LABOISSIERE, M. C., STURLEY, S. L. & RAINES, R. T. (1995) The essential function of protein-disulfide isomerase is to unscramble non-native disulfide bonds. *J Biol Chem,* 270**,** 28006-28009.

LAMANTIA, M., MIURA, T., TACHIKAWA, H., KAPLAN, H. A., LENNARZ, W. J. & MIZUNAGA, T. (1991) Glycosylation site binding protein and protein disulfide isomerase are identical and essential for cell viability in yeast. *Proc Natl Acad Sci USA,* 88**,** 4453–4457.

LANGE, H., KAUT, A., KISPAL, G. & LILL, R. (2000) A mitochondrial ferredoxin is essential for biogenesis of cellular iron-sulfur proteins. *Proc Natl Acad Sci USA,* 97**,** 1050-1055.

LANGE, H., LISOWSKY, T., GERBER, J., MUHLENHOFF, U., KISPAL, G. & LILL, R. (2001) An essential function of the mitochondrial sulfhydryl oxidase Erv1p/ALR in the maturation of cytosolic Fe/S proteins. *Embo Rep,* 2**,** 715-720.

LEE, J., HOFHAUS, G. & LISOWSKY, T. (2000) Erv1p from *Saccharomyces cerevisiae* is a FAD-linked sulfhydryl oxidase. *FEBS Lett,* 477**,** 62-66.

LI, J., SAXENA, S., PAIN, D. & DANCIS, A. (2001) Adrenodoxin reductase homolog (Arh1p) of yeast mitochondria required for iron homeostasis. *J Biol Chem,* 276**,** 1503-1509.

LI, Y., DUDEK, J., GUIARD, B., PFANNER, N., REHLING, P. & VOOS, W. (2004) The presequence translocase-associated protein import motor of mitochondria: Pam16 functions in an antagonistic manner to Pam18. *J Biol Chem,* 279**,** 38047-38054.

LILL, R., DIEKERT, K., KAUT, A., LANGE, H., PELZER, W., PROHL, C. & KISPAL, G. (1999) The essential role of mitochondria in the biogenesis of cellular iron-sulfur proteins. *Biol Chem,* 380**,** 1157-1166.

LILL, R. & KISPAL, G. (2000) Maturation of cellular Fe-S proteins: An essential function of mitochondria. *Trends Biochem Sci,* 25**,** 352-356.

LIONAKI, E., AIVALIOTIS, M., POZIDIS, C. & TOKATLIDIS, K. (2010) The N-terminal shuttle domain of Erv1 determines the affinity for Mia40 and mediates electron transfer to the catalytic Erv1 core in yeast mitochondria. *Antioxid Redox Signal*.

LIONAKI, E., DE MARCOS LOUSA, C., BAUD, C., VOUGIOUKALAKI, M., PANAYOTOU, G. & TOKATLIDIS, K. (2008) The essential function of Tim12 *in*

vivo is ensured by the assembly interactions of its C-terminal domain. *J Biol Chem,* 283**,** 15747-15753.

LISOWSKY, T. (1992) Dual function of a new nuclear gene for oxidative phosphorylation and vegetative growth in yeast. *Mol Gen Genet,* 232**,** 58-64.

LISOWSKY, T. (1994) ERV1 is involved in the cell-division cycle and the maintenance of mitochondrial genomes in *Saccharomyces cerevisiae*. *Curr Genet,* 26**,** 15-20.

LISOWSKY, T. (1996) Removal of an intron with unique 3' branch site creates an amino-terminal protein sequence directing the scERV1 gene product to mitochondria. *Yeast,* 12**,** 1501-1510.

LOCKER, J. K. & GRIFFITHS, G. (1999) An unconventional role for cytoplasmic disulfide bonds in vaccinia virus proteins. *J Biol Chem,* 144**,** 267-279.

LONGEN, S., BIEN, M., BIHLMAIER, K., KLOEPPEL, C., KAUFF, F., HAMMERMEISTER, M., WESTERMANN, B., HERMANN, J. M. & RIEMER, J. (2009) Systematic analysis of the twin CX_9C protein family. *J Mol Biol,* 393**,** 356-368.

LU, H., ALLEN, S., WARDLEWORTH, L., SAVORY, P. & TOKATLIDIS, K. (2004) Functional TIM10 chaperone assembly is redox-regulated *in vivo*. *J Biol Chem,* 279**,** 18952-18958.

LU, H. & WOODBURN, J. (2005) Zinc binding stabilizes mitochondrial Tim10 in a reduced and import-competent state kinetically. *J Mol Biol,* 353**,** 897-910.

MALOJCIĆ, G., OWEN, R. L., GRIMSHAW, J. P. & GLOCKSHUBER, R. (2008) Preparation and structure of the charge-transfer intermediate of the transmembrane redox catalyst DsbB. *FEBS Lett,* 582**,** 3301-3307.

MARGULIS, L. (1981) Symbiosis in cell evolution: Life and its environment on the early Earth. New York: W. H. Freeman.

MARQUARDT, T., HEBERT, D. N. & HELENIUS, A. (1993) Post-translational folding of influenza hemagglutinin in isolated endoplasmic reticulum-derived microsomes. *J Biol Chem,* 268**,** 19618–19625.

MEIER, S., NEUPERT, W. & HERRMANN, J. (2005) Proline residues of transmembrane domains determine the sorting of inner membrane proteins in mitochondria. *J Cell Biol,* 170**,** 881-888.

MEISINGER, C., PFANNSCHMIDT, S., RISSLER, M., MILENKOVIC, D., BECKER, T., STOJANOVSKI, D., YOUNGMAN, M. J., JENSEN, R. E., CHACINSKA, A.,

GUIARD, B., PFANNER, N. & WIEDEMANN, N. (2007) The morphology proteins Mdm12/Mmm1 function in the major β-barrel assembly pathway of mitochondria. *Embo J,* 26**,** 2229-2239.

MEISINGER, C., RISSLER, M., CHACINSKA, A., SANJUÁN SZKLARZ, L. K., MILENKOVIC, D., KOZJAK, V., SCHÖNFISCH, B., LOHAUS, C., MEYER, H. E., YAFFE, M. P., GUIARD, B., WIEDEMANN, N. & PFANNER, N. (2004) The mitochondrial morphology protein Mdm10 functions in assembly of the preprotein translocase of the outer membrane. *Dev Cell,* 7**,** 61-71.

MESECKE, N., BIHLMAIER, K., GRUMBT, B., LONGEN, S., TERZIYSKA, N., HELL, K. & HERRMANN, J. M. (2008) The zinc-binding protein Hot13 promotes oxidation of the mitochondrial import receptor Mia40. *Embo Rep,* 9**,** 1107-1113.

MESECKE, N., TERZIYSKA, N., KOZANY, C., BAUMANN, F., NEUPERT, W., HELL, K. & HERRMANN, J. M. (2005) A disulfide relay system in the intermembrane space of mitochondria that mediates protein import. *Cell,* 121**,** 1059-1069.

MEZGHRANI, A., FASSIO, A., BENHAM, A., SIMMEN, T., BRAAKMAN, I. & SITIA, R. (2001) Manipulation of oxidative protein folding and PDI redox state in mammalian cells. *Embo J,* 22**,** 6288-6296.

MIAO, B. J., DAVIS, J. E. & CRAIG, E. A. (1997) Mge1 functions as a nucleotide release factor for Ssc1, a mitochondrial Hsp70 of Saccharomyces cerevisiae. *J Mol Biol,* 265**,** 541–552.

MILENKOVIC, D., RAMMING, T., MULLER, J. M., WENZ, L. S., GEBERT, N., SCHULZE-SPECKING, A., STOJANOVSKI, D., ROSPERT, S. & CHACINSKA, A. (2009) Identification of the signal directing Tim9 and Tim10 into the intermembrane space of mitochondria. *Mol Biol Cell,* 20**,** 2530-2539.

MISSIAKAS, D., GEORGOPOULOS, C. & RAINA, S. (1994) The *Escherichia coli* dsbC (xprA) gene encodes a periplasmic protein involved in disulfide bond formation. *Embo J,* 13**,** 2013-2020.

MOBERG, P., NILSSON, S., STAHL, A., ERIKSSON, A. C., GLASER, E. & MÄLER, L. (2004) NMR solution structure of the mitochondrial $F_1\beta$ presequence from *Nicotiana plumbaginifolia*. *J Mol Biol,* 336**,** 1129-1140.

MOKRANJAC, D., BOURENKOV, G., HELL, K., NEUPERT, W. & GROLL, M. (2006) Structure and function of Tim14 and Tim16, the J and J-like components of the mitochondrial protein import motor. *Embo J,* 25**,** 4675-4685.

MOKRANJAC, D., PASCHEN, S. A., KOZANY, C., PROKISCH, H., HOPPINS, S. C., NARGANG, F. E., NEUPERT, W. & HELL, K. (2003) Tim50, a novel component of the TIM23 preprotein translocase of mitochondria. *Embo J,* 22**,** 816-825.

MOKRANJAC, D., SICHTING, M., POPOV-CELEKETIC, D., MAPA, K., GEVORKYAN-AIRAPETOV, L., ZOHARY, K., HELL, K., AZEM, A. & NEUPERT, W. (2009) Role of tim50 in the transfer of precursor proteins from the outer to the inner membrane of mitochondria. *Mol Biol Cell,* 20**,** 1400-1407.

MOLTENI, S. N., FASSIO, A., CIRIOLO, M. R., FILOMENI, G., PASQUALETTO, E., FAGIOLI, C. & SITIA, R. (2004) Glutathione limits Ero1-dependent oxidation in the endoplasmic reticulum. *J Biol Chem,* 279**,** 32667-32673.

MORGAN, B., ANG, S. K., YAN, G. & LU, H. (2009) Zinc can play chaperone-like and inhibitor roles during import of mitochondrial small Tim proteins. *J Biol Chem,* 284**,** 6818-6825.

MORGAN, B. & LU, H. (2008) Oxidative folding competes with mitochondrial import of the small Tim proteins. *Biochem J,* 411**,** 115-122.

MÜLLER, J. M., MILENKOVIC, D., GUIARD, B., PFANNER, N. & CHACINSKA, A. (2008) Precursor oxidation by Mia40 and Erv1 promotes vectorial transport of proteins into the mitochondrial intermembrane space. *Mol Biol Cell,* 19**,** 226-236.

MUHLENHOFF, U. & LILL, R. (2000) Biogenesis of iron-sulfur proteins in eukaryotes: a novel task of mitochondria that is inherited from bacteria. *Biochim Biophys Acta,* 1549**,** 370-382.

MURPHY, M. P. (2009) How mitochondria produce reactive oxygen species. *Biochem J,* 417**,** 1–13.

NAOÉ, M., OHWA, Y., ISHIKAWA, D., OHSHIMA, C., NISHIKAWA, S. I., YAMAMOTO, H. & ENDO, T. (2004) Identification of Tim40 that mediates protein sorting to the mitochondrial intermembrane space. *J Biol Chem,* 279**,** 47815-47821.

NARGANG, F. E., DRYGAS, M. E., KWONG, P. L., NICHOLSON, D. W. & NEUPERT, W. (1988) A mutant of Neurospora crassa deficient in cytochrome c heme lyase activity cannot import cytochrome c into mitochondria. *J Biol Chem,* 263**,** 9388-9394.

NELSON, J. W. & CREIGHTON, T. E. (1994) Reactivity and ionization of the active site cysteine residues of DsbA, a protein required for disulfide bond formation *in vivo*. *Biochemistry,* 33**,** 5974-5983.

NEUPERT, W. & BRUNNER, M. (2002) The protein import motor of mitochondria. *Nat Rev Mol Cell Biol,* 3**,** 555-565.

NEUPERT, W. & HERRMANN, J. M. (2007) Translocation of proteins into mitochondria. *Annu Rev Biochem,* 76**,** 723-749.

OTERA, H., TAIRA, Y., HORIE, C., SUZUKI, Y., SUZUKI, H., SETOGUCHI, K., KATO, H., OKA, T. & MIHARA, K. (2007) A novel insertion pathway of mitochondrial outer membrane proteins with multiple transmembrane segments. *J Cell Biol,* 179**,** 1355-1363.

PASCHEN, S. A., WAIZENEGGER, T., STAN, T., PREUSS, M., CYRKLAFF, M., HELL, K., RAPAPORT, D. & NEUPERT, W. (2003) Evolutionary conservation of biogenesis of β-barrel membrane proteins. *Nature,* 426**,** 862-866.

PEBAY-PEYROULA, E., DAHOUT-GONZALEZ, C., KAHN, R., TRÉZÉGUET, V., LAUQUIN, G. J. & BRANDOLIN, G. (2003) Structure of mitochondrial ADP/ATP carrier in complex with carboxyatractyloside. *Nature,* 426**,** 39-44.

PECK JR, E. J. & RAY JR, W. J. (1971) Metal complexes of phosphoglucomutase *in vivo*. Alterations induced by insulin. *J Biol Chem,* 246**,** 1160-1167.

PERKINS, G. A. & FREY, T. G. (2000) Recent structural insight into mitochondria gained by microscopy. *Micron,* 31**,** 97–111.

PFANNER, N. & NEUPERT, W. (1987) Distinct steps in the import of ADP/ATP carrier into mitochondria. *J Biol Chem,* 262**,** 7528-7536.

PIECZENIK, S. R. & NEUSTADT, J. (2007) Mitochondrial dysfunction and molecular pathways of disease. *Exp Mol Pathol,* 83**,** 84-92.

POPOV-CELEKETIĆ, J., WAIZENEGGER, T. & RAPAPORT, D. (2008) Mim1 Functions in an Oligomeric Form to Facilitate the Integration of Tom20 into the Mitochondrial Outer Membrane. *J Mol Biol,* 376**,** 671-680.

RAJE, S. & THORPE, C. (2003) Inter-domain redox communication in flavoenzymes of the quiescin/sulfhydryl oxidase family: role of a thioredoxin domain in disulfide bond formation. *Biochemistry,* 42**,** 4560-4568.

REDDEHASE, S., GRUMBT, B., NEUPERT, W. & HELL, K. (2009) The disulfide relay system of mitochondria is required for the biogenesis of mitochondrial Ccs1 and Sod1. *J Mol Biol,* 385**,** 331-338.

REHLING, P., MODEL, K., BRANDNER, K., KOVERMANN, P., SICKMANN, A., MEYER, H. E., KUHLBRANDT, W., WAGNER, R., TRUSCOTT, K. N. &

PFANNER, N. (2003) Protein insertion into the mitochondrial inner membrane by a twin-pore translocase. *Science,* 299**,** 1747.

RIETSCH, A., BESSETTE, P., GEORGIOU, G. & BECKWITH, J. (1997) Reduction of the periplasmic disulfide bond isomerase, DsbC, occurs by passage of electrons from cytoplasmic thioredoxin. *J Bacteriol,* 179**,** 6602-6608.

RISSLER, M., WIEDEMANN, N., PFANNSCHMIDT, S., GABRIEL, K., GUIARD, B., PFANNER, N. & CHACINSKA, A. (2005) The essential mitochondrial protein Erv1 cooperates with Mia40 in biogenesis of intermembrane space proteins. *J Mol Biol,* 353**,** 485-492.

ROESCH, K., CURRAN, S. P., TRANEBJAERG, L. & KOEHLER, C. M. (2002) Human deafness dystonia syndrome is caused by a defect in assembly of the DDP1/TIMM8a-TIMM13 complex. *Hum Mol Genet,* 11**,** 477-486.

ROJO, E. E., GUIARD, B., NEUPERT, W. & STUART, R. A. (1998) Sorting of D-lactate dehydrogenase to the inner membrane of mitochondria. Analysis of topogenic signal and energetic requirements. *J Biol Chem,* 273**,** 8040-8047.

ROJO, E. E., STUART, R. A. & NEUPERT, W. (1995) Conservative sorting of F0-ATPase subunit 9: export from matrix requires delta pH across inner membrane and matrix ATP. *Embo J,* 14**,** 3445-3451.

ROTHWARF, D. M. & SCHERAGA, H. A. (1992) Equilibrium and kinetic constants for the thiol-disulfide interchange reaction between glutathione and dithiothreitol. *Proc Natl Acad Sci USA,* 89**,** 7944-7948.

SAITOH, T., IGURA, M., OBITA, T., OSE, T., KOJIMA, R., MAENAKA, K., ENDO, T. & KOHDA, D. (2007) Tom20 recognizes mitochondrial presequences through dynamic equilibrium among multiple bound states. *Embo J,* 26**,** 4777-4787.

SCHAGGER, H. & VON JAGOW, G. (1987) Tricine-sodium dodecyl sulfate-polyacrylamide gel electrophoresis for the separation of proteins in the range from 1 to 100 kDa. *Anal Biochem,* 166**,** 368-379.

SCHAPIRA, A. H. (2006) Mitochondrial disease. *Lancet,* 368**,** 70-82.

SCHNEIDER, A., BERHRENS, M., SCHERER, P., PRATJE, E., MICHAELIS, G. & SCHATZ, G. (1991) Inner membrane protease I, an enzyme mediating intramitochondrial protein sorting in yeast. *Embo J,* 10**,** 247-254.

SENKEVICH, T. G., WHITE, C. L., KOONIN, E. V. & MOSS, B. (2000) A viral member of the ERV1/ALR protein family participates in a cytoplasmic pathway of disulfide bond formation. *Proc Natl Acad Sci USA,* 97**,** 12068-12073.

SENKEVICH, T. G., WHITE, C. L., KOONIN, E. V. & MOSS, B. (2002) Complete pathway for protein disulfide bond formation encoded by poxviruses. *Proc Natl Acad Sci USA,* 99**,** 6667-6672.

SESAKI, H., SOUTHARD, S. M., AIKEN HOBBS, A. E. & JENSEN, R. E. (2003) Cells lacking Pcp1p/Ugo2p, a rhomboid-like protease required for Mgm1p processing, lose mtDNA and mitochondrial structure in a Dnm1p-dependent manner, but remain competent for mitochondrial fusion. *Biochem Biophys Res Commun,* 308**,** 276-283.

SEVIER, C. S., CUOZZO, J. W., VALA, A., ASLUND, F. & KAISER, C. A. (2001) A flavoprotein oxidase defines a new endoplasmic reticulum pathway for biosynthetic disulphide bond formation. *Nat Cell Biol,* 3**,** 874-882.

SEVIER, C. S. & KAISER, C. A. (2002) Formation and transfer of disulphide bonds in living cells. *Nat Rev Mol Cell Biol,* 3**,** 836.

SEVIER, C. S. & KAISER, C. A. (2006a) Conservation and diversity of the cellular disulfide bond formation pathways. *Antioxidants and Redox Signaling,* 8**,** 797-811.

SEVIER, C. S. & KAISER, C. A. (2006b) Disulfide transfer between two conserved cysteine pairs imparts selectivity to protein oxidation by Ero1. *Mol Biol Cell,* 17**,** 2256-2266.

SEVIER, C. S., QU, H., HELDMAN, N., GROSS, E., FASS, D. & KAISER, C. A. (2007) Modulation of cellular disulfide-bond formation and the ER redox environment by feedback regulation of Ero1. *Cell,* 129**,** 333-344.

SHARIFF, K., GHOSAL, S. & MATOUSCHEK, A. (2004) The force exerted by the membrane potential during protein import into the mitochondrial matrix. *Biophys J,* 86**,** 3647-3652.

SICKMANN, A., REINDERS, J., WAGNER, Y., JOPPICH, C., ZAHEDI, R., MEYER, H. E., SCHONFISCH, B., PERSCHIL, I., CHACINSKA, A., GUIARD, B., REHLING, P., PFANNER, N. & MEISINGER, C. (2003) The proteome of *Saccharomyces cerevisiae* mitochondria. *Proc Natl Acad Sci USA,* 100**,** 13207.

SIDERIS, D. P., PETRAKIS, N., KATRAKILI, N., MIKROPOULOU, D., GALLO, A., CIOFI-BAFFONI, S., BANCI, L., BERTINI, I. & TOKATLIDIS, K. (2009) A novel intermembrane space targeting signal primes cysteines for docking onto Mia40 in mitochondrial oxidative folding. *J Cell Biol,* 187**,** 1007-1022.

SIMONS, T. J. B. (1991) Intracellular free zinc and zinc buffering in human red blood cells. *J Membr Biol,* 23**,** 63-71.

SIRRENBERG, C., ENDRES, M., FOLSCH, H., STUART, R. A., NEUPERT, W. & BRUNNER, M. (1998) Carrier protein import into mitochondria mediated by the intermembrane proteins Tim10/Mrs11 and Tim12/Mrs5. *Nature,* 391**,** 912-915.

STAAL, F. J., ROEDERER, M. & HERZENBERG, L. A. (1990) Intracellular thiols regulate activation of nuclear factor kappa B and transcription of human immunodeficiency virus. *Proc Natl Acad Sci USA,* 87**,** 9943-9947.

STEIN, G. & LISOWSKY, T. (1998) Functional comparison of the yeast scERV1 and scERV2 genes. *Yeast,* 14**,** 171-180.

STEINER, H., ZOLLNER, A., HAID, A., NEUPERT, W. & LILL, R. (1995) Biogenesis of mitochondrial heme lyases in yeast – import and folding in the intermembrane space. *J Biol Chem,* 270**,** 22842-22849.

STOJANOVSKI, D., GUIARD, B., KOZJAK-PAVLOVIC, V., PFANNER, N. & MEISINGER, C. (2007) Alternative function for the mitochondrial SAM complex in biogenesis of α-helical TOM proteins. *J Cell Biol,* 179**,** 881-893.

STOJANOVSKI, D., MILENKOVIC, D., MULLER, J. M., GABRIEL, K., SCHULZE-SPECKING, A., BAKER, M. J., RYAN, M. T., GUIARD, B., PFANNER, N. & CHACINSKA, A. (2008a) Mitochondrial protein import: Precursor oxidation in a ternary complex with disulfide carrier and sulfhydryl oxidase. *J Cell Biol,* 183**,** 195-202.

STOJANOVSKI, D., MÜLLER, J. M., MILENKOVIC, D., GUIARD, B., PFANNER, N. & CHACINSKA, A. (2008b) The MIA system for protein import into the mitochondrial intermembrane space. *Biochim Biophys Acta,* 1783**,** 610-617.

SUN, X. X. & WANG, C. C. (2000) The N-terminal sequence (residues 1-65) is essential for dimerization, activities, and peptide binding of *Escherichia coli* DsbC. *J Biol Chem,* 275**,** 22743-22749.

TAKAHASHI, Y. H., INABA, K. & ITO, A. (2004) Characterization of the menaquinone-dependent disulfide bond formation pathway of *Escherichia coli*. *J Biochem,* 279**,** 47057-47065.

TAMURA, Y., HARADA, Y., SHIOTA, T., YAMANO, K., WATANABE, K., YOKOTA, M., YAMAMOTO, H., SESAKI, H. & ENDO, T. (2009) Tim23 - Tim50 pair

coordinates functions of translocators and motor proteins in mitochondrial protein import. *J Cell Biol,* 184**,** 129-141.

TAYLOR, S. W., FAHY, E., ZHANG, B., GLENN, G. M., WARNOCK, D. E., WILEY, S., MURPHY, A. N., GAUCHER, S. P., CAPALDI, R. A., GIBSON, B. W. & GHOSH, S. S. (2003) Characterization of the human heart mitochondrial proteome. *Nat Biotech,* 21**,** 281-286.

TERZIYSKA, N., GRUMBT, B., BIEN, M., NEUPERT, W., HERMANN, J. M. & HELL, K. (2007) The sulfhydryl oxidase Erv1 is a substrate of the Mia40-dependent protein translocation pathway. *FEBS Lett,* 581**,** 1098-1102.

TERZIYSKA, N., GRUMBT, B., KOZANY, C. & HELL, K. (2009) Structural and functional roles of the conserved cysteine residues of the redox-regulated import receptor Mia40 in the intermembrane space of mitochondria. *J Biol Chem,* 284**,** 1353-1363.

TERZIYSKA, N., LUTZ, T., KOZANY, C., MOKRANJAC, D., MESECKE, N., NEUPERT, W., HERRMANN, J. M. & HELL, K. (2005) Mia40, a novel factor for protein import into the intermembrane space of mitochondria is able to bind metal ions. *FEBS Lett,* 579**,** 179-184.

THORPE, C. & COPPOCK, D. L. (2007) Generating disulfides in multicellular organisms: emerging roles for a new flavoprotein family. *J Biol Chem,* 282**,** 13929-13933.

THORPE, C., HOOBER, K. L., RAJE, S., GLYNN, N. M., BURNSIDE, J., TURI, G. K. & COPPOCK, D. L. (2002) Sulfhydryl oxidases: Emerging catalysts of protein disulfide bond formation in eukaryotes. *Arch Biochem Biophys,* 405**,** 1-12.

TIAN, G., XIANG, S., NOIVA, R., LENNARZ, W. J. & SCHINDELIN, H. (2006) The crystal structure of yeast protein disulfide isomerase suggests cooperativity between its active sites. *Cell,* 124**,** 61.

TIENSON, H. L., DABIR, D. V., NEAL, S. E., LOO, R., HASSON, S. A., BOONTHEUNG, P., KIM, S. K., LOO, J. A. & KOEHLER, C. M. (2009) Reconstitution of the Mia40-Erv1 oxidative folding pathway for the small Tim proteins. *Mol Biol Cell,* 20**,** 3481-3490.

TRUSCOTT, K. N., WIEDEMANN, N., REHLING, P., MULLER, H., MEISINGER, C. & PFANNER, N. (2002) Mitochondrial import of the ADP/ATP carrier: the essential TIM complex of the intermembrane space is required for precursor release from the TOM complex. *Mol Cell Biol,* 22**,** 7780-7789.

TSAI, B., RODIGHIERO, C., LENCER, W. I. & RAPOPORT, T. A. (2001) Protein disulfide isomerase acts as a redox-dependent chaperone to unfold cholera toxin. *Cell,* 104**,** 937-948.

TSUKIHARA, T., AOYAMA, H., YAMASHITA, E., TOMIZAKI, T., YAMAGUCHI, H., SHINZAWA-ITOH, K., NAKASHIMA, R., YAONO, R. & YOSHIKAWA, S. (1995) Structures of metal sites of oxidized bovine heart cytochrome c oxidase at 2.8 A. *Science,* 269**,** 1069-1074.

TU, B. P., HO-SCHLEYER, S. C., TRAVERS, K. J. & WEISSMAN, J. S. (2000) Biochemical basis of oxidative protein folding in the endoplasmic reticulum. *Science,* 290**,** 1571-1574.

TU, B. P. & WEISSMAN, J. (2002) The FAD- and O_2-dependent reaction cycle of Ero1-mediated oxidative protein folding in the endoplasmic reticulum. *Mol Cell,* 10**,** 983-994.

TURY, A., MAIRET-COELLO, G., PONCET, F., JACQUEMARD, C., RISOLD, P. Y., FELLMANN, D. & GRIFFOND, B. (2004) QSOX sulfhydryl oxidase in rat adenohypophysis: localization and regulation by estrogens. *J Endocrinol,* 183**,** 353-363.

UNGERMANN, C., GUIARD, B., NEUPERT, W. & CYR, D. M. (1996) The delta psi- and Hsp70/MIM44-dependent reaction cycle driving early steps of protein import into mitochondria. *Embo J,* 15**,** 735-744.

UNGERMANN, C., NEUPERT, W. & CYR, D. M. (1994) The role of Hsp70 in conferring unidirectionality on protein translocation into mitochondria. *Science,* 266**,** 1250-1253.

VALA, A., SEVIER, C. S. & KAISER, C. A. (2005) Structural determinants of substrate access to the disulfide oxidase Erv2p. *J Mol Biol,* 354**,** 952-966.

VAN DER LAAN, M., MEINECKE, M., DUDEK, J., HUTU, D. P., LIND, M., PERSCHIL, I., GUIARD, B., WAGNER, R., PFANNER, N. & REHLING, P. (2007) Motor-free mitochondrial presequence translocase drives membrane integration of preproteins. *Nat Cell Biol,* 9**,** 1152-1159.

VAN DER LAAN, M., WIEDEMANN, N., MICK, D. U., GUIARD, B., REHLING, P. & PFANNER, N. (2006) A role for Tim21 in membrane-potential-dependent preprotein sorting in mitochondria. *Curr Biol,* 16**,** 2271-2276.

VAN LOON, A. P., BRÄNDLI, A. W. & SCHATZ, G. (1986) The presequences of two imported mitochondrial proteins contain information for intracellular and intramitochondrial sorting. *Cell,* 44**,** 801-812.

VASILJEV, A., AHTING, U., NARGANG, F. E., GO, N. E., HABIB, S. J., KOZANY, C., PANNEELS, V., SINNING, I., PROKISCH, H., NEUPERT, W., NUSSBERGER, S. & RAPAPORT, D. (2004) Reconstituted TOM core complex and Tim9/Tim10 complex of mitochondria are sufficient for translocation of the ADP/ATP carrier across membranes. *Mol Biol Cell,* 15**,** 1445-1458.

VELTRI, K. L., ESPIRITU, M. & SINGH, G. (1990) Distinct genomic copy number in mitochondria of different mammalian organs. *J Cell Physiol,* 143**,** 160-164.

VERGNOLLE, M. A., ALCOCK, F. H., PETRAKIS, N. & TOKATLIDIS, K. (2007) Mutation of conserved charged residues in mitochondrial TIM10 subunits precludes TIM10 complex assembly, but does not abolish growth of yeast cells. *J Mol Biol,* 371**,** 1315-1324.

VERGNOLLE, M. A., BAUD, C., GOLOVANOV, A. P., ALCOCK, F., LUCIANO, P., LIAN, L. Y. & TOKATLIDIS, K. (2005) Distinct domains of small Tims involved in subunit interaction and substrate recognition. *J Mol Biol,* 351**,** 839-849.

VITU, E., BENTZUR, M., LISOWSKY, T., KAISER, C. A. & FASS, D. (2006) Gain of function in an ERV/ALR sulfhydryl oxidase by molecular engineering of the shuttle disulfide. *J Mol Biol,* 362**,** 89-101.

VITU, E., KIM, S., SEVIER, C. S., LUTZKY, O., HELDMAN, N., BENTZUR, M., UNGER, T., YONDA, M., KAISER, C. A. & FASS, D. (2010) Oxidative activity of yeast Ero1p on protein disulfide isomerase and related oxidoreductases of the endoplasmic reticulum. *J Biol Chem,* 285**,** 18155–18165.

VON HEIJNE, G. (1986) Mitochondrial targeting sequences may form amphiphilic helices. *Embo J,* 5**,** 1335-1342.

WAGNER, K., GEBERT, N., GUIARD, B., BRANDNER, K., TRUSCOTT, K. N., WIEDEMANN, N., PFANNER, N. & REHLING, P. (2008) The assembly pathway of the mitochondrial carrier translocase involves four preprotein translocases. *Mol Cell Biol,* 28**,** 4251-4260.

WAIZENEGGER, T., SCHMITT, S., ZIVKOVIC, J., NEUPERT, W. & RAPAPORT, D. (2005) Mim1, a protein required for the assembly of the TOM complex of nitochondria. *EMBO Rep,* 6**,** 57-62.

WANG, L., LI, S. J., SIDHU, A., ZHU, L., LIANG, Y., FREEDMAN, R. B. & WANG, C. C. (2009) Reconstitution of human Ero1-Lalpha/protein-disulfide isomerase oxidative folding pathway in vitro. Position-dependent differences in role between the a and a' domains of protein-disulfide isomerase. *J Biol Chem,* 284**,** 199-206.

WANG, W., WINTHER, J. R. & THORPE, C. (2007) Erv2p: characterization of the redox behavior of a yeast sulfhydryl oxidase. *Biochemistry,* 46**,** 3246-3254.

WEBB, C. T., GORMAN, M. A., LAZAROU, M., RYAN, M. T. & GULBIS, J. M. (2006) Crystal structure of the mitochondrial chaperone TIM9.10 reveals a six-bladed alpha-propeller. *Mol Cell,* 21**,** 123-133.

WHITE, C. L., SENKEVICH, T. G. & MOSS, B. (2002) Vaccinia virus G4L glutaredoxin is an essential intermediate of a cytoplasmic disulfide bond pathway required for virion assembly. *J Virol,* 76**,** 467-472.

WHITE, C. L., WEISBERG, A. S. & MOSS, B. (2000) A glutaredoxin, encoded by the G4L gene of vaccinia virus, is essential for virion morphogenesis. *J Virol,* 19**,** 9175-9183.

WIEDEMANN, N., KOZJAK, V., CHACINSKA, A., SCHÖNFISCH, B., ROSPERT, S., RYAN, M. T., PFANNER, N. & MEISINGER, C. (2003) Machinery for protein sorting and assembly in the mitochondrial outer membrane. *Nature,* 424**,** 565-571.

WIEDEMANN, N., PFANNER, N. & RYAN, M. T. (2001) The three modules of ADP/ATP carrier cooperate in receptor recruitment and translocation into mitochondria. *Embo J,* 20**,** 951-960.

WIEDEMANN, N., TRUSCOTT, K. N., PFANNSCHMIDT, S., GUIARD, B., MEISINGER, C. & PFANNER, N. (2004) Biogenesis of the protein import channel Tom40 of the mitochondrial outer membrane: Intermembrane space components are involved in an early stage of the assembly pathway. *J Biol Chem,* 279**,** 18188-18194.

WIEDEMANN, N., VAN DER LAAN, M., HUTU, D. P., REHLING, P. & PFANNER, N. (2007) Sorting switch of mitochondrial presequence translocase involves coupling of motor module to respiratory chain. *J Cell Biol,* 179**,** 1115-1122.

WILCOX, A. J., CHOY, J., BUSTAMANTE, C. & MATOUSCHEK, A. (2005) Effect of protein structure on mitochondrial import. *Proc Natl Acad Sci USA,* 102**,** 15435-15440.

WILKINSON, B. & GILBERT, H. F. (2004) Protein disulfide isomerase. *Biochim Biophys Acta,* 1699**,** 35-44.

WISHART, J. A., HAYES, A., WARDLEWORTH, L., ZHANG, N. & OLIVER, S. G. (2005) Doxycycline, the drug used to control the tet-regulatable promoter system, has no effect on global gene expression in *Saccharomyces cerevisiae*. *Yeast,* 22**,** 565-569.

WITTKE, I., WIEDEMEYER, R., PILLMANN, A., SAVELYEVA, L., WESTERMANN, F. & SCHWAB, M. (2003) Neuroblastoma-derived sulfhydryl oxidase, a new member of the sulfhydryl oxidase/Quiescin6 family, regulates sensitization to interferon gamma-induced cell death in human neuroblastoma cells. *Cancer Res,* 63**,** 7742-7752.

WU, C. K., DAILEY, T. A., DAILEY, H. A., WANG, B. C. & ROSE, J. P. (2003) The crystal structure of augmenter of liver regeneration: A mammalian FAD-dependent sulfhydryl oxidase. *Protein Sci,* 12**,** 1109-1118.

WU, Y. & SHA, B. (2006) Crystal structure of yeast mitochondrial outer membrane translocon member Tom70p. *Nat Struct Mol Biol,* 13**,** 589-593.

XIAO, R., WILKINSON, B., SOLOVYOV, A., WINTHER, J. R., HOLMGREN, A., LUNDSTROM-LJUNG, J. & GILBERT, H. F. (2004) The contributions of protein disulfide isomerase and its homologues to oxidative protein folding in the yeast endoplasmic reticulum. *J. Biol. Chem. ,* 279**,** 49780–49786.

YAMAMOTO, H., ESAKI, M., KANAMORI, T., TAMURA, Y., NISHIKAWA, S. I. & ENDO, T. (2002) Tim50 is a subunit of the TIM23 complex that links protein translocation across the outer and inner mitochondrial membranes. *Cell,* 111**,** 519-528.

YAMANO, K., YATSUKAWA, Y., ESAKI, M., HOBBS, A. E., JENSEN, R. E. & ENDO, T. (2008) Tom20 and Tom22 share the common signal recognition pathway in mitochondrial protein import. *J Biol Chem,* 283**,** 3799.

YEH, S. M., KOON, N., SQUIRE, C. & METCALF, P. (2007) Structures of the dimerization domains of the Escherichia coli disulfide-bond isomerase enzymes DsbC and DsbG. *Acta Crystallogr D Biol Crystallogr,* 63**,** 465-471.

YEN, K., GITSHAM, P., WISHART, J., OLIVER, S. G. & ZHANG, N. (2003) An improved *tet*O promoter replacement system for regulating the expression of yeast genes. *Yeast,* 20**,** 1255-1262.

YOUNG, J. C., HOOGENRAAD, N. J. & HARTL, F. U. (2003) Molecular chaperones Hsp90 and Hsp70 deliver preproteins to the mitochondrial import receptor Tom70. *Cell,* 112**,** 41-50.

ZAPUN, A., BARDWELL, J. C. A. & CREIGHTON, T. E. (1993) The reactive and destabilizing disulfide bond of DsbA, a protein required for protein disulfide bond formation in vivo. *Biochemistry,* 32**,** 5083-5092.

ZAPUN, A., MISSIAKAS, D., RAINA, S. & CREIGHTON, T. E. (1995) Structural and functional characterization of DsbC, a protein involved in disulfide bond formation in *Escherichia coli*. *Biochemistry,* 34**,** 5075-5089.

ZARA, V., FERRAMOSCA, A., ROBITAILLE-FOUCHER, P., PALMIERI, F. & YOUNG, J. C. (2009) Mitochondrial carrier protein biogenesis: Role of the chaperones Hsc70 and Hsp90. *Biochem J,* 419**,** 369-375.

9. APPENDICES

Appendix 1: List of oligonucleotides and DNA constructs

Table 1: Constructs generated by DNA cloning

Constructs	Characteristics	Oligonucleotides (5' to 3')	Restriction sites	DNA templates
pET24a/Erv1N	Erv1 N-terminus (1-83)	F) AAAGCCATATGAAAGC AATAGATAAAATGACGG R) AAAAAACTCGAGGTCAA CCTTCCTGTATGTTCTTG	NdeI XhoI	pET24a/Erv1-WT
pET24a/Erv1C	Erv1 C-terminus (84-189)	F) AAACGCCATATGCCTCC TGACGTAGAGCAACTAG R) AGATTGCTCGAGTTCG TCCCAGCCGTCCTTCCA	NdeI XhoI	pET24a/Erv1-WT
pGEX/Mia40C	Mia40 C-terminus (284-403)	F) AACTCGGATCCGCTTAT AACCCAGACACTG R) AACTCCTCGAGAGATCT TTAAGGTTTGGATTCCT	BamHI XhoI	Yeast genomic DNA
pGEX/Erv1-C30/33S-Myc	Erv1 mutant C30/33S with C-ter Myc tag	F) AAAGCGGATCCAAAGCA ATAGATAAAATGACGGA R1) ATGAGTTTTTGTTCTTC GTCCCAGCCGTCCTTCC ATCT R2) GATCCTCTTCTGAGATG AGTTTTTGTTCTTCGTC CCAG R3) TTTTTCTCGAGTTACAG ATCCTCTTCTGAGATGA GTTT	BamHI XhoI	pET24a/Erv1-C30/33S
pGEX/Erv1-C130/133S-Myc	Erv1 mutant C130/133S with C-ter Myc tag		BamHI XhoI	pET24a/Erv1C130/133S
pRS414/Erv1-WT	Erv1 with its promoter and terminator regions		XhoI BamHI	Yeast genomic DNA
pRS416/Erv1-C30/33S	Erv1 mutant C30/33S with its promoter and terminator regions	F) AAAAACTCGAGATTGAC GAAATTGATTCATTCCTT AGA R) AAAAAGGATCCTTCACA ATTCATAACTAAAATAG TATGC	XhoI BamHI	pRS414/Erv1-C30/33S
pRS416/Erv1-C130/133S	Erv1 mutant C130/133S with its promoter and terminator regions		XhoI BamHI	pRS414/Erv1-C130/133S

Table 2: Constructs generated by site-directed mutagenesis

Constructs	Characteristics	Oligonucleotides (5' to 3')	DNA templates
pET24a/Erv1-C30S	Erv1 mutant C30S	F) GATGGCAAACCTAGCCGATC ATGTAACACCCTACTTG R) CAAGTAGGGTGTTACATGAT CGGCTAGGTTTGCCATC	pET24a/Erv1-WT
pET24a/Erv1-C33S	Erv1 mutant C33S	F) GATGGCAAACCTTGCCGATC ATCTAACACCCTACTTG R) CAAGTAGGGTGTTAGATGAT CGGCAAGGTTTGCCATC	pET24a/Erv1-WT
pET24a/Erv1-C30/33S	Erv1 mutant C30/33S	F) GATGGCAAACCTAGCCGATC ATCTAACACCCTACTTG R) CAAGTAGGGTGTTAGATGAT CGGCTAGGTTTGCCATC	pET24a/Erv1-WT
pRS414/Erv1-C30/33S	Erv1 mutant C30/33S with its promoter and terminator regions	F) CTCTATAATAGTAGCCGATC ATCTAACACCCTACTTG R) CAAGTAGGGTGTTAGATGAT CGGCTACTATTATAGAG	pRS414/Erv1-WT
pET24a/Erv1-C130S	Erv1 mutant C130S	F) CACATATTTATCCTAGCAAC TGGTGTGCTAAAGACTTCG R) CGAAGTCTTTAGCACACCAG TTGCTAGGATAAATATGTG	pET24a/Erv1-WT
pET24a/Erv1-C133S	Erv1 mutant C133S	F) CACATATTTATCCTTGCAACT GGTCTGCTAAAGACTTCG R) CGAAGTCTTTAGCAGACCAG TTGCAAGGATAAATATGTG	pET24a/Erv1-WT
pET24a/Erv1-C130/133S	Erv1 mutant C130/133S	F) CACATATTTATCCTAGCAAC TGGTCTGCTAAAGACTTCG R) CGAAGTCTTTAGCAGACCAG TTGCTAGGATAAATATGTG	pET24a/Erv1-WT
pRS414/Erv1-C130/133S	Erv1 mutant C130/133S with its promoter and terminator regions		pRS414/Erv1-WT
pET24a/Erv1-C159S	Erv1 mutant C159S	F) GGGAGGTGGATGTCTGAAG CCCACAATAA R) TTATTGTGGGCTTCAGACAT CCACCTCCC	pET24a/Erv1-WT
pRS414/Erv1-C159S	Erv1 mutant C159S with its promoter and terminator regions		pRS414/Erv1-WT
pET24a/Erv1-C176S	Erv1 mutant C176S	F) GCCCAAATTTGACTCTAATT TCTGGGA R) TCCCAGAAATTAGAGTCAAA TTTGGGC	pET24a/Erv1-WT
pRS414/Erv1-C176S	Erv1 mutant C176S with its promoter and terminator regions		pRS414/Erv1-WT
pET24a/Erv1-C159/176S	Erv1 mutant C159/176S		pET24a/Erv1-C159S
pRS414/Erv1-C159/176S	Erv1 mutant C159/176S with its promoter and terminator regions		pRS414/Erv1-C159S
pGEX/Mia40C-C296S	Mia40C mutant C296S	F) GAGATAAATTGGGACTCTCC TTGCTTGGGAGGTATGGC R) GCCATACCTCCCAAGCAAGG AGAGTCCCAATTTATCTC	pGEX/Mia40C
pGEX/Mia40C-C298S	Mia40C mutant C298S	F) GAGATAAATTGGGACTGTCC TAGCTTGGGAGGTATGGC R) GCCATACCTCCCAAGCTAGG ACAGTCCCAATTTATCTC	pGEX/Mia40C

Table 3: Oligonucleotides used for construction of *ERV1* repressible yeast strain

Oligonucleotides (5' to 3')	Characteristics	DNA templates
P1.F) CTTCCTTTATTTCTGCTTTATAATTA TATACTAGTTATTTTTCTTCGTACGCT GCAGGTCGACGG P2.R) GCCTTCTTGTGGTGGATTATCCGTC ATTTTATCTATTGCTTTCATAGGCCAC TAGTGGATCTG	Amplification of KanMX4-*Tet*O_2 cassette containing the *ERV1* gene flanking regions	pCM324 plasmid
P3.F) GAGGCAGCTCATTGATAGTG P4.R) TTGCTCTACGTCAGGAGGGT K2.R) AACGTGAGTCTTTTCCTTACC K3.F) TCTCCTTCATTACAGAAACGG	Screening for integration of the KanMX4- *Tet*O_2 in the correct location of yeast genome by using a combination of P3.F/K2.R and K3.F/P4.R	Genomic DNA of CML476 Δerv1::KanMX4-*Tet*O_2-ERV1

The pET24a/Erv1-WT construct was a kind gift from Thomas Lisowsky (University of Düsseldorf, Germany). The plasmid pGEX was purchased from GE Healtcare, Piscataway, NJ, USA. The pRS414 plasmid was given by Nianshu Zhang (Cambridge, UK). The pRS416 plasmid was provided by Chris Grant (Manchester, UK).

Appendix 2: Publications

Publication 1

MORGAN, B., **ANG, S. K.**, YAN, G. & LU, H. (2009) Zinc can play chaperone-like and inhibitor roles during import of mitochondrial small Tim proteins. *J Biol Chem,* 284**,** 6818-6825.

THE JOURNAL OF BIOLOGICAL CHEMISTRY VOL. 284, NO. 11, pp. 6818–6825, March 13, 2009

Zinc Can Play Chaperone-like and Inhibitor Roles during Import of Mitochondrial Small Tim Proteins*

Received for publication, November 17, 2008, and in revised form, December 30, 2008 Published, JBC Papers in Press, December 31, 2008, DOI 10.1074/jbc.M808691200

Bruce Morgan, Swee Kim Ang, Guanhua Yan, and Hui Lu[1]

From the Faculty of Life Sciences, The University of Manchester, Michael Smith Building, Oxford Road, Manchester M13 9PT, United Kingdom

Zinc is an essential cofactor required for the function of ~8% of the yeast and 10% of the human proteome. All of the "small Tim" proteins of the mitochondrial intermembrane space contain a strictly conserved "twin CX_3C" zinc finger motif, which can bind zinc ions in the Cys-reduced form. We have shown previously that although disulfide bond formation is essential for the function of these proteins in mitochondria, only reduced proteins can be imported into mitochondria (Lu, H., Allen, S., Wardleworth, L., Savory, P., and Tokatlidis, K. (2004) *J. Biol. Chem.* 279, 18952–18958 and Morgan, B., and Lu, H. (2008) *Biochem. J.* 411, 115–122). However, the role of zinc during the import of these proteins is unclear. This study shows that the function of zinc is complex. It can play a thiol stabilizer role preventing oxidative folding of the small Tim proteins and maintaining the proteins in an import-competent form. On the other hand, zinc-bound forms cannot be imported into mitochondria efficiently. Furthermore, our results show that zinc is a powerful inhibitor of Erv1, an essential component of the import pathway used by the small Tim proteins. We propose that zinc plays a chaperone-like role in the cytosol during biogenesis of the small Tim proteins and that the proteins are imported into mitochondria through the apo-forms.

Zinc is an essential element required for the growth and metabolism of eukaryotic cells; it plays important structural and regulatory roles in numerous zinc finger proteins (1, 2). Whereas the total cellular zinc concentration is estimated to be 0.1–0.5 mM (2), a wide range of free or labile Zn^{2+} concentrations (10^{-5}–10^{-12}) has been reported in eukaryotic cells (3–6). The majority of cellular Zn^{2+} is bound to proteins with widely varying binding affinities. Cysteine thiol is one of the most prominent groups for zinc binding (7). Growing evidence suggests that the switch between zinc binding and disulfide bond formation plays a key role during the function of many proteins, such as the chaperone activity of Hsp33 (8–10), the regulation of anti-σ factor RsrA (9), and the biogenesis of the mitochondrial "small Tim" proteins (11–13).

The small Tim proteins of the *Saccharomyces cerevisiae* yeast mitochondrial intermembrane space (IMS)[2] play an essential role during the import of mitochondrial membrane proteins (14, 15), and they are themselves imported through the redox-regulated Mia40/Erv1 pathway (16, 17). All small Tim proteins contain a strictly conserved "twin CX_3C" zinc finger motif, which can bind zinc in the Cys-reduced form at a molar ratio of 1:1 with an observable conformational change (18). Tim9 and Tim10, the two most abundant small Tim proteins in yeast, form a hexameric Tim9-Tim10 complex for their function in the IMS. Whereas disulfide bond formation between the four Cys residues of the zinc finger motif is essential for the complex formation, oxidized proteins cannot be imported into mitochondria; only reduced proteins can (19, 20). However, whether or how zinc binding affects the mitochondrial import of the small Tim proteins is unknown. Because zinc binding and release are highly dynamic, it is difficult to distinguish between the import of apo- and zinc-bound forms. On the other hand, the apoproteins can be oxidized by GSSG under the cytosolic redox conditions, and the oxidative folding of both Tim9 and Tim10 competes directly with their mitochondrial import (11, 20). Thus, Zn^{2+} may play an important role during the biogenesis of small Tim proteins. In particular, how zinc binding influences the import of the zinc finger small Tim proteins into mitochondria needs to be addressed.

In this study, the effects of zinc on the oxidative folding and mitochondrial import of Tim9 and Tim10 were investigated. We show that zinc binding can stabilize both proteins from oxidative folding. Using mitochondrial import coupled with a buffered zinc system, our results show that whereas the precursor Tim9 was stabilized in the reduced form, the level of mitochondrial import was decreased with the increase of free zinc concentration. Furthermore, an oxygen consumption assay showed that zinc can inhibit the oxidase activity of Erv1, one of the essential components of the mitochondrial import and assembly pathway used by the small Tim proteins. A model is proposed for the function of zinc during biogenesis of the zinc finger small Tim proteins. Our studies reveal a new function for zinc acting as a chemical chaperone in the cytosol.

EXPERIMENTAL PROCEDURES

Materials—Tris(2-carboxyethyl)phosphine (TCEP) and 4-acetamido-4′-maleimidylstilbene-2,2′-disulfonic acid (AMS)

* This work was supported by Biotechnology and Biological Sciences Research Council Grant BB/C514323 and the Royal Society. The costs of publication of this article were defrayed in part by the payment of page charges. This article must therefore be hereby marked "*advertisement*" in accordance with 18 U.S.C. Section 1734 solely to indicate this fact.

[1] A Royal Society University Research Fellow. To whom correspondence should be addressed. Tel.: 44-161-2751553; Fax: 44-161-2755082; E-mail: hui.lu@manchester.ac.uk.

[2] The abbreviations used are: IMS, intermembrane space; AAC, ADP/ATP carrier; AMS, 4-acetamido-4′-maleimidylstilbene-2,2′-disulfonic acid; TCEP, tris(2-carboxyethyl)phosphine; Tricine, *N*-[2-hydroxy-1,1-bis(hydroxymethyl)ethyl]glycine.

were obtained from Molecular Probes (Invitrogen). EDTA was from BDH, and all other chemicals were obtained from Sigma at the highest grade.

Protein Preparations—Oxidized Tim9, Tim9(F43W), and Tim10 were purified as described previously in buffer A (50 mM Tris, pH 7.4, 150 mM NaCl) (11, 21). Reduced proteins were always prepared fresh immediately before use typically by incubation of oxidized proteins with 1–2 mM TCEP for 60–90 min at room temperature, followed by gel filtration using a Superdex 75 column to remove TCEP. Erv1-His_6 was expressed in *Escherichia coli* Rosetta-gami™ 2 (Novagen) and purified using His-tagged affinity beads as described for Erv2 (22). Then, Erv1 was dialyzed against buffer A and supplemented with 50 μM FAD before being stored at −80 °C. The protein was further purified, and free FAD was removed using a Superdex 75 gel filtration column before use.

AMS Assays—Oxidation of purified reduced Tim9 or Tim10 was initiated by the addition of GSSG. At various time points, aliquots were removed from the folding reaction and added to nonreducing gel sample buffer containing 10 mM AMS for 30 min in the dark at room temperature. AMS interacts specifically with free thiols of the reduced protein but not the disulfide-bonded oxidized protein. Each bound AMS molecule increases the molecular mass of the protein by ~500 Da, thus allowing efficient separation of different protein redox states by SDS-PAGE.

Fluorescence—Fluorescence measurements were acquired using a Cary Eclipse fluorescence spectrophotometer (Varian Ltd.). Tim9(F43W) and Tim10 oxidative folding was measured by recording fluorescence emission at 350 and 303 nm using excitation wavelengths of 280 and 275 nm, respectively. Slit widths for both excitation and emission were 5 nm. All experiments were performed at 25 °C.

Circular Dichroism—Analysis was performed using a JASCO J810 spectropolarimeter with a 1-mm path length quartz cuvette. Each spectrum represents an average of four scans from 200 to 260 nm at 0.2-nm intervals with the spectra for buffer alone (buffer A) subtracted.

Oxygen Consumption Assay—Oxygen consumption of Erv1 was measured at 25 °C using 2.5 mM TCEP as substrate. For all experiments, 1 μM Erv1 in buffer A, in the presence or absence of zinc was pre-equilibrated at 25 °C, followed by the addition of 2.5 mM TCEP to initiate the reaction. A Clarke-type oxygen electrode (Hansatech Instrument Ltd.) was used.

Mitochondrial Isolation—The wild type *S. cerevisiae* yeast D273-10B strain (MATα) was grown for 16 h at 30 °C, and the *tim9*ts yeast strain was grown for 30 h at 24 °C, followed by 8 h at 37 °C. Mitochondria were isolated from yeast cells as described previously (20, 23).

Import Assays—Import reactions consisted of 0.6 M sorbitol, 50 mM KCl, 0.75 mg/ml L-methionine, 1 mg/ml fatty acid-free bovine serum albumin, 50 mM Hepes-KOH, pH 7.4, 2 mM EGTA, 0.5 mg/ml mitochondria. $ZnCl_2$ was added from 0 to 2 mM where indicated. Free Zn^{2+} concentrations were calculated using WEBMAXC as described previously (24). The TnT SP6-coupled transcription/translation kit (Promega) was used to synthesize ^{35}S-labeled proteins. Typically, lysate was added to the import reaction at a final concentration of 3.3% (v/v). Import was always performed at 25 °C, and import time varied depending upon the particular experiment. Import was stopped by the addition of 5 volumes of ice-cold 0.6 M sorbitol, 20 mM Hepes, pH 7.4, containing 50 μg/ml trypsin for 20 min on ice, followed by the addition of soybean trypsin inhibitor to a final concentration of 1 mg/ml for 10 min on ice. Further post-import treatments were performed as described in the figure legends. Mitochondria were reisolated by centrifugation, followed by resuspension in gel sample buffer for Tris/Tricine/SDS-PAGE analysis and visualization by autoradiography. Import level was quantified by two-dimensional densitometry using an Aida image analyzer (Version 4.00).

For analysis of the redox states of unimported material, aliquots were removed from the import reaction, and the mitochondria were removed by centrifugation. The supernatant was added to gel sample buffer containing 10 mM AMS and incubated in the dark at room temperature for 30 min. Samples were analyzed by nonreducing Tris/Tricine/SDS-PAGE and autoradiography.

RESULTS

Zn^{2+} Binding Inhibits Oxidative Folding of Small Tim Proteins—We have previously shown that oxidized Tim9 and Tim10 are thermodynamically stable under the cytosolic glutathione conditions and that disulfide bond formation competes directly with import of both proteins (11, 20). To explore the role of zinc during the biogenesis of these proteins, we first studied the effects of zinc on the oxidative folding of Tim9 and Tim10 using purified proteins. Based on the fluorescence intensity difference between oxidized and reduced states (11, 20), oxidative folding of the reduced proteins initiated by the addition of GSSG was measured in the presence and absence of Zn^{2+} (Fig. 1, *A* and *C*). Because wild type Tim9 has no detectable fluorescence, the Tim9(F43W) mutant was used in this study. The results show that the apoproteins, both Tim9(F43W) and wild type Tim10, can be oxidized much faster than the proteins in the presence of zinc. Next, disulfide bond formation was confirmed by SDS-PAGE-based AMS thiol modification assay (Fig. 1, *B* and *D*). In the presence of EDTA, the reduced apoproteins became oxidized quickly to a partially oxidized intermediate and then fully oxidized state in a similar time scale as that measured by fluorescence. In the presence of Zn^{2+}, both proteins remained reduced over the same time course. Thus, both fluorescence and AMS methods show that Zn^{2+} binding can inhibit oxidative folding of the small Tim proteins. Furthermore, a detectable conformational change (folding) induced by zinc binding was shown by circular dichroism, but the degree of folding was small compared with that induced by disulfide bond formation for Tim9 (Fig. 1*E*) and Tim10 (24). In summary, zinc binding stabilizes both Tim9 and Tim10 from oxidative folding and induces an observable conformational change in the reduced proteins.

Effect of Zn^{2+} on Mitochondrial Import of Small Tim Proteins—First, import of purified Tim9 under various conditions was carried out using mitochondria isolated from a *tim9*ts yeast strain that has no detectable endogenous Tim9 and Tim10 (25). After import for 30 min, trypsin was added to degrade any unimported and mitochondria-associated precursor proteins.

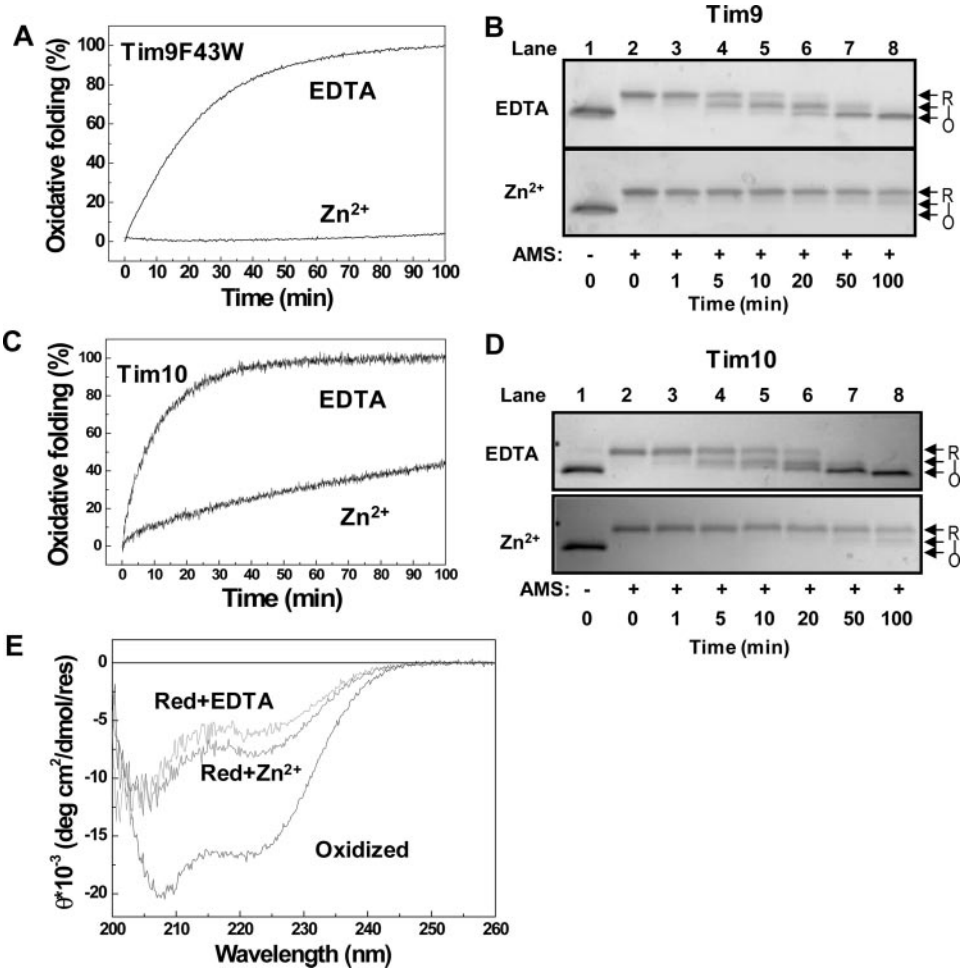

FIGURE 1. **Zn^{2+} binding inhibits oxidative folding of the small Tim proteins.** *A*, time course of oxidative folding of Tim9(F43W), followed by Trp fluorescence change at 350 nm. Oxidative folding of the protein was initiated by the addition of 1 mM GSSG in the presence of either 1 mM EDTA or 40 μM $ZnCl_2$. *B*, oxidative folding of wild type Tim9 analyzed by AMS assay. *Lane 1* is the untreated reduced Tim9. *Lanes 2–8* are the AMS-treated samples after oxidative folding for the times indicated. The fully reduced (*R*), intermediate (*I*), and oxidized (*O*) states are indicated. *C* and *D*, oxidative folding of Tim10 measured by Tyr fluorescence intensity change at 303 nm and AMS assay, respectively. *E*, CD spectra of 10 μM Tim9 in buffer A before (oxidized) and after incubation with 1 mM TCEP in the presence of 1 mM EDTA or 40 μM $ZnCl_2$. *Red*, reduced; *deg*, degrees; *res*, residues.

Furthermore, the efficiency of trypsin treatment was confirmed by mitoplasting (rupture of the mitochondrial outer membrane by osmotic swelling) performed before trypsin treatment (Fig. 2*A*, *lane 8*). Two results are shown in Fig. 2*A*. (i) The oxidized protein could not be imported into mitochondria, whereas reduced Tim9 could be imported in both the absence and presence of Zn^{2+}. (ii) The apparent import level was decreased with the increase of Zn^{2+} concentration. Thus, it was not clear whether zinc-bound protein (ZnTim9) can be imported directly into mitochondria because apoTim9 and ZnTim9 were in equilibrium dynamically. The observed Tim9 imported in the presence of Zn^{2+} might still be imported via the apo-form.

To understand whether ZnTim9 can be imported efficiently, conditions at which most (if not all) proteins can be stably maintained in the zinc-bound form are required. To this end, we used a buffered zinc system (2 mM EGTA, 0–2 mM $ZnCl_2$) to supply a sufficient amount of Zn^{2+} and at the same time control the concentration of free Zn^{2+} at μM or lower. ^{35}S-Labeled Tim9 synthesized in rabbit reticulocyte lysate was imported into wild type mitochondria under various zinc concentrations (Fig. 2, *B* and *C*), and the redox state of the unimported Tim9 was analyzed by AMS assay in parallel (Fig. 2*D*) as described previously (20). As expected, the amount of Tim9 maintained in a reduced state increased with increasing Zn^{2+} concentration. However, zinc had an opposite effect on the import level, which decreased with the increase of free zinc concentration. To confirm that Zn^{2+} does not affect the integrity of the outer membrane and the susceptibility of small Tim proteins to trypsin digestion, Western blotting of endogenous Tim10 was performed. As expected, the same level of Tim10 at the full length was observed (Fig. 2*B*). Thus, the efficiency of Tim9 import decreased with an increase in the amount of ZnTim9 or a decrease of apoTim9. The result is consistent with the finding that the import of apoTim9 is concentration-dependent (Fig. 2*E*). Furthermore, a similar zinc concentration-dependent result was obtained for Tim10 (data not shown). Thus, our results suggest that zinc-bound small Tim proteins cannot be effectively imported into mitochondria.

Zinc Affects Import of Small Tim Proteins Reversibly—Next, we tested whether the effect of zinc on Tim9 import is a reversible process by performing a sequential folding import experiment (Fig. 3*A*), in which oxidative folding of apoTim9 and ZnTim9 initiated by the addition of GSSG was followed by mitochondrial import in the presence of 5 mM EDTA. ^{35}S-Labeled Tim9 synthesized in rabbit reticulocyte lysate was ammonium sulfate-precipitated and resuspended in buffer containing 10 mM GSH and either EGTA (for apoTim9) or buffered zinc (2 mM EGTA, 2 mM $ZnCl_2$ for ZnTim9). Folding was initiated by the addition of 10 μM GSSG, and at the times indicated (Fig. 3, *B* and *C*), aliquots were removed and used for mitochondrial import in the presence of 5 mM EDTA (a stronger Zn^{2+} chelator than EGTA). Both the redox state (Fig. 3*B*) and mitochondrial import (Fig. 3*C*) of Tim9 were analyzed. In the absence of Zn^{2+}, apoTim9 was oxidized by GSSG under cytosolic redox conditions with oxidized Tim9 observed after ~5 min, and the oxidative folding resulted in a decreased level of mitochondrial import. On the other hand, ZnTim9 was maintained in the reduced form, which was imported into mitochondria (in the presence of EDTA) with the same efficiency as the reduced protein at time 0 through the same folding time course (Fig. 3*C*). Thus, zinc

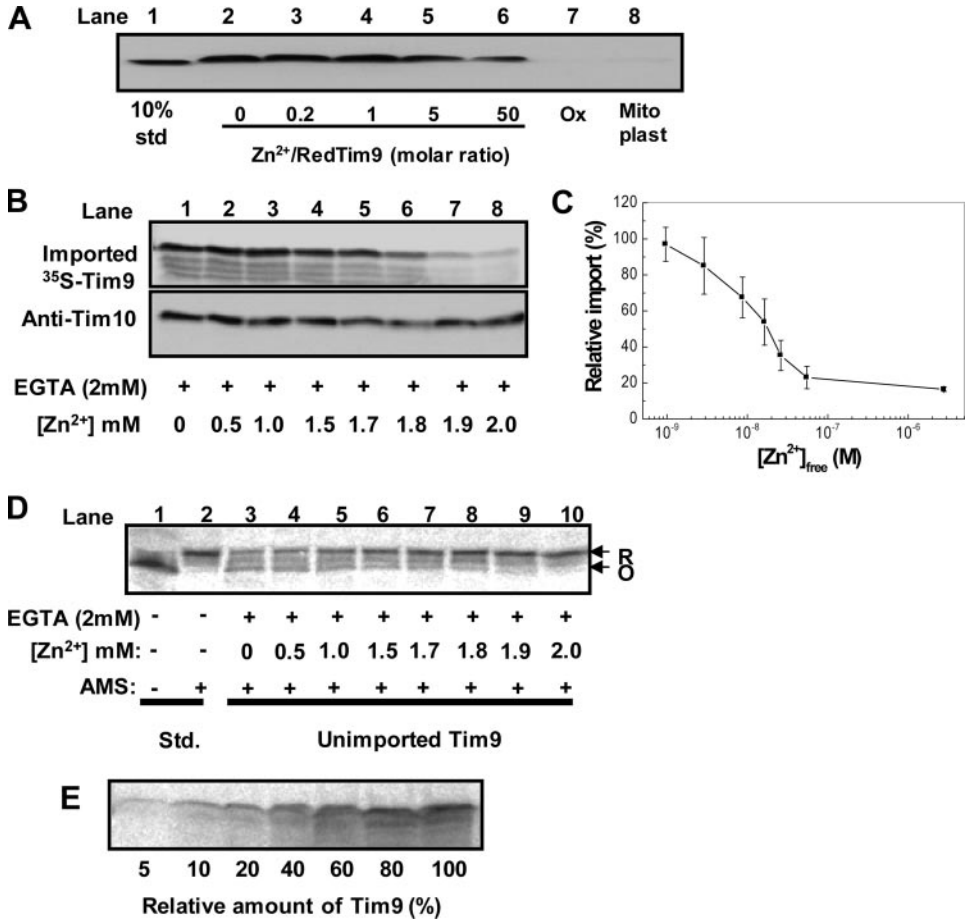

FIGURE 2. **Zn^{2+} binding inhibits the apparent mitochondrial import of small Tim proteins.** *A*, Western blotting of purified Tim9 (~10 μM) imported into *tim*9ts mitochondria. Reduced Tim9 in the absence (*lanes 2* and *8*) or presence (*lanes 3–6*) of $ZnCl_2$ at various molar ratios and oxidized (*Ox*) Tim9 (*lane 7*) were imported at 25 °C for 30 min, followed by trypsin treatment. As a control, mitoplasting was performed before trypsin treatment for Tim9 imported in the absence of zinc (*lane 8*). *Lane 1*, standard (*std*). *B*, Zn^{2+} concentration dependence of ^{35}S-labeled Tim9 import into wild type mitochondria. ^{35}S-Labeled Tim9 was imported in the presence of 2 mM EGTA and 0–2 mM $ZnCl_2$ for 30 min at 25 °C. Import was analyzed by SDS-PAGE and autoradiography. The gel was also probed with anti-Tim10 antibodies as a loading control. *C*, quantified import level in *B* plotted against $[Zn^{2+}]_{free}$. Import in the absence of Zn^{2+} was set as 100%. *Error bars* represent S.E. ($n = 3$). *D*, AMS assay of the unimported Tim9 of the experiment in *B*. Reduced (*R*) and oxidized (*O*) states are indicated. *E*, concentration dependence of Tim9 on its mitochondrial import, with 3.3% (v/v) of ^{35}S-labeled Tim9 added as 100%. Import was analyzed by SDS-PAGE and autoradiography.

binding can stabilize the protein in a reduced form, and ZnTim9 can be effectively converted to the import-competent form.

Zinc Ions Inhibit Import of Small Tim Proteins but Not the TOM or TIM Translocase Complexes—One possibility for the inhibitory effect of Zn^{2+} on the observed import of Tim9 and Tim10 is that zinc inhibits part of the general mitochondrial import machinery. Thus, the effects of Zn^{2+} on the import of the matrix-localized protein Su9-DHFR (a hybrid protein containing the presequence of subunit 9 of the mitochondrial ATP synthase coupled to dihydrofolate reductase) and the inner membrane-localized protein ADP/ATP carrier (AAC) were examined. Both precursors enter mitochondria through the TOM40 (translocase of the outer membrane) complex, after which they follow distinct import pathways of TIM23 (translocase of the inner membrane) and TIM22, respectively. Time courses of import of ^{35}S-labeled Su9-DHFR (Fig. 4, *A* and *B*) and ^{35}S-labeled AAC (Fig. 4, *C* and *D*) were performed in the absence or presence of Zn^{2+}. The results show that Zn^{2+} had no obvious effect on the import of either protein and thus no effect on the function of the TOM40, TIM22, and TIM23 translocase. In contrast, both the rate and the level of Tim9 import were significantly decreased by the addition of the same concentration of Zn^{2+} (Fig. 4, *E* and *F*), although proteins were maintained in a reduced state by zinc ions (Fig. 4*G*). The apparent initial rate of import in the presence of zinc was ~8-fold slower than that in the absence of zinc. Thus, the presence of zinc selectively inhibits the import of the small Tim proteins, not the TOM and TIM translocase complexes. We anticipate that the inhibition of Tim9 import may be a result of inhibition of the mitochondrial import and assembly pathway by zinc, and/or ZnTim9 cannot be imported directly into mitochondria.

Zinc Inhibits Oxidase Activity of Erv1—To determine whether zinc ions can inhibit the import pathway used by the small Tim proteins, the oxidase activity of Erv1, an essential component of the Mia40/Erv1 import machinery, was studied in the presence and absence of zinc ions. For this purpose, TCEP was used as the electron donor because TCEP is a strong reductant and not a chelator of zinc, unlike dithiothreitol (26). Time courses of oxygen consumption showed that Erv1 catalyzed the reaction most effectively in the presence of EDTA, with a turnover number of ~1.0 μM/s (Fig. 5, *curve a*). However, Erv1 activity was strongly impaired by the addition of 1 μM Zn^{2+} (Fig. 5, *curve b*), which gave a molar ratio of Erv1 to zinc of 1:1. Furthermore, Erv1 activity was completely inhibited by the presence of 10 μM Zn^{2+} (Fig. 5, *curve c*), and the activity could be recovered by the addition of EDTA (Fig. 5, *curve d*). Interestingly, even in the absence of added zinc and EDTA, Erv1 activity was clearly lower than in the presence of EDTA (Fig. 5, compare *curves e* and *a*); only ~80% activity was obtained in the absence of added zinc and EDTA compared with in the presence of 1 mM EDTA. Taken together, these results show that zinc has a high affinity for Erv1 and can inhibit the oxidase activity of Erv1 and hence the Mia40/Erv1 import pathway.

ZnTim9 Can Be Stably Retained in the Mitochondrial IMS—Next, we asked whether the poor Tim9 import in the presence of zinc is purely due to the inactivation of the Mia40/Erv1 pathway or because ZnTim9 itself cannot be imported directly or

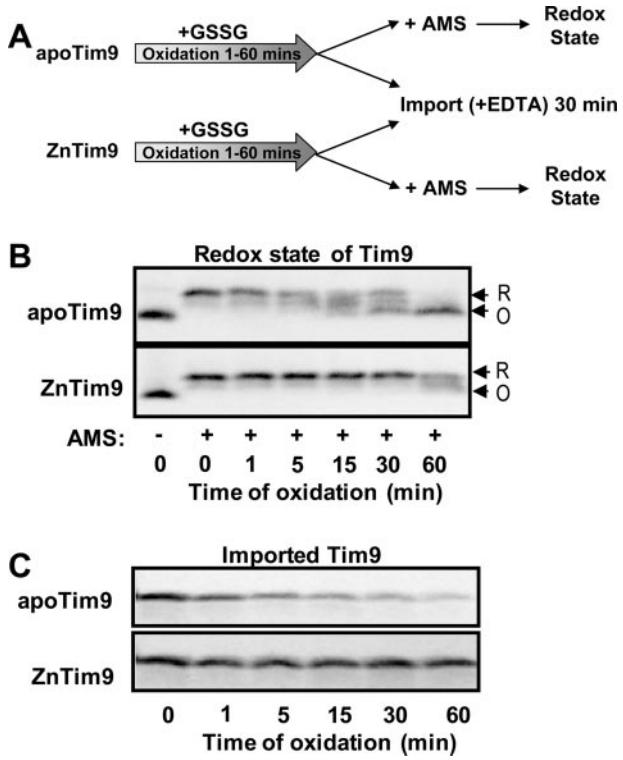

FIGURE 3. **Zn^{2+} binding stabilizes Tim9 in the reduced form, and the effect on import is reversible.** *A*, schematic diagram of the sequential oxidative folding and import experiment. Oxidative folding of reduced apoTim9 (2 mM EGTA) and ZnTim9 (2 mM EGTA, 2 mM $ZnCl_2$) was initiated by the addition of 10 μM GSSG. After various times of oxidative folding, aliquots from both folding reactions were removed and subjected to analysis by AMS assay and mitochondrial import in the presence of 5 mM EDTA. *B*, time course of the redox state change of apo- and zinc-bound ^{35}S-labeled Tim9 during the folding reactions. The reduced (*R*) and oxidized (*O*) states are indicated. *C*, analysis of the import competence of proteins removed from the folding reactions at the times indicated. Proteins were added to mitochondria immediately following removal from the folding reactions and imported in the presence of 5 mM EDTA for 30 min at 25 °C in all cases.

efficiently. To address this issue, we investigated whether the imported ZnTim9 can leak out of the mitochondrial IMS. ^{35}S-Labeled Tim9 was imported into mitochondria in the presence of Zn^{2+}, followed by trypsin treatment to remove unimported proteins. Then, the mitochondria were split into five equal aliquots and subjected to five post-import treatments: (i) untreated control and (ii–v) mitochondria resuspended in import buffer containing (ii) EGTA, (iii) EGTA + GSSG, (iv) buffered Zn^{2+}, or (v) buffered Zn^{2+}, followed by another trypsin treatment. After the treatments, each sample was further subdivided in two for analysis of import level (Fig. 6*A*, *lanes 3–7*) and redox state (*lanes 8–12*) of the imported Tim9 in parallel. The results show that the levels of imported Tim9 remained the same after all five post-import treatments (Fig. 6, *A* and *B*). Furthermore, the redox state of untreated ZnTim9 was mainly reduced (Fig. 6*A*, *lane 8*), and ZnTim9 became oxidized after EGTA treatment with or without the addition of GSSG (*lanes 9* and *10*). Interestingly, >60% of the protein remained in the reduced form when resuspended in Zn^{2+}-containing buffers (Fig. 6*A*, *lanes 11* and *12*). Taken together, these results show that ZnTim9 was trapped inside mitochondria in a reduced form and could not leak out. Thus, ZnTim9 cannot pass freely across the outer membrane, unlike the small Tim apoproteins (27). Therefore, ZnTim9 probably cannot be imported directly or at least not as efficiently as apoproteins.

DISCUSSION

In this study, we have shown that zinc can play dual roles during the biogenesis of the zinc finger small Tim proteins. The reduced small Tim apoproteins can be oxidized under the cytosolic redox conditions, which inhibit their import into mitochondria. Zinc can act as a chaperone-like thiol stabilizer preventing the proteins from oxidative folding in the cytosol and as an inhibitor of the Mia40/Erv1 import pathway used by the small Tim and many other mitochondrial IMS proteins. We propose a model for the role of zinc during biogenesis of the mitochondrial small Tim proteins as depicted in Fig. 7. Following the synthesis of the proteins in the cytosol, zinc binds to the reduced proteins to protect them from oxidative folding. Most of the proteins, if not all, are imported into mitochondria through the apo-form. It is likely that the zinc-bound form cannot be imported into mitochondria directly, or at least not as efficiently as the apoprotein, as a significantly low level of import was observed for ZnTim9, whereas imported ZnTim9 cannot leak out of the IMS. Biogenesis of the small Tim proteins will then be ensured by oxidative folding catalyzed by Mia40/Erv1 and complex formation in the IMS as shown previously.

Our import results suggest that Zn^{2+} is removed from the zinc finger small Tim proteins upon their import into the mitochondrial IMS, which is further supported by the result that zinc is detrimental to the activity of Erv1 and thus the Mia40/Erv1 import machinery located in the IMS. Consistent with our results, a similar inhibitory effect of zinc on the yeast sulfhydryl oxidase Erv2 was reported previously (22), suggesting that zinc may be an inhibitor for the activity of sulfhydryl oxidases in general. Furthermore, our results are consistent with the findings that different cell compartments are biased toward different elements (2, 28–30), and whereas the cytosol has a high level of zinc storage, the zinc level in mitochondria is low and regulated independently (31). However, how the equilibrium between the apo- and zinc-bound forms of the small Tim proteins is mediated in the cytosol is unknown. It may be mediated by another currently unknown factor or through protein-protein interactions, because zinc binding is highly regulated in the cell.

We cannot exclude that a small fraction of the proteins may be imported in a zinc-bound form, followed by zinc removal or transfer to Mia40/Erv1 to allow oxidative folding of the small Tim proteins (Fig. 7). A recent study suggested that Hot13 (helper of Tim proteins), a Cys-rich IMS protein, can promote oxidation of Mia40 by removing zinc, which otherwise inhibits the activity of Mia40 (32). Although both Mia40 and Erv1 are essential proteins for the viability of yeast cells, Hot13 is not (33). Thus, the function of Hot13 as a zinc chelator may be as a second line of security in case zinc is imported into the IMS along with the zinc finger small Tim proteins to ensure that the Mia40/Erv1 pathway works efficiently. Thus, the Hot13 studies also indicate that it is important to remove zinc from the small Tim proteins before they are imported into the mitochondrial IMS.

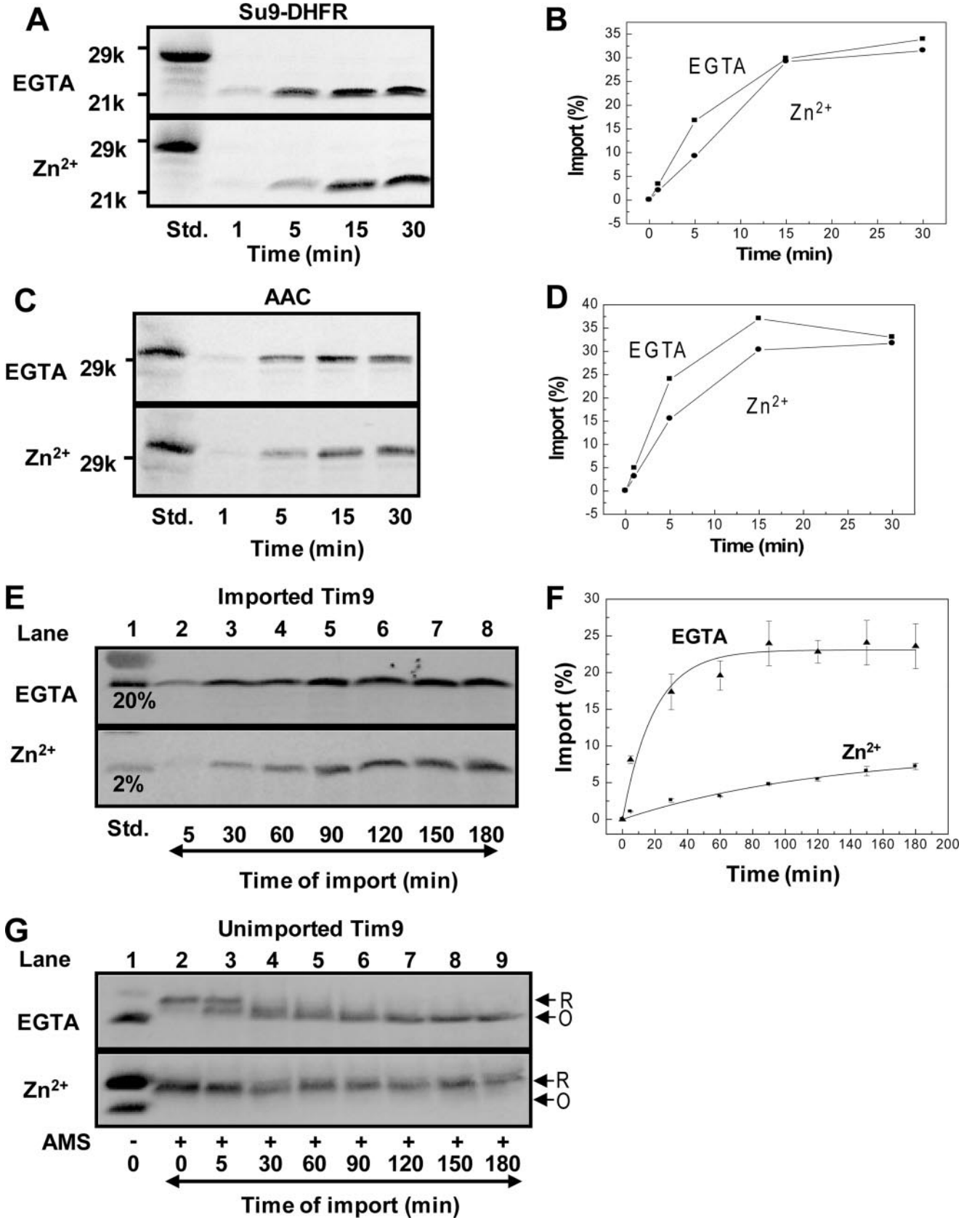

FIGURE 4. **Zinc does not inhibit the mitochondrial import of Su9-DHFR and AAC.** *A*, time course of import of ^{35}S-labeled Su9-DHFR in the absence (EGTA) or presence of buffered Zn^{2+}. *B*, quantification of import levels in *A* based on a standard (*Std.*), which represents 40% of the material in the import reaction. *C* and *D*, time course of import of ^{35}S-labeled AAC as described for Su9-DHFR. *E* and *F*, time course of import of apoTim9 (EGTA) or ZnTim9 (Zn^{2+}). Import level was determined based on a standard, which represents 20 and 2% of the material in the apoTim9 and ZnTim9 reactions, respectively. *Errors bars* represent S.E. ($n = 3$). *G*, AMS assay of the unimported Tim9 from the same import assay in *E*. All import assays were analyzed by SDS-PAGE and autoradiography.

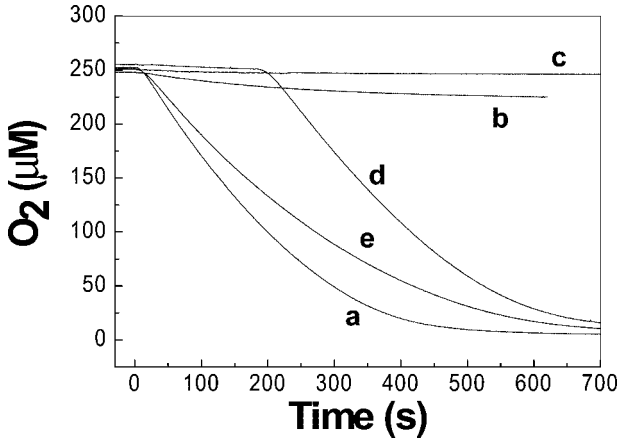

FIGURE 5. **Zinc ions inhibit the oxidase activity of Erv1.** Time courses of oxygen consumption were done with 2.5 mM TCEP as electron donor in the presence of 1 μM Erv1 in all conditions plus 1 mM EDTA (*curve a*), 1 μM $ZnCl_2$ (*curve b*), and 10 μM $ZnCl_2$ (*curves c* and *d*); 1 mM EDTA was added to *curve d* at 180 s to chelate zinc ions. No EDTA or $ZnCl_2$ was added to *curve e*. For all measurements, the solutions without TCEP were pre-equilibrated at 25 °C, followed by the addition of 2.5 mM TCEP at time 0.

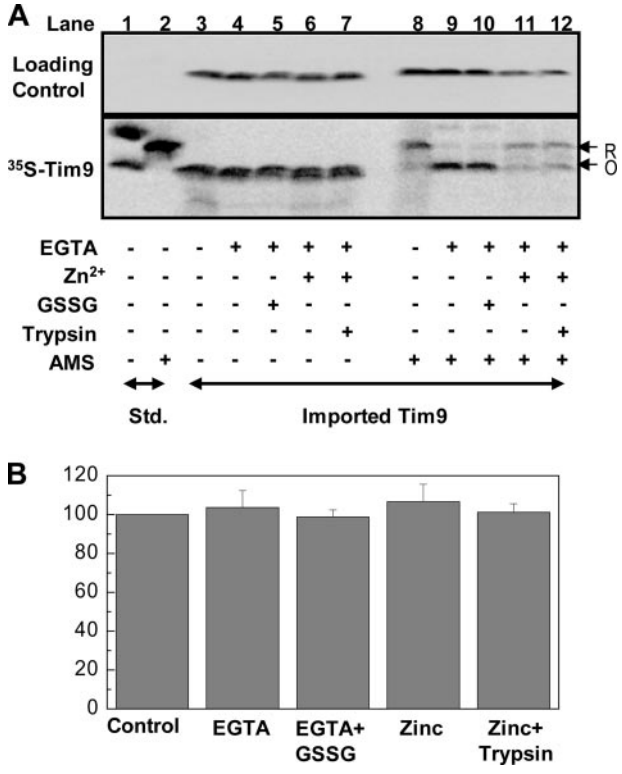

FIGURE 6. **ZnTim9 is stably trapped inside the IMS.** *A*, SDS-PAGE analysis of imported ZnTim9. ^{35}S-Labeled Tim9 was imported for 30 min at 25 °C under buffered Zn^{2+} conditions. Unimported material was removed by trypsin treatment, and the import reaction was subsequently split into five equal aliquots and resuspended in buffers under five different conditions as indicated (*lanes 3–7*) for post-import treatments. After a 30-min incubation at 25 °C, the samples were further split into sets for SDS-PAGE analysis without (*lanes 3–7*) and with (*lanes 8–12*) AMS treatment. The gel was also probed with anti-Tim10 antibodies as a loading control. *Lanes 1* and *2*, standards (*Std.*). *R*, reduced; *O*, oxidized. *B*, quantification of import levels in *A* (*lanes 3–7*). *Error bars* represent S.E. ($n = 3$).

Unlike the oxidized small Tim proteins that are completely import-incompetent, zinc-bound forms can be reversibly converted into the import-efficient state, the apo-forms. Thus, zinc binding can stabilize the small Tim proteins in a reduced and

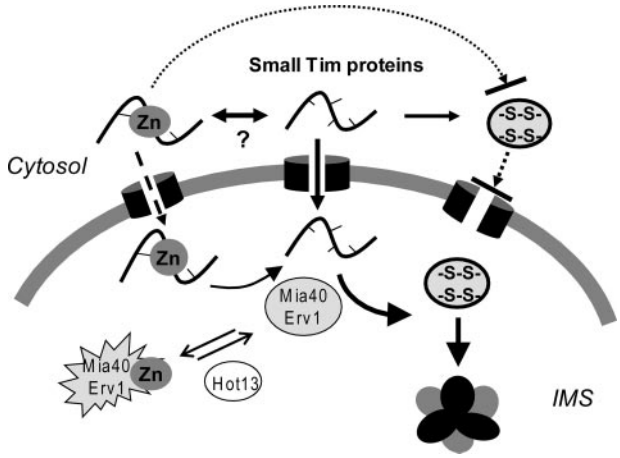

FIGURE 7. **Model for the function of zinc during biogenesis of the small Tim proteins.** Following the synthesis of the proteins in the cytosol, zinc binds to the reduced proteins to protect them from oxidative folding, as the oxidized proteins cannot be imported. The equilibrium between the apo- and zinc-bound forms may be mediated by a currently unknown cytosolic factor. Most of the proteins are imported into mitochondria through the apo-form, followed by oxidative folding catalyzed by the Mia40/Erv1 system and complex formation in the IMS. A small fraction of the proteins may be imported into the IMS in a zinc-bound form, which may inhibit the activity of the Mia40/Erv1 system and thus may require the help of Hot13.

mitochondrial import-competent form. Interestingly, unlike the structural roles played by zinc in many other zinc finger proteins (2, 34, 35), zinc binding to the small Tim proteins results in only a moderate degree of protein folding or conformational change, which is much smaller than that induced by disulfide bond formation (18, 24). This suggests that zinc binding to the small Tim proteins is highly dynamic and cannot induce or stabilize the proteins in a stable conformation, whereas the formation of two pairs of disulfide bonds in juxtaposition can bridge the two parts of each protein together covalently and more closely. The difference between the small Tim and other proteins may reflect the special role of zinc that has to balance between stabilizing the proteins in reduced states and keeping them in unfolded states ready for mitochondrial import. Our results suggest that zinc plays a new function as a small chemical chaperone in the cytosol during biogenesis of the small Tim proteins. The chaperone-like thiol stabilizer role may be an important function of zinc in many other zinc finger proteins.

In summary, this study shows that zinc has dual roles as a chaperone-like thiol stabilizer and inhibitor of the Mia40/Erv1 pathway during biogenesis of the small Tim proteins. Zinc-bound proteins cannot be imported efficiently into the mitochondrial IMS. A new biological function for zinc as a small chemical chaperone in the cytosol is revealed. It will be challenging and exciting to understand the molecular basis for the chaperone-like function of zinc in the future.

Acknowledgments—We thank Kostas Tokatlidis (Institute of Molecular Biology and Biotechnology, Crete) for Tim9, Thomas Lisowsky (Botanisches Institute) for Erv1, Nikolaus Pfanner (University Freiburg) for AAC, Kai Hell (University München) for Su9-DHFR constructs, and Carla Koehler (UCLA) for the tim9ts yeast strain. We thank Martin Pool and Neil Bullied (Manchester University) for comments on the manuscript.

REFERENCES

1. Berg, J. M., and Shi, Y. (1996) *Science* **271,** 1081–1085
2. Frausto, J. J. R., and Williams, R. J. P. (2001) *The Biological Chemistry of the Elements*, pp. 315–339, Oxford University Press, Oxford
3. Sensi, S. L., Ton-That, D., Sullivan, P. G., Jonas, E. A., Gee, K. R., Kaczmarek, L. K., and Weiss, J. H. (2003) *Proc. Natl. Acad. Sci. U. S. A.* **100,** 6157–6162
4. Sensi, S. L., Canzoniero, L. M., Yu, S. P., Ying, H. S., Koh, J. Y., Kerchner, G. A., and Choi, D. W. (1997) *J. Neurosci.* **17,** 9554–9564
5. Haase, H., Mocchegiani, E., and Rink, L. (2006) *Biogerontology* **28,** 1–4
6. Eide, D. J. (2006) *Biochim. Biophys. Acta* **1763,** 711–722
7. Maret, W. (2004) *Biochemistry* **43,** 3301–3309
8. Jakob, U., Eser, M., and Bardwell, J. C. (2000) *J. Biol. Chem.* **275,** 38302–38310
9. Li, W., Bottrill, A. R., Bibb, M. J., Buttner, M. J., Paget, M. S., and Kleanthous, C. (2003) *J. Mol. Biol.* **333,** 461–472
10. Tang, W., and Wang, C. C. (2001) *Biochemistry* **40,** 14985–14994
11. Lu, H., and Woodburn, J. (2005) *J. Mol. Biol.* **353,** 897–910
12. Chacinska, A., Pfannschmidt, S., Wiedemann, N., Kozjak, V., Sanjuan Szklarz, L. K., Schulze-Specking, A., Truscott, K. N., Guiard, B., Meisinger, C., and Pfanner, N. (2004) *EMBO J.* **23,** 3735–3746
13. Terziyska, N., Lutz, T., Kozany, C., Mokranjac, D., Mesecke, N., Neupert, W., Herrmann, J. M., and Hell, K. (2005) *FEBS Lett.* **579,** 179–184
14. Koehler, C. M. (2004) *Trends Biochem. Sci.* **29,** 1–4
15. Pfanner, N., Wiedemann, N., Meisinger, C., and Lithgow, T. (2004) *Nat. Struct. Mol. Biol.* **11,** 1044–1048
16. Tokatlidis, K. (2005) *Cell* **121,** 965–967
17. Hell, K. (2008) *Biochim. Biophys. Acta* **1783,** 601–609
18. Lu, H., Golovanov, A. P., Alcock, F., Grossmann, J. G., Allen, S., Lian, L. Y., and Tokatlidis, K. (2004) *J. Biol. Chem.* **279,** 18959–18966
19. Lu, H., Allen, S., Wardleworth, L., Savory, P., and Tokatlidis, K. (2004) *J. Biol. Chem.* **279,** 18952–18958
20. Morgan, B., and Lu, H. (2008) *Biochem. J.* **411,** 115–122
21. Ivanova, E., Jowitt, T. A., and Lu, H. (2008) *J. Mol. Biol.* **375,** 229–239
22. Wang, W., Winther, J. R., and Thorpe, C. (2007) *Biochemistry* **46,** 3246–3254
23. Meisinger, C., Pfanner, N., and Truscott, K. N. (2006) *Methods Mol. Biol.* **313,** 33–39
24. Ivanova, E., Ball, M., and Lu, H. (2008) *Proteins Struct. Funct. Bioinformat.* **71,** 467–475
25. Leuenberger, D., Curran, S. P., Wong, D., and Koehler, C. M. (2003) *Traffic* **4,** 144–152
26. Krezel, A., Latajka, R., Bujacz, G. D., and Bal, W. (2003) *Inorg. Chem.* **42,** 1994–2003
27. Muller, J. M., Milenkovic, D., Guiard, B., Pfanner, N., and Chacinska, A. (2008) *Mol. Biol. Cell* **19,** 226–236
28. Williams, R. J. (1984) *Endeavour* **8,** 65–70
29. Tottey, S., Waldron, K. J., Firbank, S. J., Reale, B., Bessant, C., Sato, K., Cheek, T. R., Gray, J., Banfield, M. J., Dennison, C., and Robinson, N. J. (2008) *Nature* **455,** 1138–1142
30. Vallee, B. L., and Auld, D. S. (1995) *EXS* (*Basel*) **73,** 259–277
31. Simm, C., Lahner, B., Salt, D., LeFurgey, A., Ingram, P., Yandell, B., and Eide, D. J. (2007) *Eukaryot. Cell* **6,** 1166–1177
32. Mesecke, N., Bihlmaier, K., Grumbt, B., Longen, S., Terziyska, N., Hell, K., and Herrmann, J. M. (2008) *EMBO Rep.* **9,** 1107–1113
33. Curran, S. P., Leuenberger, D., Leverich, E. P., Hwang, D. K., Beverly, K. N., and Koehler, C. M. (2004) *J. Biol. Chem.* **279,** 43744–43751
34. Maret, W. (2005) *J. Trace Elem. Med. Biol.* **19,** 7–12
35. Matthews, J. M., and Sunde, M. (2002) *IUBMB Life* **54,** 351–355

Publication 2

ANG, S. K. & LU, H. (2009) Deciphering structural and functional roles of individual disulfide bonds of the mitochondrial sulfhydryl oxidase Erv1p. *J Biol Chem,* 284**,** 28754-28761.

THE JOURNAL OF BIOLOGICAL CHEMISTRY VOL. 284, NO. 42, pp. 28754–28761, October 16, 2009

Deciphering Structural and Functional Roles of Individual Disulfide Bonds of the Mitochondrial Sulfhydryl Oxidase Erv1p*[S]

Received for publication, May 13, 2009, and in revised form, August 12, 2009 Published, JBC Papers in Press, August 13, 2009, DOI 10.1074/jbc.M109.021113

Swee Kim Ang and Hui Lu[1]

From the Faculty of Life Sciences, The University of Manchester, Michael Smith Building, Oxford Road, Manchester M13 9PT, United Kingdom

Erv1p is a FAD-dependent sulfhydryl oxidase of the mitochondrial intermembrane space. It contains three conserved disulfide bonds arranged in two C*XX*C motifs and one CX_{16}C motif. Experimental evidence for the specific roles of the individual disulfide bonds is lacking. In this study, structural and functional roles of the disulfides were dissected systematically using a wide range of biochemical and biophysical methods. Three double cysteine mutants with each pair of cysteines mutated to serines were generated. All of the mutants were purified with the normal FAD binding properties as the wild type Erv1p, showing that none of the three disulfides are essential for FAD binding. Thermal denaturation and trypsin digestion studies showed that the CX_{16}C disulfide plays an important role in stabilizing the folding of Erv1p. To understand the functional role of each disulfide, small molecules and the physiological substrate protein Mia40 were used as electron donors in oxygen consumption assays. We show that both C*XX*C disulfides are required for Erv1 oxidase activity. The active site disulfide is well protected thus requires the shuttle disulfide for its function. Although both mutants of the C*XX*C motifs were individually inactive, Erv1p activity was partially recovered by mixing these two mutants together, and the recovery was rapid. Thus, we provided the first experimental evidence of electron transfer between the shuttle and active site disulfides of Erv1p, and we propose that both intersubunit and intermolecular electron transfer can occur.

Disulfide bonds play very important roles in the structure and function of many proteins by stabilizing protein folding and/or acting as thiol/disulfide redox switches. The process of disulfide formation is catalyzed by dedicated enzymes *in vivo* (1–4). Erv1p is a FAD-dependent sulfhydryl oxidase located in the *Saccharomyces cerevisiae* mitochondrial intermembrane space (4–6). It is an essential component of the redox regulated Mia40/Erv1 import and assembly pathway used by many of the cysteine-containing intermembrane space proteins, such as members of the "small Tim" and Cox17 families (7–10). Upon import of a Cys-reduced substrate, Mia40 interacts with the substrate via intermolecular disulfide bond and shuttles a disulfide to its substrate. Although oxidized Mia40 promotes disulfide bond formation in the substrates, Erv1p functions in catalyzing reoxidation of the reduced Mia40 and/or release of the substrate (11–13).

The common features for the FAD-dependent sulfhydryl oxidases are that the enzymes can catalyze the electron transfer from substrate molecules (*e.g.* protein thiols) through the noncovalent bound FAD cofactor to molecular oxygen or oxidized cytochrome *c* (14). The sulfhydryl oxidases can be divided into three groups: Ero1 enzymes, multidomain quiesin sulfhydryl oxidases, and single domain Erv (essential for respiration and vegetative growth)/ALR proteins. The yeast Ero1p and the mammalian homologues (Ero1α and Ero1β) are large flavoenzymes present in the ER with at least five disulfide bonds, but only two of the disulfide bonds are conserved. The conserved cysteines are essential for the catalytic activity of Ero1p forming the active site C*XX*C and shuttle disulfide CX_4C, respectively (15, 16). Furthermore, nonconserved disulfide bonds have been shown recently to be important in regulating the activity of both yeast and mammalian Ero1 (17–19). The second group of oxidases, the multidomain quiesin sulfhydryl oxidases, have important functions in higher eukaryotes (14, 20). Quiesin sulfhydryl oxidases consist of an Erv/ALR module fused to one or more thioredoxin-like domains with two conserved C*XX*C motifs in the Erv/ALR module. Quiesin sulfhydryl oxidase enzymes are found in many subcellular and extracellular locations, but not in mitochondria. Instead, single domain Erv/ARL enzymes of the third group are found in the 7mitochondria of many eukaryotic cells (21). Erv1p belongs to this single domain Erv/ARL family, which includes the human mitochondrial ARL, plant AtErv1, and yeast Erv2p of the ER lumen.

The Erv/ARL enzymes are characterized by a highly conserved central catalytic core of ~100 amino acids, which includes an active site C*XX*C motif (Cys^{130}–Cys^{133} for Erv1p), CX_{16}C disulfide bond (Cys^{159}–Cys^{176} for Erv1p), and residues involved in FAD binding (Fig. 1*A*). Based on the partial crystal structure data of Erv2p (22) and AtErv1 (23), the catalytic core of Erv proteins contains a four-helix bundle forming the noncovalent FAD-binding site with the active site C*XX*C in close proximity to the isoalloxazine ring of FAD. In addition, the long range CX_{16}C disulfide bond of the Erv proteins brings the short fifth helix to the four-helix bundle in proximity to the adenine ring of FAD (Fig. 1*A*). Thus, the CX_{16}C disulfide bond is pro-

* This work was supported in part by the Royal Society and by Biotechnology and Biological Sciences Research Council Grant BB/C514323.
[S] The on-line version of this article (available at http://www.jbc.org) contains supplemental Fig. S1 and Table S1.
[1] Royal Society University Research Fellow. To whom correspondence should be addressed. Tel.: 44-161-2751553; Fax: 44-161-2755082; E-mail: hui.lu@manchester.ac.uk.

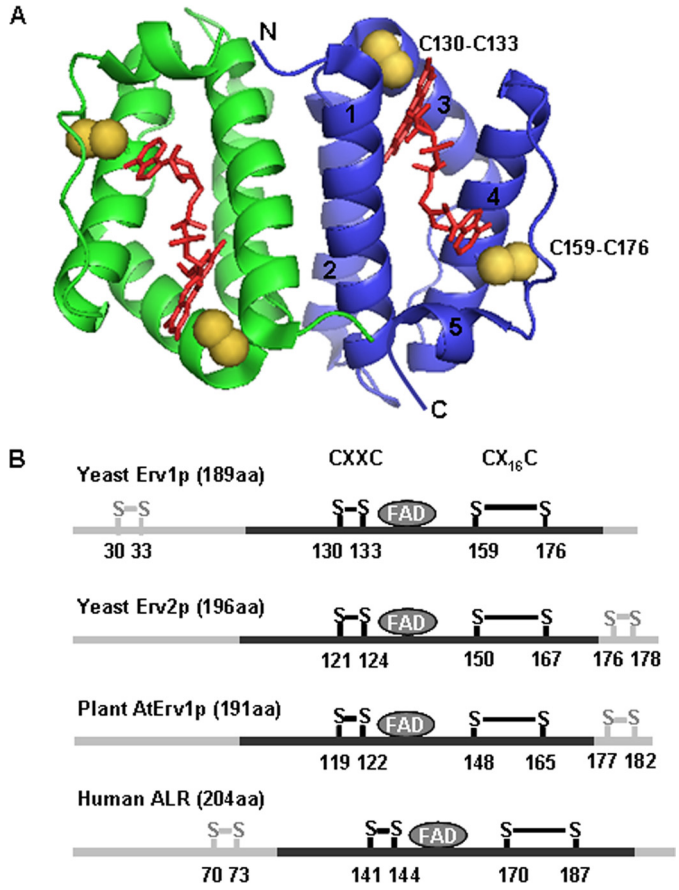

FIGURE 1. **Structure and conserved Cys motifs of Erv/ALR enzymes.** *A*, modeled structures of the conserved central catalytic core domain of Erv1p dimer based on the crystal structure data of AtErv1 (Protein Data Bank accession number 2HJ3, residues 73–173, the helix 1 starts with residue 75). The helices of the four-helix bundle and the short fifth helix are labeled from *1* to *5*. The two disulfides are shown as *yellow spheres*, and the cofactor FAD is in *red*. The Cys^{130}–Cys^{133} is the redox active disulfide located closely to the isoalloxazine ring of FAD. The N and C termini were labeled as N and C, respectively. The structure was generated using Pymol program. *B*, schematic of the primary structure of yeast, plant, and human sulfhydryl oxidase with the conserved Cys motifs. The conserved central catalytic core regions are shown as *black bars*, and the nonconserved regions are in *gray*.

posed to play a structural role in stabilizing the FAD binding and/or protein folding, but direct experimental evidence to verify the roles is lacking. Apart from the catalytic core, the other parts of the proteins seem flexible and unfolded. Importantly, all members of the Erv/ALR family have at least an additional disulfide bond located in the nonconserved N- or C-terminal region to the catalytic core (Fig. 1*B*), which is hypothesized as a shuttle disulfide based on the partial crystal structure of Erv2 (22). The hypothesized shuttle disulfide of Erv2p *CXC* and AtErv1 CX_4C are located in the C terminus, but Erv1p (Cys^{30}–Cys^{33}) and ALR have a *CXXC* shuttle disulfide located N-terminal to the catalytic core. Furthermore, structural and chemical data have suggested that Erv/ARL enzymes form homodimer or oligomers in the presence or absence of intermolecular disulfide bonds (5, 23, 24).

Yeast mitochondrial Erv1p contains a total of six Cys residues forming three pairs of disulfide bonds (residues 30–33, 130–133, and 159–176) as described above. Previous studies with single Cys mutants showed that although all three disulfide bonds are essential for Erv1p function *in vivo*, only Cys^{130}–Cys^{133} disulfide is required for the oxidase activity of Erv1p *in vitro* (24). The conclusion that only Cys^{130}–Cys^{133} disulfide is required for Erv1p oxidase activity *in vitro* was based on a study using the artificial substrate DTT[2] as the electron donor. Abnormal color changes were observed for some of the single Cys mutants of Erv1p in the previous study that were probably caused by protein misfolding or formation of non-native disulfides because of the presence of a redox active but unpaired Cys. It is clear that Cys^{130}–Cys^{133} is the active site disulfide; however, experimental evidence for the role of Cys^{30}–Cys^{33} disulfide is lacking, and the specific role played by the unique $CX_{16}C$ motif of Erv proteins is unknown.

In this study, we dissected the structural and functional roles of all three individual disulfides of Erv1p systematically. To avoid misfolding via unpaired Cys, three double Cys mutants of Erv1p were generated with each of the disulfides mutated to serines. All three mutants were successfully purified with the normal FAD binding properties of the wild type (WT) Erv1p. Various biophysical and biochemical methods were used to study the folding and oxidase activity of the WT and Erv1p mutants. Both artificial and the natural substrate (Mia40) of Erv1p were used as electron donors to understand the functional mechanism of Erv1p. Our results show that both the first (Cys^{30}–Cys^{33}) and second (Cys^{130}–Cys^{133}) disulfides are essential for Erv1 oxidase activity *in vitro*. Although none of the three disulfides are essential for FAD binding, the third disulfide (Cys^{159}–Cys^{176}) plays an important role in stabilizing the folding of Erv1p. More importantly, this study provided direct experimental evidence to show that Cys^{30}–Cys^{33} functionally acts as a shuttle disulfide passing electrons to the active site Cys^{130}–Cys^{133} disulfide. Moreover, the electron transfer seems to occur through both intersubunit and intermolecular interactions.

EXPERIMENTAL PROCEDURES

Materials—4-acetamido-4′-maleimidylstilbene-2,2′-disulfonic acid (AMS) and tris(2-carboxyethyl)phosphine (TCEP) were obtained from Molecular Probes (Invitrogen). EDTA was from BDH Co, and all other chemicals were obtained from Sigma at the highest grade. A peptide corresponding to 14 C-terminal residues of Erv1p was used to raise antibodies in rabbit against Erv1p (Eurogentec Ltd.).

Mutagenesis and Protein Preparations—Cysteine to serine mutants of Erv1 were created using QuikChange site-directed mutagenesis with *Pfu* DNA polymerase (Stratagene) and pET-24a(+) harboring the wild type complete Erv1 gene as template (5). All of the constructs were verified by DNA sequencing. Sequences of mutagenic oligonucleotides can be provided upon request. The Erv1p-His_6 proteins were expressed in the *Escherichia coli* Rosetta-gami™ 2 (Novagen) and purified using His tag affinity beads followed by fast protein liquid chromatography using Superdex75 column as described previously (25). Concentrations of the WT and Erv1p mutants

[2] The abbreviations used are: DTT, 1,4-dithiothreitol; AMS, 4-acetamido-4′-maleimidylstilbene-2,2′-disulfonic acid; TCEP, tris(2-carboxyethyl)phosphine; WT, wild type; Tricine, *N*-[2-hydroxy-1,1-bis(hydroxymethyl)ethyl]-glycine; PK, proteinase K.

were calculated using the molar extinction coefficients determined in this study as listed in Table 1. Mia40c (amino acids 284–403), the C-terminal domain of Mia40, was cloned into pGEX 4T-1 vector (GE Healthcare), expressed in the *E. coli* Rosetta-gami™ 2, and purified using GST affinity beads as described previously (11). The partially reduced Mia40c (Mia40c-pR) was prepared by incubation with 0.5 mM TCEP for 20 min at room temperature, followed by gel filtration using a Superdex75 column to remove TCEP. The protein had the same redox state as that described in Ref. 11. The concentration was determined based on a 5,5′-dithiobis(nitrobenzoic acid) assay for the free thiol groups. All of the experiments were carried out under aerobic conditions at 25 °C in buffer AE (50 mM Tris, pH 7.4, 150 mM NaCl, 1 mM EDTA), unless indicated otherwise.

AMS Assays—At various time points, protein aliquots were removed from reaction solutions and added to nonreducing gel sample buffer containing excess amount of AMS (10 mM) for 30 min in the dark at room temperature as described before (26). AMS interacts with free thiols of reduced proteins covalently, but not disulfide bonds. Each bound AMS molecule increases the molecular mass of the protein ~0.5 kDa. Different redox states of the proteins were analyzed by 16% Tricine-SDS-PAGE under nonreducing conditions.

Determination of the Extinction Coefficients—Absorption spectra of Erv1p and its mutants were recorded using a Cary 300 spectrophotometer from 250 to 700 nm, at 1-nm intervals, using a 1-cm path length quartz cuvette. The extinction coefficients and the percentage of enzyme-bound FAD for the WT and mutant Erv1p were calculated based on a molar extinction coefficient of 11.3 mM^{-1} cm^{-1} at 450 nm for free FAD and 72.68 mM^{-1} cm^{-1} for Erv1p at 275 nm as reported previously (27). FAD was released from the proteins by the addition of 1% SDS.

Circular Dichroism—CD analysis was performed using a JASCO J810 spectropolarimeter with a 1-mm path length quartz cuvette. Far-UV CD spectra were measured at 25 °C with 300 μl of 10 μM proteins as described previously (28). Each spectrum represents an average of four scans from 200 to 260 nm at 0.2-nm intervals with the spectra for buffer alone subtracted. Thermal denaturation was measured at 222 nm, at 1 °C intervals over 5–90 °C with temperature increase of 1 °C/min.

Proteinase K Digestion—20 μl of 5 μM Erv1p and its mutants were incubated with 50 μg/ml proteinase K at 25 °C for 30 min, followed by inhibition of the protease activity by the addition of 10 mM phenylmethylsulfonyl fluoride for 10 min. Then the samples were analyzed by 16% Tricine-SDS-PAGE and Western blotting with antibody raised with peptide of the C terminus of Erv1p. Mock controls were treated in exactly the same manner.

Oxygen Consumption Assay—Oxygen consumption of Erv1 was measured using a Clarke-type oxygen electrode (Hansatech Instrument Ltd.) at 25 °C as described before (25). For measurements with DTT and TCEP as electron donors, 1 or 2 μM Erv1 as indicated in the text was pre-equilibrated at 25 °C followed by the addition of 10 mM DTT or 3.5 mM TCEP to initiate the reaction. For measurements with Mia40c-pR as substrate, 50 μM freshly prepared Mia40c-pR was pre-equilibrated at 25 °C followed by the addition of 1 μM Erv1 to catalyze the reaction.

Mass Spectrometry Analysis—The WT Erv1 (5 μM) was incubated with 0 or 50 μM freshly prepared Mia40c-pR for ~10 s, and then the reaction was stopped by the addition of nonreducing SDS-PAGE sample buffer containing 4 mM iodoacetamide. The proteins were separated by nonreducing SDS-PAGE. The bands corresponding to Erv1 were excised and digested with AspN. The peptides were analyzed by mass spectrometry on a Bruker matrix-assisted laser desorption ionization time-of-flight using a positive reflection method.

RESULTS

Characterization of the WT and Three Double Cys Mutants of Erv1p—To understand the roles of individual disulfide bonds of Erv1, three double Cys mutants of Erv1p with the Cys residues corresponding to each of the three disulfides mutated to serines were generated. They are named as C30S/C33S, C130S/C133S, and C159S/C176S, respectively, in the rest of the report. All three mutants were successfully purified with the same method and yellowish color as that of the WT Erv1p. No abnormal color was observed for any of the mutants. The UV-visible spectrum of the WT Erv1p shows a characteristic bound FAD spectrum with a maximum absorbance at 460 nm and a shoulder peak at ~485 nm (supplemental Fig. S1). The absorption maximum was ~10 nm blue-shifted to 450 nm upon the addition of 1% SDS (data not shown), the same wavelength as that of free FAD confirming the release of cofactor FAD. The same protein-bound FAD spectrum as that of the WT Erv1p was observed for C30S/C33S and C159S/C176S mutants (supplemental Fig. S1), but a slightly blue-shifted spectrum with the maximum at 453 nm was obtained for C130S/C133S (supplemental Table S1). It is consistent with the fact that the active site Cys^{130}–Cys^{133} disulfide is located proximal to the isoalloxazine ring of FAD and the mutation changes bound-FAD absorption slightly. The molar extinction coefficients for the bound FAD in the WT and all three double Cys mutants were determined (see "Experimental Procedures") to be 11.9, 11.1, 12.1, and 11.9 mM^{-1} cm^{-1} at the corresponding wavelength of the absorption maximum (supplemental Table S1). These values are similar to each other and to that of other members of Erv/ALR family. The same FAD-binding yield of ~93% was obtained for the WT and all the mutants. Taken together, these results show that all three double Cys mutants were correctly folded and with FAD bound at a molar ratio of 1:1 as that of the WT. None of the three individual disulfide bonds of Erv1p is essential for FAD binding.

Structural Roles Played by Individual Disulfide Bonds of Erv1p—It was shown that Cys^{30} and Cys^{33} are involved in formation of an intermolecular disulfide bonded dimer and oligomers (5, 24). Thus, the oligomerization state of the double Cys mutants was investigated using reducing and nonreducing SDS-PAGE. For all the proteins except C30S/C33S mutant, a fraction of ~20% proteins migrated slowly on the nonreducing gel with an apparent molecular weight corresponding to a dimer (data not shown). The result is consistent with the previous observation (5, 24). Next, the effect of these mutations on the overall conformation of Erv1p was investigated using far-UV CD spectra. The WT and all of the mutants have a

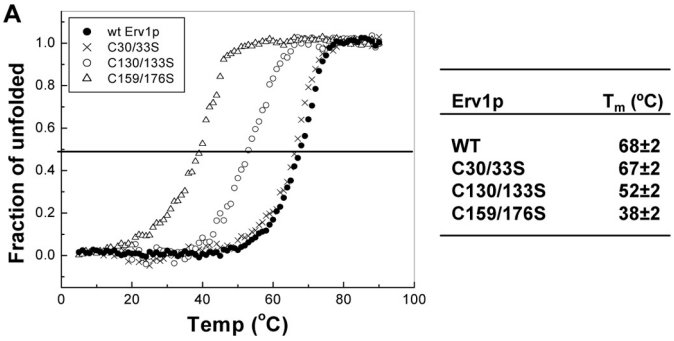

Erv1p	T_m (°C)
WT	68±2
C30/33S	67±2
C130/133S	52±2
C159/176S	38±2

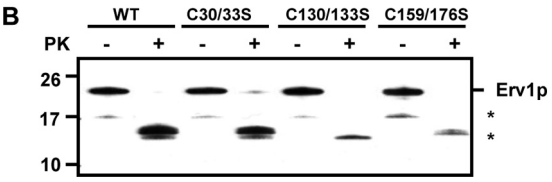

FIGURE 2. **Stability of the WT and mutant Erv1p.** *A*, thermal denaturation of the WT and Erv1p mutants measured by CD intensity change at 222 nm. The T_m of the WT Erv1p (*solid circle*), C30S/C33S (*cross*), C130S/C133S (*open circle*), and C159S/C176S (*open triangle*) mutant were determined to be 68, 67, 52, and 38 °C, respectively. *B*, Western blotting of Erv1p and its mutants using an antibody against the C-terminal of Erv1p. The proteins were untreated or treated by incubation with 0.05 mg/ml proteinase K at 25 °C for 30 min and followed by the addition of 10 mM phenylmethylsulfonyl fluoride before separation by SDS-PAGE. The full-length Erv1p and the N-terminal truncated fragments (*) are indicated.

similar spectrum profile with a conformation dominated by α-helical structures as expected (data not shown). However, an intensity decrease was observed for C30S/C33S mutant. It may be due to the absence of intermolecular disulfide bonded dimer, or the Cys^{30}–Cys^{33} disulfide may be important for the overall folding of the non-FAD-binding N-terminal segment.

To understand the possible structural role played by each disulfide, thermal denaturation of the WT and Erv1p mutants was studied using CD at 222 nm. As shown in Fig. 2*A*, the WT Erv1p is stable against heat denaturation with a melting temperature (T_m) at ~68 °C. The N-terminal double Cys mutant (C30S/C33S) had no apparent affect on the overall stability of Erv1p. In contrast, both the core domain double Cys mutants (C130S/C133S and C159S/C176S) had a clear effect on the stability of Erv1p, with a T_m of 52 °C for C130S/C133S and 38 °C for C159S/C176S (Fig. 2*A*). Mutation of the Cys^{159}-Cys^{167} disulfide alone resulted in a decrease of 30 °C in Erv1p T_m. A fraction of the C159S/C176S mutant was unfolded at the physiological temperature and as low as ~25 °C. Thus, our results show that the Cys^{159}–Cys^{176} disulfide plays a key role in stabilizing the overall folding of Erv1p.

Next, the effects of the individual disulfides on the stability of Erv1 were confirmed by proteinase K (PK) digestion analysis (Fig. 2*B*). After incubation of the WT and the mutants with or without the presence of 50 μg/ml PK at 25 °C for 30 min, the samples were analyzed by Western blotting using antibody against the C terminus of Erv1p. In the presence of PK, the WT and all three double Cys mutants were degraded (Fig. 2*B*). Although a stable C-terminal fragment of ~15 kDa was clearly observed for the WT and C30S/C33S mutant, the intensity of the same fragment was very weak for C130S/C133S and C159S/C176S mutants, and no other bands were detectable. Thus, the

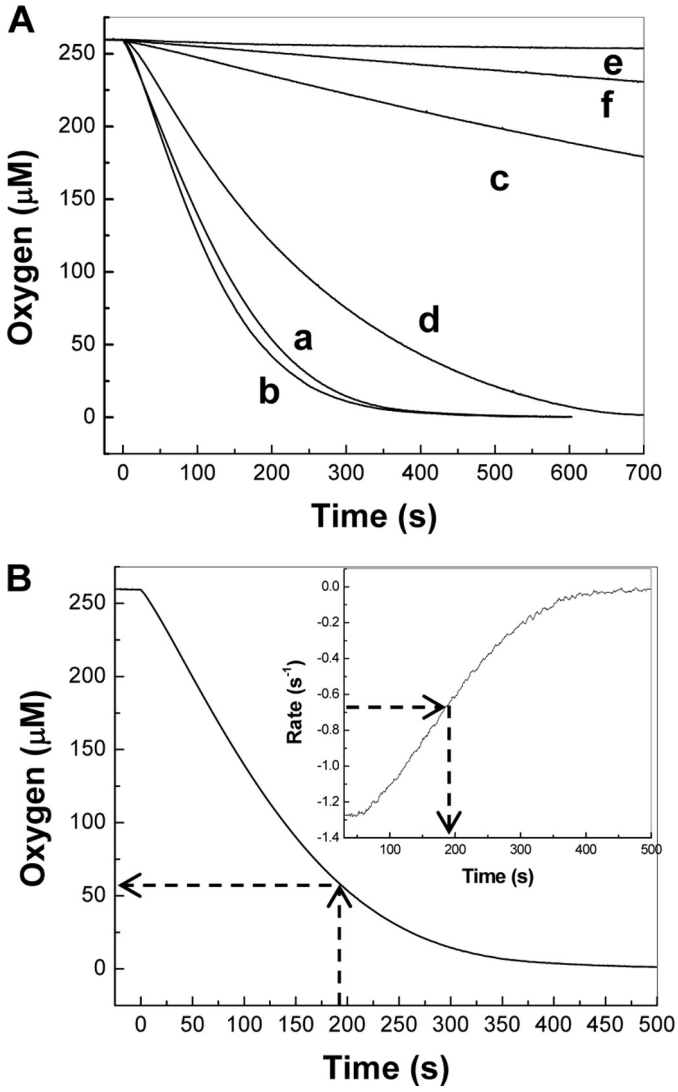

FIGURE 3. **Oxygen consumption of DTT catalyzed by the WT and Erv1p mutants.** *A*, oxygen consumption profiles of 10 mM DTT in the presence of 1 μM the WT (*curve a*), C30S/C33S (*curve b*), C130S/C133S (*curve c*), and C159S/C176S (*curve d*), respectively, and two controls of 10 mM DTT in the buffer (50 mM Tris, pH 7.4, 150 mM NaCl, 1 mM EDTA) alone (*curve e*) or plus 1 μM free FAD (*curve f*). For all measurements, DTT was injected to pre-equilibrated samples at 25 °C at time 0. *B*, oxygen consumption of 10 mM DTT catalyzed by the WT Erv1p and the time course of the rate change (*inset*) to show how k_{cat} and K_m were determined.

results of PK digestion are consistent with those of the thermal denaturation study.

Taken together, CD and PK digestion studies show that the C-terminal region of Erv1p was folded and resistant to PK digestion but not the N terminus. Therefore, although the N-terminal disulfide Cys^{30}–Cys^{33} has no effect on the stability of Erv1p, both of the central core disulfides play a role in stabilizing the folding of Erv1p, especially the Cys^{159}–Cys^{176} disulfide.

The Effects of the Individual Disulfides on the Oxidase Activity of Erv1p—The effects of individual disulfide bonds on the sulfhydryl oxidase activity of Erv1p were studied using oxygen consumption assays. First, the commonly used reducing agent DTT was employed as the electron donor with and without the presence of the WT or mutant Erv1p. As shown in Fig. 3*A*,

TABLE 1

Oxygen consumption kinetic parameters for the WT and Erv1p mutants

All of the experiments were carried out with 1 mM Erv1p proteins in 50 mM Tris buffer, pH 7.4, 150 mM NaCl, 1 mM EDTA at 25 °C. The error bars represent the standard errors ($n = 3$).

Electron donor	Erv1p	k_{cat}	K_m	k_{cat}/K_m
		s^{-1}	mM	$M^{-1} s^{-1}$
10 mM DTT	WT	1.3 ± 0.1	57 ± 4	$2.3 \pm 0.2 \times 10^4$
	C30S/C33S	1.5 ± 0.1	62 ± 5	$2.4 \pm 0.2 \times 10^4$
	C130S/C133S	<0.1		
	C159S/C176S	0.8 ± 0.1	87 ± 8	$9.2 \pm 0.2 \times 10^3$
3.5 mM TCEP	WT	1.1 ± 0.1	27 ± 3	$4.1 \pm 0.3 \times 10^4$
	C30S/C33S	<0.1		
	C130S/C133S	<0.05		
	C159S/C176S	0.7 ± 0.1	18 ± 2	$3.9 \pm 0.3 \times 10^4$

oxygen consumption was catalyzed as soon as the WT Erv1p was added. The k_{cat} was determined to be $1.3 \pm 0.1\ s^{-1}$, ~50% higher than that reported previously (24, 27). The K_m for molecular oxygen was determined to be 57 μM (Fig. 3*B* and Table 1). Different effects on the oxidase activity were observed with the three double Cys mutants. As expected, the active site C130S/C133S mutant showed no or very little activity, similar to that of a previous study using single Cys mutants (24). Interestingly, the N-terminal C30S/C33S mutant showed ~15% higher oxidase activity ($k_{cat} = 1.5 \pm 0.1\ s^{-1}$) than that of the WT enzyme. In contrast, the previous study with the corresponding single Cys mutants showed only ~30–50% activity of the WT Erv1p (24). For the C159S/C176S mutant, a decreased activity was observed (Fig. 3*A*), and the k_{cat} and K_m values were determined to be $0.8\ s^{-1}$ and 87 μM, respectively (Table 1). The enzyme specificity, ratio of k_{cat}/K_m, was the same ($2.3 \times 10^4\ M^{-1}\ s^{-1}$) for the WT and C30S/C33S and was similar to that of Ero1 proteins ($4–8 \times 10^4\ M^{-1}\ s^{-1}$) (29, 30). Taken together, these results showed that using DTT as substrate, only Cys^{130}–Cys^{133} disulfide is required for the oxidase activity of Erv1p, confirming that it is the active site disulfide.

Both Cys^{30}–Cys^{33} and Cys^{130}–Cys^{133} Disulfides Are Required for the Oxidase Activity of Erv1p toward Its Physiological Substrate—Previous yeast genetic studies demonstrated that all six Cys residues of Erv1p were required for its function *in vivo* (24). Therefore, we asked whether all three disulfides are essential for the oxidase active toward its native substrate protein Mia40. To this end, a functional C-terminal domain of Mia40, Mia40c (residues 284–403), was expressed and purified as reported previously. Mia40c contains all the six conserved Cys residues (CPC-CX_9C-CX_9C) of the protein. It has been shown that the CPC motif is the redox active site of Mia40, which can be selectively reduced and act as an electron donor for Erv1p (11). Thus, the partially reduced Mia40c (Mia40c-pR), with the Cys of CPC in the reduced form and CX_9C motifs in the oxidized form, was prepared and used as an electron donor for Erv1p. Oxygen consumption of 50 μM Mia40c-pR in the presence of 1 μM the WT or mutant Erv1p was measured. As shown in Fig. 4*A*, whereas both the WT and C159S/C176S Erv1p can catalyze the electron transfer from Mia40 to molecular oxygen, both C30S/C33S and C130S/C133S mutants were inactive (Fig. 4*A*). The initial rates for WT and C159S/C176S were ~0.6 ± 0.1 and $0.5 \pm 0.1\ s^{-1}$, respectively. Thus, for Mia40 oxidation, although C159S/C176S mutant had no significant effect on the

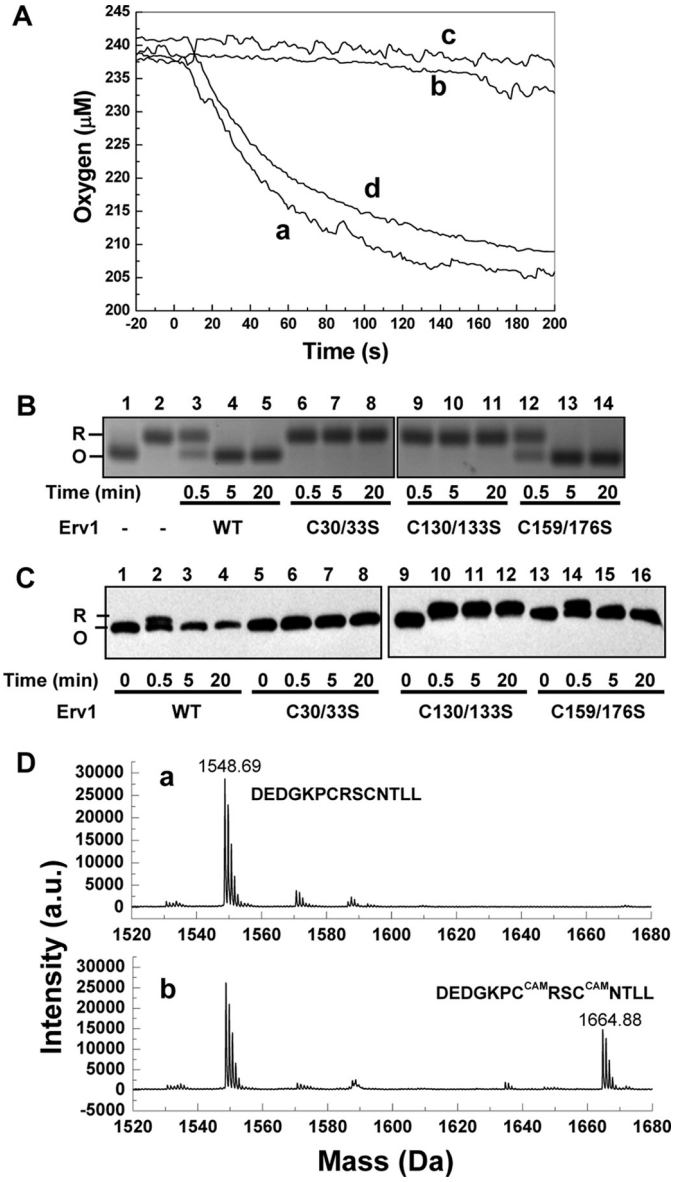

FIGURE 4. **Oxygen consumption and AMS assay of Mia40c-pR oxidation catalyzed by the WT and Erv1p mutants.** *A*, oxygen consumption profiles of 50 μM Mia40c-pR in the presence of 1 μM the WT Erv1p (*curve a*), C30S/C33S (*curve b*), C130S/C133S (*curve c*), and C159S/C176S (*curve d*), respectively. *B*, AMS assay of the redox state change of Mia40c-pR. Mia40c was detected by Coomassie Blue staining. *C*, AMS assay of the redox state change of the WT and Erv1p mutants. The proteins were detected by Western blotting with antibody against Erv1p. *D*, mass spectrometry analysis of Erv1p before (*panel a*) and after (*panel b*) incubated with Mia40c-pR for ~10 s. The peptides contain Cys^{30} and Cys^{33} in the oxidized (1548.69 Da) or reduced and alkylated (1664.88 Da) forms were shown.

oxidase activity of Erv1p, both Cys^{30}–Cys^{33} and Cys^{130}–Cys^{133} disulfides were required. It seems that less oxygen was consumed (~40 μM) than might be expected given that 50 μM Mia40 was in the reaction. This may partially be due to the fact that the protein was not 100% pure (~95% based on SDS-PAGE), due to errors of concentration as determined by the 5,5′-dithiobis(nitrobenzoic acid) assay, and/or due to the fact that oxygen consumption was very slow after the reaction for 3 min.

Furthermore, changes in the redox state of Erv1p and Mia40c were analyzed in parallel using a SDS-PAGE based AMS thiol-

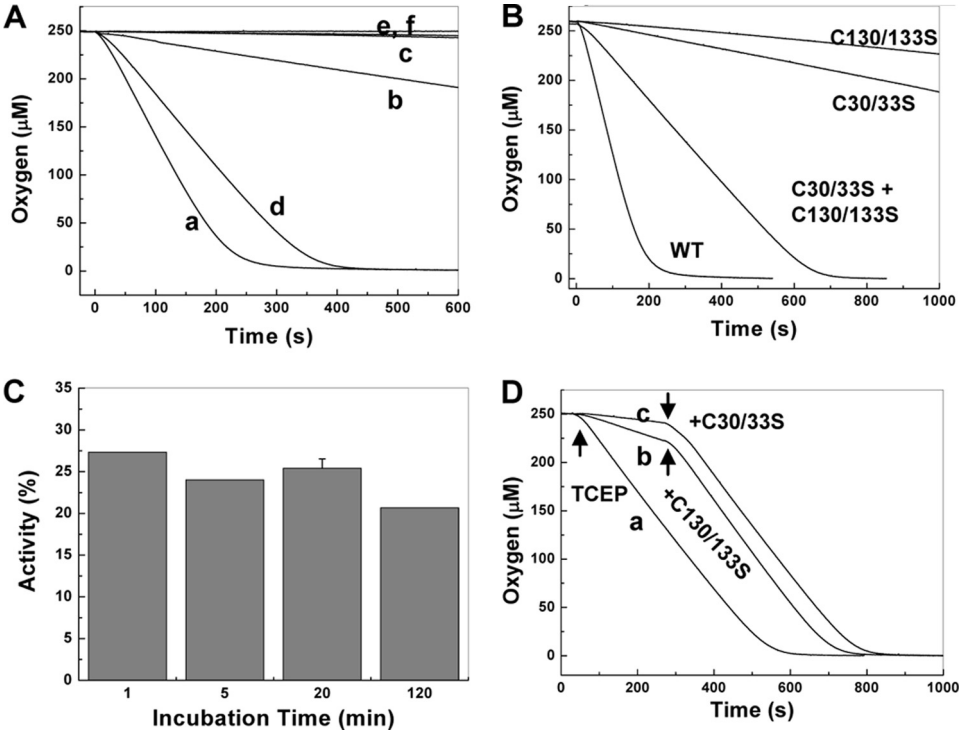

FIGURE 5. **Oxygen consumption of TCEP catalyzed by the WT and mutant Erv1.** *A*, oxygen consumption profiles of 3.5 mM TCEP in the presence of 1 μM the WT Erv1p (*curve a*), C30S/C33S (*curve b*), C130S/C133S (*curve c*), and C159S/C176S (*curve d*), respectively, and two controls of 3.5 mM TCEP in the buffer alone (*curve e*) or in the presence of 1 μM free FAD (*curve f*) as described for DTT in the legend to Fig. 4. *B*, oxygen consumption of 3.5 mM TCEP in the presence of a mixture of 1 μM C30S/C33S plus 1 μM C130S/C133S, or 2 μM of the WT, C30S/C33S, or C130S/C133S, respectively. *C*, the relative activity of C30S/C33S plus C130S/C133S plotted against the incubation time. The activity of the WT Erv1 was set as 100%. *D*, oxygen consumption of 3.5 mM TCEP catalyzed by 1 μM C30S/C33S plus 1 μM C130S/C133S. The two mutants were preincubated for 5 min before TCEP was injected (*curve a*), TCEP was injected to C30S/C33S at 30 s followed by the addition of C130S/C133S at 300 s (*curve b*), and TCEP was injected to C130S/C133S at 30 s followed by the addition of C30S/C33S at 300 s (*curve c*).

modification assay (see "Experimental Procedures"). As shown in Fig. 4*B*, a fraction of oxidized Mi40c (*O*) was observed after addition of the WT or C159S/C176S Erv1p for 0.5 min, and all of the proteins were oxidized in 5 min (Fig. 4*B*, *lanes 3–5* and *12–14*). When C30S/C33S or C130S/C133S mutant was used, Mia40c-pR remained in the reduced form (*R*), even after 20 min (Fig. 4*B*, *lanes 6–11*). Meanwhile, the redox state of Erv1p was revealed by Western blotting (Fig. 4*C*). Again, the same pattern of redox state change was observed for the WT Erv1p and C159S/C176S mutant (Fig. 4*C*, *lanes 1–4* and *13–16*), which was in agreement with the time courses of Mia40c-pR oxidation. A fraction of reduced Erv1p was detected at 0.5 min, which was reoxidized/regenerated in 5 min when all of the Mia40c-pR were oxidized. For C30S/C33S mutant, no redox state change was observed, consistent with the observation that this mutant was inactive in oxygen consumption (Fig. 4*A*, *curve b*). However, all C130S/C133S mutant was reduced after 0.5 min and remained in the reduced form through the same time course (Fig. 4*C*, *lanes 10–12*), although the mutant was enzymatically inactive (Fig. 4*A*, *curve c*). Thus, these results are consistent with the conclusion that Cys^{30}–Cys^{33} acts as a shuttle disulfide, which was reduced by Mia40c-pR, and these two Cys residues (Cys^{30} and Cys^{33}) were modified by AMS. The conclusion was confirmed by proteinase digestion coupled with mass spectrometry analysis of Erv1 before and after incubation with Mia40c-pR briefly (Fig. 4*D*). Although a peptide of 1548.69 Da corresponding to 24–37 residues of Erv1 with Cys^{30}–Cys^{33} disulfide bonded was identified in both samples, the same peptide with both Cys^{30} and Cys^{33} modified by iodoacetamide (1664.88 Da) was observed only in the sample mixed with Mia40c-pR (Fig. 4*D*, *panel b*).

In summary, oxygen consumption and AMS assays showed that both *CXXC* disulfides (Cys^{30}–Cys^{33} and Cys^{130}–Cys^{133}) are essential for Erv1p oxidase activity toward the physiological substrate Mia40c. The $CX_{16}C$ disulfide has no obvious effect on Erv1p activity and thus is not required for Erv1p oxidase function.

The Active Site Cys^{130}–Cys^{133} Disulfide Is Well Protected and Can Be Activated by Cys^{30}–Cys^{33} Disulfide through Intermolecular Electron Transfer—To understand whether Cys^{30}–Cys^{33} was required to act as a shuttle disulfide and whether that requirement was due to the fact that the active site disulfide was not accessible, we repeated the oxygen consumption experiments using TCEP as an electron donor. TCEP is a stronger reducing agent and has a slightly larger size (250 Da) than DTT (154 Da). Comparison between DTT and TCEP shows that the same kind of effects on the Erv1p activity were observed for C130S/C133S (inactive) and C159S/C176S (decreased activity) mutants, respectively (compare Figs. 3*A* and 5*A*). However, an opposite result was observed for the C30S/C33S mutant. Although a slightly increased activity was observed with DTT (Fig. 3*A*, *curve b*), little oxygen consumption was detected using TCEP as an electron donor (Fig. 5*A*, *curve b*). In the absence of Cys^{30}–Cys^{33} disulfide, TCEP is not a substrate for Erv1p. Thus, our results show that even TCEP cannot access and reduce the active site disulfide of Erv1 directly, suggesting the active site disulfide (Cys^{130}–Cys^{133}) is buried and well protected. The oxygen consumption curves of TCEP oxidation were further analyzed, and the k_{cat} values were determined to be 1.1 and 0.7 s^{-1} for the WT and C159S/C176S, respectively. The K_m values for oxygen were 27 μM for the WT and 18 μM for C159S/C176S (Table 1). A similar substrate specificity of 4×10^4 M^{-1} s^{-1} was obtained, which was ~2–4 times higher than that determined by using DTT (Table 1). Thus, TCEP is a better electron donor than DTT in terms of activation specificity. It is consistent with the finding that DTT not only can reduce Cys^{30}–Cys^{33}, but also Cys^{130}–Cys^{133} and maybe even Cys^{159}–Cys^{176}; thus some enzyme activity may be lost during the assays using DTT.

Next, to confirm that Cys^{30}–Cys^{33} can act as a shuttle disulfide, we performed the activity assay using TCEP as an electron donor in the presence of a total of 2 μM enzyme(s): WT Erv1, C30S/C33S, or C130S/C133S alone, or a mixture (preincubated for ~5 min) of the two mutants (1 μM each), respectively. As show in Fig. 5*B*, although both mutants alone were inactive, the mixture of these two mutants showed a clear Erv1p oxidase activity. The rate of oxygen consumption was ~0.36 $\mu M\ s^{-1}$, which was ~24% that of the WT enzyme (1.5 $\mu M\ s^{-1}$) at the same condition (Fig. 5*B*). The result confirms that Cys^{30}–Cys^{33} disulfide of a C130S/C133S mutant can activate C30S/C33S mutant via intersubunit or intermolecular electron transfer. If formation of a heterodimer between the two mutants is necessary for the activity, the activity will increase with the time of incubation. Interestingly, no obvious difference in the levels of activity was observed between 1, 5, and 20 min of incubation, but a slightly decreased activity was obtained when the proteins are preincubated for 2 h (Fig. 5*C*). Thus, these results suggest that heterodimer formation is not required. To confirm our finding, we carried out the experiments by incubating TCEP with one of the mutants first and followed by addition of the second mutants (Fig. 5*D*, *curves b* and *c*). As shown in Fig. 5*D*, the same rate of oxygen consumption as that of preincubated proteins (curve a) was obtained as soon as the second mutant was added in both cases. Taken together, we demonstrated experimentally for the first time that Cys^{30}–Cys^{33} functionally acts as a shuttle disulfide passing electrons to the active site Cys^{130}–Cys^{133} disulfide, and furthermore the electron transfer may occur between two different molecules via intermolecular interactions.

DISCUSSION

In this study, the structure and functional roles of all three individual disulfides of the yeast mitochondrial sulfhydryl oxidase Erv1p were analyzed using site-directed mutagenesis coupled with various biochemical and biophysical techniques. We show that whereas none of the three disulfides is essential for FAD-binding to Erv1p, they all play an important role *in vitro*. The specific roles played by each disulfide were deciphered systematically.

In this report, we provide direct experimental evidence to show that the N-terminal Cys^{30}–Cys^{33} disulfide is required to shuttle electrons from the physiological substrate Mia40 to the active site Cys^{130}–Cys^{133} disulfide. Although most *in vitro* studies on the function of FAD-dependent sulfhydryl oxidases have used a model substrate (*e.g.* DTT, reduced lysozyme, or *E. coli* thioredoxin), in this study, we used both artificial substrates (DTT and TCEP) and the physiological substrate, partially reduced Mia40, to address the functional mechanism of Erv1p. By comparison between the results, we are able to show that the active site disulfide Cys^{130}–Cys^{133} is accessible to DTT but not to TCEP and Mia40; thus, in terms of biological relevance, TCEP is a better small molecule than DTT as substrate for Erv1p studies. C30S/C33S mutant was more active than the WT toward DTT oxidation but was enzymatically inactive toward Mia40c and TCEP oxidation. Together with the fact that TCEP is a stronger reductant and larger (250 Da) than DTT (154 Da), our results suggest that the active site disulfide is highly protected. It is not accessible to Mia40 and even to TCEP. The standard redox potential for Erv1p active site disulfide (Cys^{130}–Cys^{133}) has been determined to be of −150 mV (27). The redox potentials for the mitochondrial intermembrane space, GSH, and DTT were determined to be −255, −240, and −330 mV, respectively (31, 32), and an even lower value for TCEP was predicted (33). Accordingly, the active site disulfide of Erv1p would be thermodynamically unstable in the intermembrane space or against any of above thiol reducing reagents if it was not well protected. The inaccessible nature of the active site disulfide can also explain why DTT is a poor substrate for all members of Erv/ALR and Ero1 families in general. Our conclusion is also in agreement with the finding that GSH is not a good substrate for Erv1p (data not shown) and other Erv enzymes, because GSH is a weaker reductant than DTT and larger (307 Da) than TCEP. Thus, we provided direct experimental evidence for the current hypothesis that Cys^{30}–Cys^{33} is required to serve as a shuttle disulfide transferring electrons from substrate to the active site Cys^{130}–Cys^{133} disulfide.

More importantly, the Erv1p oxidase activity was partially recovered after mixing of the two individually inactive mutants, C30S/C33S and C130S/C133S (Fig. 5, *B–D*). An optimum of 50% of the WT Erv1p activity is expected for a perfect mixing and reassembled C30S/C33S-C130S/C133S Erv1. Because all known Erv/ALR enzymes form stable dimer or oligomers, the rate of dissociation is expected to be slow and probably in a time scale of min or even hours. Moreover, our results show that the enzyme activity was recovered rapid to ~25% that of the WT Erv1p. Although we cannot exclude the possibility that the subunits rapidly scramble, our results suggest that this recovered activity was via intermolecular rather than intersubunit reaction. It seems likely that in the cells Cys^{30}–Cys^{33} can shuttle electrons to Cys^{130}–Cys^{133} through both intersubunit and intermolecular reactions and maybe even via intrachain shuttle. Similarly, for Ero1p a mechanism of both intra- and interchain electron transfer has been suggested (34).

Next, our study also suggests that Cys^{30}–Cys^{33} disulfide and/or the flexible N-terminal region may also play a role in regulating the accessibility of the active site disulfide through a conformation change induced by interacting with Mia40 and thiol/disulfide exchange. Based on the CD measurements, a clear conformation change was observed for the N-terminal C30S/C33S mutant (data not shown). It suggests that a conformation change may occur in the flexible N-terminal region upon reduction of Cys^{30}–Cys^{33} disulfide. Although the oxidase activity can be regained by mixing the active site C130S/C133S mutant with C30S/C33S, no enzyme activity was recovered by mixing C130S/C133S with Erv1-ΔN (a N-terminal 72-amino acid deleted Erv1) (data not shown). Thus, the interactions involving Erv1p N-terminal regions may play an important role during electron transfer from the shuttle disulfide to the active site disulfide and mediating the accessibility of the active site disulfide. In this way, the oxidase activity of Erv1p can be regulated effectively and specifically while circumventing or limiting nonspecific and harmful oxidation of protein thiols. Recently, a similar regulatory role played by a disulfide was demonstrated for both Ero1p and Ero1α (17–19). These regulatory disulfide bonds are among the nonconserved disulfides

of Ero1 proteins. Although Erv1p has only three conserved disulfides, the location and the spacing between the two Cys residues of the shuttle disulfides (CX_nC, n = 1, 2, or 4) are not strictly conserved among the Erv/ALR enzymes. Accordingly, this disulfide may act as a regulative disulfide with substrate specificity.

Furthermore, this report provided direct evidence to show that $CX_{16}C$ disulfide plays an important role in the overall stability of Erv1p. Based on our thermal denaturation and limited proteinase digestion studies, both disulfides (Cys^{130}–Cys^{133} and Cys^{159}–Cys^{176}) of the C terminus contribute to the overall stability of the protein. Mutation of C130S/C133S decreases the T_m of Erv1p from 68 to 53 °C, and C159S/C176S has an apparent T_m of 38 °C. A fraction of C159S/C176S mutant was unfolded at temperature as low as 25 °C. Thus, this result provides a good explanation for the report that a single mutation of C159S results in a temperature-sensitive phenotype in yeast (35). Although the mutant yeast can grow at 24 °C, it cannot grow at 37 °C.

In summary, this study shows that all three pairs of disulfide bonds play an essential or important but different role in structure and function of Erv1p. Although the first *CXXC* motif (Cys^{30}–Cys^{33}) acts as shuttle disulfide and is involved in regulating the accessibility of the active site disulfide (Cys^{130}–Cys^{133}), the C-terminal $CX_{16}C$ disulfide plays an important role in the overall stability of Erv1p. The well protected active site disulfide Cys^{130}–Cys^{133} requires a shuttle disulfide to transfer electrons from substrate, and both intersubunit and intermolecular transfer can occur.

Acknowledgments—We are grateful to Neil Bulleid, Mike Grant, Bruce Morgan, and members of the Faculty Biomolecule core facility staffs (Manchester University, UK) for help.

REFERENCES

1. Collet, J. F., and Bardwell, J. C. (2002) *Mol. Microbiol.* **44,** 1–8
2. Kadokura, H., Katzen, F., and Beckwith, J. (2003) *Annu. Rev. Biochem.* **72,** 111–135
3. Sevier, C. S., and Kaiser, C. A. (2006) *Antioxid. Redox. Signal.* **8,** 797–811
4. Stojanovski, D., Müller, J. M., Milenkovic, D., Guiard, B., Pfanner, N., and Chacinska, A. (2008) *Biochim. Biophys. Acta* **1783,** 610–617
5. Lee, J., Hofhaus, G., and Lisowsky, T. (2000) *FEBS Lett.* **477,** 62–66
6. Koehler, C. M., and Tienson, H. L. (2009) *Biochim. Biophys. Acta* **1793,** 139–145
7. Mesecke, N., Terziyska, N., Kozany, C., Baumann, F., Neupert, W., Hell, K., and Herrmann, J. M. (2005) *Cell* **121,** 1059–1069
8. Tokatlidis, K. (2005) *Cell* **121,** 965–967
9. Allen, S., Balabanidou, V., Sideris, D. P., Lisowsky, T., and Tokatlidis, K. (2005) *J. Mol. Biol.* **353,** 937–944
10. Hell, K. (2008) *Biochim. Biophys. Acta* **1783,** 601–609
11. Grumbt, B., Stroobant, V., Terziyska, N., Israel, L., and Hell, K. (2007) *J. Biol. Chem.* **282,** 37461–37470
12. Banci, L., Bertini, I., Cefaro, C., Ciofi-Baffoni, S., Gallo, A., Martinelli, M., Sideris, D. P., Katrakili, N., and Tokatlidis, K. (2009) *Nat. Struct. Mol. Biol.* **16,** 198–206
13. Stojanovski, D., Milenkovic, D., Müller, J. M., Gabriel, K., Schulze-Specking, A., Baker, M. J., Ryan, M. T., Guiard, B., Pfanner, N., and Chacinska, A. (2008) *J. Cell Biol.* **183,** 195–202
14. Thorpe, C., and Coppock, D. L. (2007) *J. Biol. Chem.* **282,** 13929–13933
15. Frand, A. R., Cuozzo, J. W., and Kaiser, C. A. (2000) *Trends Cell Biol.* **10,** 203–210
16. Gross, E., Kastner, D. B., Kaiser, C. A., and Fass, D. (2004) *Cell* **117,** 601–610
17. Sevier, C. S., Qu, H., Heldman, N., Gross, E., Fass, D., and Kaiser, C. A. (2007) *Cell* **129,** 333–344
18. Baker, K. M., Chakravarthi, S., Langton, K. P., Sheppard, A. M., Lu, H., and Bulleid, N. J. (2008) *EMBO J.* **27,** 2988–2997
19. Appenzeller-Herzog, C., Riemer, J., Christensen, B., Sørensen, E. S., and Ellgaard, L. (2008) *EMBO J.* **27,** 2977–2987
20. Coppock, D. L., and Thorpe, C. (2006) *Antioxid. Redox. Signal.* **8,** 300–311
21. Fass, D. (2008) *Biochim. Biophys. Acta* **1783,** 557–566
22. Gross, E., Sevier, C. S., Vala, A., Kaiser, C. A., and Fass, D. (2002) *Nat. Struct. Biol.* **9,** 61–67
23. Vitu, E., Bentzur, M., Lisowsky, T., Kaiser, C. A., and Fass, D. (2006) *J. Mol. Biol.* **362,** 89–101
24. Hofhaus, G., Lee, J. E., Tews, I., Rosenberg, B., and Lisowsky, T. (2003) *Eur. J. Biochem.* **270,** 1528–1535
25. Morgan, B., Ang, S. K., Yan, G., and Lu, H. (2009) *J. Biol. Chem.* **284,** 6818–6825
26. Lu, H., Allen, S., Wardleworth, L., Savory, P., and Tokatlidis, K. (2004) *J. Biol. Chem.* **279,** 18952–18958
27. Dabir, D. V., Leverich, E. P., Kim, S. K., Tsai, F. D., Hirasawa, M., Knaff, D. B., and Koehler, C. M. (2007) *EMBO J.* **26,** 4801–4811
28. Lu, H., and Woodburn, J. (2005) *J. Mol. Biol.* **353,** 897–910
29. Gross, E., Sevier, C. S., Heldman, N., Vitu, E., Bentzur, M., Kaiser, C. A., Thorpe, C., and Fass, D. (2006) *Proc. Natl. Acad. Sci. U.S.A.* **103,** 299–304
30. Wang, L., Li, S. J., Sidhu, A., Zhu, L., Liang, Y., Freedman, R. B., and Wang, C. C. (2009) *J. Biol. Chem.* **284,** 199–206
31. Hu, J., Dong, L., and Outten, C. E. (2008) *J. Biol. Chem.* **283,** 29126–29134
32. Rothwarf, D. M., and Scheraga, H. A. (1992) *Proc. Natl. Acad. Sci. U.S.A.* **89,** 7944–7948
33. Krezel, A., Latajka, R., Bujacz, G. D., and Bal, W. (2003) *Inorg. Chem.* **42,** 1994–2003
34. Sevier, C. S., and Kaiser, C. A. (2006) *Mol. Biol. Cell* **17,** 2256–2266
35. Müller, J. M., Milenkovic, D., Guiard, B., Pfanner, N., and Chacinska, A. (2008) *Mol. Biol. Cell* **19,** 226–236

Ang & Lu
Supplementary Figure 1

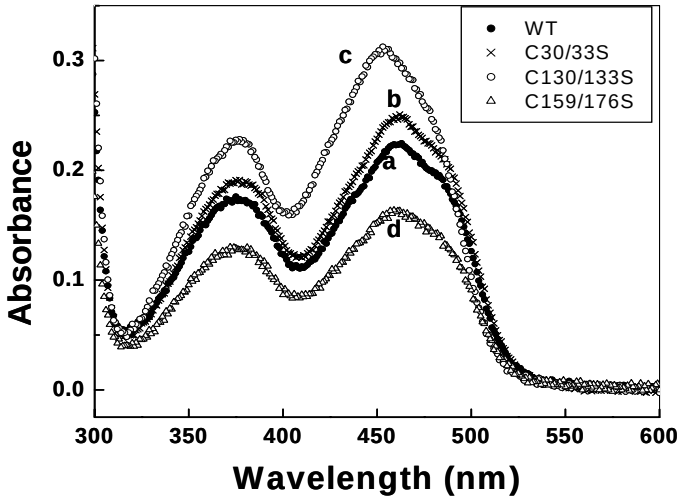

Supplementary Fig. 1. Absorption spectra of the WT (a) and the three double Cys mutants. The concentrations of FAD-bound Erv1p WT (a), C30/33S (b), C130/133S (c) and C159/176S (d) were 18.9, 22.6, 25.8 and 13.7 μM, respectively.

Ang & Lu Supplementary Table 1:

Supplementary Table 1: Spectrometric properties of the WT and Erv1p mutants

Erv1p	λ_{max} (nm)	Extinction coefficient ($mM^{-1} cm^{-1}$)	FAD-binding (%)
WT	460	11.9	93±2
C30/33S	460	11.1	93±2
C130/133S	453	12.1	93±2
C159/176S	460	11.9	91±2

The extinction coefficients and the percentage of protein bound FAD were calculated based on 11.3 $mM^{-1} cm^{-1}$ at 450 nm for free FAD and 72.68 $mM^{-1} cm^{-1}$ at 275 nm for Erv1p. The error bars represent standard errors, n=3.